



Virginia Commonwealth University
VCU Scholars Compass

Theses and Dissertations


Graduate School

2020

Investigations of Graphene-Supported Single-Atom Catalyst Model Ions in the Gas Phase

Michael Borrrome
Virginia Commonwealth University

Follow this and additional works at: <https://scholarscompass.vcu.edu/etd>

 Part of the [Inorganic Chemistry Commons](#), [Organic Chemistry Commons](#), and the [Physical Chemistry Commons](#)

© Michael Borrrome

Downloaded from

<https://scholarscompass.vcu.edu/etd/6477>

This Dissertation is brought to you for free and open access by the Graduate School at VCU Scholars Compass. It has been accepted for inclusion in Theses and Dissertations by an authorized administrator of VCU Scholars Compass. For more information, please contact libcompass@vcu.edu.

© Michael Borrome

2020 All Rights Reserved

Investigations of Graphene-Supported Single-Atom Catalyst Model Ions in the Gas Phase

A dissertation submitted in partial fulfillment of the requirements for degree of Doctor of
Philosophy from Virginia Commonwealth University

by

Michael Borrome

B.S. Chemistry, University of Connecticut 2016

Principal Investigator:

Dr. Scott Gronert

Professor, Department of Chemistry

Virginia Commonwealth University

Richmond, Virginia

October 12, 2020

ACKNOWLEDGEMENTS

As I come to the end of my academic studies, there are a few people that I would like to thank for helping me come this far. First, I would like to thank Dr. Scott Gronert, my advisor. When I joined his lab in the spring of 2017, I had a very narrow perspective of what it meant to be a scientist. I thought scientists studied hard in order to always have the correct answer. However, now I believe a scientist is someone who carefully thinks about a problem and applies a logical method in order to solve the problem and reach the answers they seek. My whole perspective on what it means to be a scientist has changed because of Dr. Gronert's guidance. Thank you for everything you have done for me! I will always appreciate it.

In a similar vein, I would like to thank my old and current committee members: Dr. Hani El-Kaderi, Dr. Vladimir Sidorov, Dr. Katharine Tibbets, Dr. Wynne, and Dr. Fugelstad. They helped me learn how to question my own work. This is crucial for eliminating any unconscious assumptions that are made when working through difficult problems. I'm sure this skill will be extremely useful as I move forward in my chemistry career. Thank you all for your help!

Of all my friends, I would like to give special thanks to my labmates Sharon Corea, Mariah Parker, and Leah Donham. Sharon and I started working in the lab at the same time and I will always appreciate her support and friendship as we faced the challenges of our studies. Mariah and Leah were senior lab members and were a great help in my training and always offered great advice when I needed it. Thank you all for being such good friends!

Finally, I would like to thank my father, my mother, and my brother. They raised me, the youngest of the family, cared for me and encouraged me to be the best person that I can be. I am here now because of their efforts. Thank you so much for all your love and support!

Table of Contents

ACKNOWLEDGEMENTS	iii
List of Figures	vii
List of Schemes	xv
List of Tables	xxi
ABSTRACT	1
Chapter 1 - Introduction to Single-Atom Catalysts	3
1.1 Size Reduction of Heterogeneous Catalysts	3
1.2 Active Site Heterogeneity	5
1.3 Single-Atom Catalysts	8
Chapter 2 - Electrospray Ionization Quadrupole Ion Trap Mass Spectrometry	14
2.1 Electrospray Ionization	14
2.2 Linear Triple Quadrupole Ion Traps	17
2.3 Ion-Molecule Reactions Using a Linear Triple Quadrupole Ion Trap	21
2.4 Gas-Phase Synthesis of Graphene-Supported Single-Atom Catalyst Model Ions	24
Chapter 3 - Gas-Phase Dehydrogenation of Alkanes: C-H Activation by a Graphene-Supported Nickel Single-Atom Catalyst Model	29
3.1 Alkane Dehydrogenation	29
3.2 Complex I in the Dehydrogenation of Cyclohexane	30
3.3 Dehydrogenation of Various Hydrocarbons	36
3.4 Dehydrogenation Mechanism	40
3.5 Sequential Dehydrogenations	42

3.6 Experimental Section.....	46
Chapter 4 - Gas-Phase Dehydrogenation of Amines and Alcohols by Graphene-Supported Single-Atom Catalyst Model Ions.....	48
4.1 Amine and Alcohol Dehydrogenation.....	48
4.2 Complexes I and II in the Dehydrogenation of Amines and Alcohols.....	49
4.3 Mechanistic Studies for the Dehydrogenation of Amines.....	56
4.4 Mechanistic Studies for the Dehydrogenation of Alcohols.....	66
4.5 Additional Reactivity.....	73
4.6 Experimental Section.....	80
Chapter 5 - Oxidative Addition of Polar Reagents by Gas-Phase Graphene-Supported Single-Atom Catalyst Model Ions.....	82
5.1 Oxidative Addition	82
5.2 Oxidative Addition of Aryl Halides by the SAC Model Complexes	83
5.3 Computation Modelling for the Oxidative Addition of Aryl Halides	92
5.4 Oxidative addition of Non-Aromatic Reagents by the SAC Model Complexes	101
5.5 Computational Modelling for the Oxidative Addition of Non-Aromatic Reagents.....	106
5.6 Experimental Section.....	113
Chapter 6 - Conclusion	115
6.1 Highlights	115
6.2 Impact and Future Directions	116
References.....	118
Appendix A – Spectra.....	131
Appendix B – Thermodynamic data.....	147

Appendix C – Computational Data.....153

List of Figures

- Figure 1.1.** Depictions of the two types of active sites on the surface of cubic, octahedral, and cuboctahedral Pd nanocrystals. Adapted with permission from Crespo-Quesada, M., Yarulin, A., Jin, M., Xia, Y. & Kiwi-Minsker, L. *J. Am. Chem. Soc.* **133**, 12787–12794 (2011). Copyright (2011) American Chemical Society.¹² 5
- Figure 1.2.** Selective production of 2-methyl-3-buten-2-ol (MBE) by Pd nanocrystals at 50% (circles) and 95% (squares) conversion of 2-methyl-3-butyn-2-ol (MBY) as a function of the amount of edge atoms. OCT = octahedral, CUB18 = 18nm cube, CUB6 = 6nm cube, COT = cuboctahedral. Adapted with permission from Crespo-Quesada, M., Yarulin, A., Jin, M., Xia, Y. & Kiwi-Minsker, L. *J. Am. Chem. Soc.* **133**, 12787–12794 (2011). Copyright (2011) American Chemical Society.¹² 7
- Figure 1.3.** Pd catalytic performance. Panel (a) – butenes selectivity as a function of conversion. Panel (b) – product distribution of butenes at 95% conversion. Adapted with permission from Yan, H. *et al. J. Am. Chem. Soc.* **137**, 10484–10487 (2015). Copyright (2015) American Chemical Society.¹⁸ 9
- Figure 1.4.** Depiction of the differences in adsorption modes on the Pd₁/graphene catalyst, resulting in higher selectivity for butenes. Adapted with permission from Yan, H. *et al. J. Am. Chem. Soc.* **137**, 10484–10487 (2015). Copyright (2015) American Chemical Society.¹⁸ 10
- Figure 1.5.** Depiction of our gas-phase SAC model ion. The model ion has been generated in our lab using four different metal centers: cobalt, nickel, copper, and palladium. 12
- Figure 2.1.** Depiction of ESI. The charged solution forms the Taylor cone and sprays a mist charged droplets. The droplets become gaseous ions and are swept towards the mass spectrometer inlet. Adapted with permission from Konermann, L., Ahadi, E., Rodriguez, A. D. & Vahidi, S. *Anal. Chem.* **85**, 2–9 (2013). Copyright (2013) American Chemical Society.⁴⁷ 14

Figure 2.2. Depiction of ion formation from charged droplets produced by ESI. The CRM proposes multiple subdivisions of charged droplets lead to gaseous ions (top). The IEM proposes solvent evaporation leads to desorption of bare gaseous ions (bottom). Adapted with permission from Nguyen, S. & Fenn, J. B. *PNAS* **104**, 1111–1117 (2007). Copyright (2007) National Academy of Sciences, U.S.A.⁵³ 16

Figure 2.3. Depiction of the linear triple quadrupole ion trap used in the modified Thermo Electron LTQ XL™.⁵⁸ Ions are directed into the front section by ion optics. The front and back sections focus ion streams into the center section. Ion trapping occurs in the center section. 17

Figure 2.4. Depiction of the potential wells caused by rf voltages. Panel (a) – ions are trapped in the radial dimension. Ions with sufficient kinetic energy can move towards the center. Panel (b) – ions are trapped in the axial dimension. Ions are accelerated towards the center of the trap. Adapted with permission from Weil, C., Nappi, M., Cleven, C. D., Wollnik, H. & Cooks, R. G. *Rapid Communications in Mass Spectrometry* **10**, 742–750 (1996). Copyright © 1996 John Wiley & Sons, Ltd.⁶⁰ 18

Figure 2.5. Depiction of ions sent to the detection system from the center section of the linear triple quadrupole ion trap.⁵⁸ All ions can be sent out to the detection system by sweeping rf voltages. Alternatively, specific ions can be isolated in the trap based on their m/z value. 20

Figure 2.6. Schematic of the external inlet system. The neutral reagent is introduced into a fast flow of helium at a constant rate. The helium-reagent mixture is drawn into the ion trap by a restriction capillary and the rest is vented to exhaust.³⁶ Adapted with Permission from Gronert, S. *Mass Spectrom. Rev.* **24**, 100–120 (2005). Copyright © 2004 Wiley Periodicals, Inc., A Wiley Company. 21

Figure 2.7. Depiction of the issues creating the Fe and Pt SAC model ions. CID reduction of the Fe precursor ion led to the metal oxide species likely due to adventitious oxygen in the ion trap. Attempts to generate the Pt precursor ion were unsuccessful. 27

Figure 3.1. Transfer dehydrogenation reaction. A sacrificial hydrogen acceptor is used to drive the reaction towards products. 29

Figure 3.2. Mass spectra for the reduction of the Ni of the precursor ion. Panel (a) Isolation of Ni precursor complex. Panel (b) Product spectrum for the CID of the Ni precursor complex. The two-electron and one-electron reduction pathways lead to the products at m/z 267 and 311, respectively. 31

Figure 3.3. Mass spectra for the reduction of the Ni complex with fluorene-9-carboxylate. Panel (a) Isolation of the Ni complex with fluorene-9-carboxylate. Panel (b) CID of the Ni complex with fluorene-9-carboxylate. Complex **I** appears at m/z 223. The fluorenyl anion appears at m/z 165. Products of adduct formation with adventitious nitrogen appears at m/z 251. The peak at m/z 227 may be an adduct of fluorene-9-carboxylate and water. 32

Figure 3.4. Mass spectra for reaction of **I** with cyclohexane. Panel (a) Isolation of **I** prior to introduction of cyclohexane. Panel (b) Product spectrum after introduction of cyclohexane. Dehydrogenation and alkane adduct products appear at m/z 305 and 307, respectively. Peak broadening of the alkane adduct is observed due to the relative instability of the ion during the instrument scans.³⁶ Complex **I** appears at m/z 223. Products of adduct formation with adventitious water, nitrogen, and methanol appear at m/z 241, 251, and 255 respectively. The peak at m/z 227 may be an adduct of fluorene-9-carboxylate and water formed through secondary reactions. There are also peaks (not shown) at m/z 90, an oxide from reaction with adventitious oxygen, and m/z 107, an unidentified species that is independent of the neutral reagent. 33

Figure 3.5. Cyclohexane- d_{12} experiments. Panel (a) Reaction of **I** with cyclohexane- d_{12} . Panel (b) Isotope effect experiment. Alkene complex (C_6H_{10} and C_6D_{10} complexes) and alkane adduct (C_6H_{12} and C_6D_{12} adducts) peaks appear at m/z 305, 315, 307 and 319, respectively. Peak broadening is observed for the alkane adduct peak due to the relative instability of the product ion during the instrument scans. Complex **I** appears at m/z 223. Products of adduct formation with water, nitrogen, and methanol appear at m/z 241, 251, and 255 respectively. The peak at m/z 227 may be an adduct of fluorene-9-carboxylate and water formed through secondary reactions. There

are also peaks (not shown) at m/z 90, an oxide from reaction with adventitious oxygen, and m/z 107, an unidentified adduct that is independent of the neutral reagent. 35

Figure 3.6. Reaction of complex **I** with 2,2-dimethylbutane. Panel (a) depicts the product spectrum. Two products are observed: the dehydrogenation product (m/z 307) and the alkane adduct (m/z 309). Panel (b) depicts which C-H bonds lead to the products. Insertion into the red C-H groups leads to the dehydrogenation product. When approaching the blue C-H groups dehydrogenation cannot occur, resulting in the alkane adduct. 38

Figure 3.7. Product spectrum for the reaction of complex **I** with tert-butylbenzene. The alkane adduct (m/z 357) was the only product observed. Complex **I** appears at m/z 223. Adduct formation products of complex **I** with water, nitrogen, and methanol appear at m/z 241, 251, and 255 respectively. The peak at m/z 227 may be an adduct of fluorene-9-carboxylate and water formed through secondary reactions. There are also peaks (not shown) at m/z 90, an oxide from reaction with adventitious oxygen, and m/z 107, an unidentified adduct that is independent of the neutral reagent. 39

Figure 3.8. Potential energy surface for the dehydrogenation of cyclohexane by complex **I**. Calculations were completed at the M06/6-311 + G** level. Detailed information on the structure and frequencies of the calculated species are shown in Appendix C. 40

Figure 3.9. Potential energy surface for the dehydrogenation of cyclohexadiene. Calculations were completed at the M06/6-311 + G** level. Detailed information on the structure and frequencies of the calculated species are shown in Appendix C. 45

Figure 4.1. Spectra for the reaction of **I** with n-butylamine. Panel (a) Isolation of complex **I** prior to introduction of n-butylamine. Panel (b) Product spectrum after introduction of n-butylamine. The dehydrogenation product appears at m/z 294. Products of adduct formation with adventitious water, nitrogen, and methanol are also present and appear at m/z 241, 251, and 255 respectively. The peak at m/z 227 may be an adduct of fluorene-9-carboxylate and water formed through secondary reactions. There are also peaks (not shown) at m/z 90, a nickel oxide from reaction with

adventitious oxygen, and m/z 107, an unidentified species that is independent of the neutral reagent..... 52

Figure 4.2. Spectra for the reaction of **II** with n-butylamine. Panel (a) Isolation of complex **II** prior to introduction of n-butylamine. Panel (b) Product spectrum after introduction of n-butylamine. The dehydrogenation and amine adduct products appear at m/z 295 and m/z 297, respectively. Peak broadening of the amine adduct is observed due to the relative instability of the ion during the instrument scans.³⁶ Products of adduct formation with adventitious water are present at m/z 242 and 260. A cobalt complex with adventitious methanol appears at m/z 91 and is the base peak (not shown). Unidentified species that are independent of the neutral reagent appear at m/z 180 and 228..... 53

Figure 4.3. Product spectrum for the reaction of **I** with n-butanol. The dehydrogenation and alcohol adduct products appear at m/z 295 and 297, respectively. The peaks at m/z 283 and 227 may be adducts of fluorene-9-carboxylate with n-butanol and water, respectively, formed through secondary reactions. The peak at m/z 223 is complex **I**. Cyclohexene and cyclohexane adduct products formed via reaction with the cyclohexane solvent appear m/z 305 and 307. Products of adduct formation with adventitious water, nitrogen, and methanol are also present and appear at m/z 241, 251, and 255 respectively. The increased signal of m/z 251 also suggests a carbon monoxide adduct. The peak at m/z 283 is likely formed via secondary reactions with adventitious species. There are also peaks (not shown) at m/z 90, a nickel oxide from reaction with adventitious oxygen, and m/z 107, an unidentified species that is independent of the neutral reagent. 55

Figure 4.4. Product spectrum for the reaction of **II** with n-butanol. The dehydrogenation and alcohol products appear at m/z 296 and 298, respectively. Complex **II** appears at m/z 224. A metal adduct with adventitious methanol appears at m/z 91. Peaks at m/z 93, 107, 147, 284, and 300 are likely formed via secondary reactions with adventitious species. An unidentified species that is independent of the neutral reagent appears at m/z 180..... 56

Figure 4.5. Product spectra for reactions of deuterium-labeled n-butylamine reagents with complex **I**. Panel (a) depicts the reaction of **I** with n-butylamine- d_9 . The imine adduct peak for this reaction appears at m/z 302. Panel (b) depicts the reaction of **I** with n-butylamine- ND_2 . An alkene

adduct appears at m/z 296. An imine adduct appears at m/z 295 with loss of HD. The peak at m/z 294 is likely an imine adduct formed with the loss of D_2 , due to HD exchange between the N and the α -C. Products of adduct formation with adventitious water, nitrogen, and methanol are also present and appear at m/z 241, 251, and 255 respectively. The peaks at m/z 242 and 243 are likely formed via HD exchange between the water adduct and the neutral reagent. The peak at m/z 227 may be an adduct of fluorene-9-carboxylate and water formed through secondary reactions. The peak at m/z 228 is likely formed via HD exchange between the m/z 227 species and the neutral reagent. There are also peaks (not shown) at m/z 90, an oxide from reaction with adventitious oxygen, and m/z 107, an unidentified species that is independent of the neutral reagent. 60

Figure 4.6. Transition states for the dehydrogenation of butylamine by complex **I** to give the imine and alkene adduct products. Panel (a) depicts N-H insertion followed by α -C elimination. Panel (b) depicts α -C insertion followed by N-H elimination. Panel (c) depicts α -C insertion followed by β -C elimination. Enthalpies for transition states are in kcal/mol. DFT calculations were performed at the M06/6-311+G** level. Detailed information on the structures and frequencies of the calculated species are shown in Appendix C. 61

Figure 4.7. Potential energy surface for the dehydrogenation of butylamine by complex **I**. DFT calculations performed at the M06/6-311+G** level. Detailed information on the structures and frequencies of the calculated species are shown in Appendix C. 63

Figure 4.8. Transition states for the dehydrogenation of diethylamine by complex **II** to give the imine adduct product. Panel (a) depicts N-H insertion followed by α -C elimination. Panel (b) depicts α -C insertion followed by N-H elimination. Enthalpies for transition states are in kcal/mol. DFT calculations were performed at the M06/6-311+G** level. Detailed information on the structures and frequencies of the calculated species are shown in Appendix C. 64

Figure 4.9. Potential energy surface for the dehydrogenation of diethylamine by complex **II**. DFT calculations performed at the M06/6-311+G** level. Detailed information on the structures and frequencies of the calculated species are shown in Appendix C. 65

Figure 4.10. Transition states for the dehydrogenation of butanol by complex **I** to give the aldehyde and alkene adduct products. Panel (a) depicts O-H insertion followed by α -C elimination. Panel (b) depicts α -C insertion followed by O-H elimination. Panel (c) depicts α -C insertion followed by β -C elimination. Enthalpies for transition states in kcal/mol. DFT calculations were performed at the M06/6-311+G** level. Detailed information on the structures and frequencies of the calculated species are shown in Appendix C. 68

Figure 4.11. Potential energy surface for the dehydrogenation of butanol by complex **I**. DFT calculations performed at the M06/6-311+G** level. Detailed information on the structures and frequencies of the calculated species are shown in Appendix C. 69

Figure 4.12. Transition states for the dehydrogenation of butanol by complex **II** to give the aldehyde adduct products. Panel (a) depicts O-H insertion followed by α -C elimination. Panel (b) depicts α -C insertion followed by O-H elimination. Enthalpies for transition states are in kcal/mol. DFT calculations were performed at the M06/6-311+G** level. Detailed information on the structures and frequencies of the calculated species are shown in Appendix C. 72

Figure 4.13. Potential energy surface for the dehydrogenation of butanol by complex **II**. DFT calculations performed at the M06/6-311+G** level. Detailed information on the structures and frequencies of the calculated species are shown in Appendix C. 73

Figure 5.1. Spectra for the reaction of bromobenzene with complex **III**. Panel (a) Isolation of complex **III** prior to introduction of bromobenzene. Panel (b) Product spectrum after introduction of bromobenzene. The insertion and halide addition products appear at m/z 219 and 307, respectively. The peak at m/z 228 is complex **III**. The peak at m/z 260 is an adduct with oxygen. 86

Figure 5.2. Spectra for the reaction of iodobenzene with complex **IV**. Panel (a) Isolation of complex **IV** prior to introduction of iodobenzene. Panel (b) Product spectrum after introduction of iodobenzene. Iodide appears at m/z 127, indicating aryl addition. The oxidative addition product appears at m/z 475. The peaks at m/z 360 and m/z 437 are $[\text{PdI}_2]^-$ and $[\text{PdI}_2\text{C}_6\text{H}_5]^-$, respectively,

and are formed through secondary reactions with iodobenzene. The peaks at m/z 299 and m/z 303 are adducts of molecular nitrogen and oxygen, respectively. 87

Figure 5.3. Product distributions for the oxidative addition reactions of fluorobenzene, chlorobenzene, bromobenzene, and iodobenzene by complex **II**, panel (a), and complex **III**, panel (b). Products of reactions between the SAC model ions and adventitious species in the ion trap are not shown. 89

Figure 5.4. Product distributions for the oxidative addition reactions of fluorobenzene, chlorobenzene, bromobenzene, and iodobenzene by complex **I**, panel (a), complex **IV**, panel (b). Products of reactions between the SAC model ions and adventitious species in the ion trap are not shown. 91

Figure 5.5. Product distributions for the oxidative addition reactions of various polar reagents by complexes **II**, panel (a), and **III**, panel (b). Products of reactions between the SAC model ions and adventitious species in the ion trap are not shown. 103

Figure 5.6. Product distributions for the oxidative addition reactions of various polar reagents by complexes **I** and **IV**. Products of reactions between the SAC model ions and adventitious species in the ion trap are not shown. 105

List of Schemes

- Scheme 1.1.** Partial oxidation of styrene by supported Au₅₅ nanoparticles using solely O₂. The ~1.5 nm Au nanoparticles were derived from 55-atom Au clusters by using a loading of 0.6 wt%.⁹ 4
- Scheme 1.2.** Reaction pathways for the hydrogenation of 2-methyl-3-butyn-2-ol (MBY). Semihydrogenation leads to 2-methyl-3-buten-2-ol (MBE) while full hydrogenation leads to 2-methyl-3-butan-2-ol (MBA). Adapted with permission from Crespo-Quesada, M., Yarulin, A., Jin, M., Xia, Y. & Kiwi-Minsker, L. *J. Am. Chem. Soc.* **133**, 12787–12794 (2011). Copyright (2011) American Chemical Society.¹² 7
- Scheme 2.1.** Gas-phase synthesis of the graphene-supported SAC model ion. CID of the precursor ion leads to reductive decarboxylations. The two-electron reduction pathway is shown in blue. The one-electron reduction pathway is shown in red..... 25
- Scheme 2.2.** Gas-phase synthesis of the Pd SAC model ion. The sequence of decarboxylations that lead to the Pd SAC model ion differs from the order observed with Ni, Co, and Cu..... 26
- Scheme 3.1.** Gas-phase synthesis of Complex I..... 30
- Scheme 3.2.** Dehydrogenation mechanism of alkanes by complex I..... 42
- Scheme 3.3.** Cyclohexane dehydrogenation pathways. Reaction enthalpies were calculated at the M06/6-311+G** level. Detailed information on the structure and frequencies of the calculated species are shown in Appendix C. 43
- Scheme 3.4.** Reaction enthalpies for the formation of the H₂ adduct with release of cyclohexadiene or benzene. 44
- Scheme 4.1.** Typical reaction sequence for the dehydrogenation of amines and alcohols. The depiction is based on work from Doberiner and Crabtree.⁷⁶ 49

Scheme 4.2. Gas-phase synthesis of Complex II	50
Scheme 4.3. n-Butylamine dehydrogenation reaction by complexes I and II . The imine is shown as the dehydrogenation product – confirmation of this assignment is provided below.....	51
Scheme 4.4. Decarbonylation of butanal by complex I . DFT calculations suggest this process is exothermic by 45.5 kcal/mol. DFT calculations performed at the M06/6-311+G** level. Detailed information on the structures and frequencies of the calculated species are given in Appendix C.	55
Scheme 4.5. Calculations used to obtain KIE values for the dehydrogenation of amines and alcohols by complexes I and II	57
Scheme 4.6. Mechanism for the dehydrogenation of amines by complexes I and II	66
Scheme 4.7. Mechanism for the dehydrogenation of alcohols by complex I	70
Scheme 4.8. Dehydrogenation pathways for reaction of piperidine with complex I . Reaction enthalpies were performed at the M06/6-311+G** level. Detailed information on the structures and frequencies of the calculated species are shown in Appendix C.	74
Scheme 4.9. Observed fluorenyl scaffold fragmentation products via CID activation of the 2,3,4,5-tetrahydropyridine adduct with complex I . DFT calculations performed at the M06/6-311+G** level. Detailed information on the structures of the calculated species are shown in Appendix C.	75
Scheme 4.10. Reaction pathways for the CID of the butan-1-imine adduct with complex I . DFT calculations performed at the M06/6-311+G** level. Detailed information on the structures of the calculated species are shown in Appendix C.....	76

Scheme 4.11. Reaction pathways for the CID of the butan-1-imine adduct with complex **II**. DFT calculations performed at the M06/6-311+G** level. Detailed information on the structures of the calculated species are shown in Appendix C. 77

Scheme 4.12. Reaction pathways for the CID of the N-ethylethanimine adduct of complex **II**. DFT calculations performed at the M06/6-311+G** level. Detailed information on the structures of the calculated species are shown in Appendix C. 77

Scheme 4.13. Reaction pathways for the CID of the butanal adducts of complexes **I** and **II**. Panel (a) depicts CID of the butanal adduct of complex **I**. Panel (b) depicts CID of the butanal adduct of complex **II**. DFT calculations performed at the M06/6-311+G** level. Detailed information on the structures of the calculated species are shown in Appendix C. 78

Scheme 4.14. Reaction pathways for the CID of the acetone adducts of complexes **I** and **II**. Panel (a) depicts CID of the acetone adduct of complex **I**. Panel (b) depicts CID of the acetone adduct of complex **II**. DFT calculations performed at the M06/6-311+G** level. Detailed information on the structures of the calculated species are shown in Appendix C. 79

Scheme 5.1. Classic depiction of an oxidative addition reaction. 82

Scheme 5.2. Typical cross-coupling cycle. 83

Scheme 5.3. Oxidative addition of aryl halides by complexes **I-IV**. Due to the excess energy gained by the ion-molecule attraction and thermodynamics of reaction, the oxidative addition product often breaks apart into three fragment products: the insertion product (top), the halogen addition product (middle), and the halide (bottom) product. 84

Scheme 5.4. Two other possible insertion products. These products occur less often than the insertion product depicted in Scheme 5.3. 85

Scheme 5.5. Energies for adduct formation and oxidative addition of fluorobenzene by complex **IV**. Panel (a) depicts adduct formation. Panel (b) depicts oxidative addition. Enthalpies in

kcal/mol. Calculations were completed with M06 functional and a mixed lanl2dz/6-311+G** basis set. Detailed information on the structures of the calculated species are shown in Appendix C. 93

Scheme 5.6. Energies for adduct formation and oxidative addition of fluorobenzene by complex **I**. Panel (a) depicts adduct formation. Panel (b) depicts oxidative addition. Enthalpies in kcal/mol. Calculations were completed at the M06/6-311+G** level. Detailed information on the structures of the calculated species are shown in Appendix C..... 94

Scheme 5.7. Enthalpies for the TS and oxidative addition products of the reaction between chlorobenzene and complex **II**. Enthalpies in kcal/mol. Calculations suggest that two binding modes are favorable for the formation of the oxidative addition product. Calculations were completed at the M06/6-311+G** level. Detailed information on the structures of the calculated species are shown in Appendix C. 95

Scheme 5.8. Enthalpies for the TS and oxidative addition products of the reaction between chlorobenzene and complex **I**. Enthalpies in kcal/mol. Calculations suggest that two binding modes are favorable for the formation of the oxidative addition product. Calculations were completed at the M06/6-311+G** level. Detailed information on the structures of the calculated species are shown in Appendix C. 96

Scheme 5.9. Enthalpies for the TS and oxidative addition products of the reaction between chlorobenzene and complex **IV**. Enthalpies in kcal/mol. Calculation suggest that two binding modes are favorable for the formation of the oxidative addition product. Calculations were completed with M06 functional and a mixed lanl2dz/6-311+G** basis set. Detailed information on the structures of the calculated species are shown in Appendix C. 97

Scheme 5.10. Enthalpies for TS and product of the halogen addition pathway of the reaction between chlorobenzene and the Cu SAC model ion. Enthalpies in kcal/mol. Calculations were completed at the M06/6-311+G** level. Detailed information on the structures of the calculated species are shown in Appendix C. 98

Scheme 5.11. Enthalpies for the reaction between chlorobenzene and complex **II**. The insertion product was considered in both the singlet and triplet spin states. (s) = singlet, (t) = triplet. The reactant ion was calculated in the doublet spin state. Calculations were completed at the M06/6-311+G** level. Detailed information on the structures of the calculated species are shown in Appendix C. 99

Scheme 5.12. Enthalpies for the reaction between chlorobenzene and complex **I**. Ion products calculated in the doublet, (d), spin state. The reactant ion was calculated in the singlet spin state. Calculations were completed at the M06/6-311+G** level. Detailed information on the structures of the calculated species are shown in Appendix C. 100

Scheme 5.13. Enthalpies for the reaction between chlorobenzene and complex **IV**. The insertion product is comprised of Pd complexed with Cl and benzyne. The reactant and product ions were calculated in the singlet, (s), spin state. Energetic information for the oxidative addition product (not shown) is depicted in Scheme 5.9. Calculations were completed with M06 functional and a mixed lan12dz/6-311+G** basis set. Detailed information on the structures of the calculated species are shown in Appendix C. 100

Scheme 5.14. Enthalpies for the reaction between chlorobenzene and complex **III**. Enthalpies The insertion product was calculated in the doublet, (d), spin state. Energetic information for the halogen addition product, (d), is depicted in Scheme 5.10. Calculations were completed at the M06/6-311+G** level. Detailed information on the structures of the calculated species are shown in Appendix C. 101

Scheme 5.15. Reaction of the SAC model ions with cis-1,2-dichloroethylene to produce the di-halogen addition product. The product ion is formed with the release of acetylene and the fluorenyl radical. 104

Scheme 5.16. Formation of the alkyl addition product. 104

Scheme 5.17. Enthalpies for the TS state and oxidative addition product of the reaction between allyl chloride and complex **II**. Enthalpies in kcal/mol. Calculations were completed at the M06/6-

311+G** level. Detailed information on the structures of the calculated species are shown in Appendix C. 106

Scheme 5.18. Enthalpies for the TS and oxidative addition product of the reaction between allyl chloride and complex **I**. Calculations suggest formation of the oxidative addition product is favored in two different bonding schemes. Enthalpies are in kcal/mol. Calculations were completed at the M06/6-311+G** level. Detailed information on the structures of the calculated species are shown in Appendix C. 108

Scheme 5.19. Enthalpies for the TS and oxidative addition product of the reaction between allyl chloride and complex **IV**. Calculations suggest formation of the oxidative addition product is favored in two different bonding schemes. Enthalpies are in kcal/mol. Calculations were completed with M06 functional and a mixed lanl2dz/6-311+G** basis set. Detailed information on the structures of the calculated species are shown in Appendix C. 108

Scheme 5.20. Enthalpies for the TS and halogen addition product of the reaction between allyl chloride and complex **III**. The TS is a one-electron process that leads to the halogen addition product. Enthalpies in kcal/mol. Calculations were completed at the M06/6-311+G** level. Detailed information on the structures of the calculated species are shown in Appendix C. 109

Scheme 5.21. Enthalpies for the reaction of allyl chloride with the Co SAC model ion. Complex **II** was calculated in the doublet, (d), spin state Both singlet and triplet states were considered for the resulting product ion. (s) = singlet, (t) = triplet. Calculations were completed at the M06/6-311+G** level. Detailed information on the structures of the calculated species are shown in Appendix C. 110

Scheme 5.22. Enthalpies for the reaction of allyl chloride with complex **I**. Ion reactants and products were calculated in the singlet state. DFT calculations suggest exothermic η^1 and η^3 binding modes for the insertion product. Calculations were completed at the M06/6-311+G** level. Detailed information on the structures of the calculated species are shown in Appendix C. 111

Scheme 5.23 Enthalpies for the reaction of allyl chloride with complex **IV**. Energetic information for the oxidative addition product (not shown) is depicted in Scheme 5.19. Ion reactants and products were calculated in the singlet (s), spin state. Calculations were completed with M06 functional and a mixed lanl2dz/6-311+G** basis set. Detailed information on the structures of the calculated species are shown in Appendix C..... 111

Scheme 5.24. Enthalpies for the reaction of allyl chloride with complex **III**. The reactant ion was calculated in the doublet, (d), spin state. Product ions were considered in the singlet spin state, (s). Calculations were completed at the M06/6-311+G** level. Detailed information on the structures of the calculated species are shown in Appendix C..... 112

List of Tables

Table 1. Relative rates of dehydrogenation reactions of alkanes with complex **I**. 36

Table 2. Kinetic isotope effects for amine and alcohol dehydrogenations. 57

ABSTRACT

Many chemical transformations are effectively carried out using homogeneous and heterogeneous catalysis. There are a number of differences between the two types of catalysts but the most important advantage that homogeneous catalysts have over heterogeneous catalysts are their uniform active sites, which allow for selective reactions. The various active sites in small scale heterogeneous catalysts can often result in undesired side reactions, making selective reactions difficult to carry out. However, due to their nature, heterogeneous catalysts also have an important advantage: facile catalyst separation from the reaction system. Separation of homogeneous catalysts can be complicated and costly. An ideal catalyst would exhibit the best features of both homogeneous and heterogeneous catalysts. Recent developments in heterogeneous catalysis has led to the conception of single-atom catalysts (SACs), a class of catalysts based on isolated metal atoms anchored to a support scaffold. SACs are often much more reactive and can offer better selectivity when compared to nano-scale catalysts. Also, like all heterogeneous catalysts, SACs can be easily separated from reaction products. In order to realize the full potential of SACs, a sound understanding of the underlying catalytic mechanisms is required. This knowledge is crucial for the development of catalysis using SACs. However, surface analysis tools can become less effective in studying catalytic mechanisms at the atomic scale.

Mass spectrometry has proven to be a robust technique for studying organometallic catalytic mechanisms at the single-molecule level. Using a modified linear triple quadrupole ion trap mass spectrometer (modified Thermo Electron LTQ XLTM) equipped with an electrospray ionization (ESI) source, we can isolate a specific ionic species and probe its reactivity via ion-molecule reactions. By employing established gas-phase synthetic techniques, we have generated zero-

valent metal complexes that can act as experimental model ions for pristine graphene-supported SACs. Our studies on the SAC model ions may shed some light on graphene-supported SAC reactivity and the underlying mechanisms.

When using Ni as the active center, the model ion is capable of the dehydrogenation of alkanes via two sequential C-H activations. By introducing energy into the system, additional dehydrogenations occur, enabling processes such as the transformation of cyclohexane to benzene. Both the Ni and Co SAC model ions are capable of the selective dehydrogenation of amines and alcohols via a similar dehydrogenation pathway. We have also generated the model ion using Cu and Pd as the active centers. The Ni, Co, and Pd model ions are capable of engaging in oxidative addition with a variety of polar reagents. The Cu model ion seems to react with polar reagents via one-electron transfer processes. Our work suggests that graphene-supported SACs are capable of engaging in dehydrogenation via C-H activation and oxidative addition depending on the metal used for the active center. Kinetic isotope effects and DFT calculations support the proposed mechanisms.

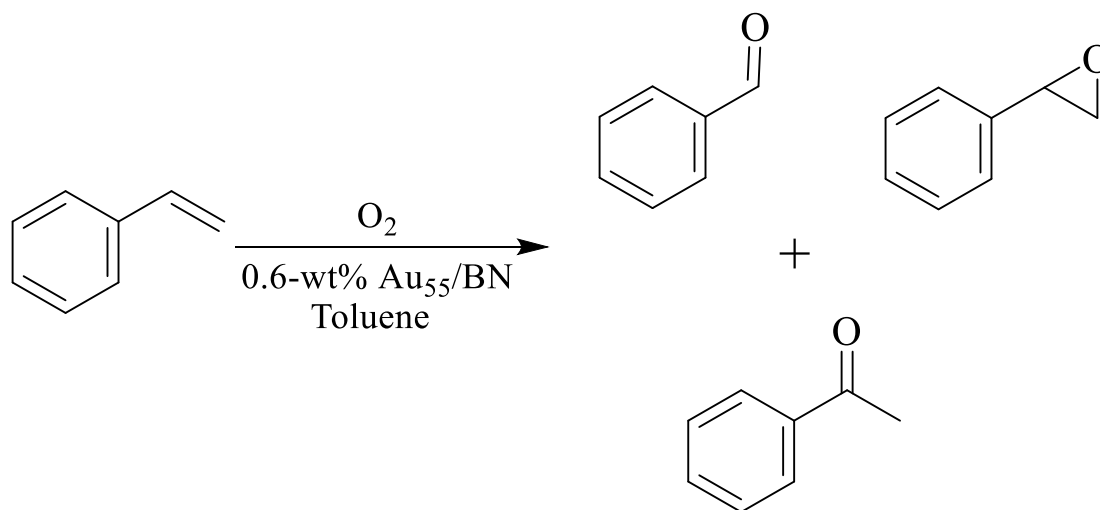
Chapter 1 - Introduction to Single-Atom Catalysts

1.1 Size Reduction of Heterogeneous Catalysts

Catalysts are an important component in many areas of chemistry. The impact of catalysis is so large that more than 90% of chemical industry rely on catalysts to effectively carry out many chemical transformations.^{1,2} While both homogeneous and heterogeneous catalysts have found their place in chemical industry, heterogeneous catalysts make up the majority of industrial catalysis.³⁻⁶ This is largely due to the fact that heterogeneous catalysts can be easily separated from reaction products, while homogeneous catalysts can require more complicated separation techniques which can often be costly. In addition to catalyst removal, heterogeneous catalysts are generally robust (can handle higher operating temperatures) and are usually recyclable, while homogeneous catalysts are often thermally unstable and have short-lifetimes.⁷

Over the years, drastic improvements in transition metal heterogeneous catalysis have been achieved by decreasing catalyst particle size and anchoring them to a support scaffold.⁸ Size reduction of the catalyst causes two important benefits: (i) the number of metal atoms available on the surface to participate in catalysis increases,⁵ and (ii) the coordination number of the metal atoms decreases, often resulting in higher activity.³ Many metal nanoparticle catalysts have been reported to produce interesting results due to their small scale nature. A study by Turner et al. on Au nanoparticles as partial oxidation catalysts can serve as an example.⁹ The authors synthesized Au nanoparticles on inert supports (such as boron nitride and SiO₂) of various sizes and tested their performance in the partial oxidation of styrene, a commonly used reactant to assess selective oxidation activity.¹⁰ Nanoparticles that were about 3.0 nm in diameter produced trace amounts of partial oxidation and larger nanoparticles (~17.0 and 30 nm) resulted in no reaction. Au

nanoparticles about 1.5 nm in diameter successfully participated in the partial oxidation of styrene (Scheme 1.1). However, larger nanoparticles are active when coupled with a peroxy compound as the initiator.¹⁰ The differences in reactivity of these Au gold nanoparticles can be explained by a study by Miller et al.¹¹ The authors investigated the bond length and electronic properties of Au nanoparticles with various particle sizes and various supports. For Au nanoparticles smaller than ~3 nm, the Au-Au bond lengths decreased as the particle size decreased (independent of the type of support), whereas little change in bond length was observed in particles larger than ~4 nm. Also, a decrease in the white line intensity of the XANES spectrum was observed as particle size decreased. These observations led the authors to conclude that decreasing Au particle below 3 nm led to an increase in the sp-d band gap and hence the d-electron density of the Au atoms. In this study, this effect allowed the particles smaller than ~3 nm to be oxidized by air. In the study by Turner et al., this effect allowed small Au nanoparticles to act as partial oxidation catalysts without a sacrificial initiator, presumably via dissociative chemisorption of O₂.



Scheme 1.1. Partial oxidation of styrene by supported Au₅₅ nanoparticles using solely O₂. The ~1.5 nm Au nanoparticles were derived from 55-atom Au clusters by using a loading of 0.6 wt%.⁹

1.2 Active Site Heterogeneity

As mentioned previously, decreasing the size of transition metal catalyst particles increases the atoms available on the surface for catalysis. While this can lead to increased catalytic activity, not all surface atoms offer equal reactivity. Therefore, controlling the size and morphology of the catalyst is key when considering selectivity. This is evident in the study by Crespo-Quesada et al. on shape- and size-controlled Pd nanocrystals.¹² The authors synthesized Pd nanocrystals of three different shapes: cubic, octahedral, and cuboctahedral (Figure 1.1). Two types of active sites are present on

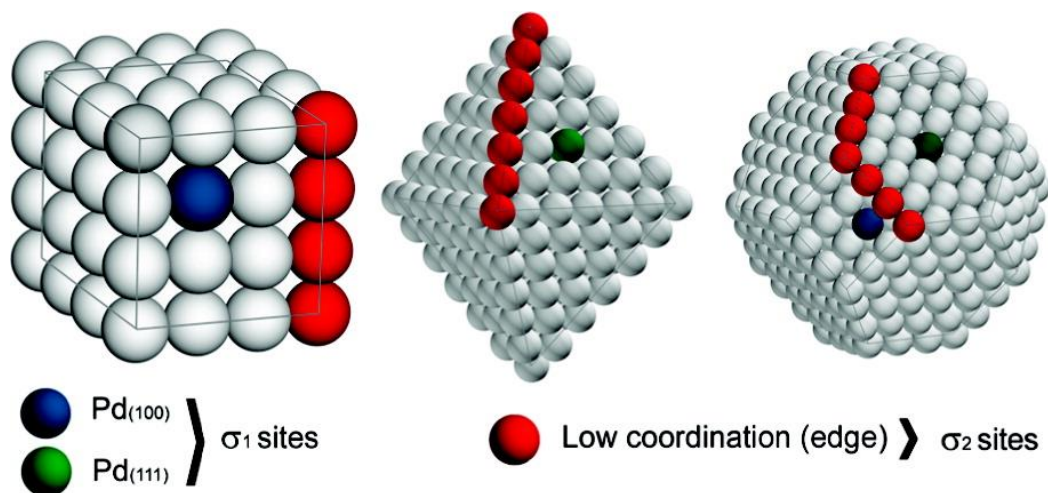
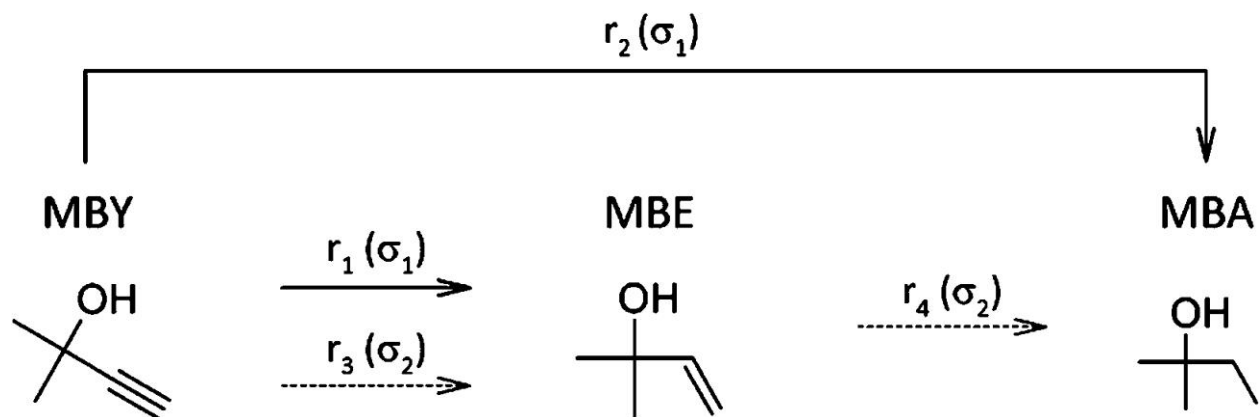


Figure 1.1. Depictions of the two types of active sites on the surface of cubic, octahedral, and cuboctahedral Pd nanocrystals. Adapted with permission from Crespo-Quesada, M., Yarulin, A., Jin, M., Xia, Y. & Kiwi-Minsker, L. *J. Am. Chem. Soc.* **133**, 12787–12794 (2011). Copyright (2011) American Chemical Society.¹²

the surface of the nanocrystals: plane atoms (σ_1 sites) and edge atoms (σ_2 sites). The ratio of plane to edge atoms can vary depending on the size and shape of the nanocrystal. The authors tested these nanocrystals in the hydrogenation of 2-methyl-3-butyn-2-ol (MBY) and found that the

active sites displayed reactivities that can be used to reach a selective reaction (Scheme 1.2). Experimental data and kinetic modelling suggest that the active sites provide two pathways to the fully hydrogenated product, 2-methyl-3-butan-2-ol (MBA): direct hydrogenation for the plane atoms and overhydrogenation for the edge atoms. Both active sites can produce 2-methyl-3-buten-2-ol (MBE) via partial-hydrogenation but the edge atoms are 4-fold less active in the production of MBE production than the plane atoms. Also, as shown in Figure 1.2, Crespo-Quesada et al. determined that both active sites were selective towards MBE production at lower conversions (~95% selective for MBE at ~50% conversion of MBY). This is due to the higher adsorption strengths of alkynes compared to alkenes.¹³ However, as conversion of MBY increases, the concentration of MBE overtakes that of MBY and the overhydrogenation pathway of the edge atoms becomes competitive, resulting in an increased production of MBA. It is due to this effect that the nanocrystals with a higher fraction of edge surface atoms are less selective towards MBE at higher conversions of MBY. Therefore, if selectivity for MBE needs to be maximized, then Pd nanocrystals with minimal edge atoms are required. Multiple active sites present in transition metal heterogeneous catalysts can lead to different products. Studies such as the report by Crespo-Quesada et al. make it very clear that by generating a heterogeneous catalyst with uniform active sites (or close to it), selective reactions can be achieved.



Scheme 1.2. Reaction pathways for the hydrogenation of 2-methyl-3-butyn-2-ol (MBY). Semihydrogenation leads to 2-methyl-3-buten-2-ol (MBE) while full hydrogenation leads to 2-methyl-3-butan-2-ol (MBA). Adapted with permission from Crespo-Quesada, M., Yarulin, A., Jin, M., Xia, Y. & Kiwi-Minsker, L. *J. Am. Chem. Soc.* **133**, 12787–12794 (2011). Copyright (2011) American Chemical Society.¹²

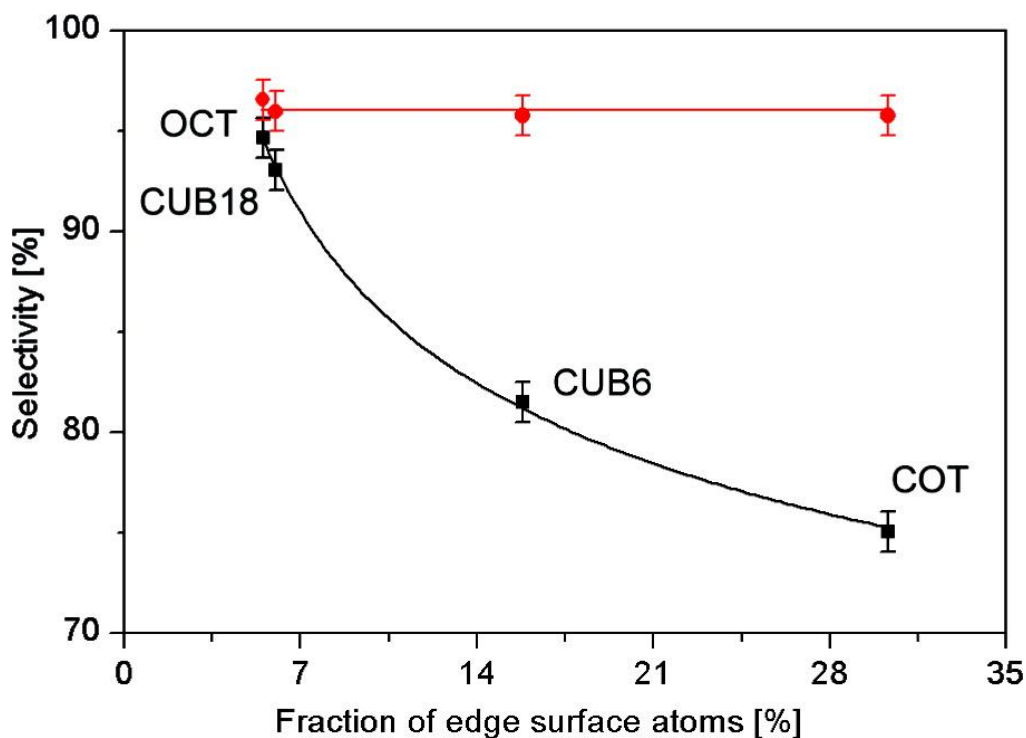


Figure 1.2. Selective production of 2-methyl-3-buten-2-ol (MBE) by Pd nanocrystals at 50% (circles) and 95% (squares) conversion of 2-methyl-3-butyn-2-ol (MBY) as a function of the amount of edge atoms. OCT = octahedral, CUB18 = 18nm cube, CUB6 = 6nm cube, COT = cuboctahedral. Adapted with permission from Crespo-Quesada, M., Yarulin, A., Jin, M., Xia, Y. & Kiwi-Minsker, L. *J. Am. Chem. Soc.* **133**, 12787–12794 (2011). Copyright (2011) American Chemical Society.¹²

1.3 Single-Atom Catalysts

Uniform active sites are an innate feature in homogeneous catalysts and are the reason that many selective reactions belong to homogeneous catalysts rather than heterogeneous systems. Among other issues (e.g. deactivation, leaching, etc.), low selectivity is one of the most significant drawbacks to heterogeneous catalysis. Generally, an ideal catalyst would have the benefits of both homogeneous and heterogeneous catalysis, i.e. a highly active catalyst with uniform active sites that can lead to selective reactions and is also easy to separate from reaction systems. One solution to this endeavor are single-atom catalysts (SACs), a class of isolated metal atoms anchored on a support scaffold. SACs are considered the ultimate-limit in heterogeneous catalysis for a few reasons: (i) the atom-sized active centers display maximum benefits from the size-reduction effects mentioned previously, (ii) uniform dispersion of the active centers can offer selective reactions, and (iii) the heterogeneous nature of the catalyst allows for easy separation.^{8,14-17}

While the field of single-atom catalysis is relatively new, there are many reports in the literature that demonstrate the potential of SACs. A good example is the study by Yan et al. about a Pd SAC supported on graphene oxide.¹⁸ The authors tested the activity of their Pd SAC (Pd₁/graphene) in the hydrogenation of 1,3-butadiene, a reaction important in chemical industry for the purification of alkene streams produced by petroleum cracking.¹⁹

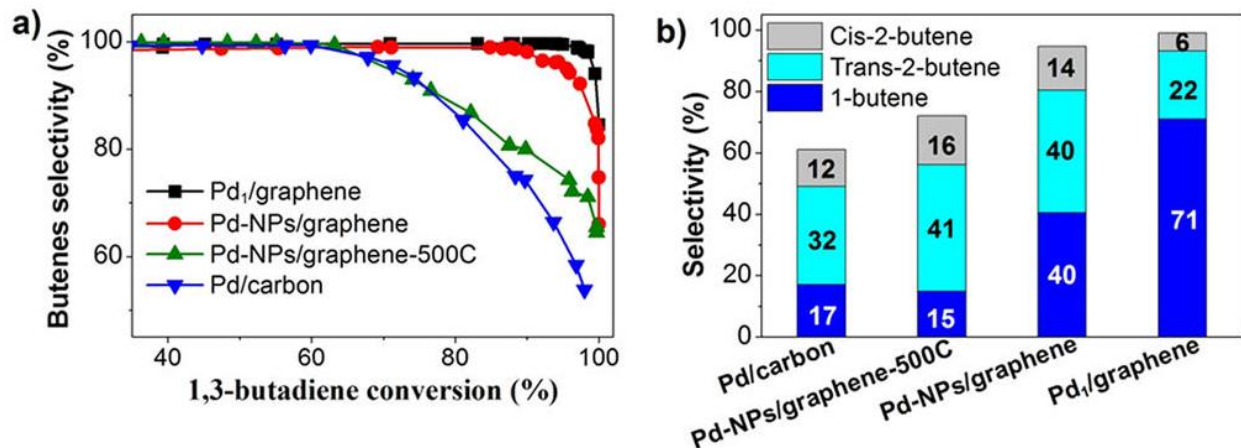


Figure 1.3. Pd catalytic performance. Panel (a) – butenes selectivity as a function of conversion. Panel (b) – product distribution of butenes at 95% conversion. Adapted with permission from Yan, H. *et al. J. Am. Chem. Soc.* **137**, 10484–10487 (2015). Copyright (2015) American Chemical Society.¹⁸

The performance of Pd₁/graphene was compared to Pd nanoparticles on graphene (Pd-NPs/graphene) and commercial Pd/carbon, as shown in Figure 1.3 a). Pd₁/graphene demonstrated the highest selectivity for butene products (~100%) compared to the other Pd catalysts. However, the butene products that result from hydrogenation of 1,3-butadiene can be a mixture of cis-2-butene, trans-2-butene, and/or 1-butene. Therefore, the authors investigated the product distribution of the butene products produced by each catalyst and the results are displayed in Figure 1.3 b). Yan et al. report that their Pd₁/graphene had the largest 1-butene selectivity of 71% at 95% conversion of 1,3-butadiene. This is very important since 1-butene is the most desired product in industrial hydrogenation of 1,3-butadiene and the selectivity for 1-butene displayed by Pd₁/graphene was the best reported in the literature at that time.^{18,19}

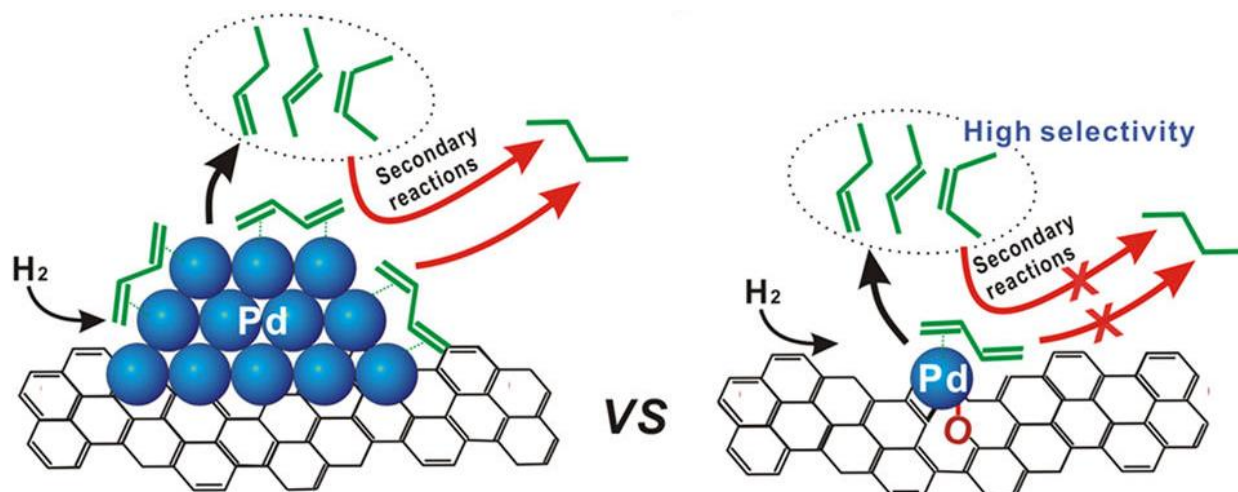


Figure 1.4. Depiction of the differences in adsorption modes on the Pd₁/graphene catalyst, resulting in higher selectivity for butenes. Adapted with permission from Yan, H. *et al. J. Am. Chem. Soc.* **137**, 10484–10487 (2015). Copyright (2015) American Chemical Society.¹⁸

The authors attribute the selectivity displayed by their catalyst to presumable differences in binding modes, depicted in Figure 1.4. Butadiene likely adsorbs on larger Pd particles via the di- π -adsorption mode due to the presence of multiple Pd atoms and can lead to simultaneous hydrogenation of both carbon-carbon double bonds. In the case of the atomically dispersed Pd₁/graphene, butadiene molecules likely adsorb via the mono- π -adsorption mode, thus encouraging 1,2-hydrogen addition to form 1-butene with high selectivity. Also, the isolated atomic nature of the Pd₁/graphene catalyst likely leads to a higher packing density of the butadiene reactant on the Pd atoms, resulting in inhibition of secondary hydrogenation reactions. This report by Yan et al. clearly demonstrates how SACs can greatly improve selectivity and there have been many other studies exploring other SACs to tune activity and selectivity.^{20–22}

Investigations on SACs have included various types of support scaffolds, including metal oxides, alloys, and carbon-based supports.^{8,14–17,23} There is great interest in using graphene as a support, due to its high surface area and facile production.^{24–26} However, in order to create a stable SAC,

support interactions must be strong enough to avoid migrations of the metal atoms that lead to agglomeration. While it is difficult to achieve such interactions on pristine graphene due to metal agglomeration,^{27,28} there are reports that demonstrate how to work around this issue. Modifications that introduce heteroatoms into the graphene lattice can be made in order to create better anchor sites for the isolated metal atoms^{18,29,30} (such as the study by Yan et al). Stable anchor points can also be introduced by generating structural defects in the graphene lattice.^{28,31–33} Recently, Zhang et al. were able to use of graphene defects to trap single Ni atoms.³⁴ The catalyst demonstrated excellent activity and stability in hydrogen and oxygen evolution reactions (comparable with commercial Pt/C for hydrogen evolution and outperforming commercial Ir/C catalyst for oxygen evolution).

As information about graphene-supported SACs grows, so does the need to understand the mechanisms responsible for the observed activity. While there are tools that can provide some insight into SAC mechanisms,²⁰ elucidation of the reactive intermediates involved in these catalytic cycles using surface analysis tools can become less effective at the atomic scale.³⁵ Robust single-molecule techniques may prove to be an effective method for studying SAC mechanisms. Quadrupole ion trap mass spectrometry equipped with an electrospray ionization (ESI) source has proven to be an effective single molecule technique for studying organometallic reactions.^{36–40} While experiments using this instrumentation occur in the gas phase, mass spectrometry investigations of organometallic systems may prove useful for SACs as bare metals and metal clusters generated in the gas phase have been used as model systems for heterogeneous catalysts in the past.^{41–45} The goal of the work presented in this dissertation is to generate a gas-phase ionic species that can act as a model system for graphene-supported SACs and to investigate the reactivity of the novel species in fundamental organometallic reactions. Our intention is to aid non

gas-phase chemists in their studies on graphene-supported SACs by providing guidance on reaction systems and the underlying mechanisms that graphene-supported SACs may perform. Our model ion is depicted in Figure 1.5.

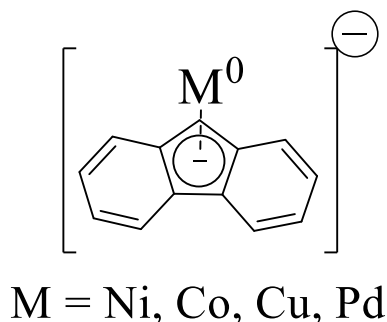


Figure 1.5. Depiction of our gas-phase SAC model ion. The model ion has been generated in our lab using four different metal centers: nickel, cobalt, copper, and palladium.

Our gas-phase SAC model ion is comprised of a zero-valent metal atom coordinated to the fluorenyl anion. The rationale is that if SACs truly operate through a single metal atom, the reactivity of these catalysts mainly depends on the local environment and therefore, metals supported on a simple polycyclic aromatic molecule, such as the fluorenyl anion, can serve as a model system for SACs supported on graphene. As mentioned above, defects in the graphene lattice can be used to trap metal atoms. Zhang et al. reported that a major portion of the defects used to trap Ni atoms in their study were Stone-Wales defects.³⁴ Since the structure of our model ion most closely resembles a metal atom adsorbed on a Stone-Wales graphene defect,⁴⁶ the work presented in this dissertation may guide studies on single metal atoms supported on graphene containing Stone-Wales defects.

In order to study the reactivity of our SAC model ion system, ion-molecule reactions were carried out in the gas phase. We have observed our model system engaging in the dehydrogenation of

simple organic species, as well as the oxidation addition of various polar reagents. Before further explanation of these studies, it is important to understand how a mass spectrometer can be used to study ion-molecule reactions.

Chapter 2 - Electrospray Ionization Quadrupole Ion Trap Mass Spectrometry

2.1 Electrospray Ionization

A mass spectrometer is an instrumental tool capable of characterizing gaseous chemical species via their mass to charge (m/z) values. Mass spectrometers are generally comprised of three hardware systems: (i) the ionization source, (ii) the mass analyzer, and (iii) the detector. Different combinations of ionization sources and mass analyzers can drastically change the capabilities of a mass spectrometer. While various ionization sources and mass analyzers have been engineered, mass spectrometry is mostly known for chemical compound identification and/or quantification. However, beyond their role in analytical chemistry, mass spectrometers can be used as a reaction vessel to carry out and study chemical reactions in the gas phase.

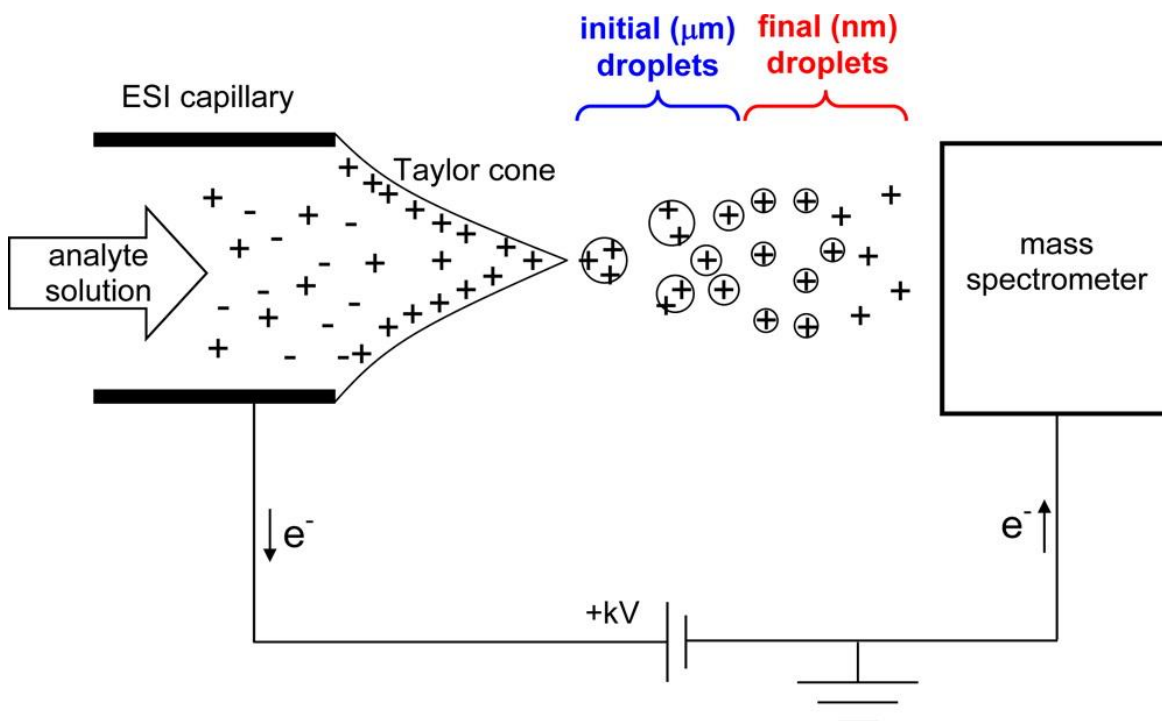


Figure 2.1. Depiction of ESI. The charged solution forms the Taylor cone and sprays a mist charged droplets. The droplets become gaseous ions and are swept towards the mass spectrometer inlet. Adapted with permission from Konermann, L., Ahadi, E., Rodriguez, A. D. & Vahidi, S. *Anal. Chem.* **85**, 2–9 (2013). Copyright (2013) American Chemical Society.⁴⁷

For decades, instruments such as flowing after glow, ion cyclotron resonance, guided ion beam, and triple quadrupole mass spectrometers have been used to study gas-phase ion-molecule reactions.^{37,48-52} Studies presented in this dissertation were performed using a modified linear triple quadrupole ion trap mass spectrometer (modified Thermo Electron LTQ XL™) equipped with an ESI source. The ESI source is capable of transferring ions in solution into the gas phase, as depicted in Figure 2.1.⁴⁷ When an ionic solution is passed through a capillary and sprayed with an electric field, the solution forms into a Taylor cone and produces a mist of charged droplets that flow from the capillary (anode) to the inlet of the mass spectrometer (cathode). On the path into the mass analyzer, the relatively large droplets eventually become bare gaseous ions with one or more charges.

The process by which the droplets become gaseous species has been debated over the years but there still isn't a single prevailing explanation. However, there are two widely known theories that offer reasonable explanations and each may be active under different experimental conditions. The charged residue model (CRM) is depicted at the top of Figure 2.2.⁵³ In this theory, originally proposed by Dole et al.,⁵⁴ solvent gradually evaporates and reduces the droplet size. The decreased droplet size reaches a point where the repulsion of the ions in the droplet exceeds the surface tension of the droplet (Rayleigh limit), resulting in the fission of the droplet into smaller droplets. This process continues until the solvent of a droplet containing a single ion evaporates, leaving behind the bare ion.

Iribarne and Thompson proposed an alternative theory called the ion evaporation model (IEM).⁵⁵ As shown at the bottom of Figure 2.2, this theory also proposes that solvent evaporation of the charged droplets leads to increased charge repulsion forces. However, when charge repulsion

reaches a maximum, the droplet relieves the tension by “pushing” out an ion from the droplet into the surrounding atmosphere. This process continues until all the ions are forced into the gas phase.

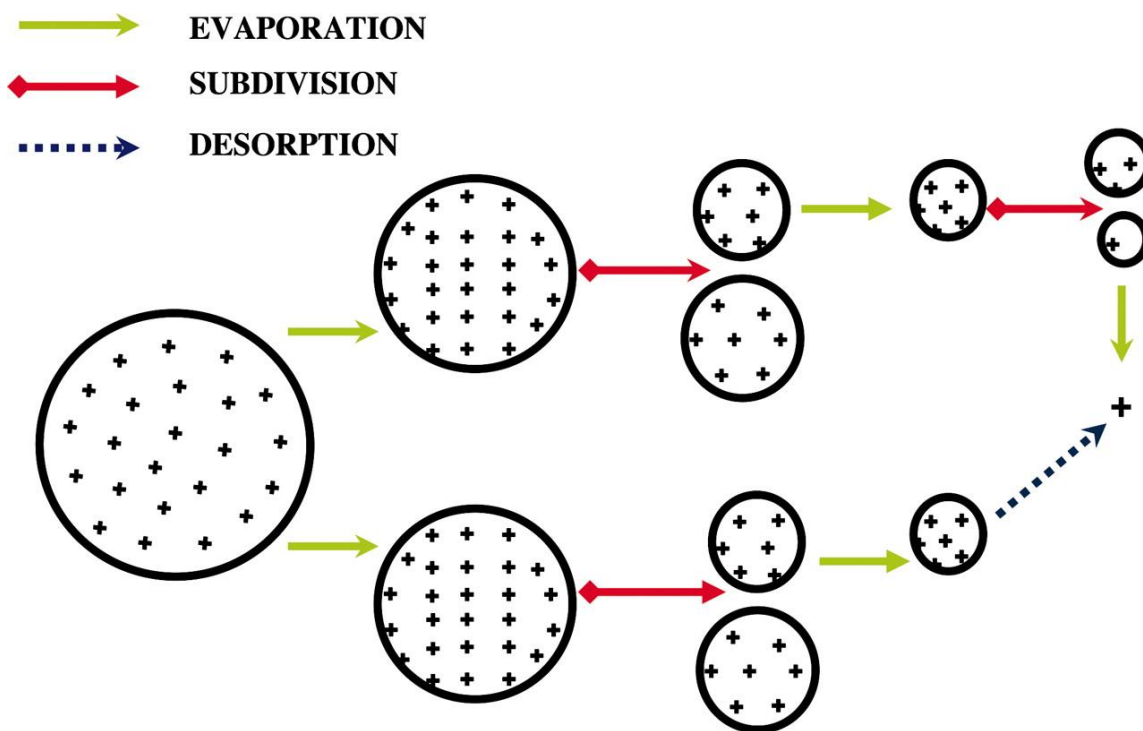


Figure 2.2. Depiction of ion formation from charged droplets produced by ESI. The CRM proposes multiple subdivisions of charged droplets lead to gaseous ions (top). The IEM proposes solvent evaporation leads to desorption of bare gaseous ions (bottom). Adapted with permission from Nguyen, S. & Fenn, J. B. *PNAS* **104**, 1111–1117 (2007). Copyright (2007) National Academy of Sciences, U.S.A.⁵³

Even though the method of ionization is not totally clear, ESI has revolutionized mass spectrometry. ESI is known as a “soft” ionization technique because of the ability to transfer liquid ionic samples into the gas phase without much or any fragmentation. Upon introduction of ESI technology, chemists were able to conduct gas-phase studies with much larger species than they believed to be possible. Many areas of study, including the study of organometallic species, benefited from the use of ESI. The impact was so large that John Fenn shared the Nobel prize in 2002 for developing the technique.⁵⁶

2.2 Linear Triple Quadrupole Ion Traps

ESI is not the only mass spectrometry invention that was awarded with a Nobel prize. Wolfgang Paul shared the physics Nobel prize in 1989 for developing the ion trap.⁵⁷ The mass analyzer in our modified instrument is a linear triple quadrupole (LTQ) ion trap. Even though the original invention was the 3D ion trap, the fundamentals of linear ion traps are the same. The LTQ used in our instrument is depicted in Figure 2.3.⁵⁸ Rf and dc voltages are applied to the four symmetric surfaces of the LTQ in order to manipulate ion motion. The LTQ is comprised of three sections that are electrically isolated (front, center, and back). The front and back sections are used to help focus ions into the center section.

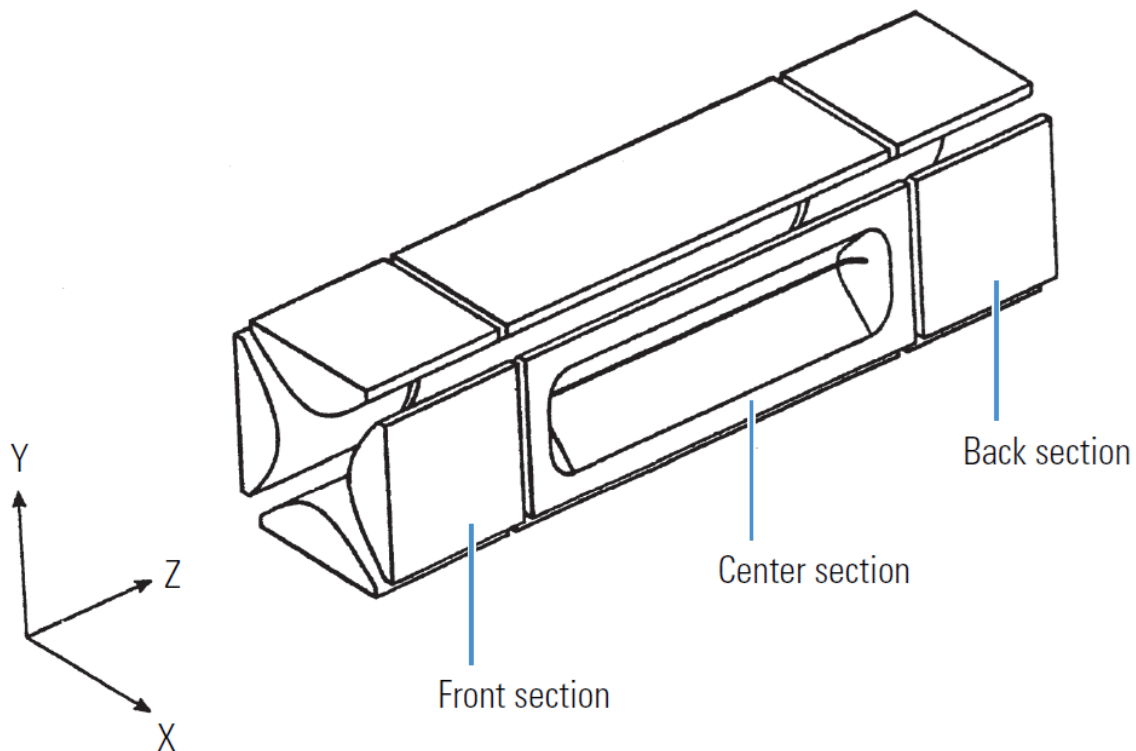


Figure 2.3. Depiction of the linear triple quadrupole ion trap used in the modified Thermo Electron LTQ XLTM.⁵⁸ Ions are directed into the front section by ion optics. The front and back sections focus ion streams into the center section. Ion trapping occurs in the center section.

Ions from the ESI source are directed along the z-axis into the front section of the LTQ by ion optics located at the inlet of the instrument. The back section can be used to direct a second ion stream into the center section, but this capability is not used for the work presented in this dissertation. The center section of the LTQ acts as the ion trap. Rf voltages applied in the center section cause the ions to oscillate about the middle of the center section.⁵⁹

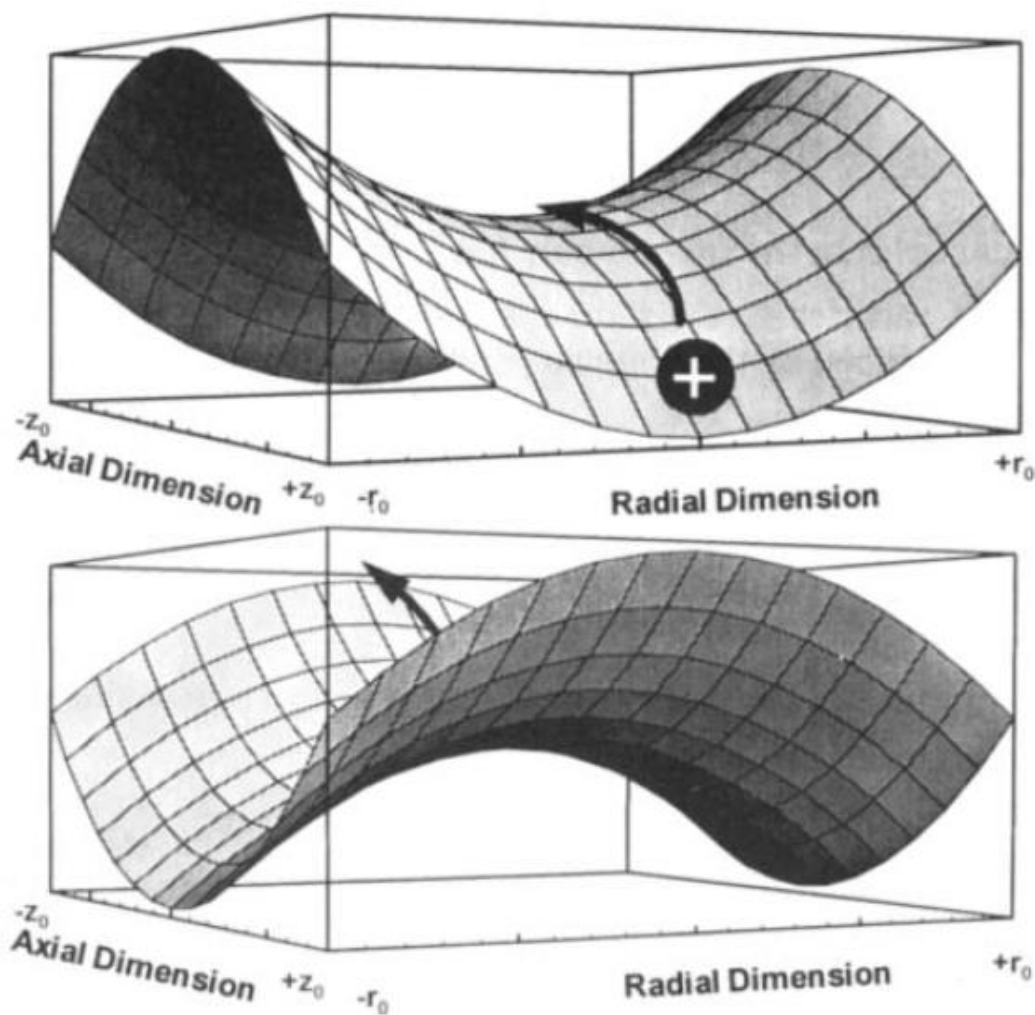


Figure 2.4. Depiction of the potential wells caused by rf voltages. Panel (a) – ions are trapped in the radial dimension. Ions with sufficient kinetic energy can move towards the center. Panel (b) – ions are trapped in the axial dimension. Ions are accelerated towards the center of the trap. Adapted with permission from Weil, C., Nappi, M., Cleven, C. D., Wollnik, H. & Cooks, R. G. *Rapid Communications in Mass Spectrometry* **10**, 742–750 (1996). Copyright © 1996 John Wiley & Sons, Ltd.⁶⁰

Figure 2.4 depicts potential wells that help describe ionic motion in the trap. Voltages applied to the walls of the trap can create the saddle-shaped potential well in Figure 2.4 (a) that traps ions in the radial direction.⁶⁰ This will drive ions towards opposing electrodes. However, when the applied rf voltages flip polarity, the field is inverted as depicted in Figure 2.4 (b).⁶⁰ This will cause ions to be accelerated back towards the radial center of the trap.

Ions are most effectively controlled by the rf voltages when they are radially near the center of the ion trap.⁶¹ In order to help keep the ions around the center of the trap, helium is introduced into the ion trap at about 10^{-3} torr. At this concentration, frequent collisions between helium and the much larger ions dampen the motion of the ions without imparting too much energy and helps shift the trajectory of the ions to the center of the trap.^{61,62} This also aids in correcting any factors that may displace ionic motion from the center of the trap, resulting in significant increases in resolution and sensitivity.^{36,61,63}

Ions in the LTQ are sent out to the detectors through slits on either side of the center section (Figure 2.5). This is accomplished by the application of increasing rf voltage to the center section which shifts frequency of motion of the ions and consequently the range of m/z which is stable in the ion trap. A strong ion ejection rf is also applied and when ions become resonant with that applied rf, they are promptly ejected. As the rf voltage increases, ions become unstable from low to high m/z .⁶³ By applying resonant ejection frequencies pertaining to all but a single m/z , it is possible to isolate and hold a singular set of ions in the ion trap for a given time period.^{36,37,59} However, since manipulation of the ions depends on their m/z , attempts to isolate an ion may trap more than one species if there are multiple ions present with the same m/z . While this can be mitigated with careful control of the ESI solution being introduced, this possibility should always be considered when interpreting mass spectra results.

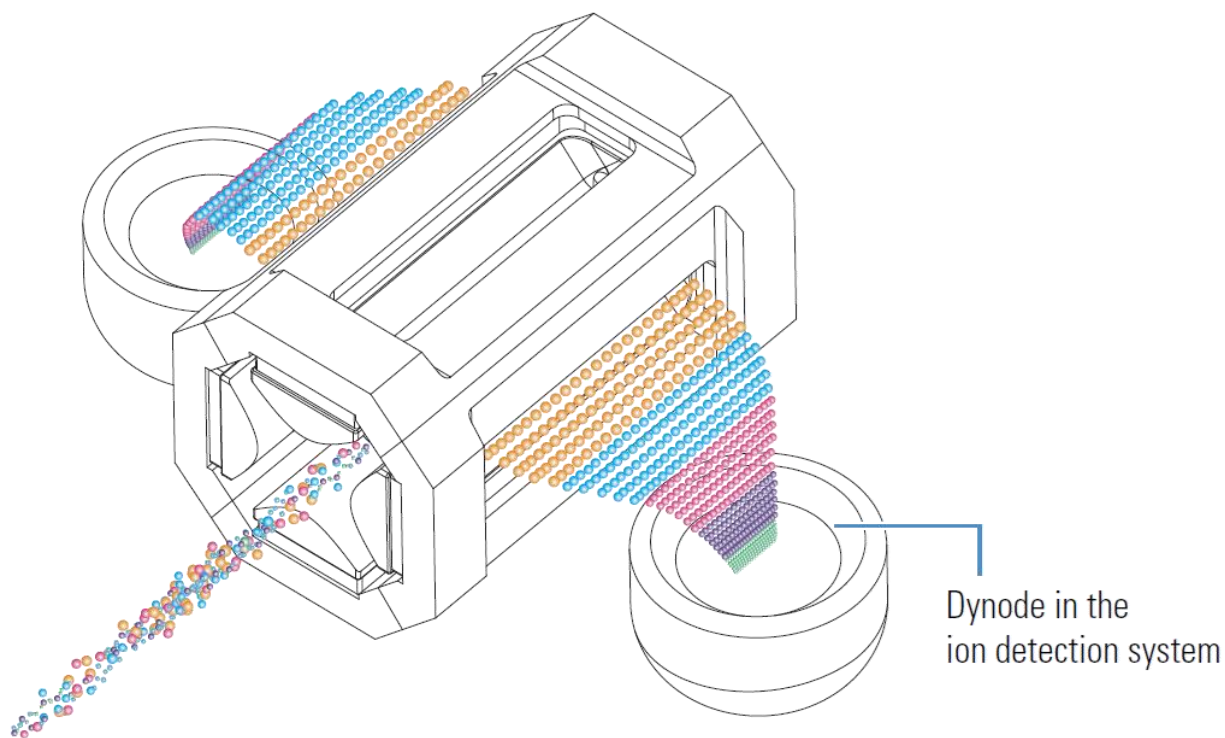


Figure 2.5. Depiction of ions sent to the detection system from the center section of the linear triple quadrupole ion trap.⁵⁸ All ions can be sent out to the detection system by sweeping rf voltages. Alternatively, specific ions can be isolated in the trap based on their m/z value.

The helium background gas in the trap can also be used for collision-induced dissociation (CID). In this process, ionic motion is accelerated by applying rf voltages resonant with a specific m/z causing more frequent and energetic collisions with helium. The collisional energy imparted on the ions leads to ion fragmentation which provides a few benefits. The most common benefit is that structural information of parent ions can be deduced from the resulting fragment ions.⁶⁴ In addition to structural analysis, fragmentation can also be used to create new ionic species of interest. Lastly, while investigating ion-molecule reactions, ionic species can be given energy via CID which may aid in the observation of new reactivity that may have been hidden by energetic barriers.

2.3 Ion-Molecule Reactions Using a Linear Triple Quadrupole Ion Trap

Neutral molecules cannot be introduced via ESI due to the lack of charge. In order to use quadrupole ion trap mass spectrometers to study ions engaging in reactions with neutral molecules, ion traps can be modified to introduce neutral reagents into the ion trap via the helium flow. The modification used in our lab is depicted in Figure 2.6.³⁶

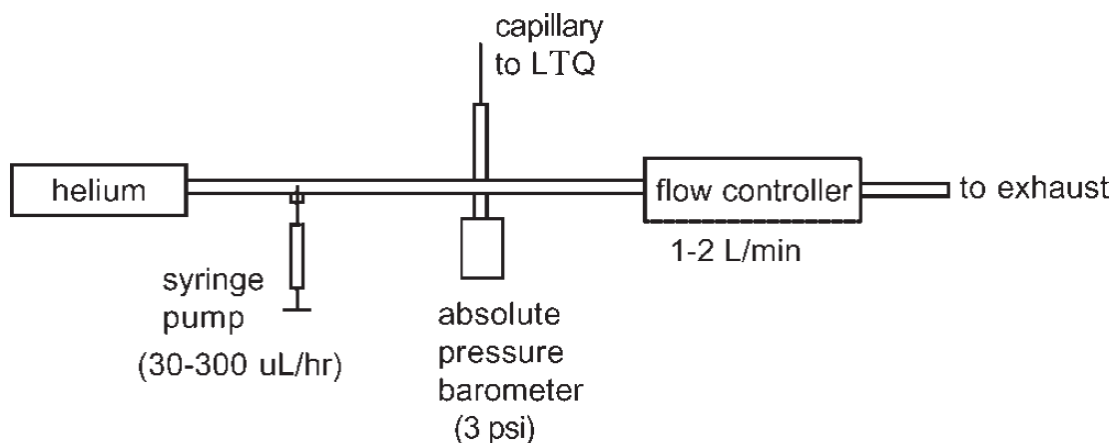


Figure 2.6. Schematic of the external inlet system. The neutral reagent is introduced into a fast flow of helium at a constant rate. The helium-reagent mixture is drawn into the ion trap by a restriction capillary and the rest is vented to exhaust.³⁶ Adapted with Permission from Gronert, S. *Mass Spectrom. Rev.* **24**, 100–120 (2005). Copyright © 2004 Wiley Periodicals, Inc., A Wiley Company.

In this modification, the helium gas is routed through an external manifold before entering the ion trap. Helium flow is adjusted to a constant flow of 1-2 L/min by a mass flow controller to create the necessary dilution of the neutral reagent.³⁶ The liquid neutral reagent is introduced into the fast flow of helium through a septum port, via a syringe pump, at a constant rate of 30-300 $\mu\text{L/hr}$. The neutral reagent is volatilized and mixes with the helium, resulting in helium-reagent mixing ratios of 100-100,000 : 1. A small portion of the helium-reagent mixture is drawn into the ion trap by a

restriction capillary while the rest is vented to exhaust. Once in the trap, the neutral species can collide with ionic species held in the trap and undergo ion-molecule reactions.

Previous studies have focused on assigning a temperature to ions in the ion trap.⁶⁵⁻⁶⁷ While the neutral reagents introduced via the helium flow are at ambient temperature, it was unclear whether the energy imparted on ions by the trapping voltages would increase the temperature of the ions, resulting in non-thermalized reactions. It has been shown that collisions with the helium buffer gas effectively cool the ions to a much greater extent than the effect of the trapping voltages, providing near thermal conditions in ion traps.^{68,69}

It is also important to note that kinetic information for ion/molecule reactions can also be determined using this system, since ions can be held in the trap and allowed to react with neutral reagents for a pre-determined time period before reactant ions and resulting products are sent to the detector. As mentioned previously, the helium-reagent mixture flows into the ion trap, at a constant rate, through the restriction capillary. Taking the mixing ratios into account, this means neutral reagent pressures are between 10^{-5} torr – 10^{-8} torr with a helium pressure of about 10^{-3} torr. These neutral reagent pressures are in great excess to the reactant ion densities and can be considered constant, enabling kinetic studies under pseudo first-order conditions. This allows kinetic studies to be simplified to the expressions shown in equations (1) and (2), where [A] is the concentration of the ion, [B] is the concentration of the neutral reagent, k is the absolute rate constant, and k' is the pseudo first-order rate constant. By plotting the natural log of the intensity of the reactant ion against the reaction time, pseudo first-order rate constants can be obtained experimentally. The overall pressure of the helium-neutral reagent buffer gas in the ion trap is about 1.75×10^{-3} torr. This pressure is a result of a restriction capillary that controls the flow of helium into the ion trap. The pressure is controlled by the balance of the helium flow and the rate

that it is pumped out of the ion trap via the vacuum manifold. We calibrate our ion trap pressure by routinely running reactions with a known rate constant, typically $\text{Br}^- + \text{CH}_3\text{I}$, and back calculating the helium pressure (the rate constant used is a literature value from flowing afterglow studies).

Neutral reagent pressures can be deduced from the overall helium pressure by using equation (3),³⁶ where F_B is the neutral reagent flow rate, F_{He} is the helium flow rate, d_B is the neutral reagent density, MW_B is the neutral reagent molecular weight, and MW_{He} is the atomic weight of helium (a background He pressure of 1.75 mTorr is assumed in this equation). The final term in equation (3) is required to account for the differential effusion of the reagent and helium from the ion trap. The pseudo-first order rate constant and the neutral reagent concentration can then be entered into equation (2) in order to calculate the absolute rate constant. Because reagent gas pressures are calculated in number densities, the rates of reaction determined in our system are measured in $\text{cm}^3 \text{molecule}^{-1} \text{s}^{-1}$.

$$\text{rate} = k[A][B] = k'[A] \quad (1)$$

$$k' = k[B] \quad (2)$$

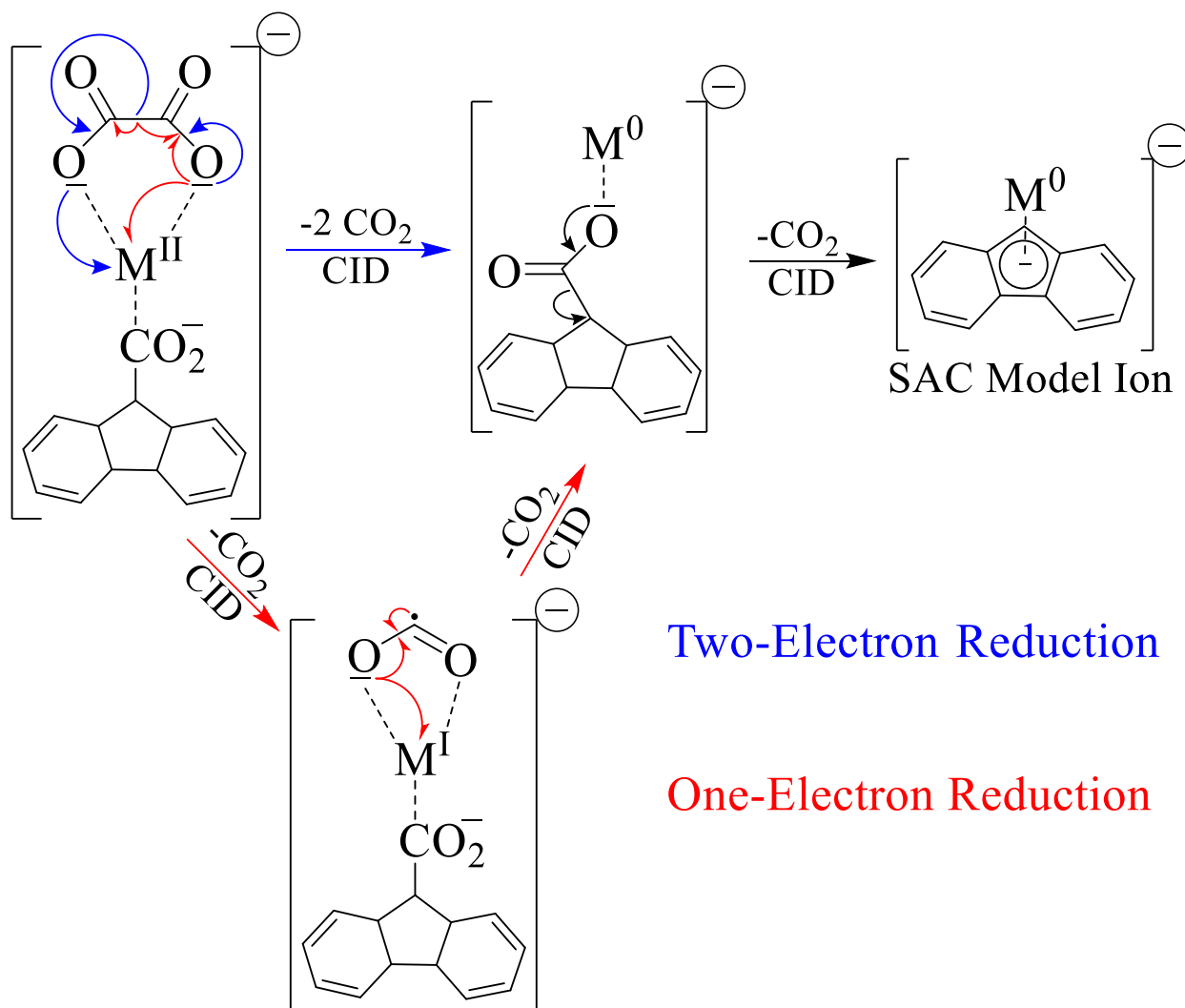
$$[B] = 1.75 \times 10^{-3} \times \frac{F_B}{F_{\text{He}}} \times \frac{d_B}{MW_B} \times \left(\frac{MW_B}{MW_{\text{He}}} \right)^{1/2} \quad (3)$$

It is clear that the ion trap is able to manipulate trapped species in various ways. However, the true potential of the ion trap is realized by linking all these operations together, sequentially in time, in order to effect tandem mass spectrometry (MS^n). This allows for a variety of robust and flexible operational methods to study ion behavior. As an example, a typical experiment performed in our

lab is as follows: (i) a reactive species of interest is isolated from a mixture of ions introduced by ESI (or it can be created from a parent ion in the solution by CID), (ii) once a steady signal of the reactant ion is achieved, a neutral reagent is introduced into the ion trap through the external manifold, as previously discussed, (iii) the ionic species is allowed to react with the neutral species for a given time period, (iv) product ion species are produced and can be identified/isolated through their m/z values and (v) product ions can be studied further via CID, or can be allowed to participate in additional ion-molecule reactions.

2.4 Gas-Phase Synthesis of Graphene-Supported Single-Atom Catalyst Model Ions

Generation of a zero-valent metal supported on a fluorenyl scaffold in the condensed phase is difficult due to the oxidation state of the metal. However, established gas-phase synthetic techniques have demonstrated that decarboxylations via CID can easily lead to reductions of metal centers.^{70,71} Through judicious ligand choice and tandem mass spectrometry, we were able to generate our SAC model ion from a precursor ion, via gas-phase reductive decarboxylations. The precursor ion, comprised of a di-valent metal coordinated to oxalate and fluorene-9-carboxylate, was made in solution by mixing salt solutions of each component together and was introduced into the mass spectrometer via the ESI source. The precursor ion was isolated in the ion trap and subjected to CID. Scheme 2.1 depicts two observed decarboxylation sequences that lead to the SAC model ion, along with our proposed mechanisms. In the two-electron reduction pathway, CID of the precursor ion results in the loss of two neutral CO_2 molecules by decomposition of the

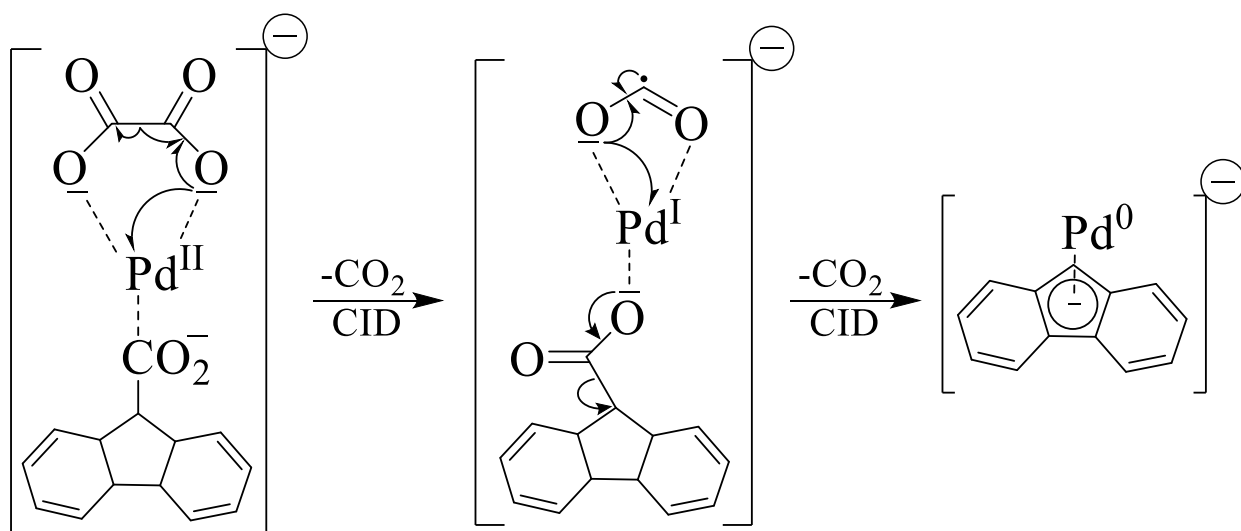


Scheme 2.1. Gas-phase synthesis of the graphene-supported SAC model ion. CID of the precursor ion leads to reductive decarboxylations. The two-electron reduction pathway is shown in blue. The one-electron reduction pathway is shown in red.

oxalate and a two-electron reduction of the metal. The resulting ion can be isolated in the ion trap and subjected to another round of CID, resulting in the loss of another CO₂ molecule, formation of the fluorenyl anion ligand, and, therefore, generation of the target ion. The SAC model ion can also be generated via sequential one-electron reductions. In this pathway, subjecting the precursor ion to CID results in the loss of a CO₂ molecule, formation of the CO₂ anion ligand and a one-electron reduction of the metal. A second round of CID leads to loss of a second CO₂ molecule

and another one-electron reduction of the metal. Finally, a third round of CID results in the loss of another CO₂ molecule and the formation of the SAC model ion.

We have successfully generated the gas-phase model ion using Ni, Co, Cu, and Pd metal centers. The Co SAC model ion was generated through the one-electron reduction pathway, while the Ni and Cu SAC model ions can be generated using either of the reduction pathways. When using Pd, two rounds of CID were required to transform the precursor ion into the ion of interest. The first round of CID resulted in the loss of one CO₂ molecule while the second round of CID caused the loss of two CO₂ molecules. Scheme 2.2 depicts our proposed mechanism for the formation of the Pd SAC model ion. The first round of CID releases a CO₂ molecule resulting in the formation of a CO₂ anion ligand and a one-electron reduction of the metal. The second round of CID releases two CO₂ molecules, resulting in the formation of the fluorenyl anion ligand and another one-electron reduction of the metal.



Scheme 2.2. Gas-phase synthesis of the Pd SAC model ion. The sequence of decarboxylations that lead to the Pd SAC model ion differs from the order observed with Ni, Co, and Cu.

Attempts to generate the model ion using Fe and Pt centers were unsuccessful. We believe there are two issues that made these attempts unsuccessful (Figure 2.7). Our gas-phase synthetic strategy relies on decarboxylations to generate the SAC model ion. This means that in order to generate the SAC model ion, a precursor ion with carboxylate ligands must form in the condensed phase and the carboxylate groups must be released when subjected to CID. When working with Fe as the metal center, CID did not result in the model ion. Instead, the metal oxide supported on the fluorenyl anion was formed. This is likely caused by adventitious O_2 present in the ion trap and the oxyphilic nature of Fe. The metal oxide was isolated and neutral reagents were introduced into the trap to probe any reactivity, but no reaction was observed. In the case of Pt, attempts to generate the precursor ion were unsuccessful which may be explained by the hard-soft acid-base (HSAB) theory. Pt, which lies in the 5th row of the d-block, may be too “soft” to bind to three oxygen-based ligands via simple coordination chemistry under our conditions.

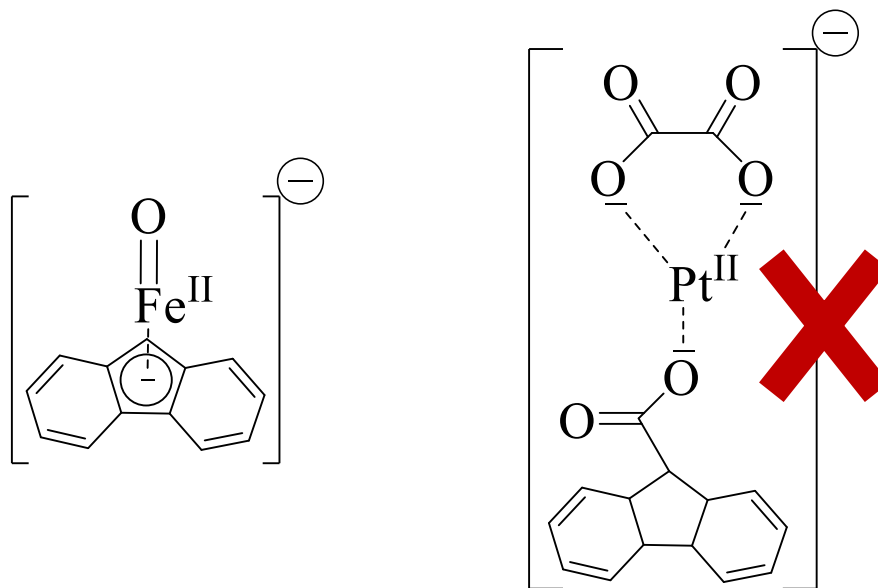


Figure 2.7. Depiction of the issues creating the Fe and Pt SAC model ions. CID reduction of the Fe precursor ion led to the metal oxide species likely due to adventitious oxygen in the ion trap. Attempts to generate the Pt precursor ion were unsuccessful.

Using Ni, Co, Cu, and Pd metal centers, we were able to probe the reactivity of the SAC model ion system via ion-molecule reactions. In addition to experiments, computational modelling of the observed reaction systems was also completed. Gas phase studies are well suited for comparison to computational calculations, due to the lack of solvent, and can be used to gain further insight into reaction chemistry.^{37,40,45,48,72} DFT calculations were performed and provide a reasonable overview of the energetics of the reaction processes and information on transition states. Modern DFT methods and current generation computers make even these relatively large molecular systems amenable to computation modelling. The studies presented in this dissertation focus on dehydrogenation of organic molecules (alkanes, amines, and alcohols), and oxidative addition of a variety of polar reagents.

Chapter 3 - Gas-Phase Dehydrogenation of Alkanes: C-H Activation by a Graphene-Supported Nickel Single-Atom Catalyst Model

3.1 Alkane Dehydrogenation

The dehydrogenation of alkanes allows for the transformation of unreactive and inexpensive alkanes to alkenes that can be used as valuable feedstocks in various industrial processes.⁷³ Transition metals have successfully been used to perform catalytic dehydrogenation of alkanes in both heterogeneous and homogeneous systems. While various noble metal and metal oxide catalysts have dominated the heterogeneous systems in chemical industry, the most used and well-studied catalysts are platinum-based and CrO_x systems.^{74,75} Homogeneous systems are also dominated by noble metals, with a heavy focus on iridium.⁷⁶ Many of the reports on catalytic dehydrogenations occur via transfer dehydrogenations.⁷⁷⁻⁸⁴ In these reactions, the catalyst transfers hydrogen from the saturated alkane to a sacrificial unsaturated hydrogen acceptor (Figure 3.1). The use of the hydrogen acceptor provides the benefit of eliminating the hydrogen being generated and shifting the equilibrium towards the products. However, the stoichiometric sacrificial reagent also makes the reaction uneconomic. Due to this consequence, many studies have focused on acceptor-less dehydrogenation systems.^{76,85,86} Our Ni SAC model ion, complex **I**, is capable of the acceptor-less dehydrogenation of alkanes via C-H activation.

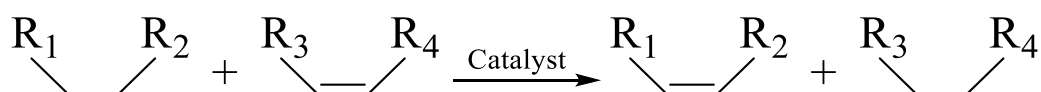
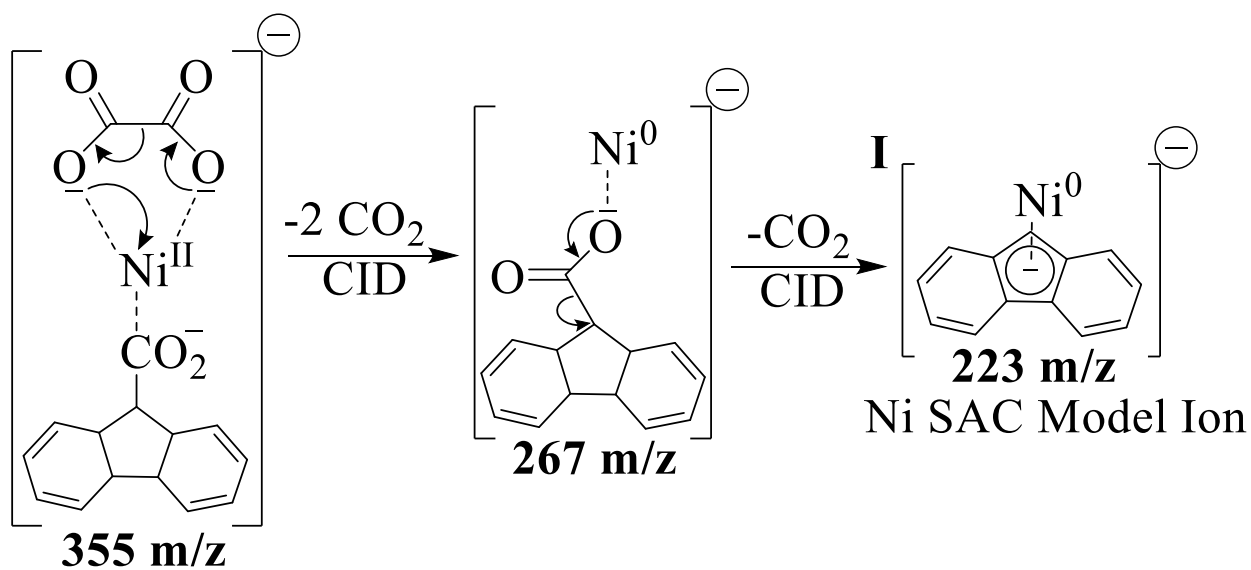


Figure 3.1. Transfer dehydrogenation reaction. A sacrificial hydrogen acceptor is used to drive the reaction towards products.

3.2 Complex I in the Dehydrogenation of Cyclohexane

Using our modified ion-trap mass spectrometer,³⁶ complex **I** can be formed in the gas phase using CID via the two-electron reduction pathway, as depicted in Scheme 3.1. While complex **I** can also be generated using the one-electron reduction pathway described in Scheme 2.1, the two-electron reduction pathway was utilized to maximize ion intensities. Mass spectra for the formation of complex **I** via CID is shown in Figures 3.2 and 3.3. The reactivity of complex **I** was probed by isolating the complex in the ion trap and allowing it to participate in ion/molecule reactions with a variety of substrates. In a survey of its reactivity with typical oxidative addition reagents (e.g., organohalides), we discovered that complex **I** underwent dehydrogenation reactions with the cyclohexane solvent used to dilute the reagent. This reaction resulted in the loss of H₂ and the formation of a cyclohexene complex with the metal ligand system. Reactivity of the Co, Cu, and Pd SAC ions was also probed but these metal complexes did not engage in alkane dehydrogenation. Their oxidative addition chemistry is discussed in later chapters.



Scheme 3.1. Gas-phase synthesis of Complex I.

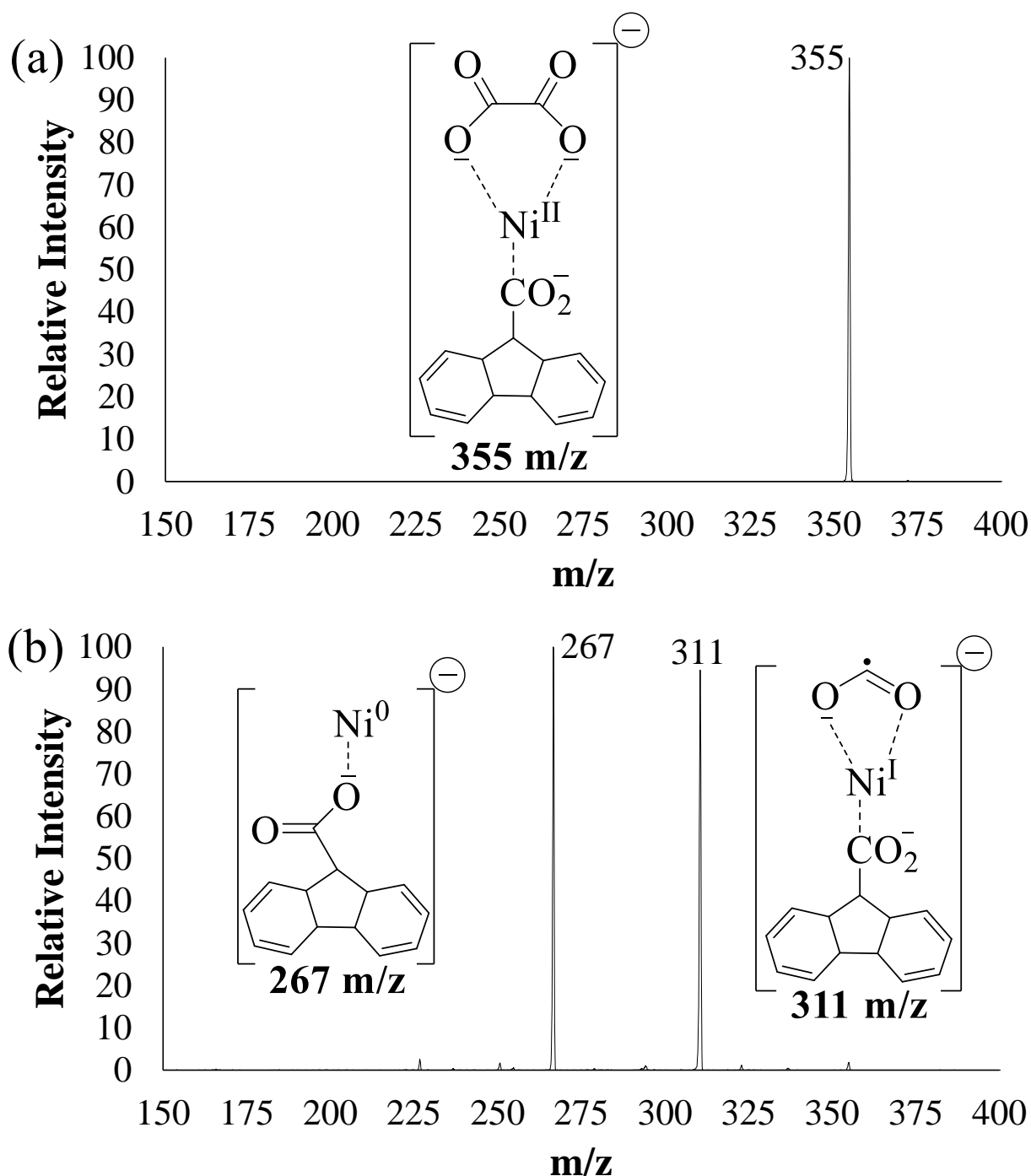


Figure 3.2. Mass spectra for the reduction of the Ni of the precursor ion. Panel (a) Isolation of Ni precursor complex. Panel (b) Product spectrum for the CID of the Ni precursor complex. The two-electron and one-electron reduction pathways lead to the products at m/z 267 and 311, respectively.

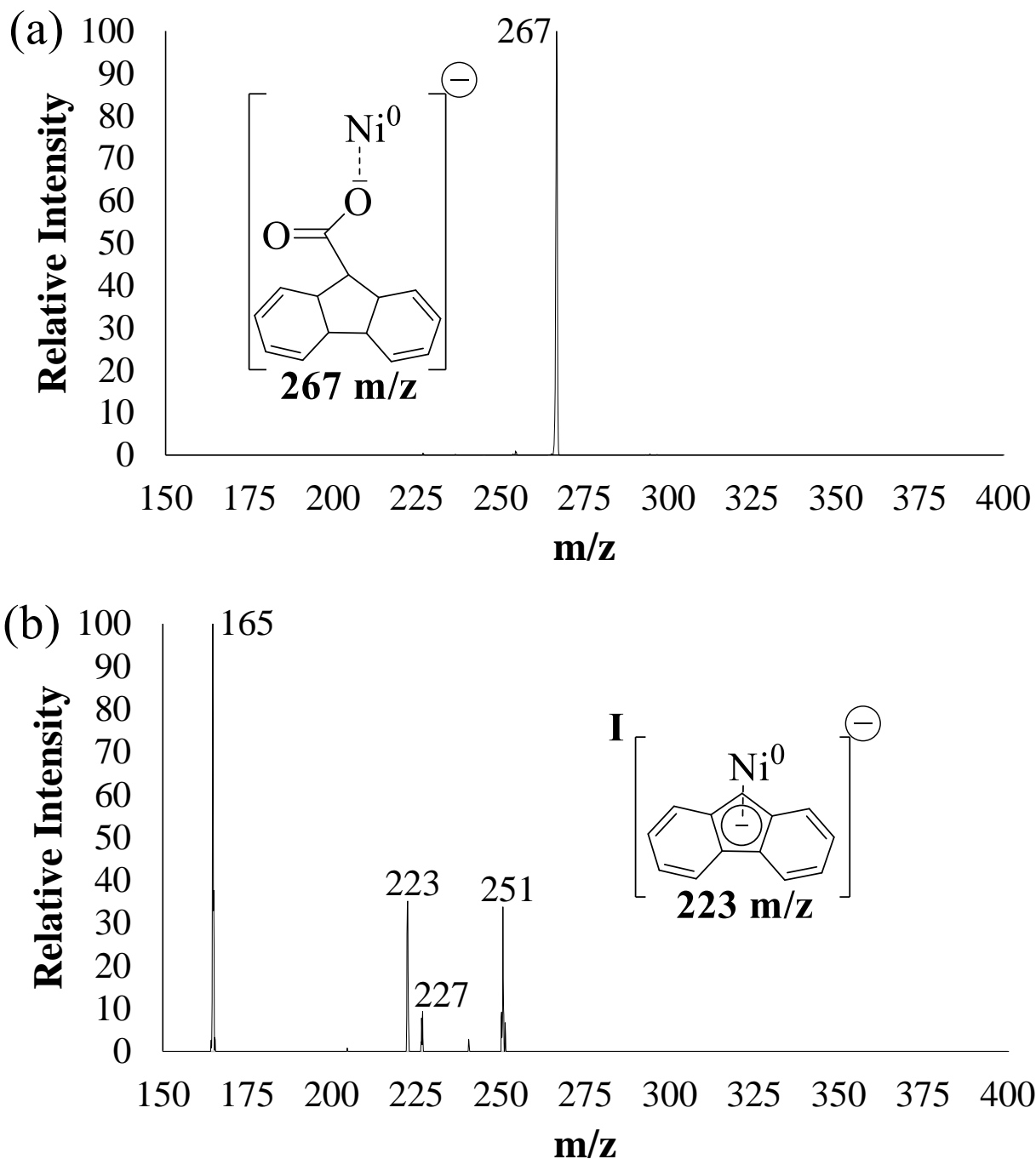


Figure 3.3. Mass spectra for the reduction of the Ni complex with fluorene-9-carboxylate. Panel (a) Isolation of the Ni complex with fluorene-9-carboxylate. Panel (b) CID of the Ni complex with fluorene-9-carboxylate. Complex **I** appears at m/z 223. The fluorenyl anion appears at m/z 165. An adduct with adventitious nitrogen appears at m/z 251. The peak at m/z 227 may be an adduct of fluorene-9-carboxylate and water.

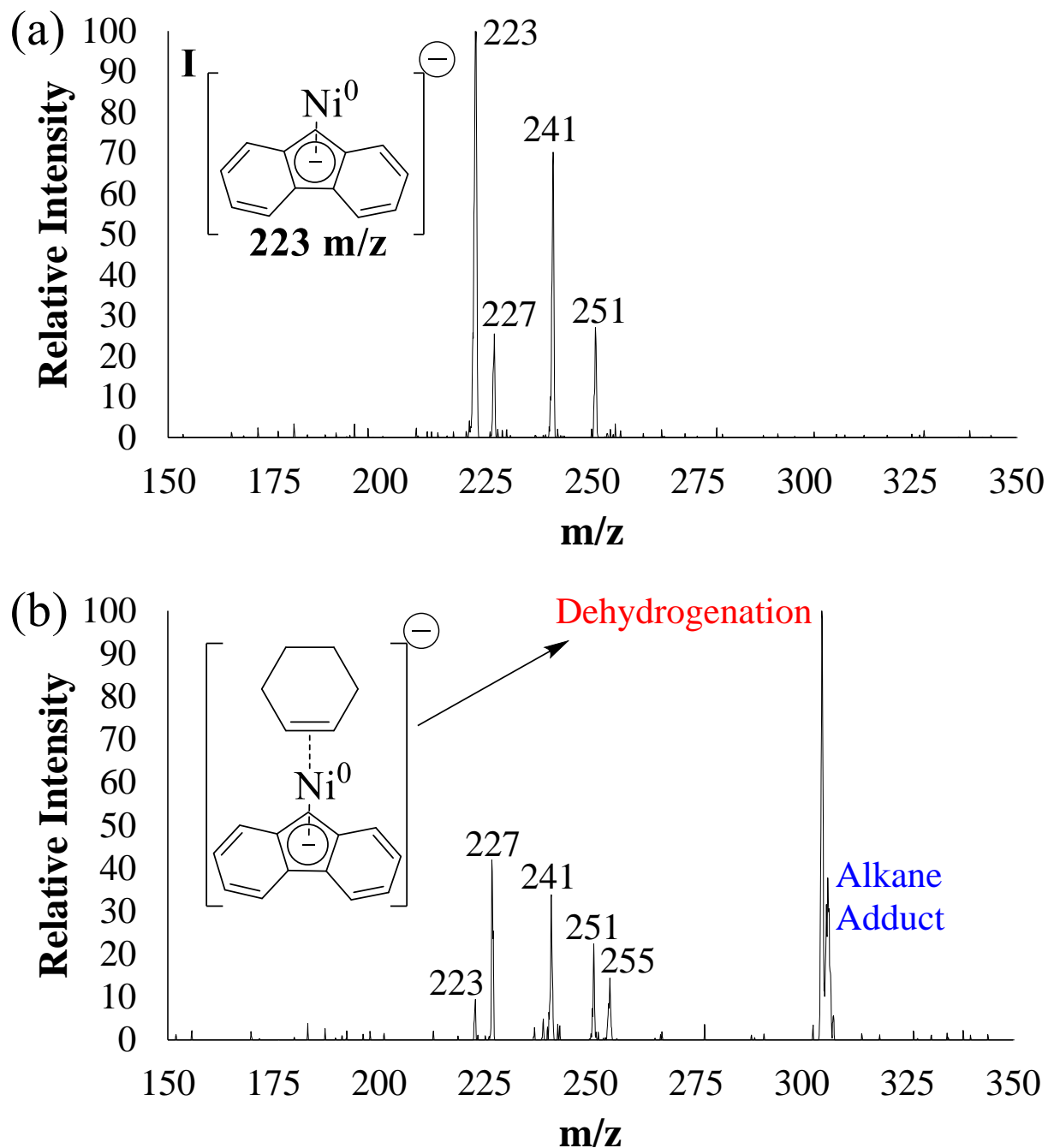


Figure 3.4. Mass spectra for reaction of **I** with cyclohexane. Panel (a) Isolation of **I** prior to introduction of cyclohexane. Panel (b) Product spectrum after introduction of cyclohexane. Dehydrogenation and alkane adduct products appear at m/z 305 and 307, respectively. Peak broadening of the alkane adduct is observed due to the relative instability of the ion during the instrument scans.³⁶ Complex **I** appears at m/z 223. Products of adduct formation with adventitious water, nitrogen, and methanol appear at m/z 241, 251, and 255 respectively. The peak at m/z 227 may be an adduct of fluorene-9-carboxylate and water formed through secondary reactions. There are also peaks (not shown) at m/z 90, an oxide from reaction with adventitious oxygen, and m/z 107, an unidentified species that is independent of the neutral reagent.

Figure 3.4 depicts the reaction spectra for the dehydrogenation of cyclohexane by complex **I**. Two products result from the reaction with cyclohexane (other peaks are from reactions with adventitious gases in the ion trap, see figure caption for details). The peak at m/z 305 is the dehydrogenation product of cyclohexane, *i.e.*, the cyclohexene adduct of complex **I**. It is important to note that collisions with the helium buffer gas cool reactant ions to near room temperature within a few milliseconds.⁸⁷ Since the cooling is significantly faster than the time scale of reactions, ion-molecule reactions in our system proceed at near thermal energies even after subjecting the ion to trapping voltages or CID.^{68,69} However, dehydrogenations generally require elevated temperatures in the condensed phase. The key driving force in our system is that the cyclohexene coordinates much more strongly with **I** than cyclohexane, providing more than enough energy to overcome the inherently endothermic nature of the dehydrogenation process. The cyclohexane adduct of **I** also appears in the spectrum.

When complex **I** is allowed to react with cyclohexane- d_{12} , the dehydrogenation product is appropriately shifted to m/z 315, as shown in Figure 3.5 (a). Complex **I** was also allowed to react with a 50%/50% by volume mixture of cyclohexane and cyclohexane- d_{12} , as shown in Figure 3.5 (b). Since the intensities of ion-molecule reaction products in our system are proportional to their rate of reaction (except for very modest mass discrimination effects in this narrow m/z range), kinetic isotope effect (KIE) values can be determined via a simple comparison of the appropriate reaction product intensities. In this case, the intensity of the C_6H_{10} complex was taken relative to the intensity of the C_6D_{10} complex and revealed a KIE of 2.4. This strongly suggests that activation of a C-H(D) bond is part of the rate-limiting step in the dehydrogenation.

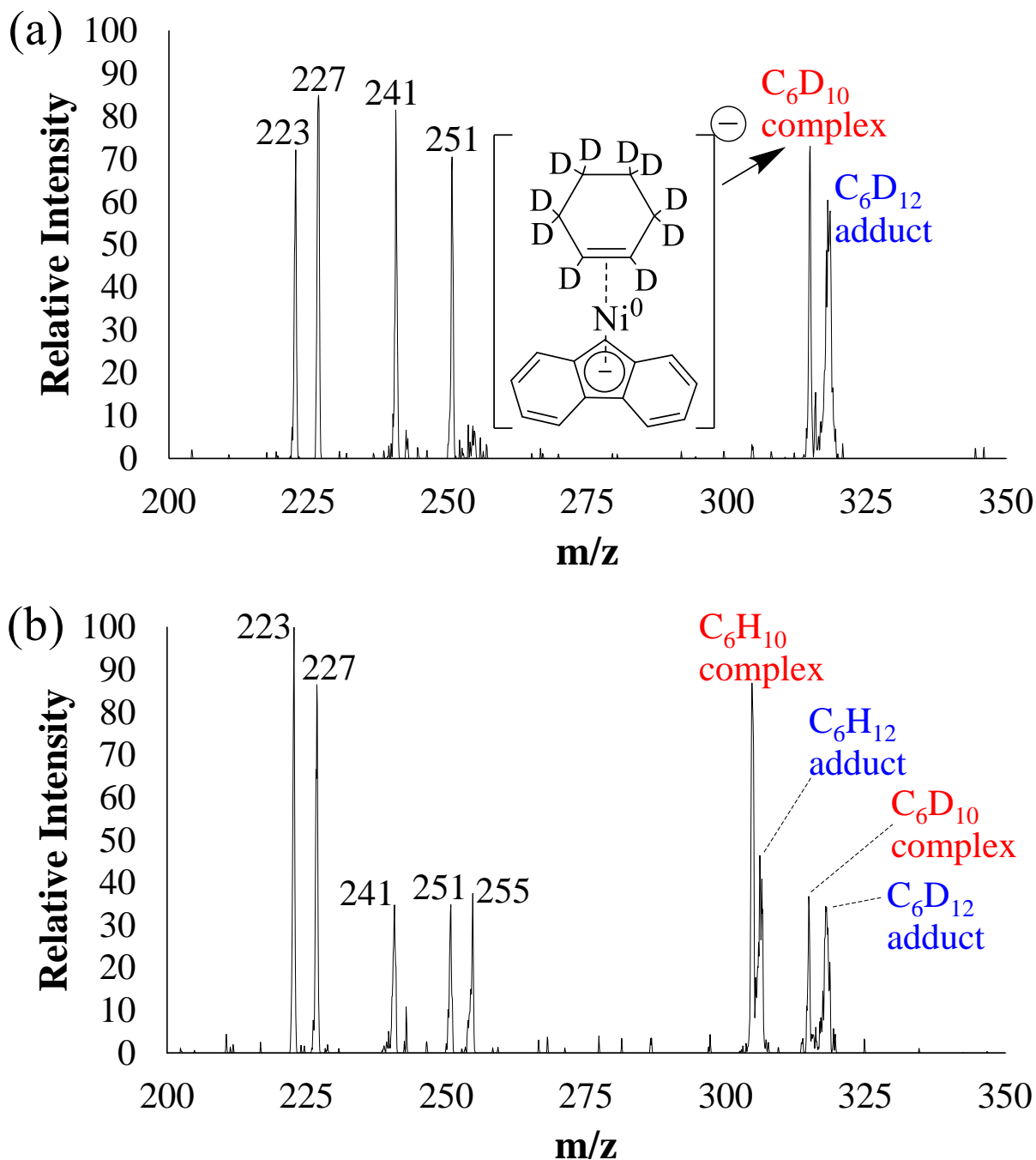
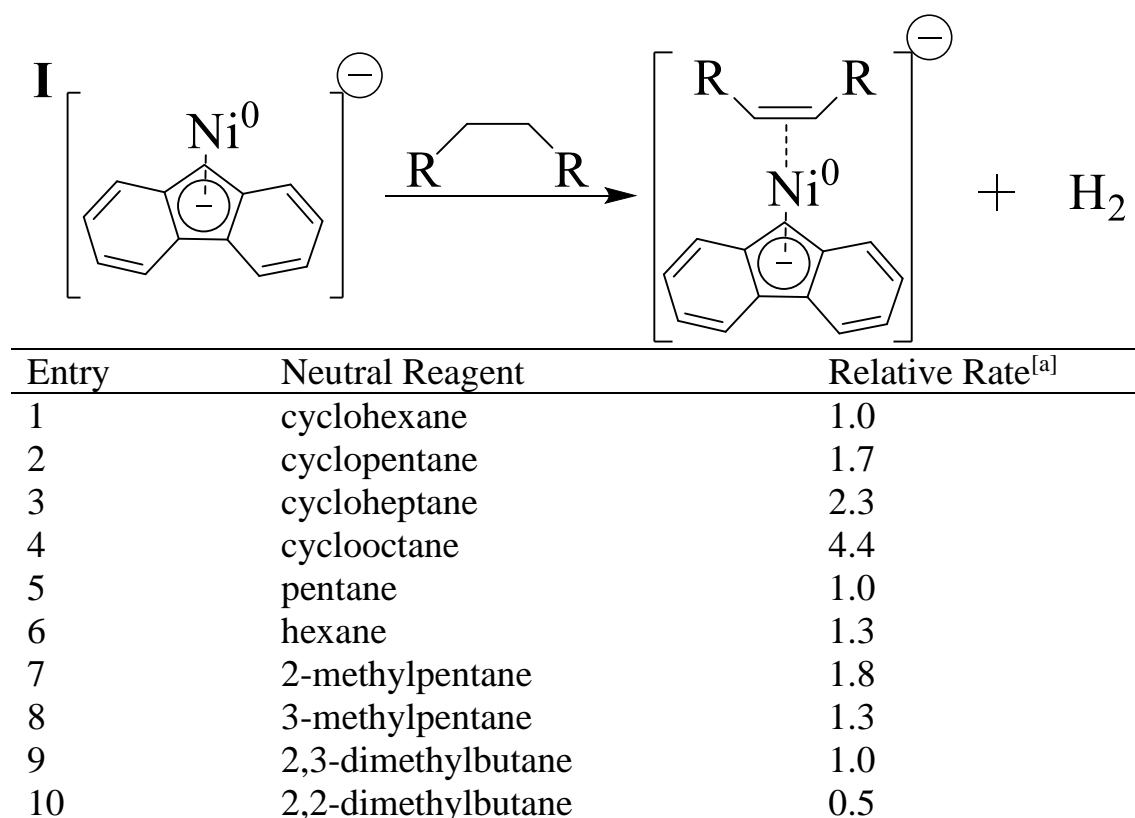


Figure 3.5. Cyclohexane-d₁₂ experiments. Panel (a) Reaction of **I** with cyclohexane-d₁₂. Panel (b) Isotope effect experiment. Alkene complex (C₆H₁₀ and C₆D₁₀ complexes) and alkane adduct (C₆H₁₂ and C₆D₁₂ adducts) peaks appear at m/z 305, 315, 307 and 319, respectively. Peak broadening is observed for the alkane adduct peak due to the relative instability of the product ion during the instrument scans. Complex **I** appears at m/z 223. Products of adduct formation with water, nitrogen, and methanol appear at m/z 241, 251, and 255 respectively. The peak at m/z 227 may be an adduct of fluorene-9-carboxylate and water formed through secondary reactions. There are also peaks (not shown) at m/z 90, an oxide from reaction with adventitious oxygen, and m/z 107, an unidentified adduct that is independent of the neutral reagent.

3.3 Dehydrogenation of Various Hydrocarbons

We also allowed **I** to react with the other alkanes listed in Table 1 and observed alkene formation in each reaction. Cyclic alkanes display a range of relative rates, spanning four-fold across the series from cyclopentane to cyclooctane. The slowest of the group is cyclohexane ($k = 1.6 \times 10^{-10} \text{ cm}^3 \text{ molecule}^{-1} \text{ s}^{-1}$), suggesting that restrictions in conformational freedom can play a significant role in limiting reaction rates. Reactions with linear and branched alkanes exhibited less variation and were similar to that of cyclohexane, with the exception of 2,2-dimethylbutane which was significantly slower (0.5).

Table 1. Relative rates of alkane dehydrogenation reactions with complex **I**.



[a] Relative to cyclohexane reaction. $k = (1.6 \pm 0.4) \times 10^{-10} \text{ cm}^3 \text{ molecule}^{-1} \text{ s}^{-1}$

The product spectrum for the reaction with 2,2-dimethylbutane is shown in Figure 3.6 (a). For this reaction, the dehydrogenation product (m/z 307) and the alkane adduct (m/z 309) appear with almost equal intensity. The prominence of the latter product in this particular reaction is likely due to the presence of the quaternary carbon. When complex **I** approaches and reacts with one of the branched methyl C-H bonds, the substrate lacks a hydrogen on the β -carbon needed to proceed with dehydrogenation to generate the alkene (Figure 3.6 (b)). The other alkanes listed in Table 1 do not have a quaternary carbon that could block dehydrogenation activity and the alkane adduct peaks (i.e. non-dehydrogenation) appear at a much lower intensity, as seen in the reaction with cyclohexane.

Dehydrogenation among the branched methyl groups of 2,2-dimethylbutane could generate a three-membered ring adduct that is isobaric with the alkene adduct (i.e. 1-ethyl-1-methylcyclopropane). Since mass spectrometry would be unable to distinguish between these two products, complex **I** was allowed to react with tert-butylbenzene (Figure 3.7). Unlike 2,2-dimethylbutane, the branched end of tert-butylbenzene is the only position that dehydrogenation could occur. However, dehydrogenation did not occur with tert-butylbenzene. The adduct was the sole product of this reaction. This suggests that the reaction with 2,2-dimethylbutane forms the dehydrogenation product on carbons 3 and 4 rather than cyclopropane formation.

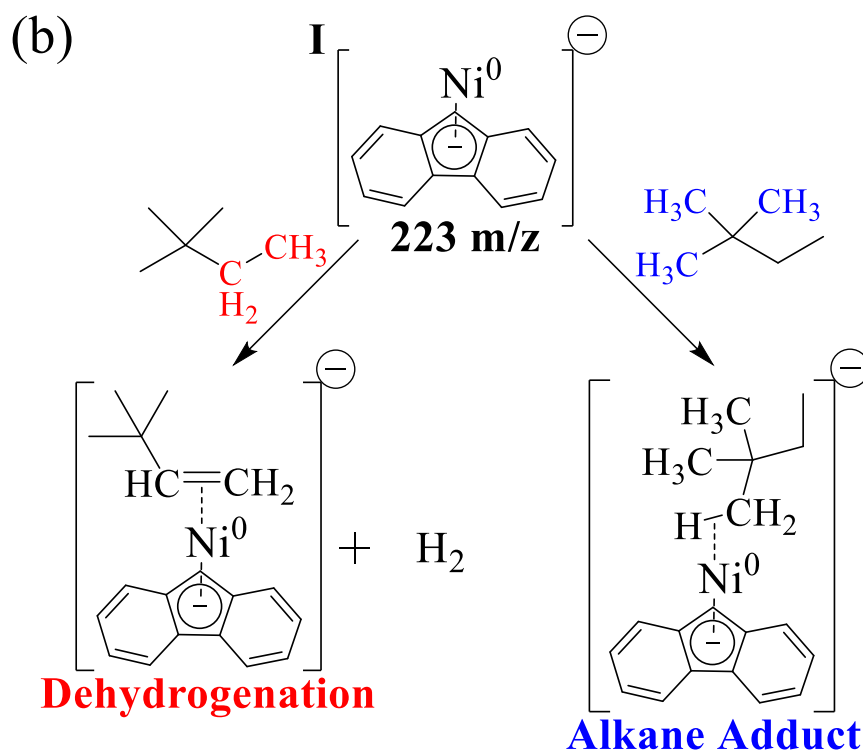
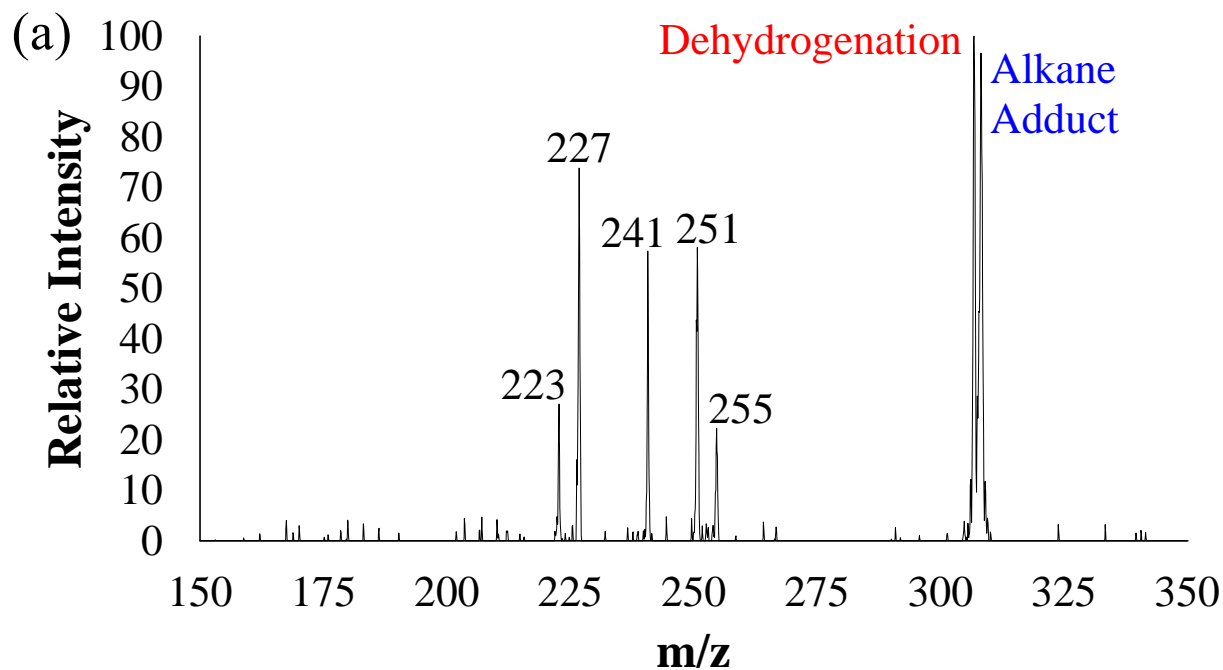


Figure 3.6. Reaction of complex **I** with 2,2-dimethylbutane. Panel (a) depicts the product spectrum. Two products are observed: the dehydrogenation product (m/z 307) and the alkane adduct (m/z 309). Panel (b) depicts which C-H bonds lead to the products. Insertion into the red C-H groups leads to the dehydrogenation product. When approaching the blue C-H groups dehydrogenation cannot occur, resulting in the alkane adduct.

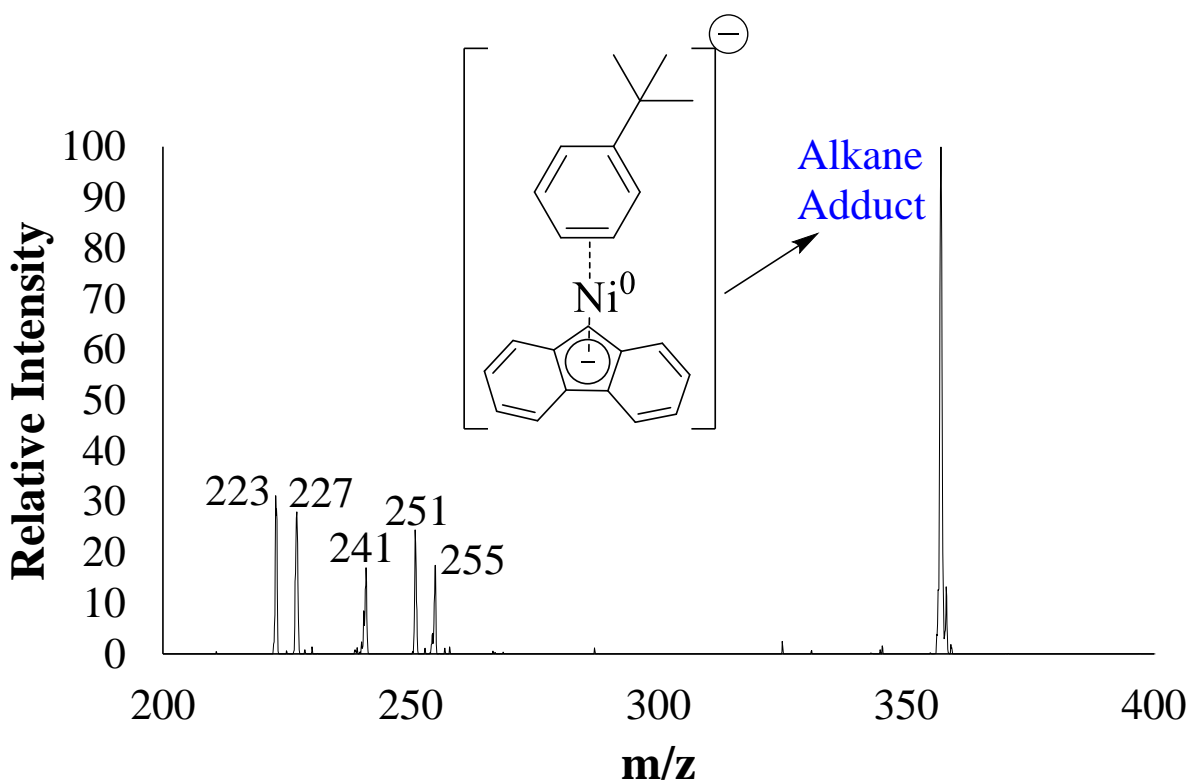


Figure 3.7. Product spectrum for the reaction of complex **I** with tert-butylbenzene. The alkane adduct (m/z 357) was the only product observed. Complex **I** appears at m/z 223. Adduct formation products of complex **I** with water, nitrogen, and methanol appear at m/z 241, 251, and 255 respectively. The peak at m/z 227 may be an adduct of fluorene-9-carboxylate and water formed through secondary reactions. There are also peaks (not shown) at m/z 90, an oxide from reaction with adventitious oxygen, and m/z 107, an unidentified adduct that is independent of the neutral reagent.

Benzene and toluene were also used to probe dehydrogenation reactivity. Dehydrogenation of these neutral reagents was not expected due to their aromatic nature. However, C-H activation on the aromatic ring could still prove useful for functionalization. Reactions with these reagents resulted in one product peak with the combined mass of complex **I** and the reagent. While the Ni model ion and the neutral reagents are clearly interacting, the product spectra alone cannot identify the products as C-H insertion products or adducts. In order to identify the products, relative kinetic studies using benzene- d_6 and toluene- d_8 were performed and revealed KIE values of 1.2. These

relatively low values suggest that the observed products are adducts instead of C-H insertion products.

3.4 Dehydrogenation Mechanism

DFT calculations for the dehydrogenation of cyclohexane, completed at the M06/6-311+G** level, provide added insight into the mechanisms of these C-H activations and dehydrogenation processes (it should be noted that a Natural Population Analysis⁸⁸ of the wavefunction with this basis set places the majority of the charge, 70%, on the fluorenyl scaffold, suggesting that the species is best described as a nickel atom on a fluorenyl ligand). The energy surface for the dehydrogenation of cyclohexane by **I** is depicted in Figure 3.8.

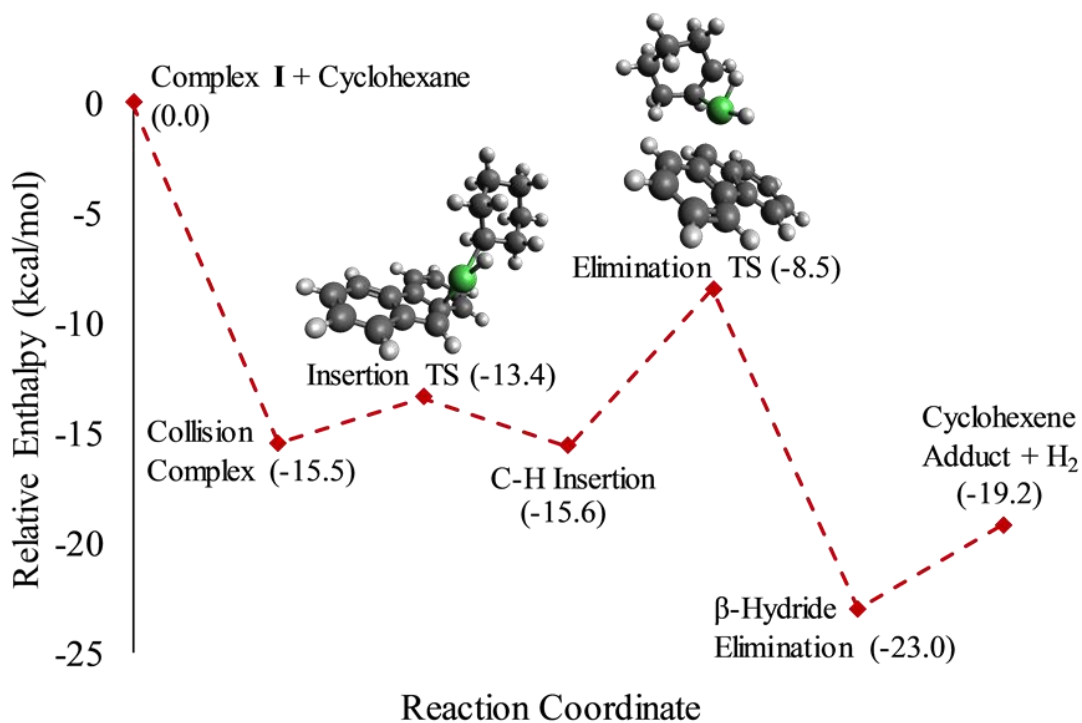


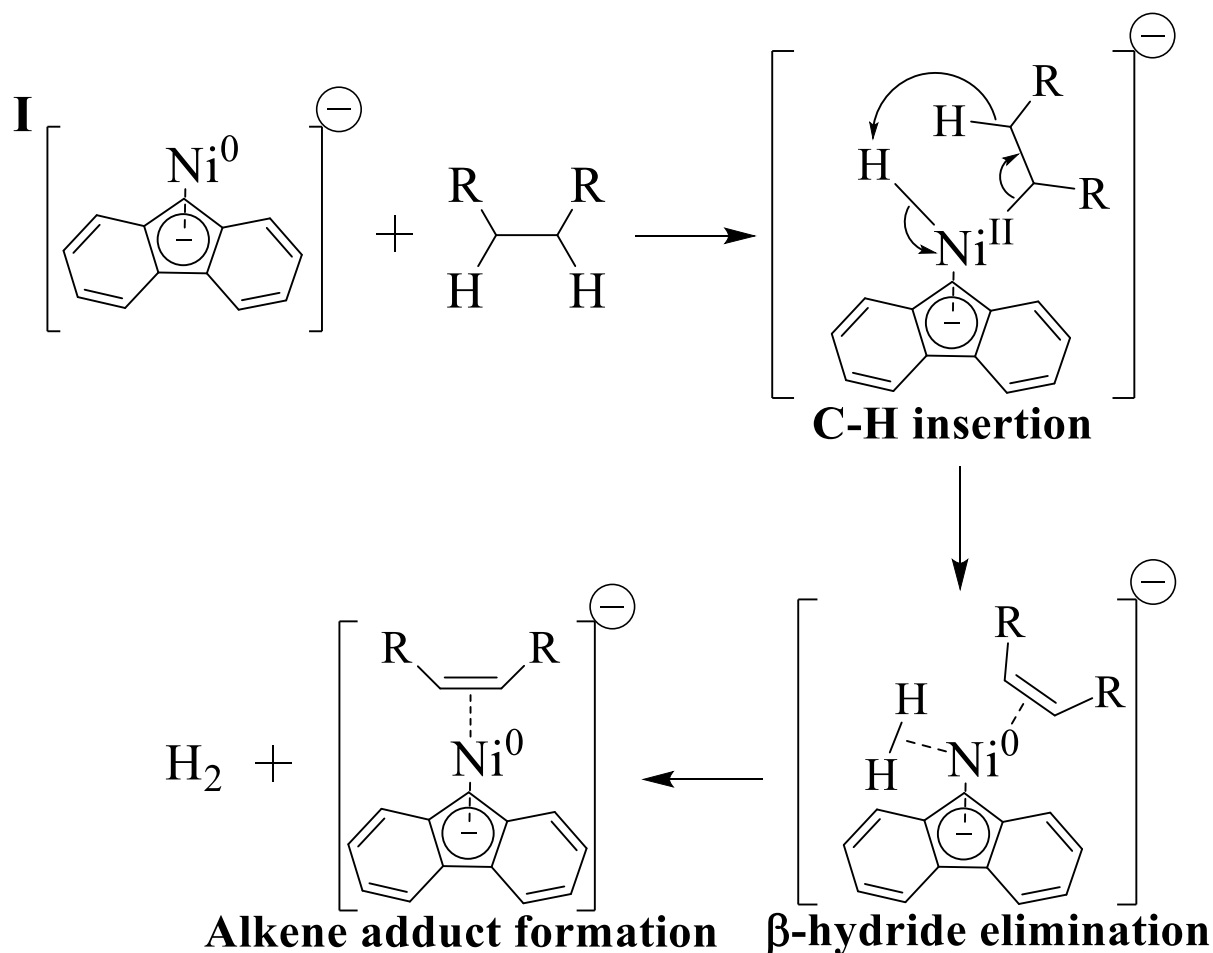
Figure 3.8. Potential energy surface for the dehydrogenation of cyclohexane by complex **I**. Calculations were completed at the M06/6-311 + G** level. Detailed information on the structure and frequencies of the calculated species are shown in Appendix C.

DFT calculations suggest that complex **I** inserts into a C-H bond via a transition state (TS) that is 13.4 kcal/mol below the reactants (2.1 kcal/mol above the collision complex) and gives a reaction that is exothermic by 15.6 kcal/mol. Subsequently, **I** performs a β -hydride elimination as part of the next C-H activation, leading to a complex of **I** with cyclohexene and molecular hydrogen. The elimination TS suggests that the nickel is able to bring the β -hydrogen close to the initially abstracted hydrogen, facilitating the formation of an H-H bond (-8.5 kcal/mol). Finally, the Ni center can expel the hydrogen molecule and form the complex with cyclohexene and the fluorenyl anion. The DFT calculations indicate an overall reaction enthalpy of -19.2 kcal/mol. The calculations point to the β -hydride elimination as the rate-limiting step, which is consistent with the deuterium kinetic isotope effect studies noted above. The low coordination environment of the metal leads to favorable interactions between nickel and the substrate, allowing the process to proceed with barriers below the energy of the reactants.

Bare nickel atoms are unreactive towards unstrained alkanes.⁸⁹ Anionic nickel atoms have been shown to react with acetonitrile under collisional activation, whereas anionic metal clusters react with alkanes at efficiencies less than 10%.^{90,91} Our Ni SAC model anion reacts at 10% efficiency with simple alkanes, although reactions with highly branched alkanes can result in more inefficient reactions. Cationic nickel atoms react at about a 10% efficiency with simple alkanes via C-H and C-C activation.⁹²⁻⁹⁵ Ligated transition metal cations have been studied extensively in the gas phase and give a variety of reactivities.^{94,96-100}

The dehydrogenation mechanism of alkanes by complex **I** is depicted in Scheme 3.2. Ethene and other light olefins are valuable building blocks in chemical industry and can be used to make a wide host of chemicals.⁷⁴ While we are unable to introduce gaseous neutral reagents into the ion trap using our experimental setup, DFT calculations suggest complex **I** would display similar

dehydrogenation reactivity with smaller, gaseous alkanes, such as ethane and butane (Appendix B.1 & B.2).

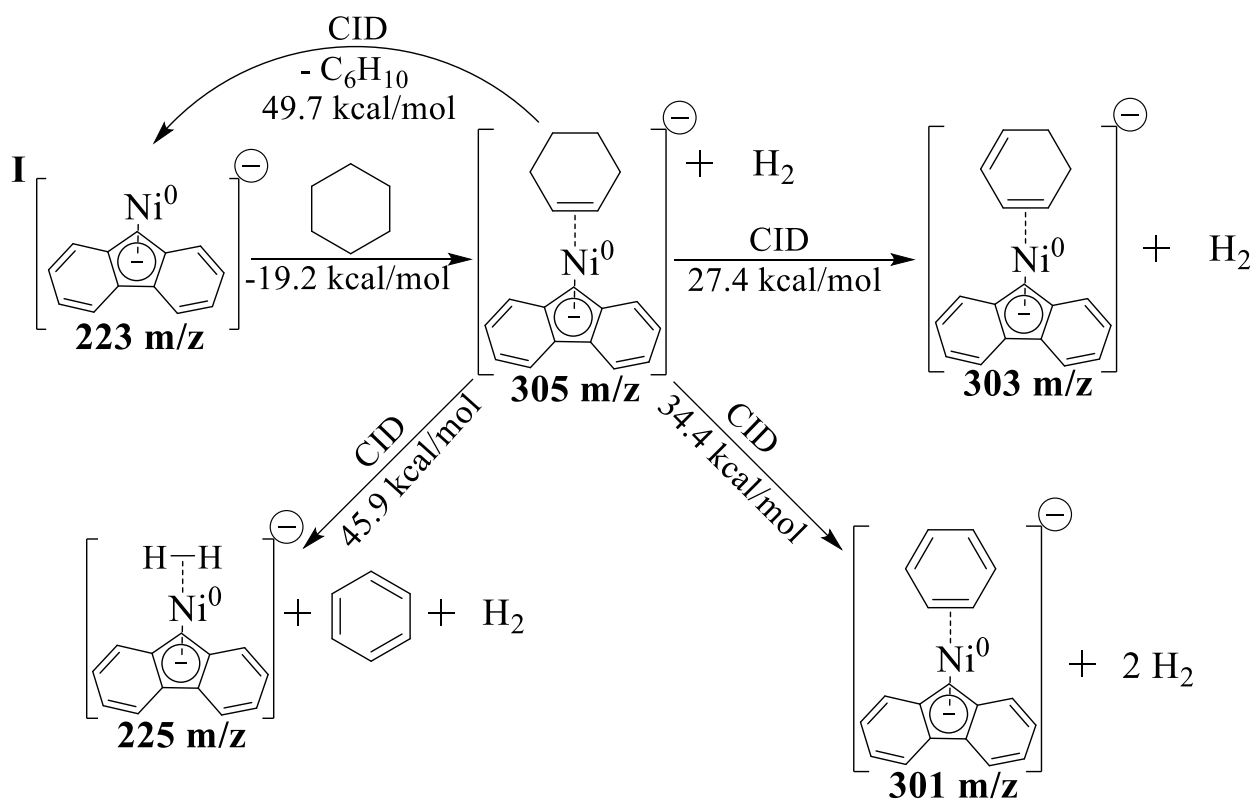


Scheme 3.2. Dehydrogenation mechanism of alkanes by complex **I**.

3.5 Sequential Dehydrogenations

Surprisingly, the reactivity of **I** with alkanes does not end with alkene formation. Tandem mass spectrometry revealed that complex **I** can perform sequential dehydrogenations. The reaction pathways for cyclohexane are shown in Scheme 3.3. When the cyclohexene complex with **I** is isolated and subjected to CID, additional dehydrogenations occur, resulting in complexes of **I** with

cyclohexadiene or benzene. These processes are endothermic and require 27.4 and 34.4 kcal/mol of activation, respectively. Recovery of complex **I**, by release of cyclohexene, is observed and requires 49.7 kcal/mol of activation. Formation of a complex of **I** with a hydrogen molecule is also observed when the cyclohexene complex of **I** is subjected to CID (endothermic by 45.9 kcal/mol). These additional dehydrogenations are not observed spontaneously at room temperature and require the energy introduced via CID in order to occur. The relevant CID spectra are shown in Appendix A.3.



Scheme 3.3. Cyclohexane dehydrogenation pathways. Reaction enthalpies were calculated at the M06/6-311+G** level. Detailed information on the structure and frequencies of the calculated species are shown in Appendix C.

This pattern of multiple dehydrogenations was also seen with other alkanes in Table 1. However, second dehydrogenations were not observed with 2,2-dimethylbutane, cyclopentane, and

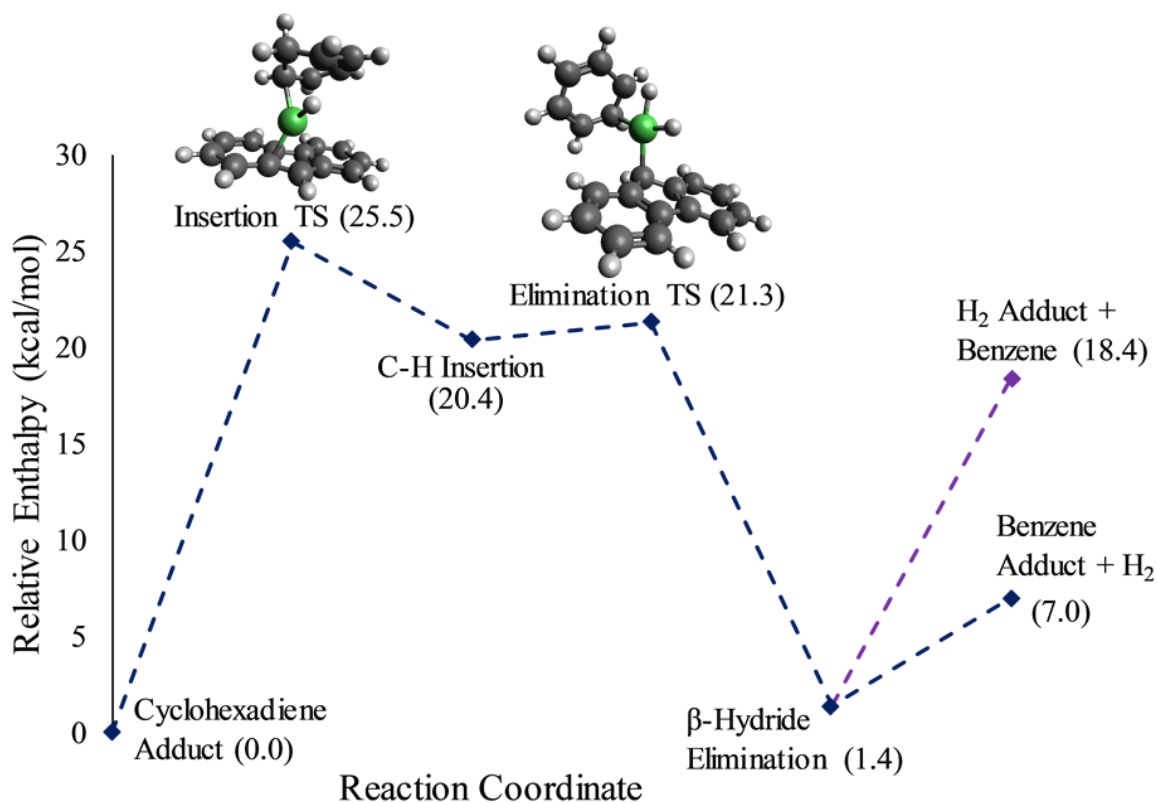


Figure 3.9. Potential energy surface for the dehydrogenation of cyclohexadiene. Calculations were completed at the M06/6-311 + G** level. Detailed information on the structure and frequencies of the calculated species are shown in Appendix C.

The aromaticity of benzene also has an effect on the dehydrogenation energy surface (Figure 3.9). While DFT calculations suggest the β -hydride elimination step is the rate-limiting step for the dehydrogenation of cyclohexane and cyclohexene (Appendix B.3), this is not the case for the third dehydrogenation. Aromaticity formation stabilizes the elimination TS, indicating that C-H insertion is the rate-limiting step. After elimination, the Ni center can expel the hydrogen molecule to form the complex with benzene. Alternatively, as noted above, the Ni center can expel benzene, resulting in the complex with the hydrogen molecule (18.4 kcal/mol). While mass spectrometry cannot distinguish this complex from the isobaric metal dihydride species, DFT calculations indicate that the hydrogen molecule adduct of complex **I** is favored over formation of the metal

dihydride (Appendix B.4), supporting the formation of the hydrogen molecule during dehydrogenation.

This study reports that a novel Ni SAC model system is capable of alkane dehydrogenation via C-H activation. The experimental data and computational modeling suggest two distinct C-H activations are required to enact dehydrogenation: metal insertion into a C-H bond and β -hydride elimination. In the condensed phase, defects in the graphene lattice are used to trap single metal atoms.^{28,31} If graphene containing Stone-Wales defects can be used to trap atomic nickel, our results suggest that it could be a potent dehydrogenation catalyst.

3.6 Experimental Section

All experiments were executed in a modified linear triple quadrupole ion trap mass spectrometer (modified Thermo Electron LTQ XLTM) equipped with an electrospray ionization (ESI) source. Nickel(II) acetate tetrahydrate and fluorene-9-carboxylic acid were each dissolved in methanol at 10^{-4} M. Potassium oxalate monohydrate was dissolved in a water/methanol mixture at 10^{-4} M. These solutions were mixed in a 1:5:2.5 ratio by volume, respectively, and passed into the ion trap via ESI. Typical ESI conditions involved flow rates of $5\mu\text{L}/\text{min}$, needle potentials between 4-5 kV and heated capillary temperatures between 230-275 °C. A notched waveform was used to isolate the precursor complex. The precursor complex was subjected to sequential rounds of CID to form complex **I**. Once a steady signal of complex **I** was achieved, neutral reagents were introduced into the ion trap via the external manifold, as previously described.^{36,68}

Reaction spectra were averaged over 200 scans in order to minimize noise. Absolute kinetic measurements were measured under pseudo-first order conditions due to the excess of neutral

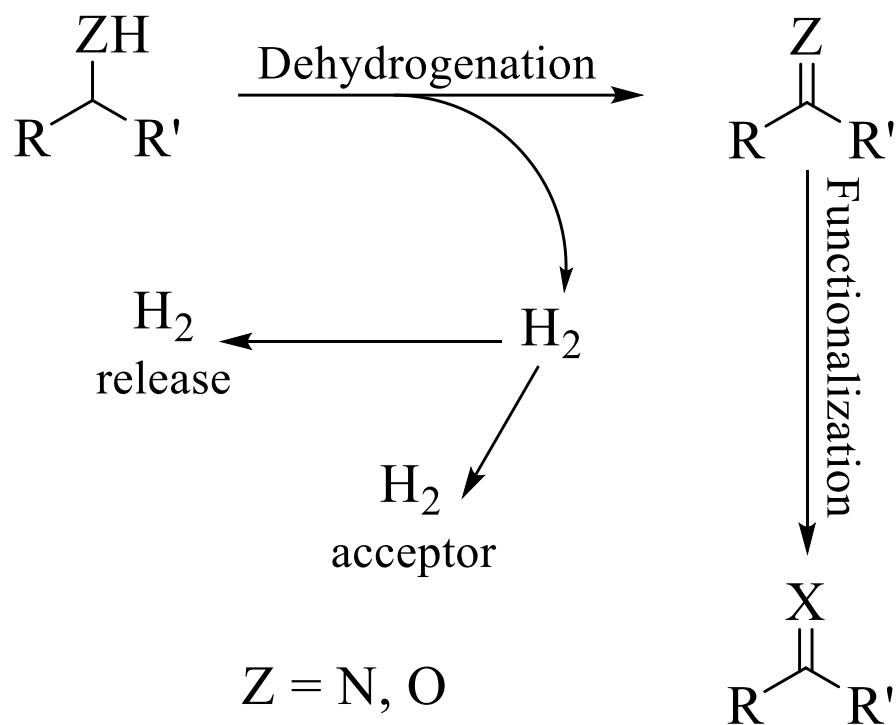
reagent (reagent/anion = 10^5 - 10^6). Reagent flow rates and time delays were varied to obtain plots that covered 2-3 half-lives of the anion. Ten different time delays were used at each flow rate and the kinetic data were obtained over six days. Relative kinetic measurements were completed by allowing complex **I** to react with an alkane and cyclohexane simultaneously. The hydrocarbons were introduced into the external manifold in a 1:1 ratio by volume. Molar ratios were used to adjust the peak heights of the alkane and cyclohexane dehydrogenation products and the resulting intensities were compared. All neutral reagents were purchased commercially in the highest purity available and used without further purification.

Density functional calculations were completed using the Gaussian16¹⁰¹ suite of quantum mechanical programs. All calculations were performed at the M06/6-311+G** level. All transition states were verified using intrinsic reaction coordinate (IRC) calculations to link them to reactants and products.

Chapter 4 - Gas-Phase Dehydrogenation of Amines and Alcohols by Graphene-Supported Single-Atom Catalyst Model Ions

4.1 Amine and Alcohol Dehydrogenation

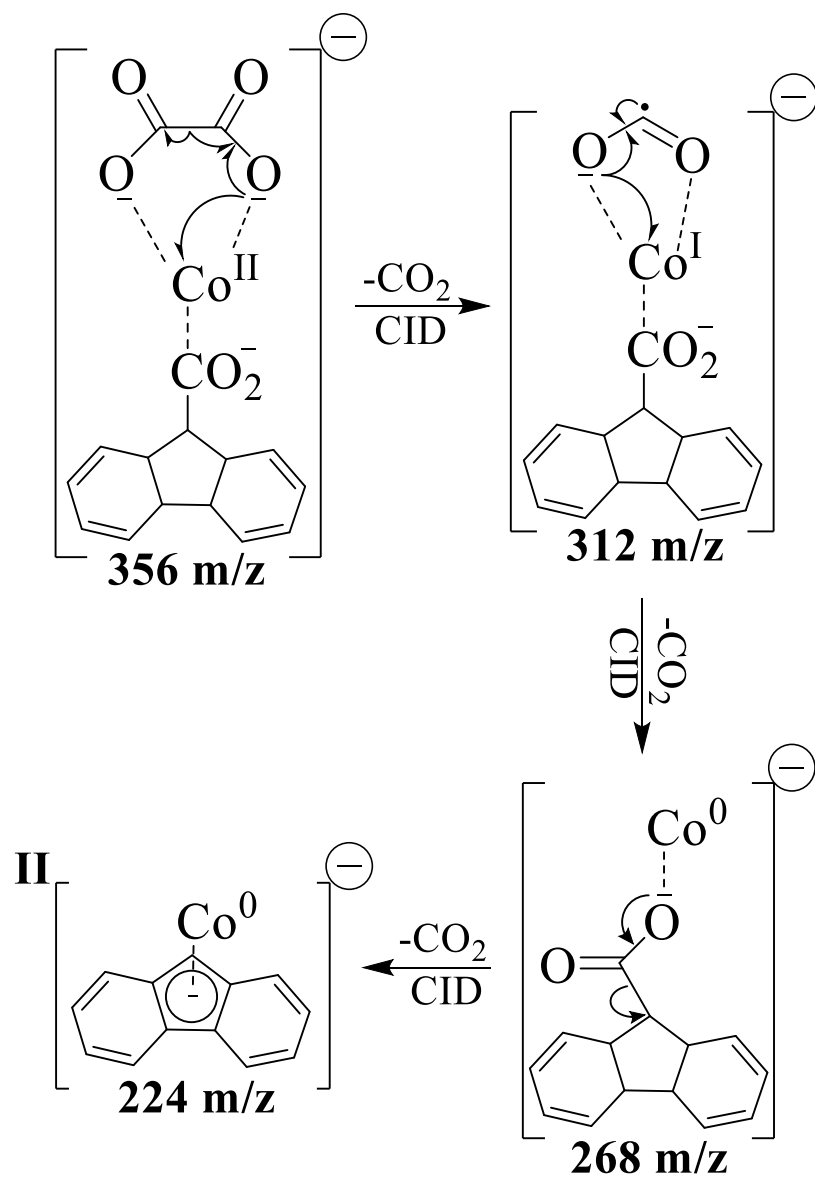
Amines and alcohols can also be activated via dehydrogenation. Catalytic dehydrogenative activation of these substrates can enable lower waste synthetic processes while using less toxic starting materials. There is great potential for using catalytic processes to convert these substrates to more valuable materials. Dehydrogenation of these functional groups occur in much the same fashion as the alkane dehydrogenations described in the previous chapter. However, the wider reactivity of the imine and carbonyl containing products of these processes provide a much wider scope of application. Many reactions that are inaccessible to the parent compounds are available in the unsaturated products. Thus, catalytic dehydrogenation of amines and alcohols is usually followed by functionalization of the unsaturated products (Scheme 4.1).⁷⁶ Once again, the dehydrogenation step can be classified into two groups: transfer dehydrogenations or acceptorless dehydrogenations. In the former case, hydrogen is transferred to a hydrogen acceptor. While the hydrogen acceptor can be a sacrificial component solely intended to help drive the reaction forward, judicious choice of the acceptor can lead to the hydrogenation of a molecule of interest. In many cases the hydrogen is used to reduce the functionalized product. This paradigm has been used to enable a variety of transformations such as transamination, nitrile formation, N-alkylation by alcohols, and Guerbet reactions.^{102–106} Acceptorless dehydrogenations result in the liberation of the hydrogen and can also be used to enable transformations to create more valuable products.^{107–113} Both the Ni and Co SAC model ions are capable of the acceptorless dehydrogenation of amines and alcohols, resulting in the formation of imine and carbonyl adducts and the loss H₂.



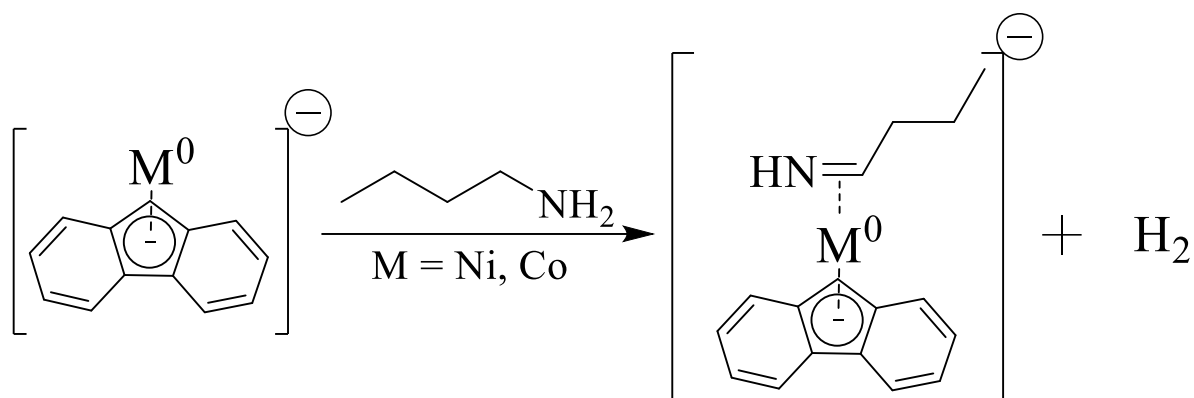
Scheme 4.1. Typical reaction sequence for the dehydrogenation of amines and alcohols. The depiction is based on work from Doberiner and Crabtree.⁷⁶

4.2 Complexes **I** and **II** in the Dehydrogenation of Amines and Alcohols

Complex **I** was generated as described in the previous chapter. The Co SAC model ion, complex **II**, was generated via the one-electron reduction pathway (described in chapter 2.4), depicted in Scheme 4.2. Experiments with n-butylamine resulted in imine adducts of both metal complexes, as depicted in Scheme 4.3. Reaction spectra for these dehydrogenations are depicted in Figures 4.1 and 4.2, respectively. **I** and **II** also performed dehydrogenations when reacting with piperidine and diethylamine (Appendix A.4 – A.7).



Scheme 4.2. Gas-phase synthesis of Complex II.



Scheme 4.3. n-Butylamine dehydrogenation reaction by complexes **I** and **II**. The imine is shown as the dehydrogenation product – confirmation of this assignment is provided below.

The peak at m/z 294 in Figure 4.1 is the dehydrogenation product for the reaction with complex **I**, i.e. the butan-1-imine adduct with complex **I**. The dehydrogenation product is the only product observed - all other peaks in the product spectrum are adducts with adventitious species in the ion trap (see figure caption). When complex **II** was allowed to react with n-butylamine, two products were observed (Figure 4.2). The peak at m/z 295 is the dehydrogenation product (i.e. the butan-1-imine adduct of complex **II**). The peak at m/z 297 is the amine adduct of complex **II**. Dehydrogenation to form the alkene product would result in the same m/z as the imine adduct. This possibility must be taken into consideration since it is already known that **I** can produce alkenes via dehydrogenation. However, experiments with n-butylamine- d_9 solely exhibited HD loss, confirming the identity of the dehydrogenation product to be the butan-1-imine adducts with each metal complex (Appendix A.8 & A.9). In other words, **I** and **II** are capable of selective dehydrogenative imine formation. Ion-molecule reactions in our system occur at room temperature even after subjecting the ion to isolation voltages or CID, due to the collision-cooling of the helium buffer gas.^{68,69,87} However, elevated temperatures are typically required to overcome the inherent endothermicity of the dehydrogenation process. The impetus for the dehydrogenation of amines in our system is the strong coordination of the metal complexes to the imine products.

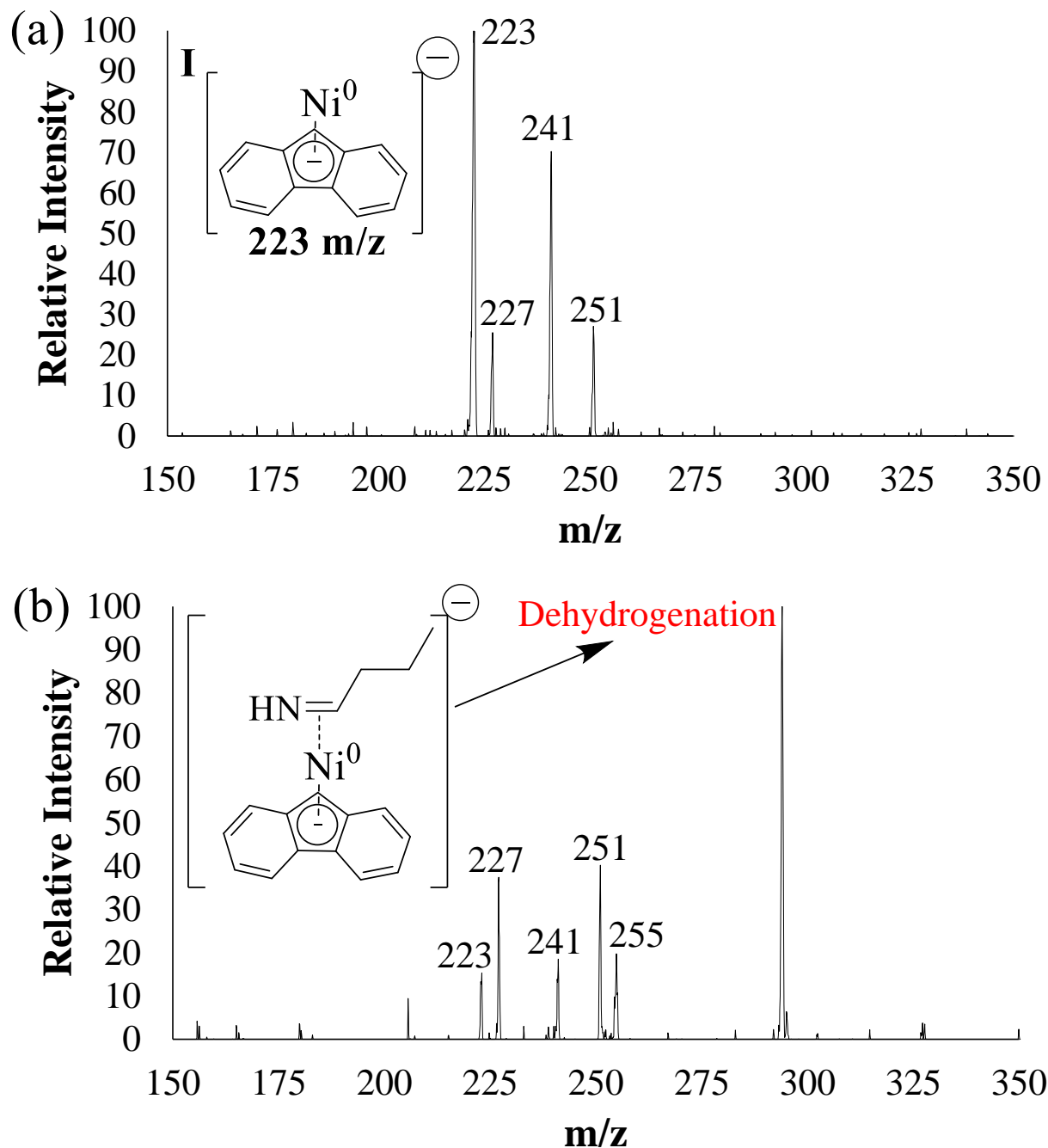


Figure 4.1. Spectra for the reaction of **I** with n-butylamine. Panel (a) Isolation of complex **I** prior to introduction of n-butylamine. Panel (b) Product spectrum after introduction of n-butylamine. The dehydrogenation product appears at m/z 294. Products of adduct formation with adventitious water, nitrogen, and methanol are also present and appear at m/z 241, 251, and 255 respectively. The peak at m/z 227 may be an adduct of fluorene-9-carboxylate and water formed through secondary reactions. There are also peaks (not shown) at m/z 90, a nickel oxide from reaction with adventitious oxygen, and m/z 107, an unidentified species that is independent of the neutral reagent.

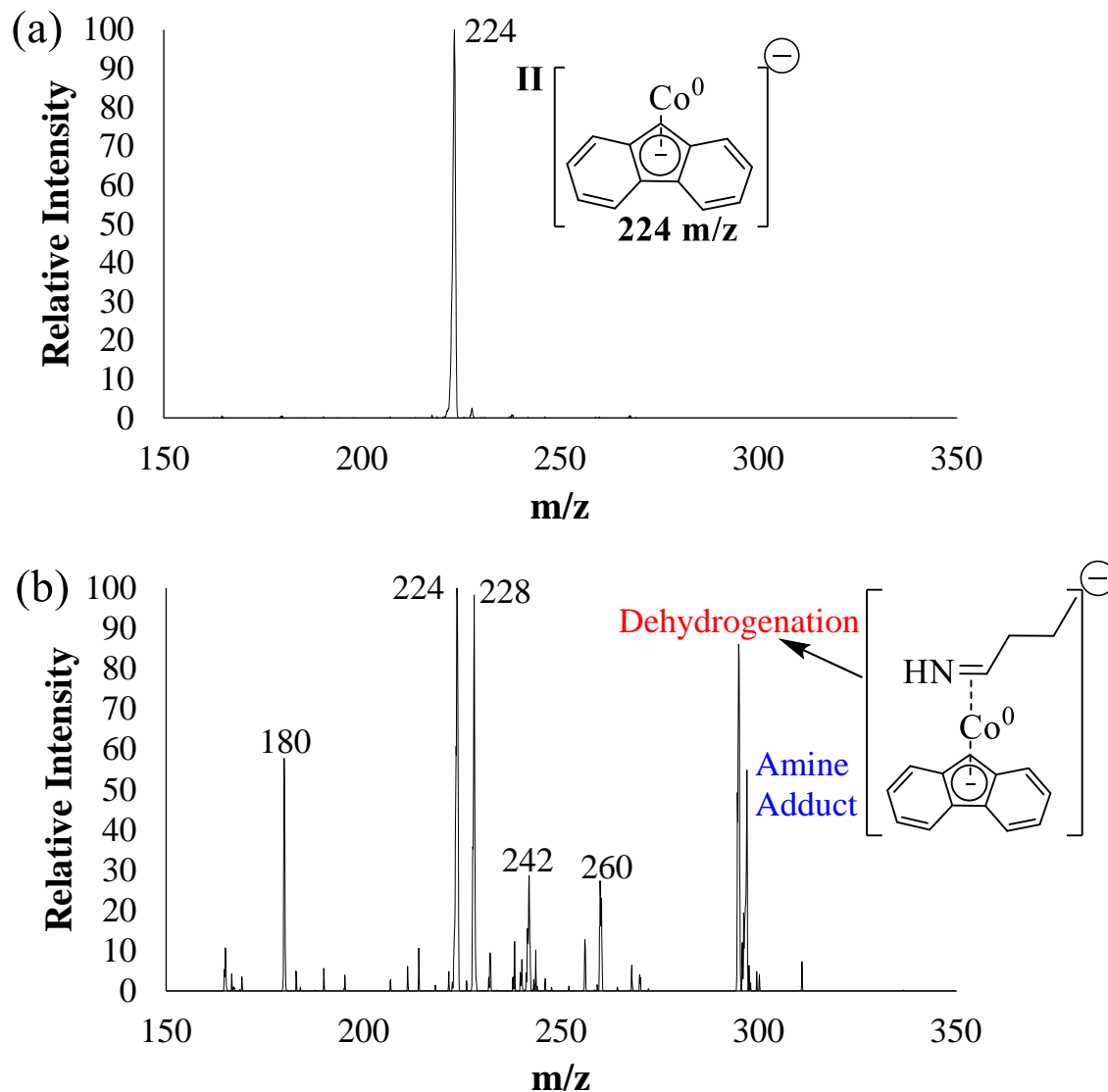


Figure 4.2. Spectra for the reaction of **II** with n-butylamine. Panel (a) Isolation of complex **II** prior to introduction of n-butylamine. Panel (b) Product spectrum after introduction of n-butylamine. The dehydrogenation and amine adduct products appear at m/z 295 and m/z 297, respectively. Peak broadening of the amine adduct is observed due to the relative instability of the ion during the instrument scans.³⁶ Products of adduct formation with adventitious water are present at m/z 242 and 260. A cobalt complex with adventitious methanol appears at m/z 91 and is the base peak (not shown). Unidentified species that are independent of the neutral reagent appear at m/z 180 and 228.

Complexes **I** and **II** are also capable of the dehydrogenation of alcohols. The reaction spectrum for the dehydrogenation of n-butanol by complex **I** is presented in Figure 4.3. Products of reactions

with butanol appear as four peaks. Similar to the alkane dehydrogenations, both the dehydrogenation (i.e. the butanal adduct with complex **I**) and the alcohol adduct products are formed (m/z 295 and 297, respectively). The peak at m/z 283 likely is an adduct of fluorene-9-carboxylate and *n*-butanol formed through secondary reactions. While the peak at m/z 251 appears without introduction of neutral reagent due to adduct formation with adventitious nitrogen, the significant increase in the peak intensity during experiments with *n*-butanol suggests a second species with m/z 251. DFT calculations indicate formation of an adduct of carbon monoxide of complex **I** with m/z 251 is exothermic and can be formed through decarbonylation of the butanol (Scheme 4.4). All other products are formed via reactions with adventitious species or the cyclohexane solvent used for dilution (see figure caption for details). Reactions with *n*-butanol-1,1,2,2- d_4 and *n*-butanol-3,3,4,4,4- d_5 confirmed the identity of the dehydrogenation product to be the butanal complex (Appendix A.10 & A.11).

Figure 4.4 depicts the dehydrogenation of *n*-butanol by complex **II**. The dehydrogenation and alcohol adduct peaks appear at m/z 296 and 298, respectively. Various products presumably formed via secondary reactions are also observed (see figure caption for details). Experiments with *n*-butanol-OD led to loss of HD and confirmed the identity of the dehydrogenation product to be the butanal complex (Appendix A.12). The product spectra for reaction with alcohols are more complicated than reactions with amines and alkanes. This is likely due to the very reactive nature of the aldehyde products. However, similar to the other dehydrogenation processes, the reactions with alcohols are likely driven by the strong coordination of the metal complexes to the aldehyde products. Isopropanol was also allowed to react with complexes **I** and **II**, resulting in acetone complexes (Appendix A.13 & A.14).

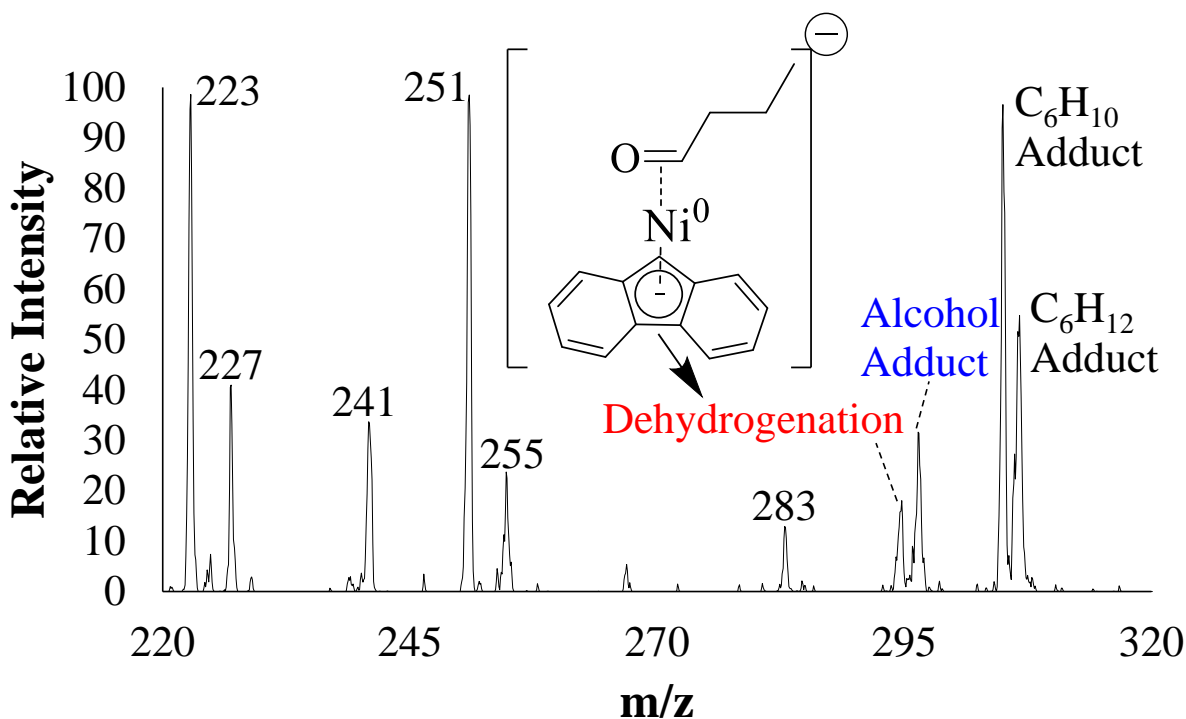
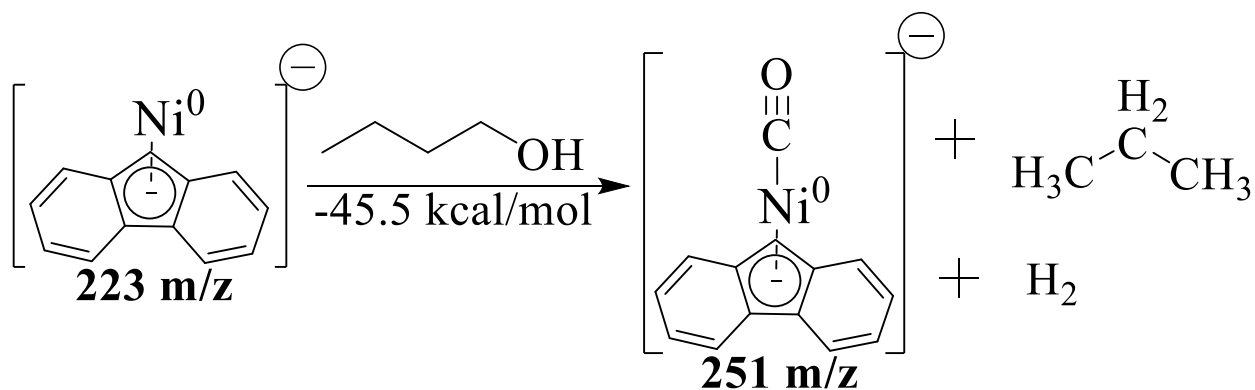


Figure 4.3. Product spectrum for the reaction of **I** with n-butanol. The dehydrogenation and alcohol adduct products appear at m/z 295 and 297, respectively. The peaks at m/z 283 and 227 may be adducts of fluorene-9-carboxylate with n-butanol and water, respectively, formed through secondary reactions. The peak at m/z 223 is complex **I**. Cyclohexene and cyclohexane adduct products formed via reaction with the cyclohexane solvent appear m/z 305 and 307. Products of adduct formation with adventitious water, nitrogen, and methanol are also present and appear at m/z 241, 251, and 255 respectively. The increased signal of m/z 251 also suggests a carbon monoxide adduct. There are also peaks (not shown) at m/z 90, a nickel oxide from reaction with adventitious oxygen, and m/z 107, an unidentified species that is independent of the neutral reagent.



Scheme 4.4. Decarbonylation of butanal by complex **I**. DFT calculations suggest this process is exothermic by 45.5 kcal/mol. DFT calculations performed at the M06/6-311+G** level. Detailed information on the structures and frequencies of the calculated species are given in Appendix C.

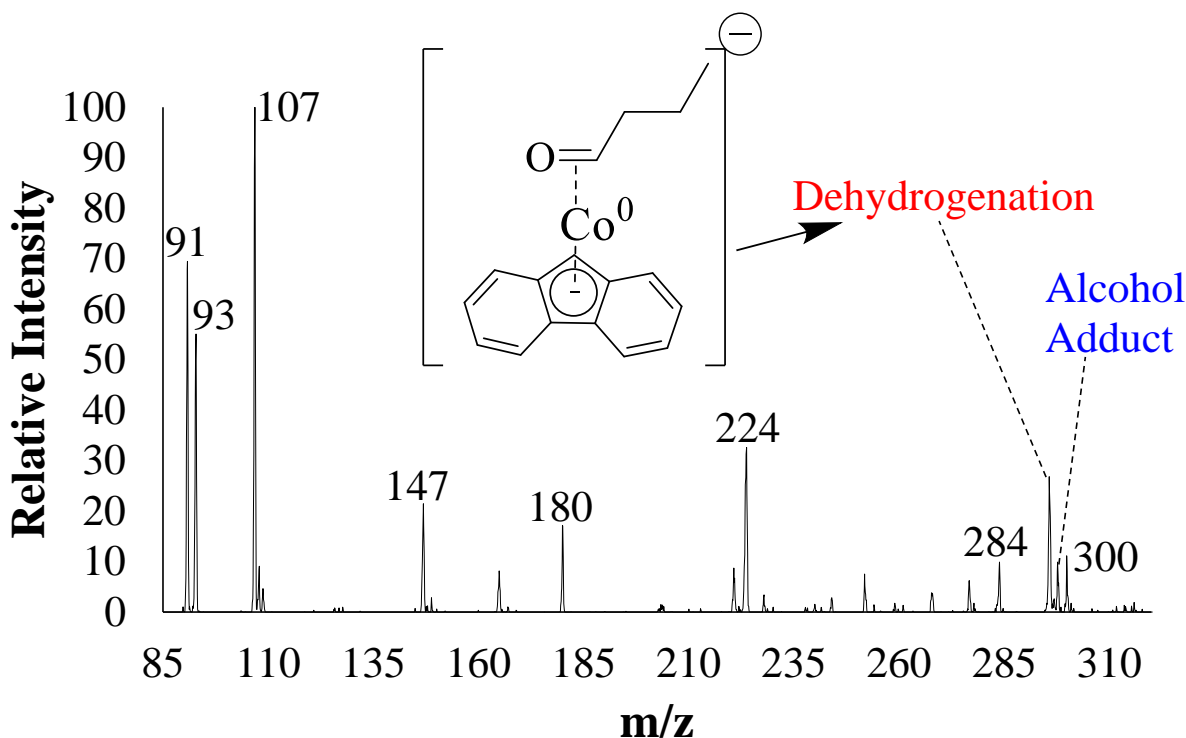


Figure 4.4. Product spectrum for the reaction of **II** with n-butanol. The dehydrogenation and alcohol products appear at m/z 296 and 298, respectively. Complex **II** appears at m/z 224. A metal adduct with adventitious methanol appears at m/z 91. Peaks at m/z 93, 107, 147, 284, and 300 are likely formed via secondary reactions with adventitious species. An unidentified species that is independent of the neutral reagent appears at m/z 180.

4.3 Mechanistic Studies for the Dehydrogenation of Amines

Kinetics experiments with deuterium-labeled neutral reagents were performed to determine KIEs which are shown in Table 2. The two methods used to calculate KIE values in this study are shown in Scheme 4.5. Intensities of products generated via ion-molecule reactions in our system are directly proportional to the rate of their respective reactions. Method A requires data from two separate reactions: dehydrogenation of the hydrogen-labeled reagent and dehydrogenation of the deuterium-labeled reagent. The intensity of the dehydrogenation product for the hydrogen-labeled reagent was taken relative to an unrelated product ion from an adventitious species that is in both reactions. The same calculation was performed for the dehydrogenation product of the deuterium-labeled reagent. A ratio of the two resulting values provided the KIE values.

Table 2. Kinetic isotope effects for amine and alcohol dehydrogenations.

M = Ni, Co
Z = NH, OH

Metal Complex	Neutral Reagent	KIE
I	Piperidine-ND	2.0
I	n-Butanol-OD	0.9
I	n-Butanol-1,1-d ₂	1.5
II	Diethylamine-ND	1.7
II	n-Butanol-OD	0.9
II	n-Butanol-1,1,2,2-d ₄	1.3

<p>Method A</p> $\frac{\text{Intensity of H-dehydrogenation}}{\text{Intensity of unrelated product}} = \text{Relative } k_H$ $\frac{\text{Intensity of D-dehydrogenation}}{\text{Intensity of unrelated product}} = \text{Relative } k_D$ $\frac{\text{Relative } k_H}{\text{Relative } k_D} = \text{KIE}$
<p>Method B</p> $\frac{\text{Intensity of H-dehydrogenation}}{\text{Intensity of D-dehydrogenation}} = \text{KIE}$

Scheme 4.5. Calculations used to obtain KIE values for the dehydrogenation of amines and alcohols by complexes **I** and **II**.

Method A was used to determine KIEs in the reactions with complex **I**. The methanol adduct was used as the adventitious product in the calculations for piperidine-ND. In the calculations for the

alcohol KIEs, the cyclohexene adduct, formed by reaction with the cyclohexane solvent, was used as the adventitious product. Method A was also used to determine KIEs for the reactions of diethylamine-ND and n-butanol-OD with complex **II**. In the experiments to determine the KIE of the diethylamine-ND reaction, chlorobenzene was mixed in with the amine reagents since complex **II** was capable of engaging in oxidative addition reactions with aryl halides (see chapter 5). The insertion product of the reaction with chlorobenzene was used as the unrelated product in the calculations for diethylamine. In experiments to determine the KIE of n-butanol-OD, n-butanol- d_{10} was mixed in with the other butanol reagents to produce a separate dehydrogenation product in the spectra. This product was used as the unrelated product in the calculations for n-butanol-OD.

Method B was used to calculate the KIE of n-butanol-1,1,2,2- d_4 . In this method, the deuterated neutral reagent was mixed with butanol to obtain a 50% by volume solution which was introduced into the ion trap for reaction with the metal complex. Due to the wide m/z separation of the dehydrogenation products, the intensity of the hydrogen-labeled product was taken relative to the deuterium labeled product intensity, resulting in the KIE value. Method A has more uncertainty than method B because it assumes that the reactions with adventitious or added species are consistent across two experiments. However, method B is only possible when the m/z values of the products of interest are distinct. Dehydrogenation of reagents such as piperidine-ND result in the same product as the dehydrogenation of the hydrogen-labeled reagent and are indistinguishable when formed in the same experiment. In these cases, method A is better suited for KIE determination.

Dehydrogenation of piperidine-ND by complex **I** revealed a KIE of 2.0 (Table 2). This value strongly suggests N-H(D) bond activation during the rate-limiting step of the reaction. This is

corroborated by the dehydrogenation of butylamine- d_9 and butylamine- ND_2 by complex **I**, as depicted in Figure 4.5. When reacting with butylamine- d_9 , the only product observed is the imine adduct that appears at m/z 302. However, in the reaction with butylamine- ND_2 , two dehydrogenation products are observed. The imine adduct appears at m/z 295 while an alkene adduct appears at m/z 296. These results indicate that imine formation is not greatly hindered by an isotope effect in the C-H activation component if the alpha carbon is deuterated. Alkene formation would be hindered in this case by deuteration at both alpha and beta sites. Conversely, the imine formation process is hindered by an isotope effect in the N-H activation if nitrogen is deuterated, allowing alkene formation to become a competitive outlet because it suffers from no isotope effects.

Barriers for imine and alkene formation in the dehydrogenation of n-butylamine by complex **I** were computed using DFT calculations, performed at the M06/6-311+G** level, and the results are shown in Figure 4.6. Panels (a) and (b) depict two potential pathways to imine formation. In panel (a), the first TS is an insertion into the N-H bond by complex **I** that is 15.2 kcal/mol below the entrance channel. The second TS is a β -hydride elimination which involves C-H activation on the alpha carbon and is 19.5 kcal/mol below the reactants. In Panel (b) the activation order is reversed. The first TS is an insertion into a C-H bond on the alpha carbon that sits 17.4 kcal/mol below the reactants. The second TS is a β -hydride elimination which activates the N-H bond and is 7.9 kcal/mol below the reactants. Both suggested pathways indicate N-H activation is the rate-determining step and are in accordance with the deuterium-labeled isotope effect studies mentioned above. Both pathways are favorable, however, there is a preference for the pathway in panel (a). In addition to imine formation, alkene formation is depicted in panel (c). In Panel (c), the first TS is the same C-H insertion shown in panel (b). However, in order to generate the alkene,

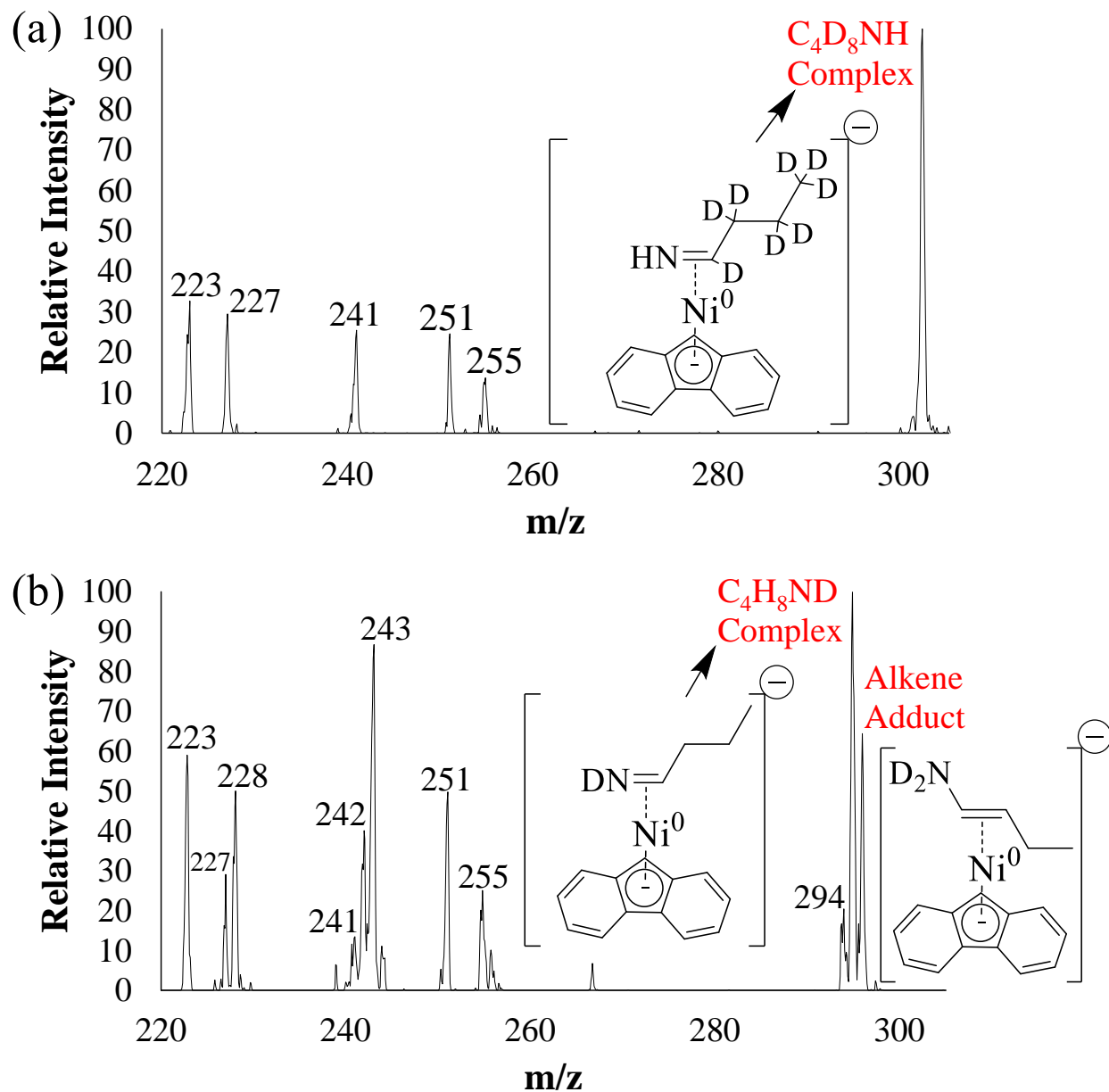


Figure 4.5. Product spectra for reactions of deuterium-labeled n-butylamine reagents with complex I. Panel (a) depicts the reaction of I with n-butylamine-d₉. The imine adduct peak for this reaction appears at m/z 302. Panel (b) depicts the reaction of I with n-butylamine-ND₂. An alkene adduct appears at m/z 296. An imine adduct appears at m/z 295 with loss of HD. The peak at m/z 294 is likely an imine adduct formed with the loss of D₂, due to HD exchange between the N and the alpha C. Products of adduct formation with adventitious water, nitrogen, and methanol are also present and appear at m/z 241, 251, and 255 respectively. The peaks at m/z 242 and 243 are likely formed via HD exchange between the water adduct and the neutral reagent. The peak at m/z 227 may be an adduct of fluorene-9-carboxylate and water formed through secondary reactions. The peak at m/z 228 is likely formed via HD exchange between the m/z 227 species and the neutral reagent. There are also peaks (not shown) at m/z 90, an oxide from reaction with adventitious oxygen, and m/z 107, an unidentified species that is independent of the neutral reagent.

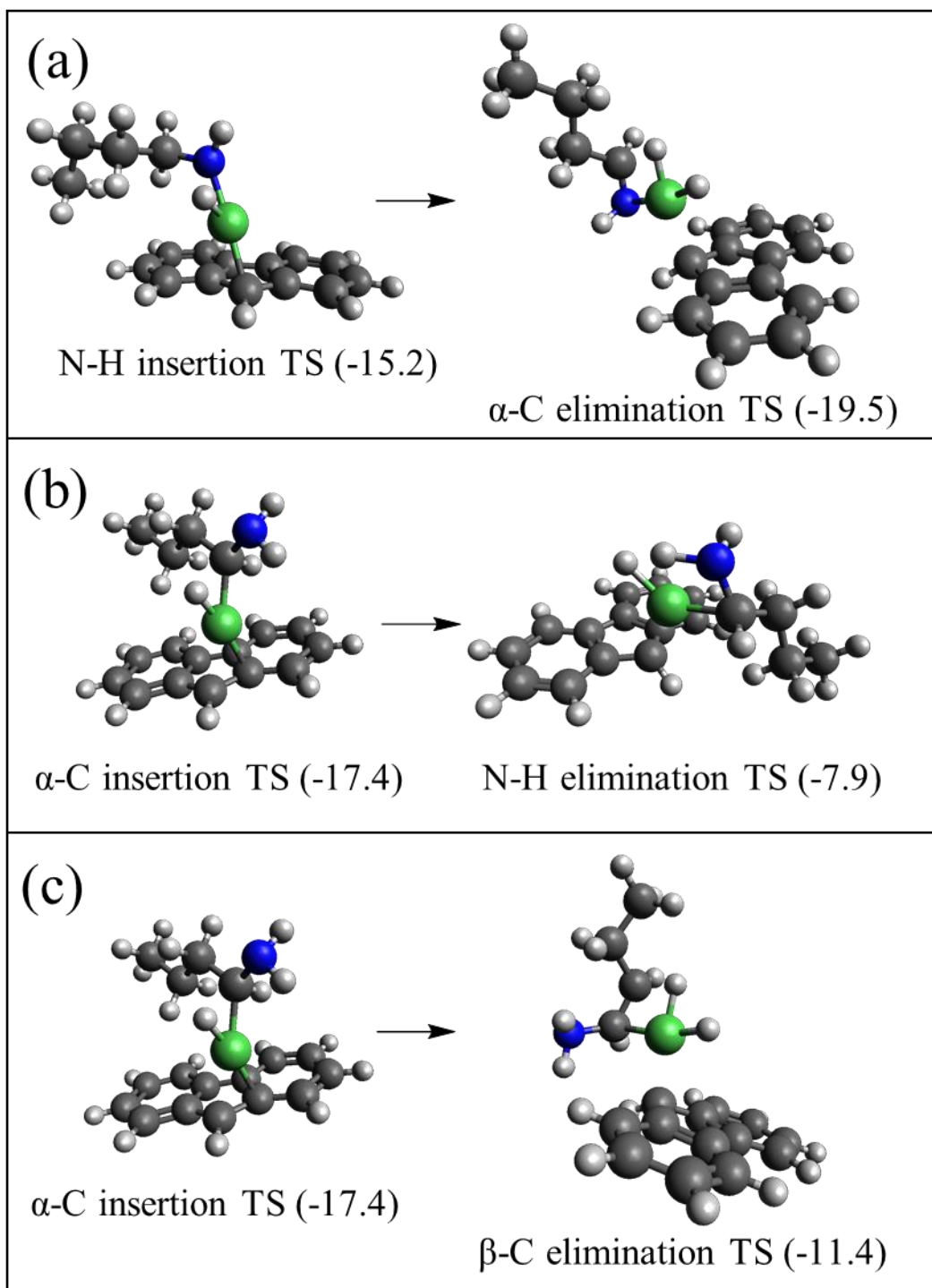


Figure 4.6. Transition states for the dehydrogenation of butylamine by complex **I** to give the imine and alkene adduct products. Panel (a) depicts N-H insertion followed by α -C elimination. Panel (b) depicts α -C insertion followed by N-H elimination. Panel (c) depicts α -C insertion followed by β -C elimination. Enthalpies for transition states are in kcal/mol. DFT calculations were performed at the M06/6-311+G** level. Detailed information on the structures and frequencies of the calculated species are shown in Appendix C.

the second TS is a β -hydride elimination that activates a C-H bond on the beta carbon and is 11.4 kcal/mol below the reactants. In other words, when initial activation occurs on the alpha carbon, alkene formation is favored by 3.5 kcal/mol. If alpha carbon activation occurred first, one might expect to see the appearance of the alkene adduct product in the reaction with butylamine- d_9 despite the isotope effect. On the contrary, the product spectrum solely reveals imine formation. The initial C-H and N-H insertion barriers are relatively similar, so it is difficult to make any definitive mechanistic statements with respect to the pathways in Figure 4.6.

As an example pathway, DFT calculations were used to link the TSs in panel (a) to the respective intermediates and the resulting potential energy surface is depicted in Figure 4.7. The first step which proceeds via the N-H insertion TS gives a reaction that is exothermic by 30.7 kcal/mol. In the following β -hydride elimination TS, the structure suggests the metal is able to bring the β -hydrogen close to the initially abstracted hydrogen, resulting in an adduct with both the hydrogen molecule and the imine (exothermic by 29 kcal/mol). Lastly, the metal center expels the hydrogen molecule to form the adduct with butan-1-imine, resulting in an overall reaction that is exothermic by 26.2 kcal/mol.

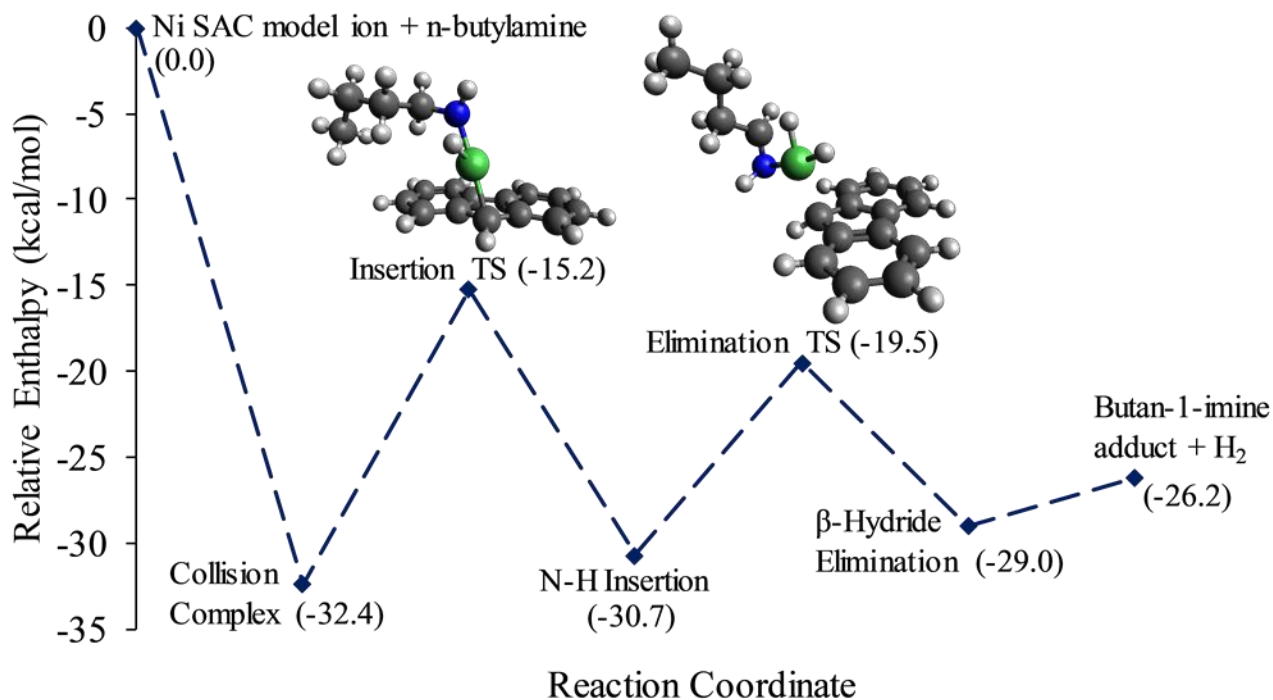


Figure 4.7. Potential energy surface for the dehydrogenation of butylamine by complex **I**. DFT calculations performed at the M06/6-311+G** level. Detailed information on the structures and frequencies of the calculated species are shown in Appendix C.

Isotope effects of amine dehydrogenations by complex **II** are similar. Experiments with diethylamine-ND reveal a KIE of 1.7 for dehydrogenation by complex **II**, suggesting N-H bond breakage during the rate-limiting step. DFT calculations suggest a viable pathway to dehydrogenation via the two TSs depicted in Figure 4.8 (a). The first step is an N-H insertion by complex **II** that is 11.9 kcal/mol below the reactants. The second step is C-H activation of the alpha carbon via a β -hydride elimination TS that is 16.6 kcal/mol below the reactants. A pathway to dehydrogenation via initial C-H insertion was also explored and is depicted in Figure 4.8 (b). C-H insertion on the alpha carbon proceeds via a TS that is 8.0 kcal/mol below the reactants. The following TS for the β -hydride elimination of the N-H bond is 4.2 kcal/mol above the reactants. The calculations suggest that both N-H activation steps of the pathways depicted in Figure 4.8 (a) and (b) are the rate-limiting steps. However, N-H activation in panel (a) is favored by 16.1

kcal/mol. This preference suggests that complex **II** performs the dehydrogenation of diethylamine via the pathway depicted in Figure 4.8 (a). The potential energy surface for the dehydrogenation of diethylamine by complex **II** is depicted in Figure 4.9. While the surface is higher in energy compared to complex **I**, DFT calculations suggest the overall dehydrogenation reaction is exothermic by 5.9 kcal/mol. The mechanism for the dehydrogenation of amines by complexes **I** and **II** is shown in Scheme 4.6.

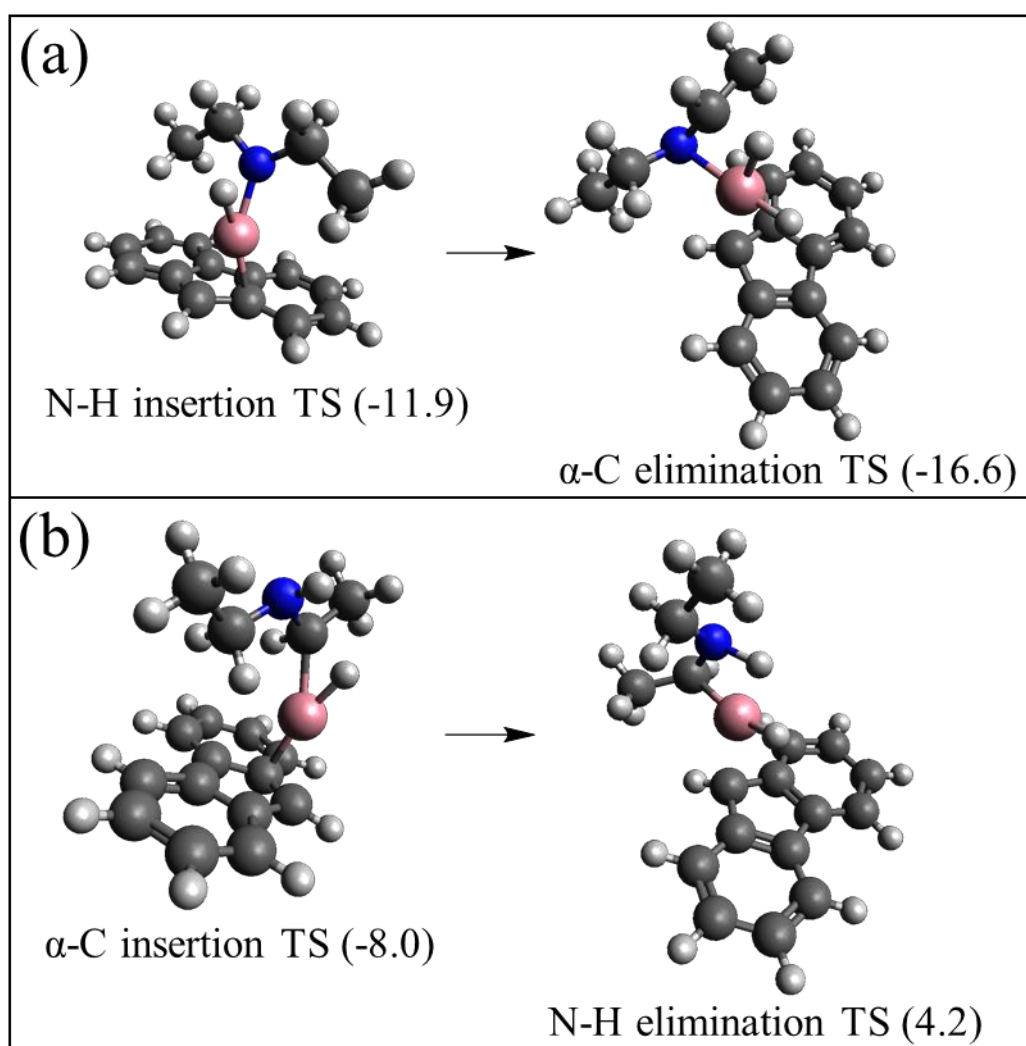


Figure 4.8. Transition states for the dehydrogenation of diethylamine by complex **II** to give the imine adduct product. Panel (a) depicts N-H insertion followed by α -C elimination. Panel (b) depicts α -C insertion followed by N-H elimination. Enthalpies for transition states are in kcal/mol. DFT calculations were performed at the M06/6-311+G** level. Detailed information on the structures and frequencies of the calculated species are shown in Appendix C.

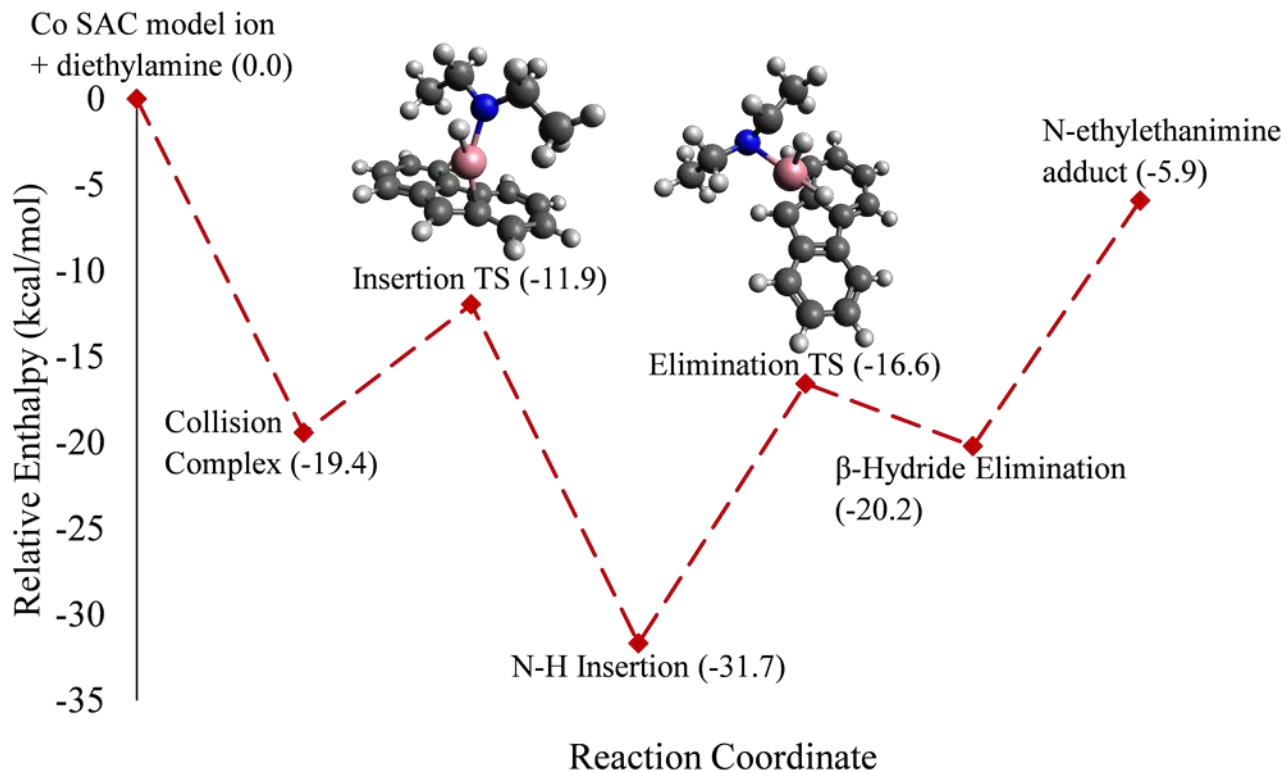
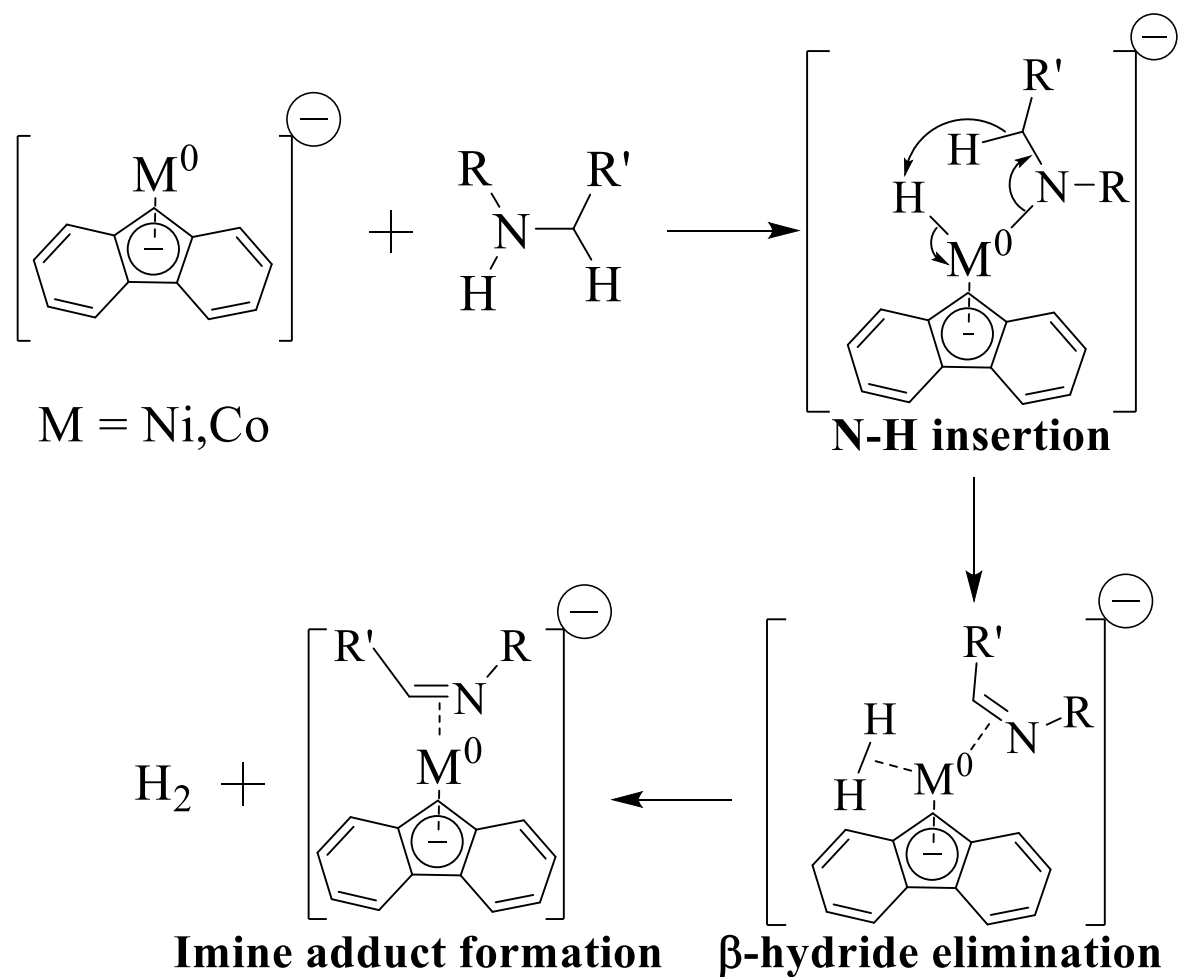


Figure 4.9. Potential energy surface for the dehydrogenation of diethylamine by complex **II**. DFT calculations performed at the M06/6-311+G** level. Detailed information on the structures and frequencies of the calculated species are shown in Appendix C.



Scheme 4.6. Mechanism for the dehydrogenation of amines by complexes **I** and **II**.

4.4 Mechanistic Studies for the Dehydrogenation of Alcohols

Dehydrogenation of butanol-OD and butanol-1,1-d₂ by complex **I** revealed KIEs of 0.9 and 1.5, respectively. These deuterium effects do not provide strong evidence for a particular dehydrogenation mechanism, so DFT calculations were used to gain further insight into the reaction mechanism. Figure 4.10 depicts two dehydrogenation pathways that can generate the aldehyde adduct. In panel (a), the first TS is an insertion into the O-H bond that is 12.3 kcal/mol below the reactants. The second TS is a β -hydride elimination which activates a C-H bond on the

alpha carbon and is 28.5 kcal/mol below the reactants. In panel (b), the first TS is an insertion into a C-H bond of the alpha carbon that is 18.8 kcal/mol below the reactants. The second TS is a β -hydride elimination that activates the O-H bond and is 11.1 kcal/mol below the reactants. These calculations suggest a small preference for the pathway in panel (a) by 1.2 kcal/mol. Alkene formation was also explored and is depicted in Figure 4.10 (c). The first TS for alkene formation is insertion into a C-H bond of the alpha carbon, as seen in the first TS in panel (b) at 18.8 kcal/mol below the reactants. The second TS is a β -hydride elimination which activates a C-H bond on the beta carbon and is 13.3 kcal/mol below the reactants. The calculations suggest that, compared to the pathway in panel (b), alkene formation is favorable by 2.2 kcal/mol. If complex **I** enacted dehydrogenation by initial insertion into a C-H bond on the alpha carbon, then alkene formation would also be expected to appear in the reaction spectra. However, experiments with n-butanol-1,1,2,2-d₄ resulted in a loss of HD instead of D₂ (Appendix A.11). These results and the experiments with n-butanol-3,3,4,4,4-d₅ (Appendix A.12) confirm that complex **I** does not form an alkene on any portion of the alkyl chain. Therefore, dehydrogenation to form the aldehyde adduct likely occurs via the pathway depicted in Figure 4.10 (a). The preference for aldehyde formation might be driven by the initial complexation of the nickel to the oxygen, which predisposes the system to a reaction along the C-O bond. Using DFT calculations, the TSs in panel (a) were linked to their respective intermediates to produce a potential energy surface, depicted in Figure 4.11.

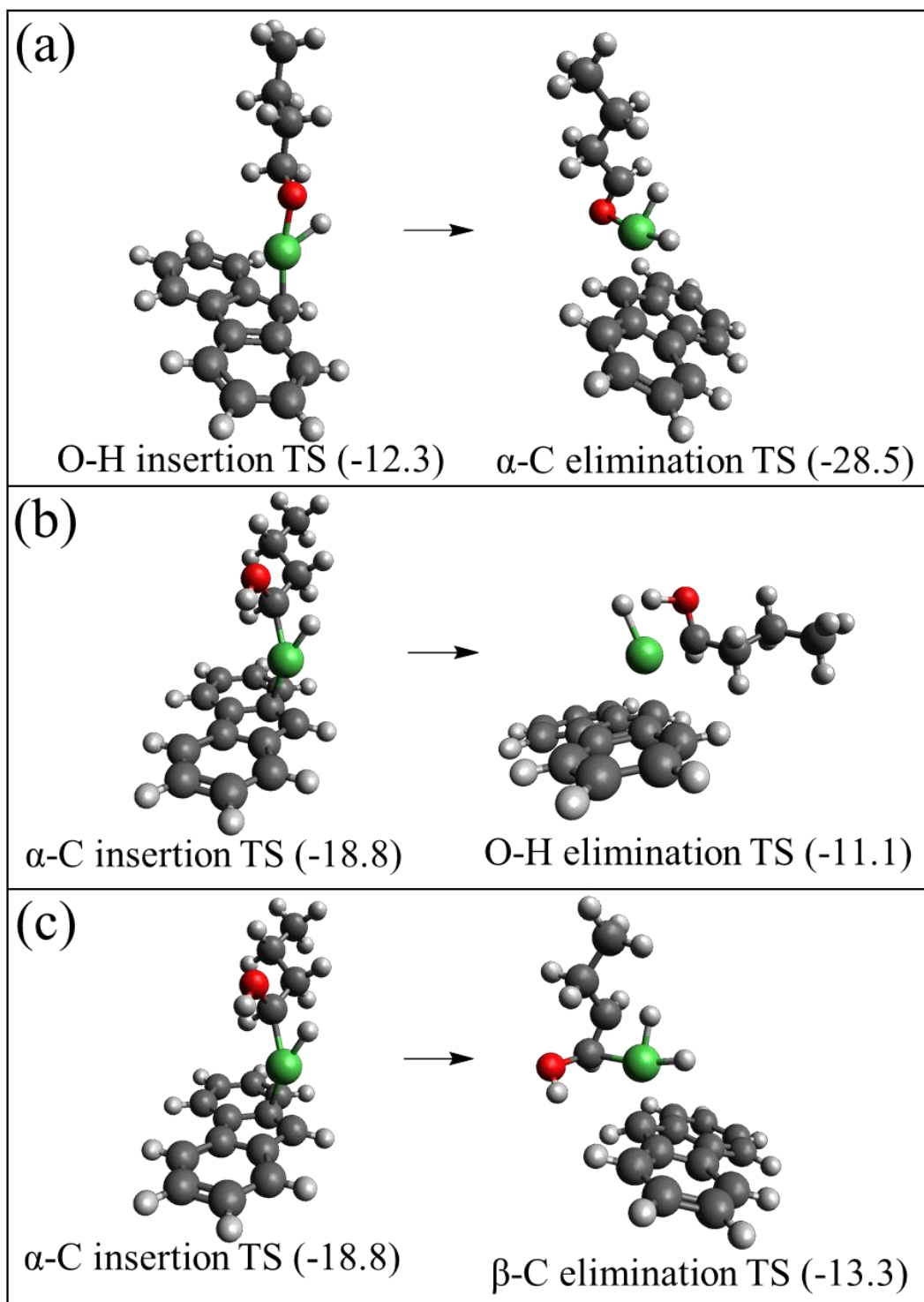


Figure 4.10. Transition states for the dehydrogenation of butanol by complex **I** to give the aldehyde and alkene adduct products. Panel (a) depicts O-H insertion followed by α -C elimination. Panel (b) depicts α -C insertion followed by O-H elimination. Panel (c) depicts α -C insertion followed by β -C elimination. Enthalpies for transition states in kcal/mol. DFT calculations were performed at the M06/6-311+G** level. Detailed information on the structures and frequencies of the calculated species are shown in Appendix C.

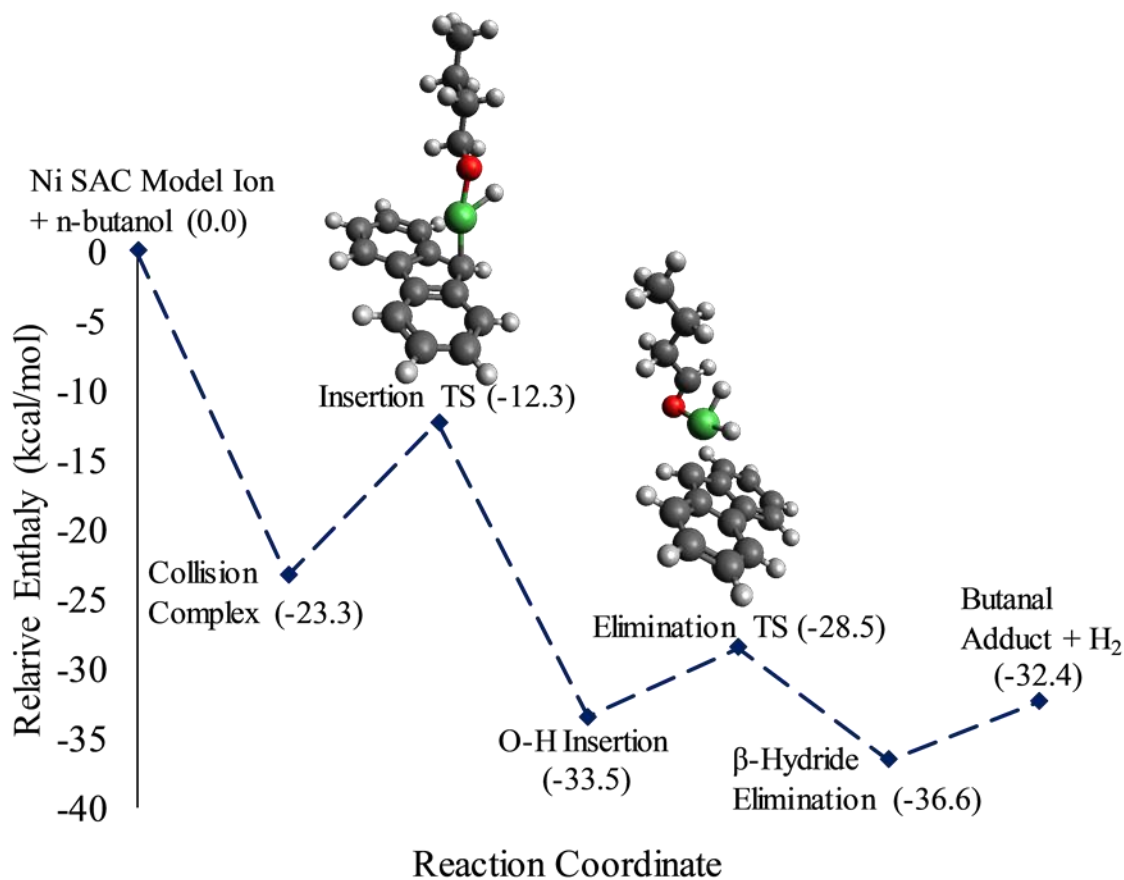
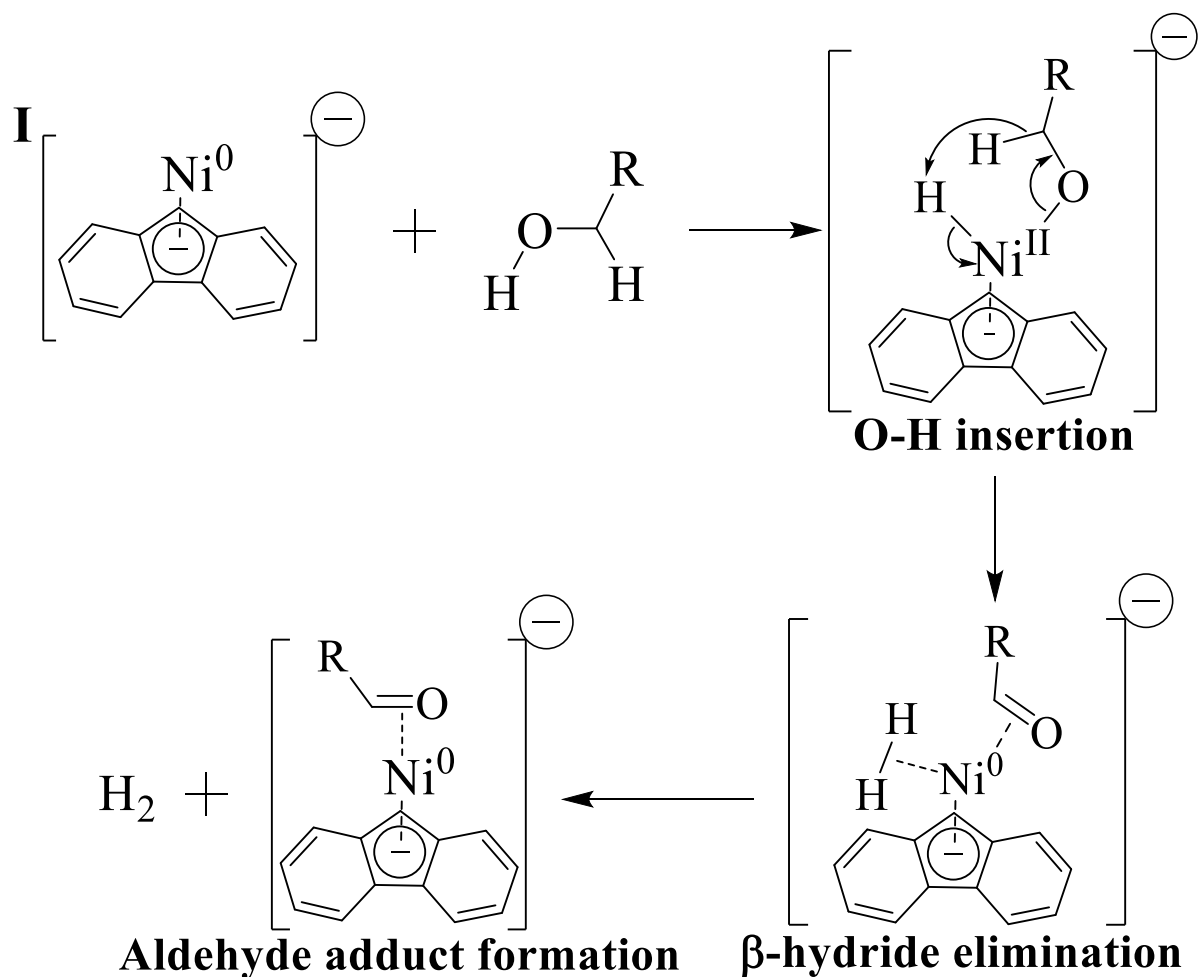


Figure 4.11. Potential energy surface for the dehydrogenation of butanol by complex **I**. DFT calculations performed at the M06/6-311+G** level. Detailed information on the structures and frequencies of the calculated species are shown in Appendix C.

The dehydrogenation of n-butanol by complex **I** is exothermic by 32.4 kcal/mol. While TSs for the amine dehydrogenation were closer in energy, the elimination TS for the dehydrogenation of n-butanol is much lower in energy than the insertion TS. This is likely due to the stronger coordination of the metal to the carbonyl. The general mechanism for the dehydrogenation of alcohols by complex **I** is shown in Scheme 4.7.



Scheme 4.7. Mechanism for the dehydrogenation of alcohols by complex **I**.

Similar to the experiments with complex **I**, dehydrogenations of butanol-OD and butanol-1,1,2,2- d_4 by complex **II** revealed KIEs of 0.9 and 1.3, respectively. Again, these deviations from unity are not large enough to confidently suggest mechanistic information. However, DFT calculations suggest two competitive pathways for the dehydrogenation of butanol by complex **II**, depicted in Figure 4.12. In panel (a), the first TS is an insertion into the O-H bond by complex **II** that is 6.0 kcal/mol below the reactants. The second TS is a β -hydride elimination that activates a C-H bond on the alpha carbon and is 26.0 kcal/mol below the reactants. The second pathway in panel (b) involves initial C-H insertion on the alpha carbon via a TS that is 9.5 kcal/mol below the reactants.

The following TS is a β -hydride elimination which activates the O-H bond and is 6.9 kcal/mol below the reactants. These calculations indicate the pathway in panel (b) is favored by 0.9 kcal/mol. However, this preference is not large enough to distinguish between the two pathways and, unlike the dehydrogenation mechanism described previously, complex **II** may enact alcohol dehydrogenation via both pathways. DFT calculations were used to link the TSs of panel (a) to their respective intermediates to produce a representative potential energy surface, depicted in Figure 4.13. The calculations suggest the dehydrogenation process is exothermic by 23.0 kcal/mol.

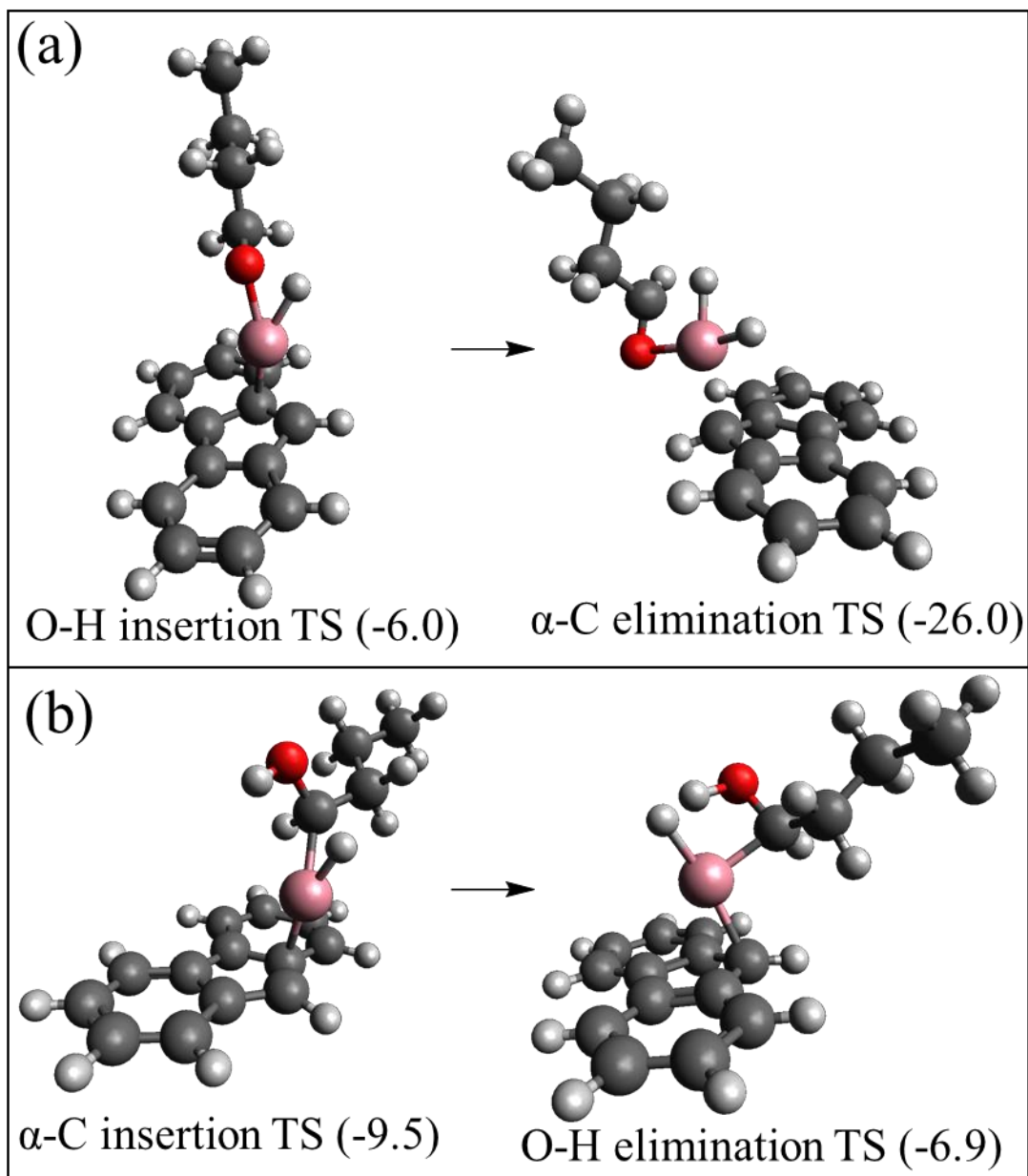


Figure 4.12. Transition states for the dehydrogenation of butanol by complex **II** to give the aldehyde adduct products. Panel (a) depicts O-H insertion followed by α -C elimination. Panel (b) depicts α -C insertion followed by O-H elimination. Enthalpies for transition states are in kcal/mol. DFT calculations were performed at the M06/6-311+G** level. Detailed information on the structures and frequencies of the calculated species are shown in Appendix C.

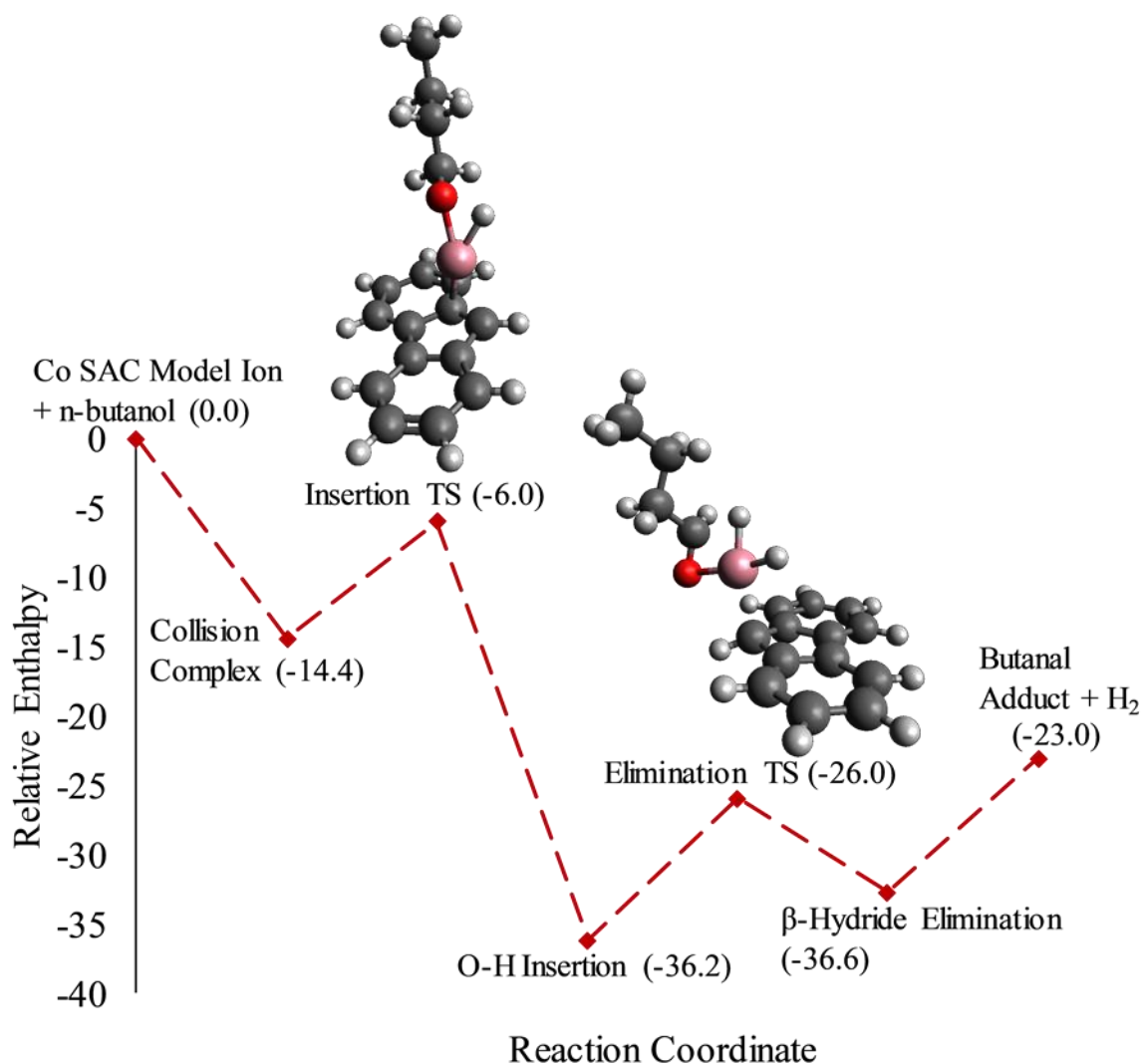
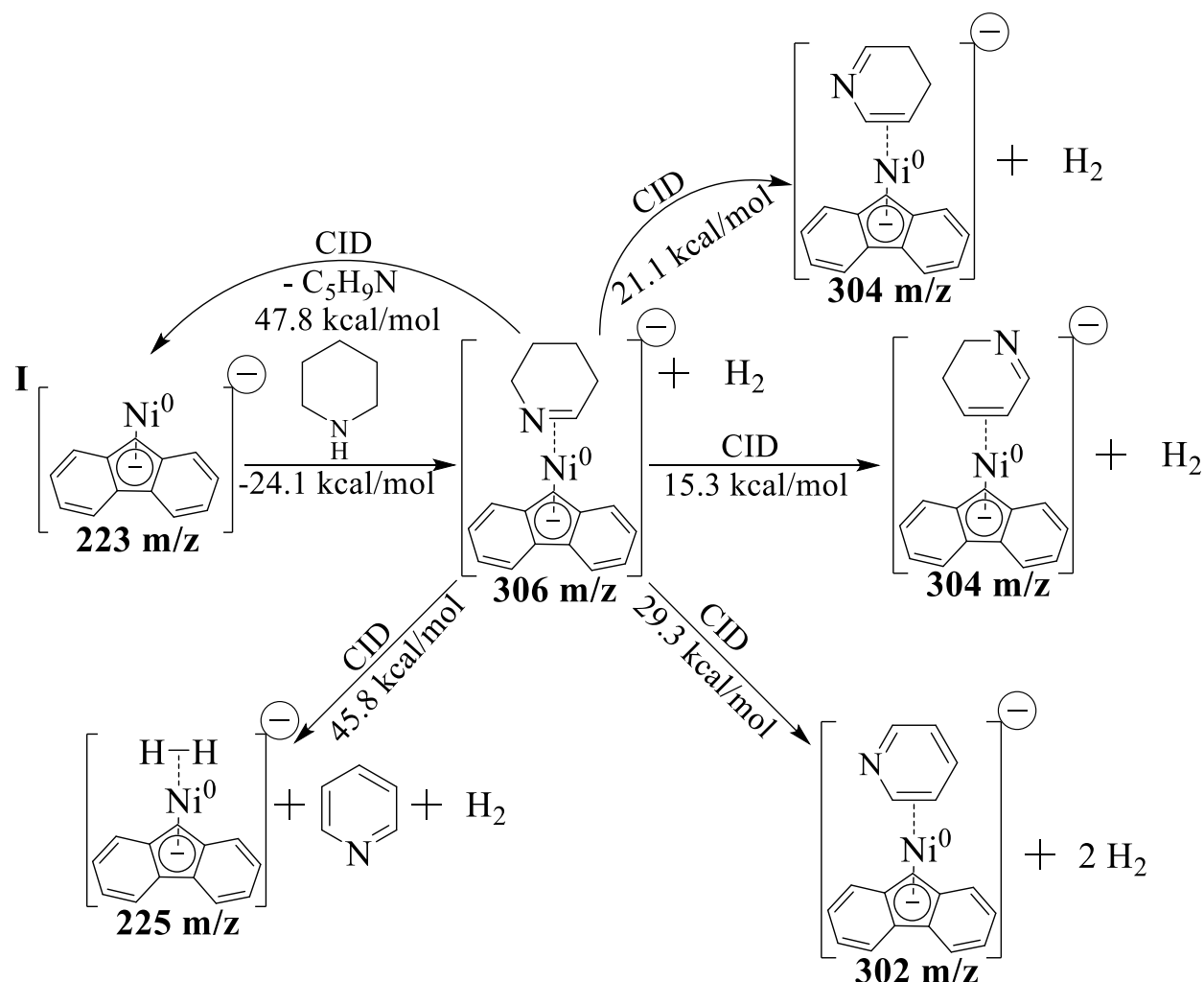


Figure 4.13. Potential energy surface for the dehydrogenation of butanol by complex **II**. DFT calculations performed at the M06/6-311+G** level. Detailed information on the structures and frequencies of the calculated species are shown in Appendix C.

4.5 Additional Reactivity

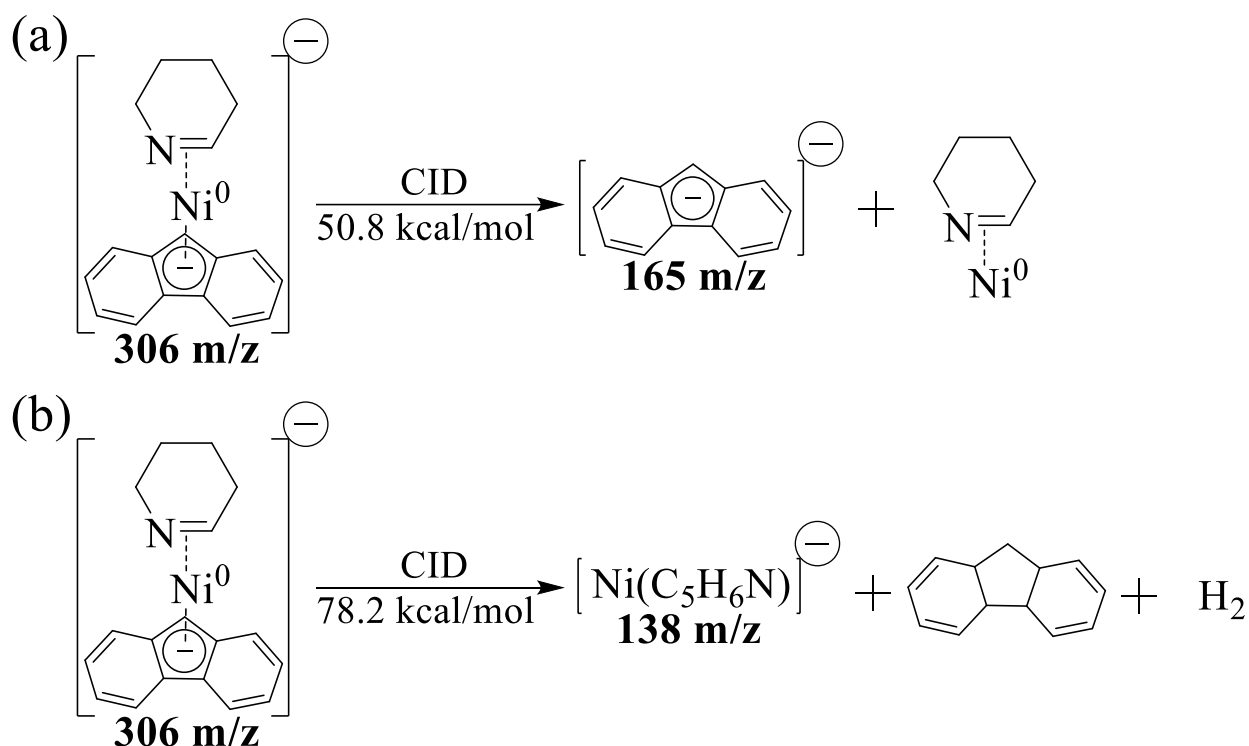
In the previous chapter, complex **I** was capable of sequential dehydrogenations when the alkene adduct products were subjected to CID. To explore this possibility, tandem mass spectrometry experiments were carried out with products from the reactions with amine and alcohols and the results indicated that the product complexes are also capable of additional reactivity. Scheme 4.8 depicts the reaction pathways for piperidine and complex **I**. When the 2,3,4,5-tetrahydropyridine complex with **I** is isolated and subjected to CID, additional dehydrogenations occur, resulting in

the formation of 3,4-dihydropyridine, 2,3-dihydropyridine, and pyridine. These processes are endothermic by 21.1 kcal/mol, 15.3 kcal/mol, and 29.3 kcal/mol, respectively. CID provides the energy necessary to enable these reactions. While formation of 2,3-dihydropyridine is favored over 3,4-dihydropyridine by 5.8 kcal/mol, the excess energy provided via the collisions with buffer gas will likely allow for the production of both adducts. The hydrogen molecule adduct of complex **I** is observed and requires 45.8 kcal/mol of activation. Recovery of complex **I**, by release of 2,3,4,5-tetrahydropyridine, is also observed and requires 47.8 kcal/mol of activation.



Scheme 4.8. Dehydrogenation pathways for reaction of piperidine with complex **I**. Reaction enthalpies were performed at the M06/6-311+G** level. Detailed information on the structures and frequencies of the calculated species are shown in Appendix C.

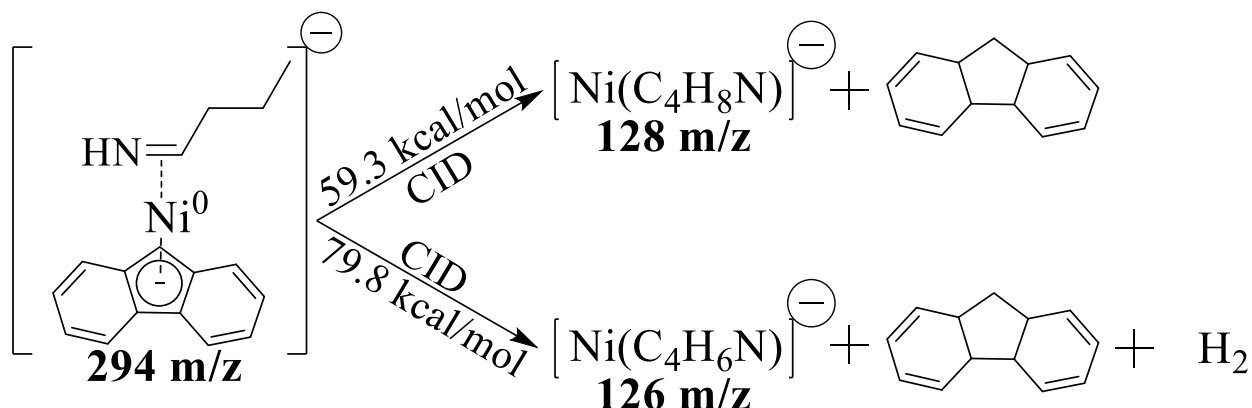
In addition to sequential dehydrogenations, release of the fluorenyl scaffold was also observed as two products (Scheme 4.9). In panel (a), the fluorenyl anion is released. Panel (b), depicts release of fluorene and formation of an anion comprised of either 2,3-dihydropyridine or 3,4-dihydropyridine bound to Ni. Based on the observed m/z value, it seems this process occurs after a second dehydrogenation has taken place and a hydrogen molecule has been released. At this point, due to the input of energy via CID, the fluorenyl scaffold can abstract a hydrogen from the imine ring, facilitating the formation of fluorene and the observed organometallic anion.



Scheme 4.9. Observed fluorenyl scaffold fragmentation products via CID activation of the 2,3,4,5-tetrahydropyridine adduct with complex **I**. DFT calculations performed at the M06/6-311+G** level. Detailed information on the structures of the calculated species are shown in Appendix C.

Tandem mass spectrometry revealed similar reactivity in reactions of complex **I** with *n*-butylamine (Scheme 4.10). When the butan-1-imine adduct of complex **I** was isolated and subjected to CID, a product ion at m/z 128 was observed. This product ion may be formed via a hydrogen abstraction

from the nitrogen, alpha carbon, or beta carbon of the imine by the fluorenyl scaffold to form fluorene. A product ion at 126 m/z is also observed, indicating the loss of the fluorene scaffold, followed by dehydrogenation of the amine ligand.

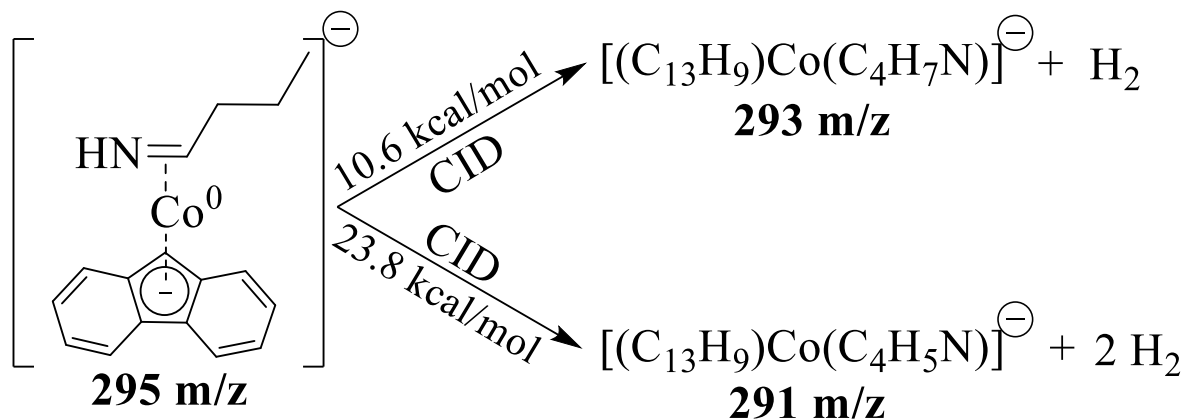


Scheme 4.10. Reaction pathways for the CID of the butan-1-imine adduct with complex **I**. DFT calculations performed at the M06/6-311+G** level. Detailed information on the structures of the calculated species are shown in Appendix C.

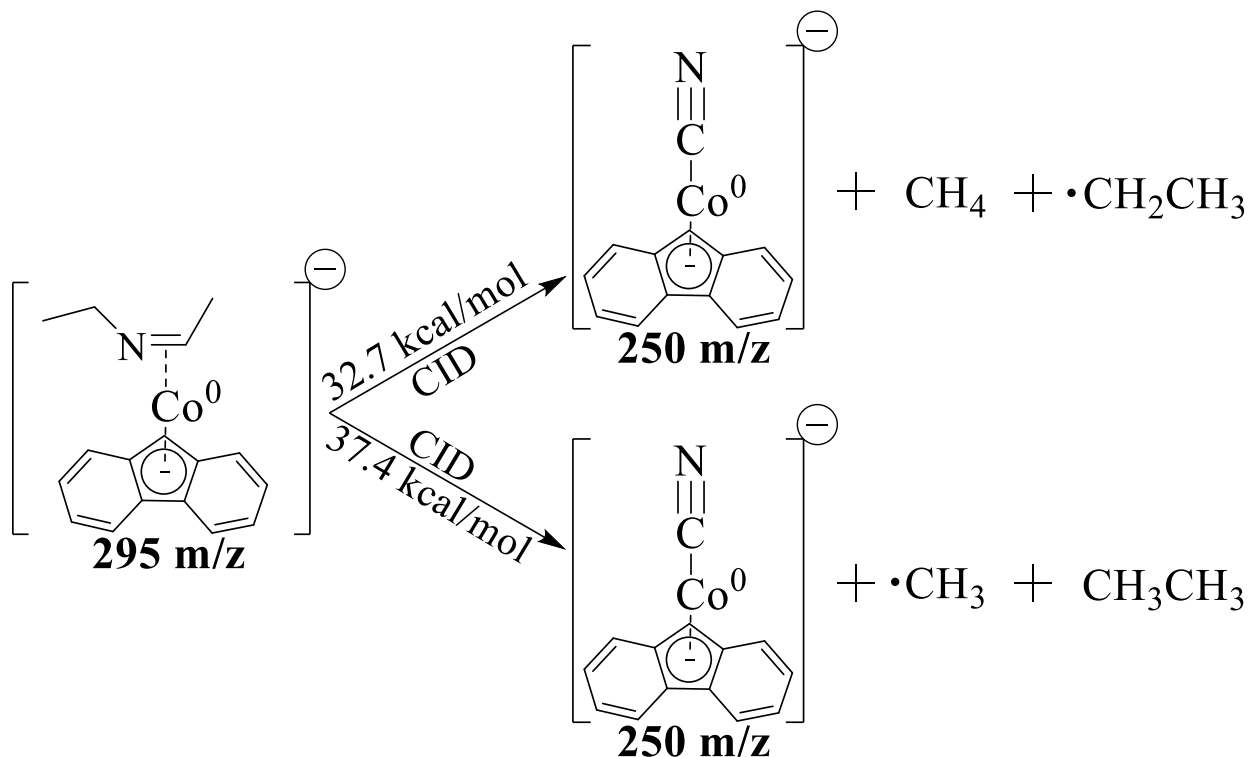
Additional dehydrogenations were observed when the butan-1-imine adduct of complex **II** was isolated and subjected to CID (Scheme 4.11). Product ions at m/z 293 and 291 indicate dehydrogenations of the imine ligand.

CID experiments of the dehydrogenation product for the reaction of diethylamine with complex **II** did not result in additional dehydrogenations (Scheme 4.12). Instead, when the dehydrogenation product was isolated and subjected to CID, a product at m/z 250 was observed, indicating oxidation of the imine to a cyano group. This process can occur with either the loss of methane and an ethyl radical (32.7 kcal/mol), or loss of a methyl radical and ethane (37.4 kcal/mol). While the loss of methane and the ethyl radical is favored by 4.7 kcal/mol, the energy introduced via CID may enable both processes. The signal intensity of the dehydrogenation of piperidine by complex **II** was not high enough to isolate and subject the ion to CID. In these cases, the complexity and uncertainty

of the reaction pathways made it impractical to fully map out mechanisms and identify transition states.

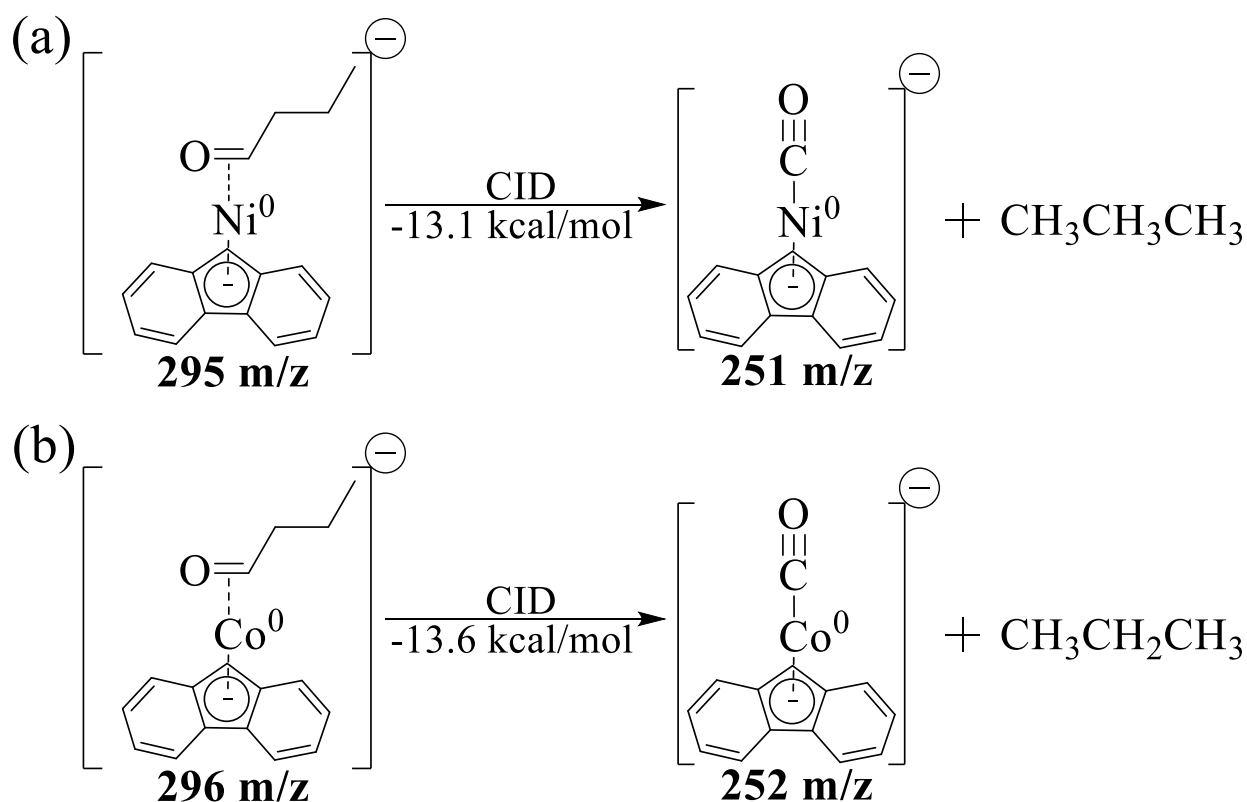


Scheme 4.11. Reaction pathways for the CID of the butan-1-imine adduct with complex **II**. DFT calculations performed at the M06/6-311+G** level. Detailed information on the structures of the calculated species are shown in Appendix C.

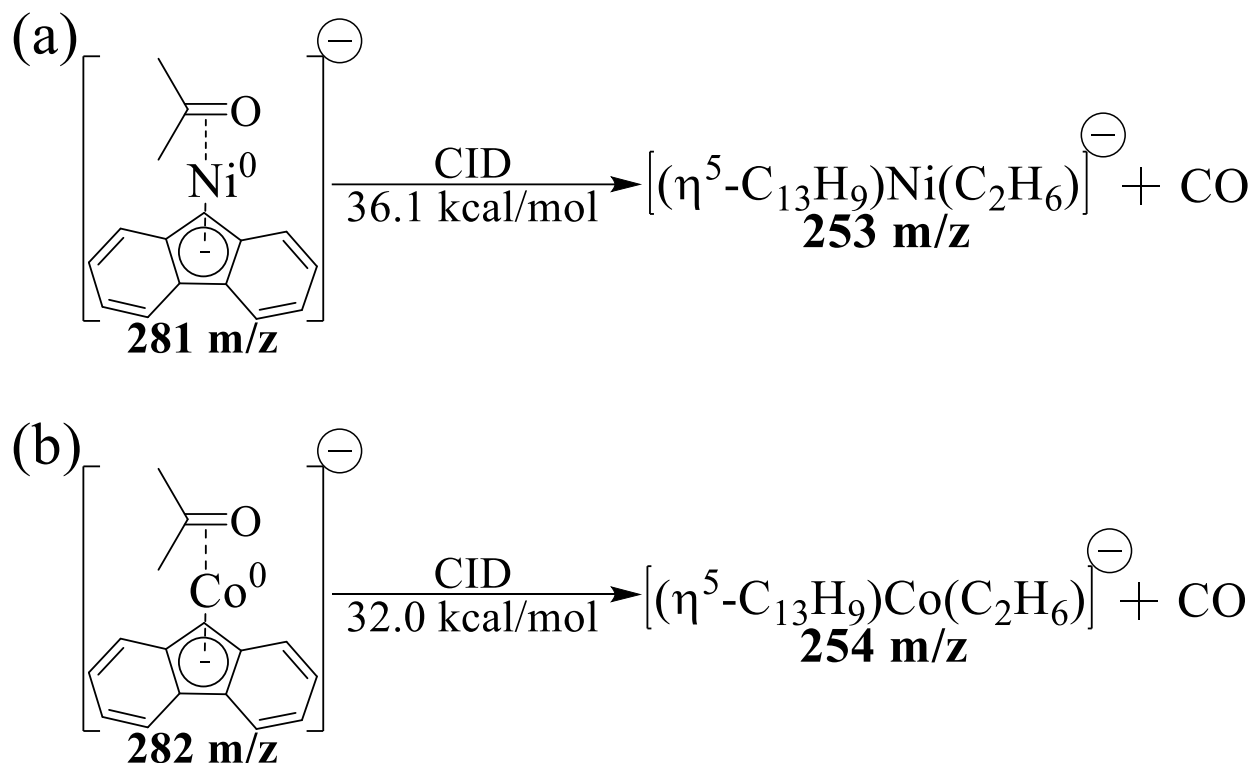


Scheme 4.12. Reaction pathways for the CID of the N-ethylethanamine adduct of complex **II**. DFT calculations performed at the M06/6-311+G** level. Detailed information on the structures of the calculated species are shown in Appendix C.

CID studies of the dehydrogenation products generated via reactions with alcohols led to decarbonylation by complexes **I** and **II**. The butanal adducts were isolated and subjected to CID, enabling decarbonylation to produce CO complexes of the metal with the release of propane (Scheme 4.13). This process is exothermic by 13.1 kcal/mol and 13.6 kcal/mol for complexes **I** and **II**, respectively. In experiments with isopropanol, decarbonylation of the acetone adducts also occurred. Unlike the experiments with butanol, decarbonylation of acetone resulted in the release of CO, leaving the alkyl moiety to form an anion with both metal complexes (Scheme 4.14). DFT calculations suggest this process is endothermic by 36.1 kcal/mol and 32.0 kcal/mol for complexes **I** and **II**, respectively.



Scheme 4.13. Reaction pathways for the CID of the butanal adducts of complexes **I** and **II**. Panel (a) depicts CID of the butanal adduct of complex **I**. Panel (b) depicts CID of the butanal adduct of complex **II**. DFT calculations performed at the M06/6-311+G** level. Detailed information on the structures of the calculated species are shown in Appendix C.



Scheme 4.14. Reaction pathways for the CID of the acetone adducts of complexes **I** and **II**. Panel (a) depicts CID of the acetone adduct of complex **I**. Panel (b) depicts CID of the acetone adduct of complex **II**. DFT calculations performed at the M06/6-311+G** level. Detailed information on the structures of the calculated species are shown in Appendix C.

In conclusion, our Ni and Co SAC model ions are capable of the dehydrogenation of amines and alcohols to produce imines, aldehydes, and ketones. Kinetics experiments and DFT calculations suggest that both model ions perform the dehydrogenations via N/O-H insertion followed by β -hydride elimination on the alpha carbon. Reactions with alcohols also led to decarbonylation products. Additional reactivity for amine and alcohol dehydrogenation products was observed by subjecting the product ions to CID. Our model ions most closely resemble metals supported on Stone-Wales graphene defects. If a Stone-Wales graphene-supported SAC was created using Ni or Co, it may be useful for generating activated products via amine or alcohol dehydrogenation.

4.6 Experimental Section

All experiments were executed in a modified linear triple quadrupole ion trap mass spectrometer (modified Thermo Electron LTQ XLTM) equipped with an electrospray ionization (ESI) source. The precursor ions for complexes **I** and **II** were made by mixing solutions of each component. For the nickel complex, nickel(II) acetate tetrahydrate and fluorene-9-carboxylic acid were each dissolved in methanol at 10^{-4} M. Potassium oxalate monohydrate was dissolved in a water/methanol mixture at 10^{-4} M. These solutions were mixed in a 1:5:2.5 ratio by volume, respectively, and passed into the ion trap via ESI. For the cobalt complex, Co(II) benzoate and fluorene-9-carboxylic acid were each dissolved in methanol at 10^{-4} M. Potassium oxalate monohydrate was dissolved in a water/methanol mixture at 10^{-4} M. These solutions were mixed in a 1:4:0.6 ratio by volume, respectively, and passed into the ion trap via ESI. Typical ESI conditions involved flow rates of $5\mu\text{L}/\text{min}$, needle potentials between 4-5 kV and heated capillary temperatures between 230-275 °C. A notched waveform was used to isolate the precursor complexes. The precursor complexes were subjected to sequential rounds of CID to form the respective SAC model ions. Once a steady signal of the ion of interest was achieved, neutral reagents were introduced into the ion trap via the external manifold, as previously described.^{36,68}

Temperatures of the ion trap environment have been shown to be near room temperature.^{68,69} Reaction spectra were averaged over 200 scans in order to minimize noise. Kinetic measurements were completed as described in Scheme 4.5.

Piperidine-ND and butylamine-ND₂ were synthesized as follows:

Piperidine-ND – 500 μL of piperidine and 2mL of D₂O were placed in a 25mL round-bottom flask.

The reaction flask was placed into an oil bath and reaction mixture was stirred and heated to $\sim 80^\circ$

C. D₂O (2mL) was added to the reaction mixture twice in one-hour increments after the reaction mixture began heating. At 3 hours, the reaction flask was taken off heat and allowed to cool. The deuterated amine was extracted in diethyl ether (2 x 3mL and 1 x 2mL) and the organic layer was distilled. Piperidine-ND was verified by ¹H-NMR.

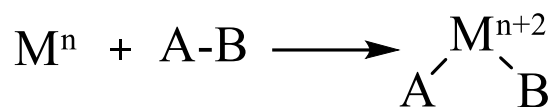
Butylamine-ND₂ – 500μL of butylamine and 6mL of D₂O were placed in a 25mL round-bottom flask. The reaction mixture was stirred at room temperature for 24 hours. The deuterated amine was extracted in diethyl ether (2 x 3mL and 1 x 2 mL) and the organic layer was distilled. Butylamine-ND₂ was verified by ¹H-NMR.

All other neutral reagents were purchased commercially in the highest purity available and used without further purification. Density functional calculations were completed using the Gaussian16¹⁰¹ suite of quantum mechanical programs. All calculations were performed at the M06/6-311+G** level. All transition states were verified using intrinsic reaction coordinate (IRC) calculations.

Chapter 5 - Oxidative Addition of Polar Reagents by Gas-Phase Graphene-Supported Single-Atom Catalyst Model Ions

5.1 Oxidative Addition

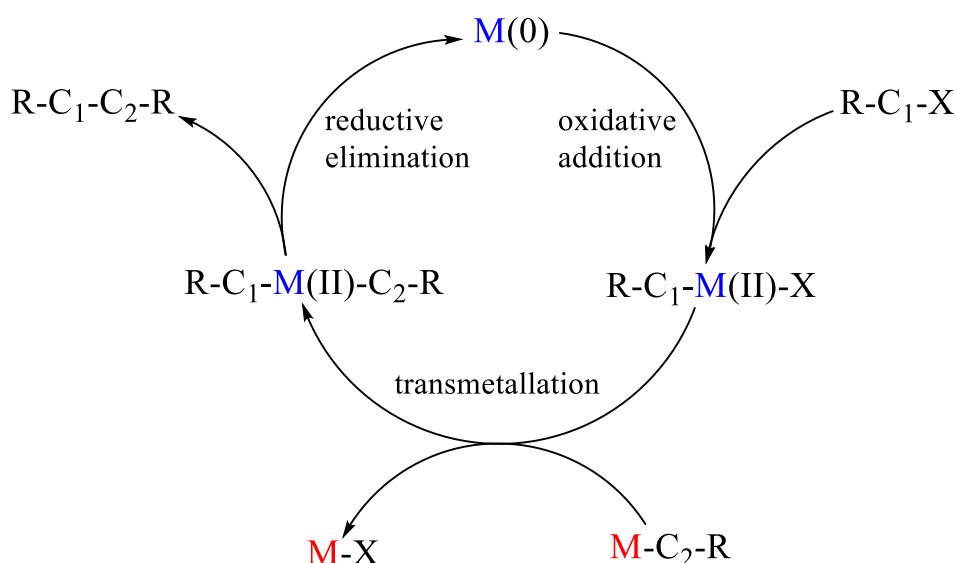
Classically defined as the formal oxidation of a metal by 2 via the addition of two ligands produced by a reductive cleavage of a substrate bond (Scheme 5.1), oxidative addition is a fundamental organometallic reaction and is a key step in many catalytic processes.¹¹⁴⁻¹¹⁷



Scheme 5.1. Classic depiction of an oxidative addition reaction.

For example, the Monsanto process employs oxidative addition as the initial step in producing acetic acid, a large scale industrial product, using the four coordinate Rh complex, $[RhI_2(CO)_2]^-$.^{114,118} The Cativa process generates acetic acid using an Ir-based complex that engages in oxidative addition during the catalytic cycle.¹¹⁹ Oxidative additions also play a role in metal-catalyzed cross coupling cycles (Scheme 5.2). The first step in a typical cross coupling cycle is oxidative addition of a polar reagent, where the metal inserts into the C-X bond resulting in the addition of two ligands along with an increase in the oxidation state by 2. While there is a laundry list of polar reagents that can be used for this step, alkyl/aryl halides are most commonly seen. In the second step, transmetalation, a second metal complex is used to exchange ligands, resulting in a new C-R ligand for the catalyst. Finally, reductive elimination releases the product via C-C bond formation and recovers the metal catalyst. The ability to form new C-C bonds via cross-couplings has had a large impact on areas of research and development involving synthetic

transformations¹²⁰⁻¹²⁸ and Professors Heck, Negishi, and Suzuki were awarded the Nobel prize in 2010 for originally developing Pd catalyzed cross-coupling reactions.¹²⁹ Since oxidative addition is a key step in the practical applications described above, it is important to identify and understand metal-centered species that engage in this reaction. Recent studies report the successful use of Pd-based SACs, supported on metal-oxides and carbon-scaffolds, in Suzuki and Sonogashira coupling reactions.¹³⁰⁻¹³²

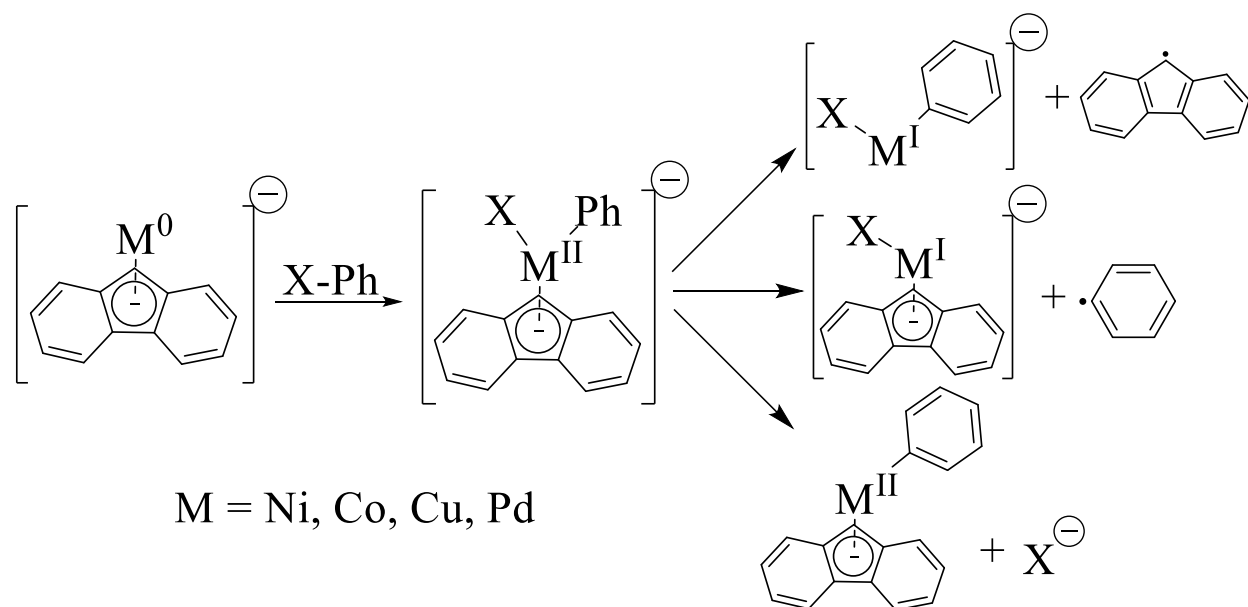


Scheme 5.2. Typical cross-coupling cycle.

5.2 Oxidative Addition of Aryl Halides by the SAC Model Complexes

All four of our SAC model ions are capable of engaging in oxidative additions with polar reagents. Most of the reagents included in our study are organic halides due to the common use of these chemicals in practical applications.¹¹⁴ A general depiction of the reaction between the SAC model ions and aryl halides is shown in Scheme 5.3. When the aryl halide is introduced into the ion trap, the first step is the insertion of the metal center into the C-X bond. The resulting product ion is

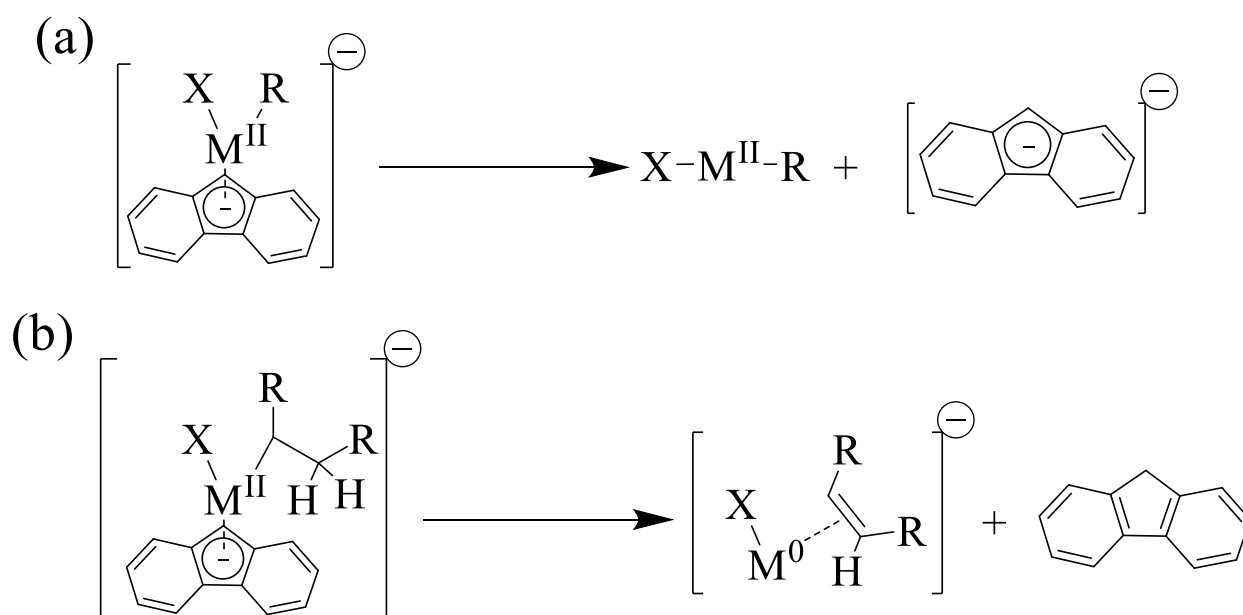
burdened by an excess of energy which results from the initial ion-molecule attraction and the enthalpy of reaction. The relatively small product ion often releases the excess energy by breaking apart into fragment ions. The initial oxidation addition intermediate has three ligands and can expel any of them as a radical or an anion. Three fragment ions are often observed in the oxidative addition product spectra. The insertion product is indicated by an anion comprised of the metal inserted into the C-X bond of the aryl halide. In this pathway, the fluorenyl scaffold is released as a fluorenyl radical. An anion formed by halogen addition suggests the release of the R group (phenyl in this case) as a radical. In the third fragmentation pathway, the metal complex can release the free halide, resulting in a neutral species comprised of the metal complex with a phenyl ligand. Generally, one or more of these fragmentation products are observed in the reaction spectra.



Scheme 5.3. Oxidative addition of aryl halides by complexes **I-IV**. Due to the excess energy gained by the ion-molecule attraction and thermodynamics of reaction, the oxidative addition product often breaks apart into three fragment products: the insertion product (top), the halogen addition product (middle), and the halide (bottom) product.

It is important to note that the insertion process can also be indicated by two other ions (Scheme 5.4). As depicted in panel (a), instead of releasing the fluorenyl radical, the carbon scaffold can be

released as the fluorenyl anion, leaving behind a neutral complex comprised of the metal atom inserted in the polar bond. In another pathway, shown in panel (b), the fluorenyl anion engages in a β -elimination of a proton, resulting in an anionic metal π -complex and a fluorene molecule. While these products are observed occasionally, the most commonly observed insertion product is shown in Scheme 5.3.



Scheme 5.4. Two other possible insertion products. These products occur less often than the insertion product depicted in Scheme 5.3.

Figure 5.1 depicts the product spectrum for the reaction of bromobenzene with the Cu SAC model ion, complex **III**. The insertion product appears at m/z 219 while the halogen addition product appears at m/z 307. The presence of bromine in these products is identified by the characteristic Br-81 isotopologues at m/z 221 and m/z 309, respectively. In some cases, the full oxidative addition product is also observed. For example, two primary products are observed in the product spectrum of the oxidative addition of iodobenzene and the Pd SAC model ion, complex **IV** (Figure 5.2).

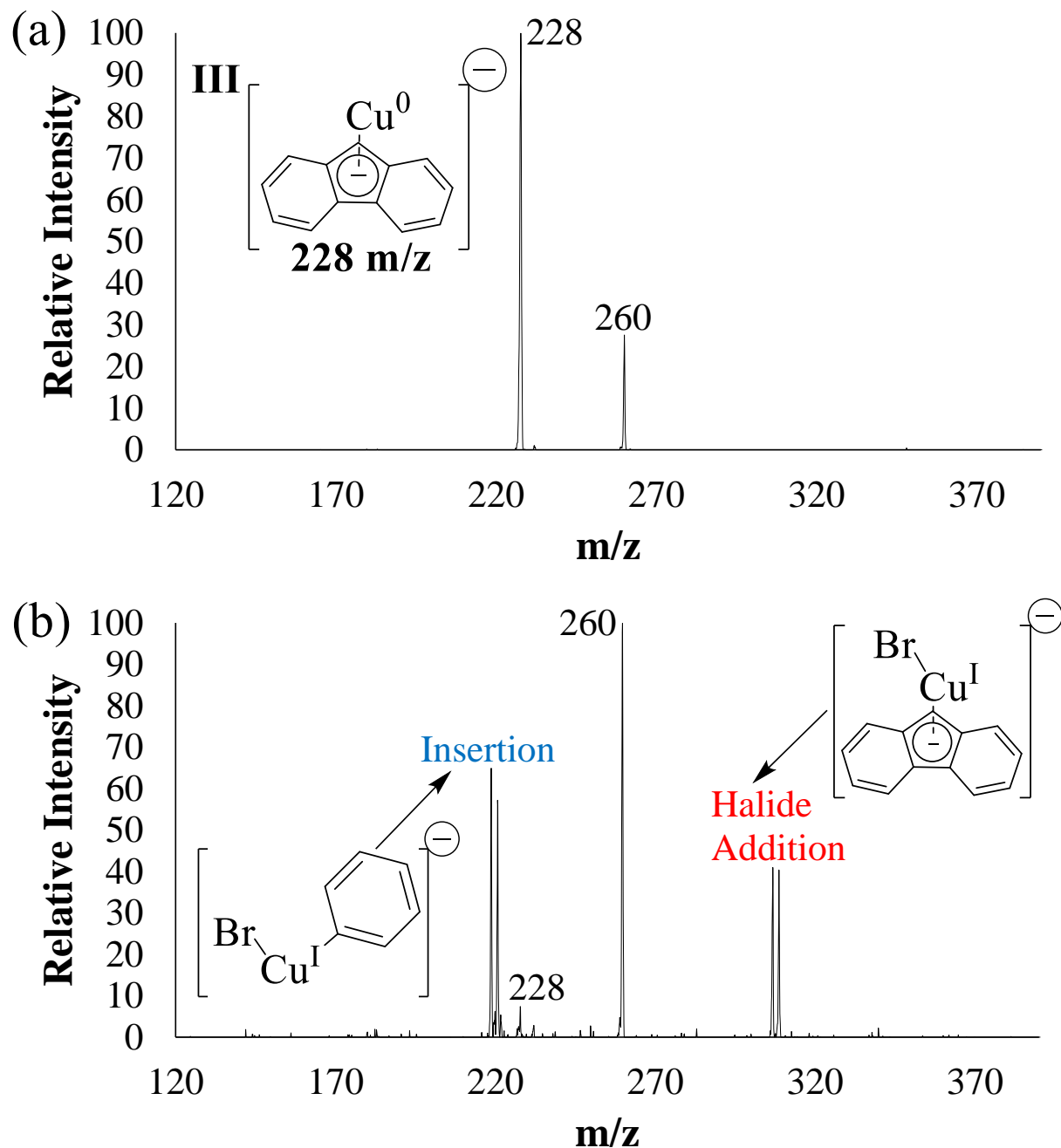


Figure 5.1. Spectra for the reaction of bromobenzene with complex **III**. Panel (a) Isolation of complex **III** prior to introduction of bromobenzene. Panel (b) Product spectrum after introduction of bromobenzene. The insertion and halogen addition products appear at m/z 219 and 307, respectively. The peak at m/z 228 is complex **III**. The peak at m/z 260 is an adduct with oxygen.

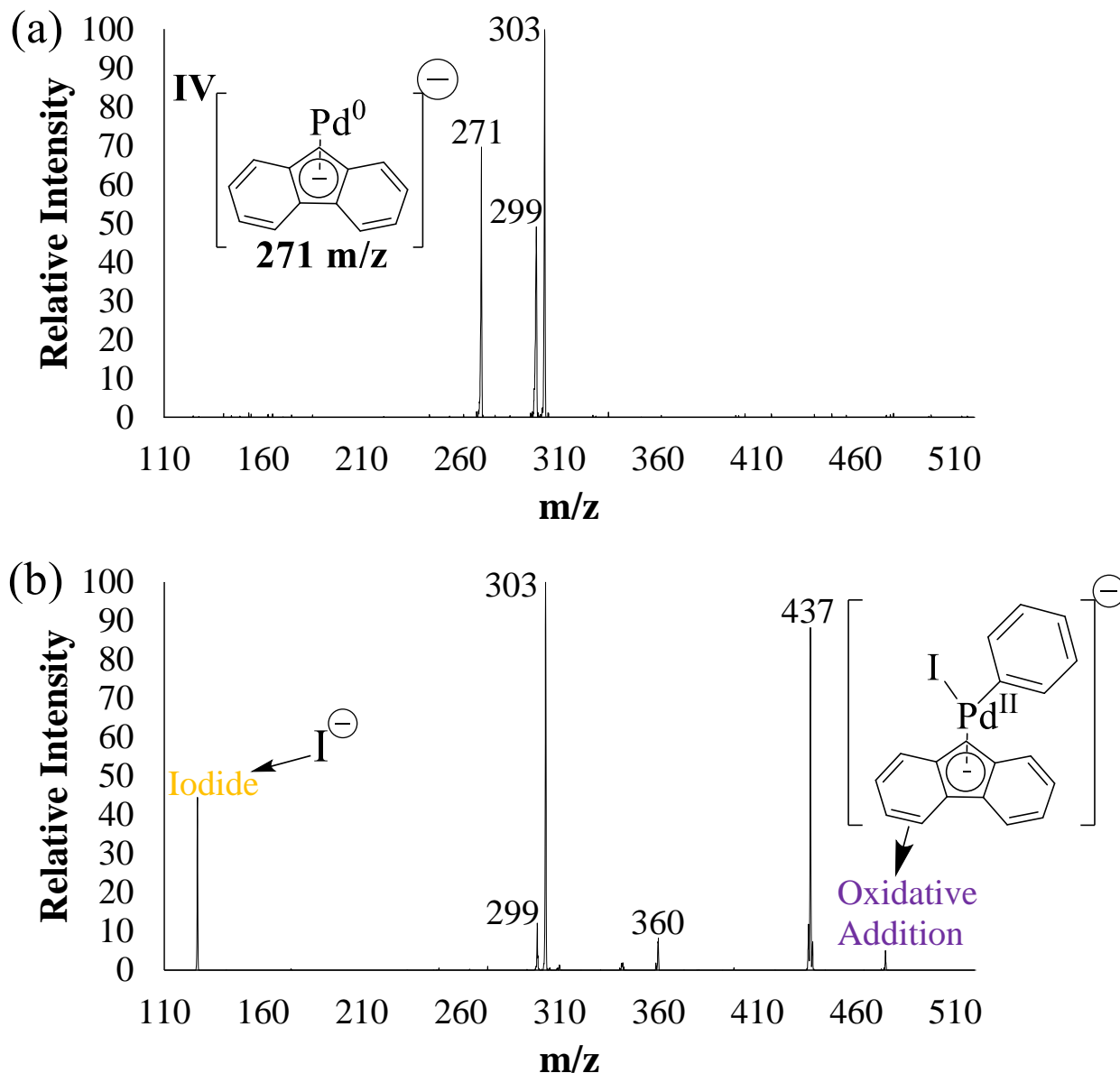
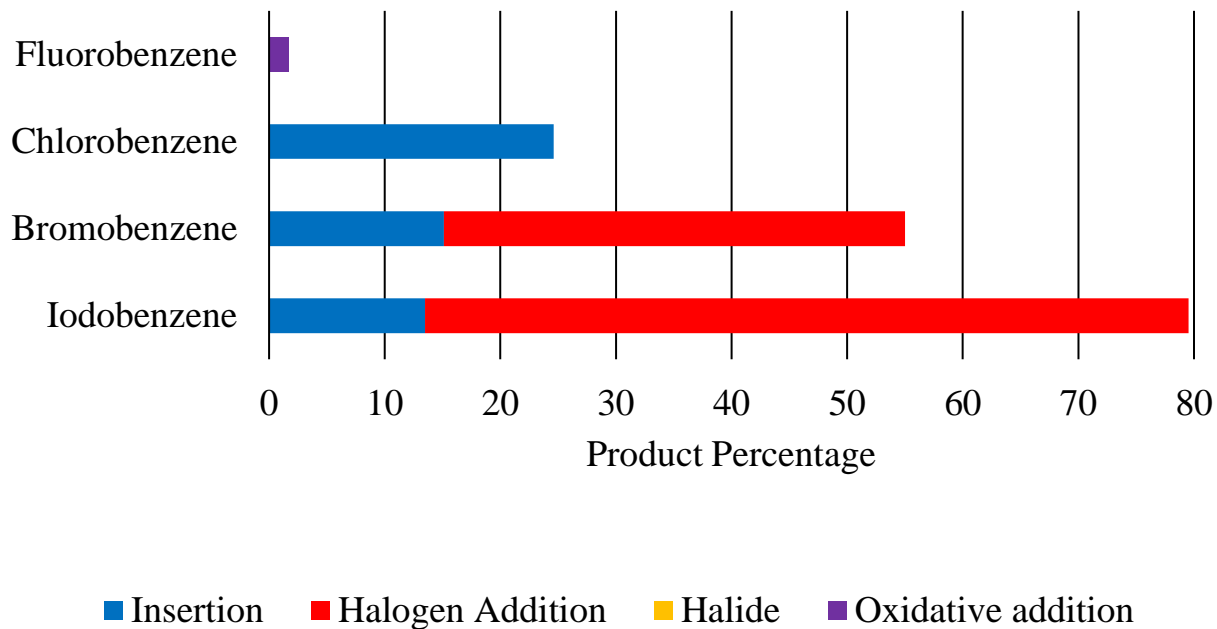


Figure 5.2. Spectra for the reaction of iodobenzene with complex **IV**. Panel (a) Isolation of complex **IV** prior to introduction of iodobenzene. Panel (b) Product spectrum after introduction of iodobenzene. Iodide appears at m/z 127, indicating aryl addition. The oxidative addition product appears at m/z 475. The peaks at m/z 360 and m/z 437 are $[\text{PdI}_2]^-$ and $[\text{PdI}_2\text{C}_6\text{H}_5]^-$, respectively, and are formed through secondary reactions with iodobenzene. The peaks at m/z 299 and m/z 303 are adducts of molecular nitrogen and oxygen, respectively.

The full oxidative addition appears at m/z 475 while iodide appears at m/z 127, indicating aryl addition. Two other products are also observed in the spectrum. The peak at m/z 360 is an anion comprised of Pd ligated to two iodides while the peak at m/z 437 indicates an anion comprised of Pd coordinated with a phenyl ring and two iodides. These products are a result of secondary reactions of product ions with a second iodobenzene molecule. Similar secondary products were observed in many of the reactions in this study. However, most of these reactions occurred between insertion products and a second molecule of the polar reagent and therefore do not reflect the reactivity of the SAC model ions featuring the fluorenyl anion as a scaffold (Appendix B.5). It is important to remember that the fragmentation products are a consequence of the gas-phase ion-molecule reactions. If graphene-supported SACs engage in oxidative additions, the excess energy imparted by the exothermicities of the reactions would likely dissipate through the many vibrational modes of the graphene lattice, resulting in simple oxidative addition.

All four SAC model ions were allowed to react with fluorobenzene, chlorobenzene, bromobenzene, and iodobenzene. Product distributions for the oxidative addition reactions of these aryl halides by complexes **II** and **III** are shown in Figure 5.3. As shown in panel (a), complex **II** had very little reactivity with fluorobenzene leading only to the oxidative addition product (which might also be a simple adduct). These results are not surprising given the notorious difficulty of C-F bond activation under mild conditions.¹³³ More significant reactivity was observed with chlorobenzene, with the insertion fragment appearing as the only product. Even more reactivity was observed in reactions with bromobenzene and iodobenzene. Both insertion and halogen addition products were observed in these reactions. This increasing trend in reactivity can be attributed to the relative bond strengths. C-X bonds weaken moving down the halogen group on the periodic table due to the increase in the halogen's atomic size and decrease in electronegativity.

(a) Co SAC Model Ion - Aryl Halide Product Distribution



(b) Cu SAC Model Ion - Aryl Halide Product Distribution

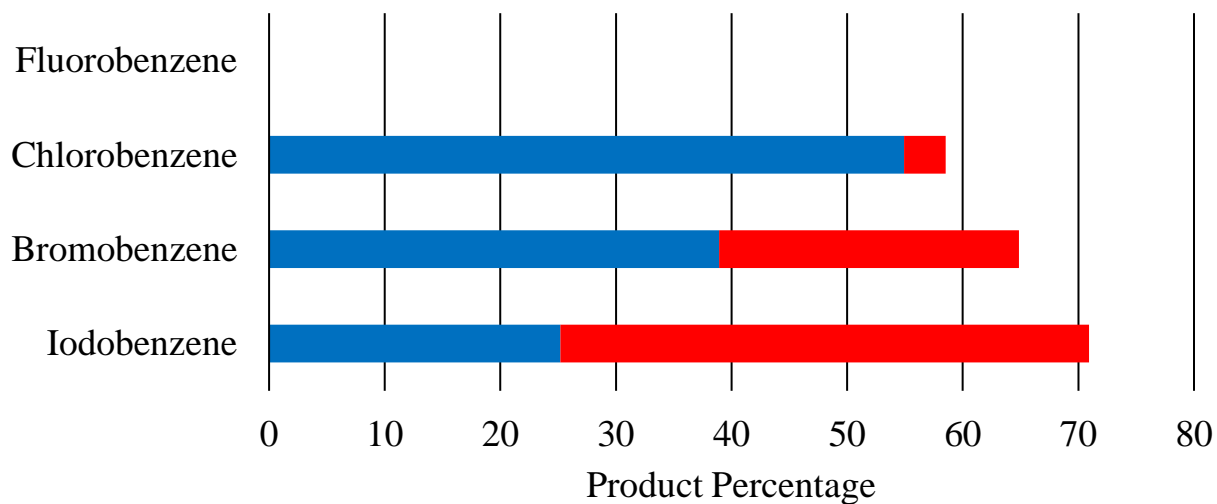


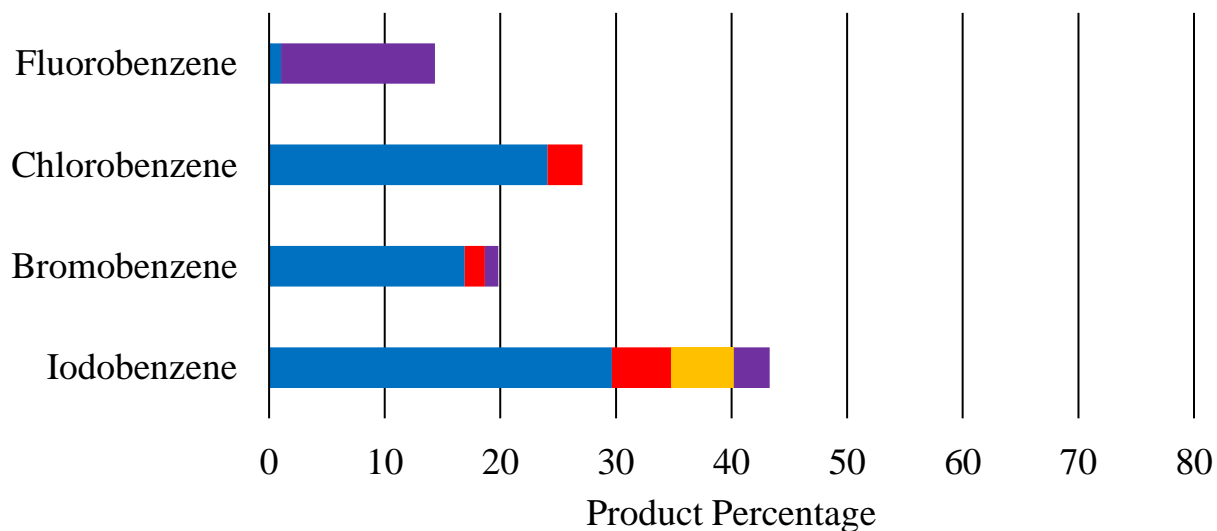
Figure 5.3. Product distributions for the oxidative addition reactions of fluorobenzene, chlorobenzene, bromobenzene, and iodobenzene by complex **II**, panel (a), and complex **III**, panel (b). Products of reactions between the SAC model ions and adventitious species in the ion trap are not shown.

These trends likely result in lower barriers for C-X bond activation by the SAC model ions. Complex **III** displayed very similar reactivity to complex **II** and both trended towards more halogen addition in the series from fluorine to iodine, but there are two main differences. Complex **III** did not react with fluorobenzene at all, meaning the metal complex was unable to activate the C-F bond. Also, compared to the Co SAC model ion, complex **III** had much more reactivity with chlorobenzene. The insertion fragment was the main product of this reaction, but the halogen addition product also appeared.

Product distributions for the oxidative addition reactions of the aryl halides with complexes **I** and **IV** are shown in Figure 5.4. The insertion product was the most commonly observed product for complex **I**. The halogen addition product was observed as a minor product in the reactions with chlorobenzene, bromobenzene, and iodobenzene (along with the halide product in the reaction with iodobenzene). Oxidative addition products appeared more often in the reactions with complex **I** than in the reactions shown in Figure 5.3. This was the major product in the reaction with fluorobenzene and also appeared as a minor product in the reactions with bromobenzene and iodobenzene. While overall reactivity was relatively low compared to reactions with the other aryl halides and SAC model ions, complex **I** was the most capable of C-F bond activation.

Reactions with complex **IV** resulted in a wide spread of products for the aryl halide reactions. In the reaction with iodobenzene, the halide appeared as the major product while the oxidative addition product appeared as the minor product. The major and minor products in the reaction with chlorobenzene were the oxidative addition and insertion products, respectively. In the reaction with bromobenzene, both products appeared in about equal amounts. It is noteworthy that the product distributions for complex **IV** are tilted towards products with a Pd-C bond, with no evidence of halide additions.

(a) Ni SAC Model Ion - Aryl Halide Product Distribution



■ Insertion ■ Halogen Addition ■ Halide ■ Oxidative addition ■ Adduct

(b) Pd SAC Model Ion - Aryl Halide Product Distribution

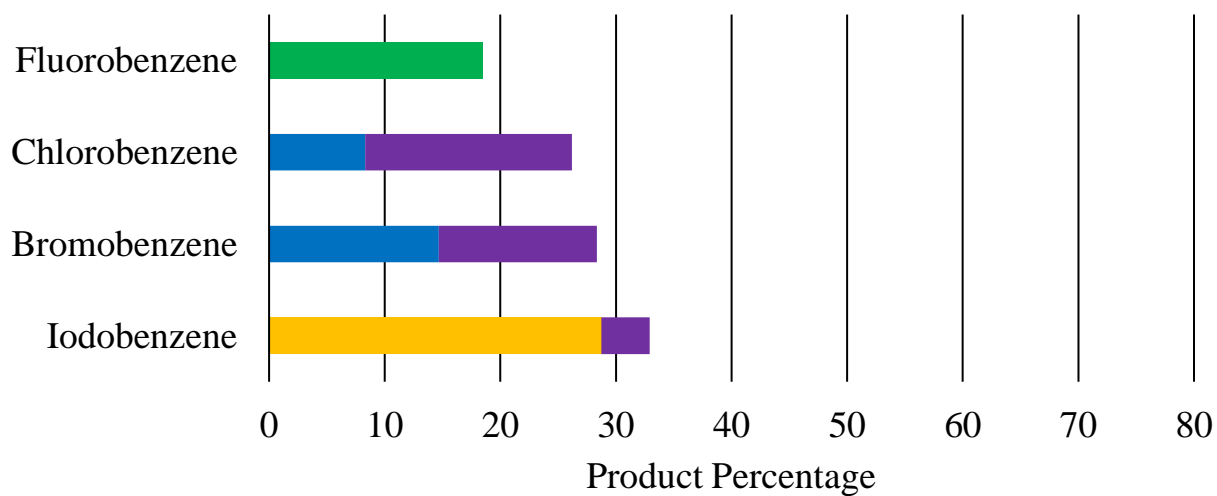
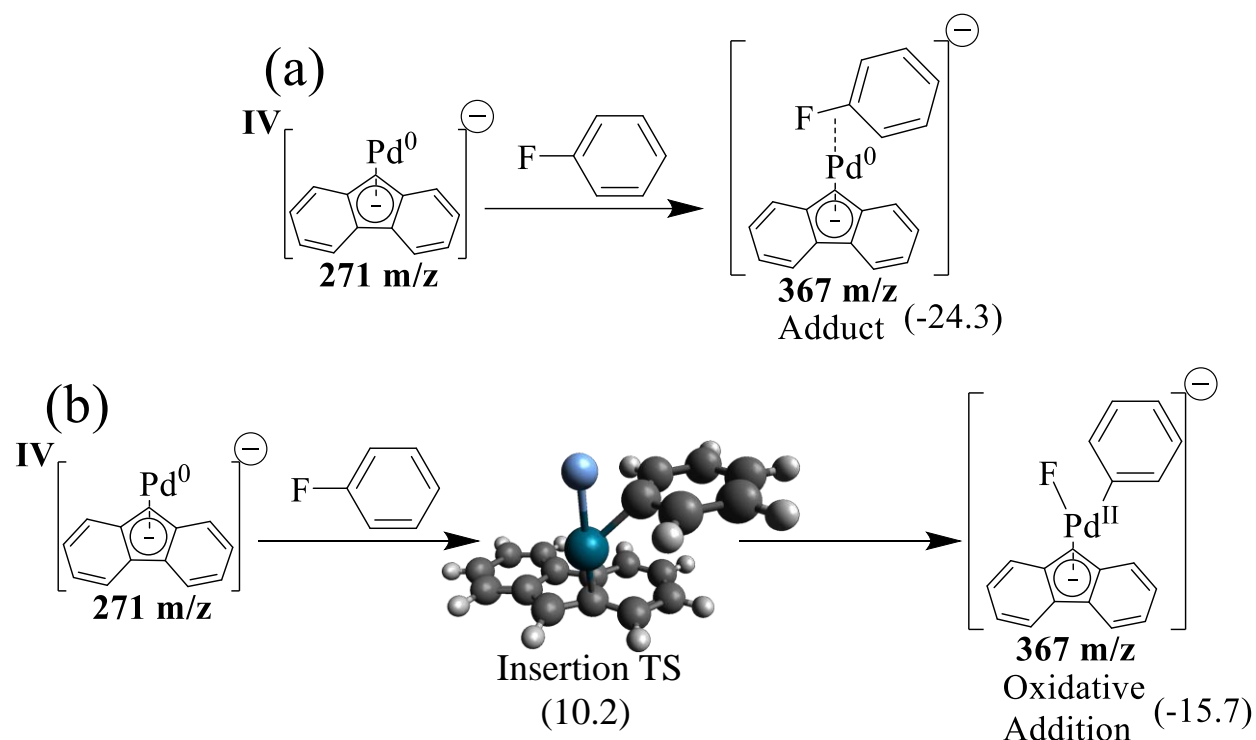


Figure 5.4. Product distributions for the oxidative addition reactions of fluorobenzene, chlorobenzene, bromobenzene, and iodobenzene by complex **I**, panel (a), complex **IV**, panel (b). Products of reactions between the SAC model ions and adventitious species in the ion trap are not shown.

The only product observed in the reaction with fluorobenzene was an adduct. Since the adduct and oxidative addition products are isobaric and therefore indistinguishable using mass spectrometry alone, computational modelling was used in order to obtain insightful energetic information that led to this conclusion (see below).

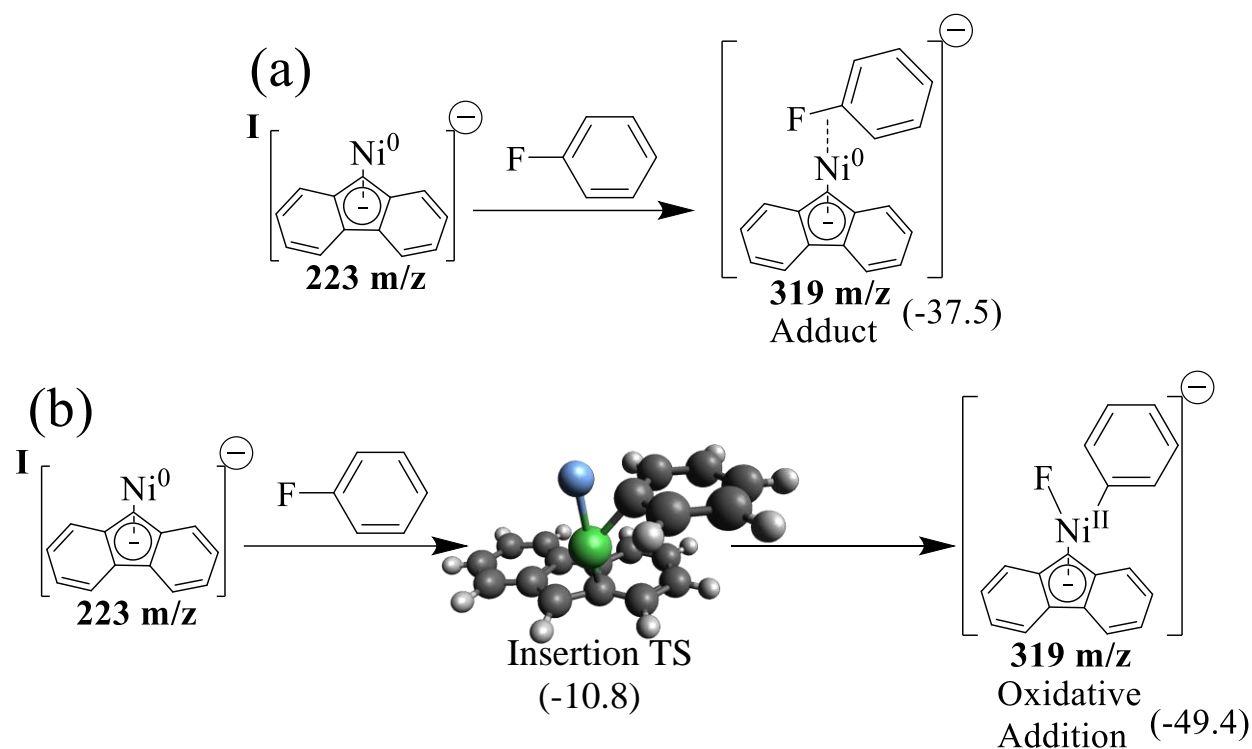
5.3 Computation Modelling for the Oxidative Addition of Aryl Halides

DFT calculations were performed using the M06 functional with an effective core potential (ECP) basis set on Pd (lanl2dz) and a 6-311+G** basis set on the other atoms. Energies are reported from single-point calculations at the M06/QZVP level with thermal enthalpy corrections from the calculations with the mixed ECP/6-311+G** basis set for all reactions. Scheme 5.5 depicts the energetics for the reaction of fluorobenzene with the complex **IV**. Panel (a) depicts adduct formation and DFT calculations suggest the process is exothermic by 24.3 kcal/mol. Since the process does not involve bond breakage, there is no associated TS. Panel (b) depicts the oxidative addition of fluorobenzene by complex **IV**. While the overall reaction is exothermic by 15.7 kcal/mol, there must be an associated TS in order to break the C-F bond. DFT calculations suggest a three-centered TS that is above the reactants by 10.2 kcal/mol. This three-centered TS is typical for oxidative addition reactions, especially when using unsaturated reagents such as aryl halides.¹¹⁴ Under our reaction conditions, this TS is too high to allow the oxidative addition to occur on the timescale of the experiment and the adduct would be preferred over the oxidative addition product at equilibrium. Therefore, the identity of the observed product ion is likely the adduct of fluorobenzene with the Pd SAC model ion.



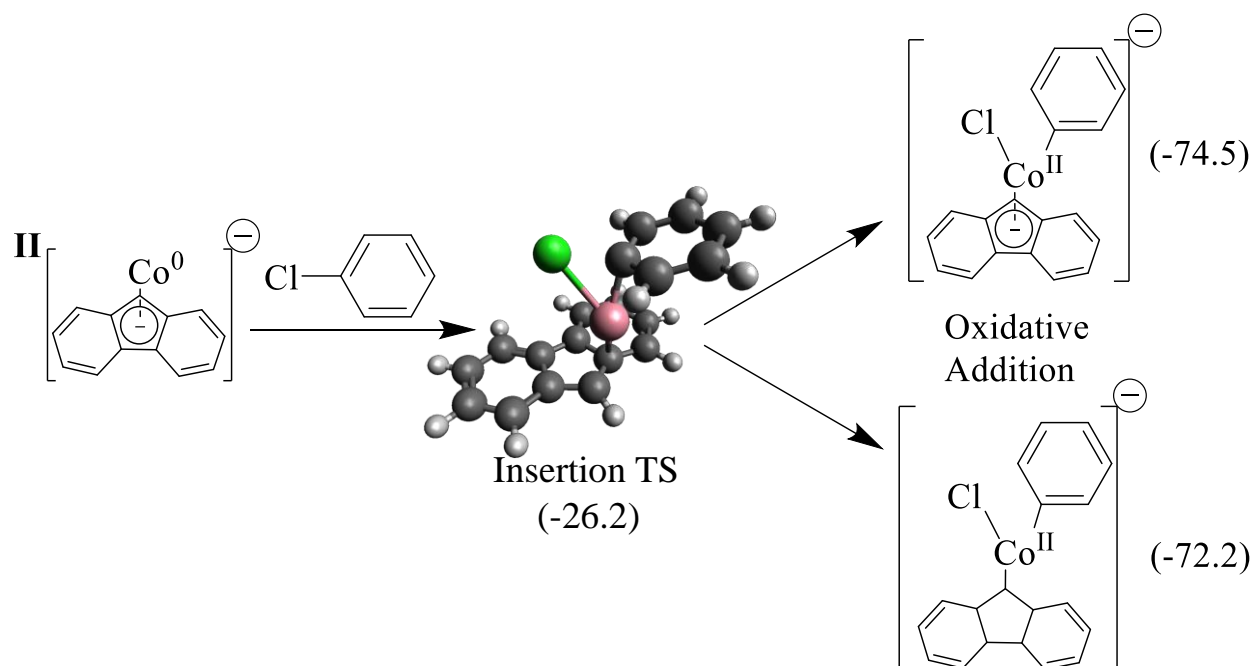
Scheme 5.5. Energies for adduct formation and oxidative addition of fluorobenzene by complex **IV**. Panel (a) depicts adduct formation. Panel (b) depicts oxidative addition. Enthalpies in kcal/mol. Calculations were completed with M06 functional and a mixed lan12dz/6-311+G** basis set. Detailed information on the structures of the calculated species are shown in Appendix C.

As mentioned previously, complex **I** also produced an oxidative addition product in the reaction with fluorobenzene (Scheme 5.6). As shown in panel (a), DFT calculations suggest adduct formation is exothermic by 37.5 kcal/mol. The oxidative addition of fluorobenzene, shown in panel (b), occurs via a three-centered TS that is below the energy of the reactants by 10.8 kcal/mol, resulting in a reaction that is exothermic by 49.4 kcal/mol. The energetically accessible TS and overall reaction exothermicity indicate that the identity of the observed product is likely the oxidative addition of fluorobenzene by the Ni SAC model ion. DFT calculations also suggest a favorable TS for the reaction between fluorobenzene and the Co SAC model ion (Appendix B.6).



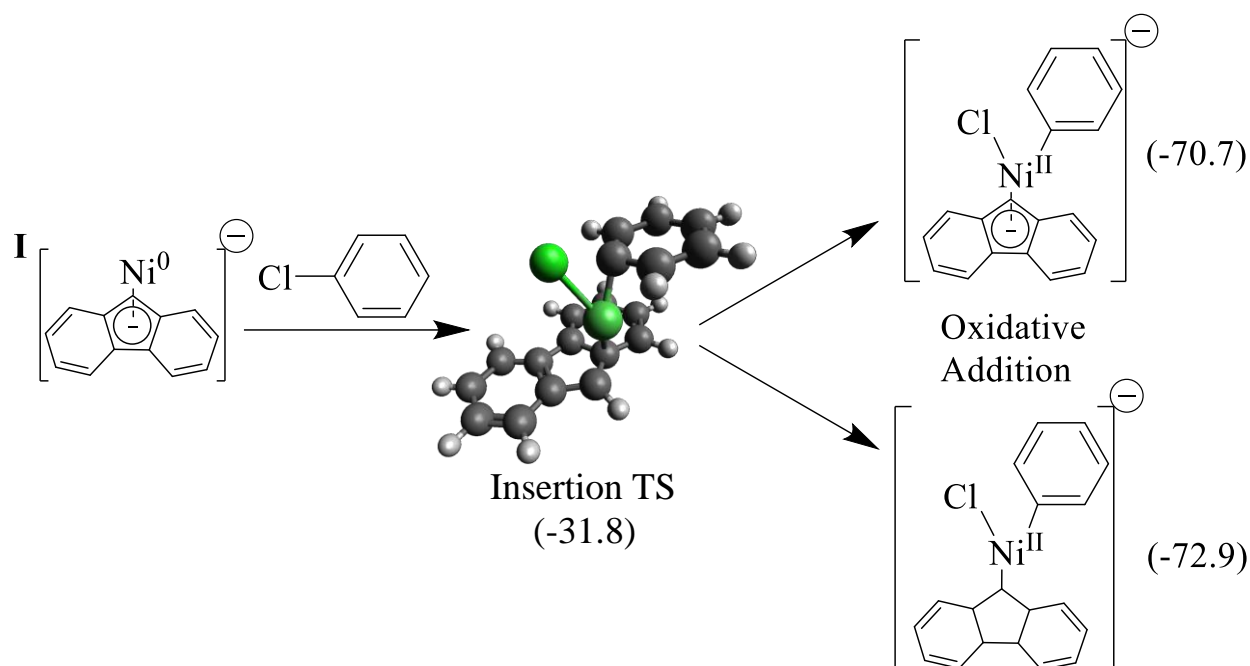
Scheme 5.6. Energies for adduct formation and oxidative addition of fluorobenzene by complex **I**. Panel (a) depicts adduct formation. Panel (b) depicts oxidative addition. Enthalpies in kcal/mol. Calculations were completed at the M06/6-311+G** level. Detailed information on the structures of the calculated species are shown in Appendix C.

As mentioned earlier, the weaker C-X bonds of the other aryl halides likely lead to lower activation barriers. In order to confirm and gain further insight into the observed reactivity of all four SAC model ions, energetic information on the reactions with chlorobenzene were also obtained via DFT calculations. Scheme 5.7 depicts the reaction between chlorobenzene and complex **II**. DFT calculations suggest the Co center is able to split the C-Cl bond via a three-centered insertion TS that is 26.2 kcal/mol below the reactants. Insertion into the C-Cl bond leads to the oxidative addition product but DFT calculations suggest two viable structures. If the Co center is coordinated to the aromatic 5-membered ring of the fluorenyl scaffold, the reaction is exothermic by 74.5 kcal/mol.



Scheme 5.7. Enthalpies for the TS and oxidative addition products of the reaction between chlorobenzene and complex **II**. Enthalpies in kcal/mol. Calculations suggest that two binding modes are favorable for the formation of the oxidative addition product. Calculations were completed at the M06/6-311+G** level. Detailed information on the structures of the calculated species are shown in Appendix C.

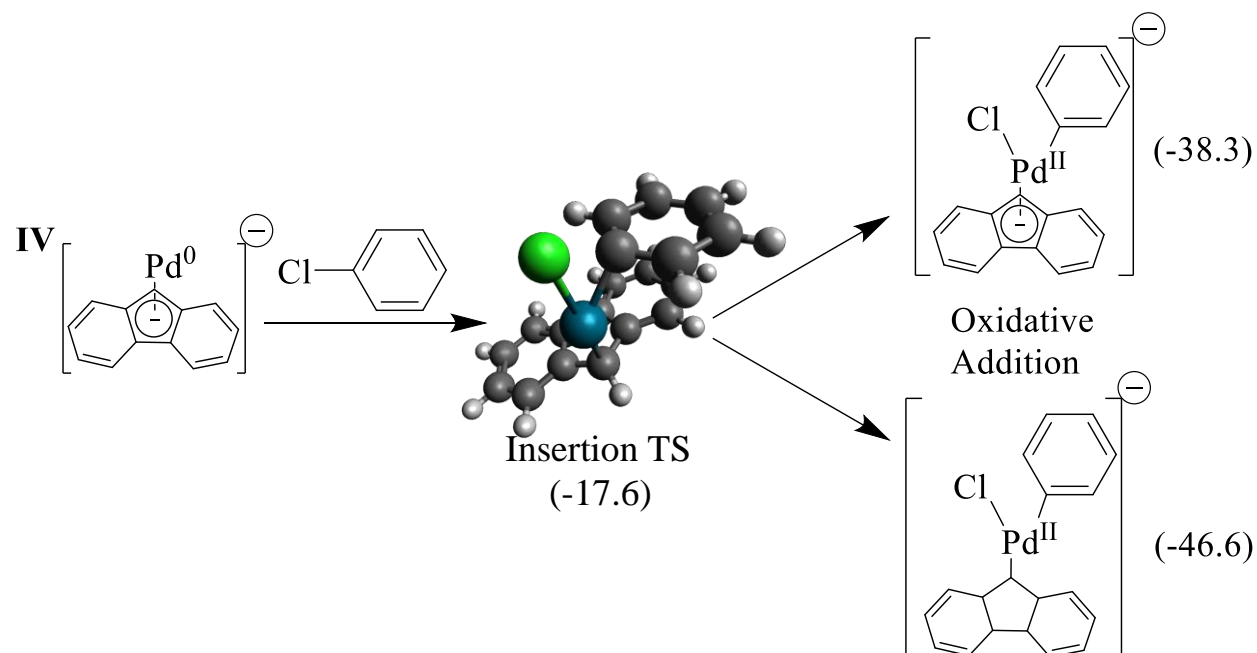
However, Co can also coordinate to a pyramidalized 9-carbon on the fluorenyl scaffold (η_1), resulting in a reaction that is exothermic by 72.2 kcal/mol. Since these products are so close in energy, it is not clear which structure is the actual product or if the product is fluxional. If there is a small barrier to interconvert between the two structures, it may be that both structures are present. However, it is important to note that in both possibilities, chlorobenzene has been separated and added to Co as two distinct ligands.



Scheme 5.8. Enthalpies for the TS and oxidative addition products of the reaction between chlorobenzene and complex **I**. Enthalpies in kcal/mol. Calculations suggest that two binding modes are favorable for the formation of the oxidative addition product. Calculations were completed at the M06/6-311+G** level. Detailed information on the structures of the calculated species are shown in Appendix C.

Similar results were found for the reactions with complexes **I** and **IV**. As shown in Scheme 5.8, complex **I** carries out oxidative addition of chlorobenzene via a three-centered TS that is below the reactants by 31.8 kcal/mol. The metal center can either be coordinated to the fluorenyl scaffold or solely the 9-carbon of the fluorenyl anion, resulting in reactions that are exothermic by 70.7 kcal/mol and 72.9 kcal/mol, respectively. The reaction with complex **IV** features a similar TS that is below the reactants by 17.6 kcal/mol (Scheme 5.9). This results in a reaction that is exothermic by 38.3 kcal/mol when the Pd center is coordinated to the fluorenyl scaffold. If the metal center is bonded to just the 9-carbon of the fluorenyl anion, the oxidative addition product is exothermic by 46.6 kcal/mol. The exothermicities associated with the oxidative addition products for the

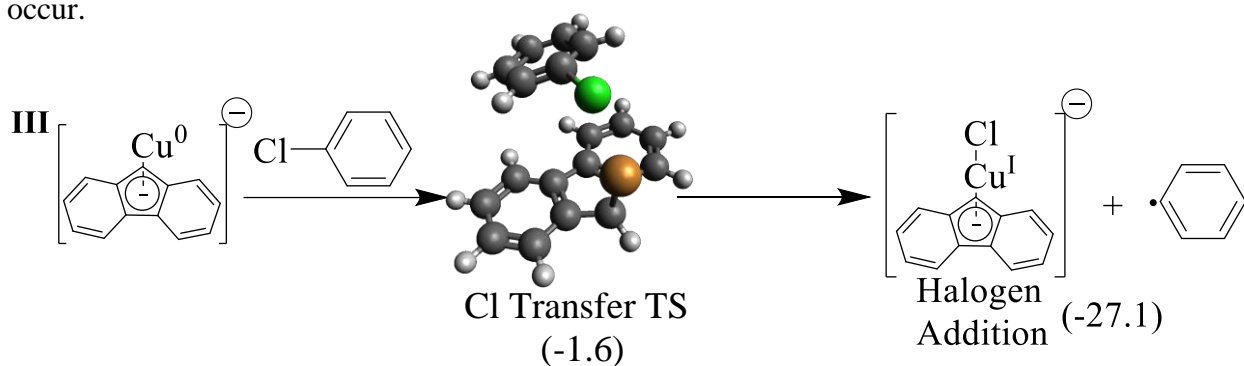
chlorobenzene reactions discussed thus far likely lead to the fragmentation products observed in experiments.



Scheme 5.9. Enthalpies for the TS and oxidative addition products of the reaction between chlorobenzene and complex IV. Enthalpies in kcal/mol. Calculation suggest that two binding modes are favorable for the formation of the oxidative addition product. Calculations were completed with M06 functional and a mixed lanl2dz/6-311+G** basis set. Detailed information on the structures of the calculated species are shown in Appendix C.

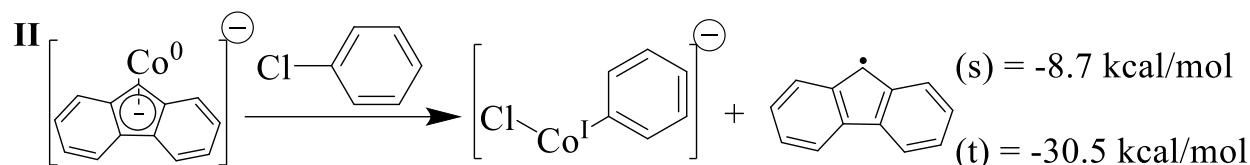
Unlike the other SAC model ions, the Cu SAC model ion seems to follow a different mechanism (Scheme 5.10). In attempts to locate a typical oxidative addition TS, DFT calculations indicated that the Cu SAC model ion abstracts Cl from the phenyl ring via a one-electron transfer TS that is 1.6 kcal/mol below the reactants. This TS leads directly to the halogen addition product and the release of a phenyl radical. The overall reaction is exothermic by 27.1 kcal/mol. The difference in mechanism may be due to the high electron count of the initial Cu complex (17-electron species). If the ion were to engage in a classic oxidative addition, the resulting complex would be a 19-

electron species, surpassing the often stable 18-electron count. However, by engaging in the one-electron transfer of Cl, the Cu complex becomes an 18-electron complex. This rationale aligns well with previous reports about halogen atom abstraction by 17-electron metal complexes.^{114,134} Organometallic systems that employ this mechanism use a second metal complex to retrieve the organic radical or to add a new moiety to the radical. Therefore, oxidative addition likely would not occur by a Cu graphene-supported SAC on its own. However, the other SAC model ions have lower electron counts which likely allow for two-electron processes, such as oxidative addition, to occur.



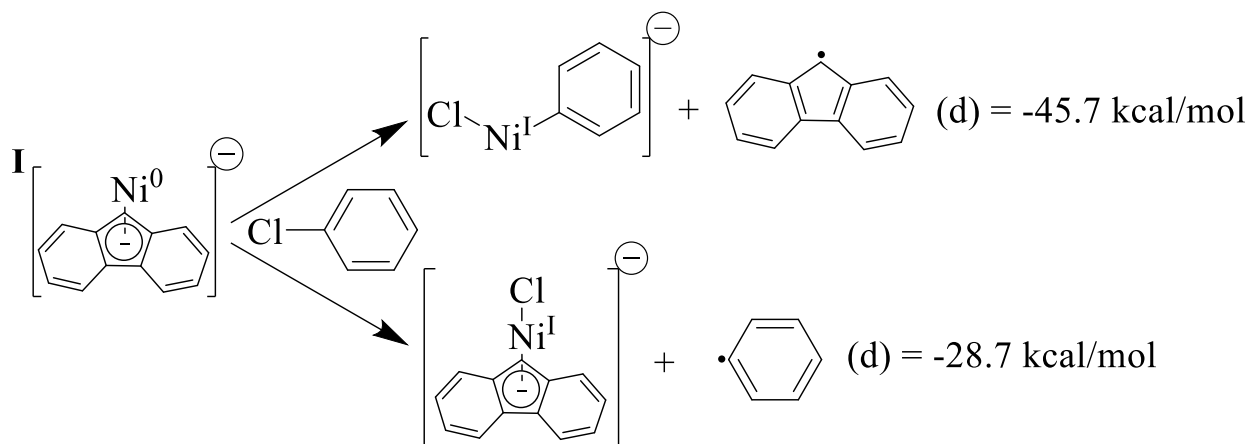
Scheme 5.10. Enthalpies for TS and product of the halogen addition pathway of the reaction between chlorobenzene and the Cu SAC model ion. Enthalpies in kcal/mol. Calculations were completed at the M06/6-311+G** level. Detailed information on the structures of the calculated species are shown in Appendix C.

DFT calculations were also performed to gain information on the overall energetics of product formation. Scheme 5.11 depicts the energies for the fragment products formed in the reaction between chlorobenzene and complex **II**. The insertion product was considered in both the singlet and triplet states and DFT calculations suggest both spin states give favorable reactions. The reaction is exothermic by 8.7 kcal/mol and 30.5 kcal/mol when forming the product in the singlet and triplet states, respectively.

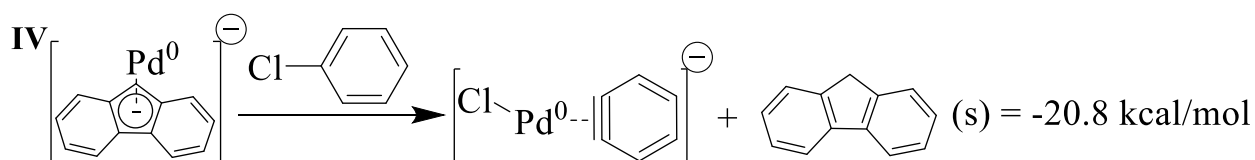


Scheme 5.11. Enthalpies for the reaction between chlorobenzene and complex **II**. The insertion product was considered in both the singlet and triplet spin states. (s) = singlet, (t) = triplet. The reactant ion was calculated in the doublet spin state. Calculations were completed at the M06/6-311+G** level. Detailed information on the structures of the calculated species are shown in Appendix C.

Formation of the products observed in the reactions between chlorobenzene and complexes **I** and **IV** were also favorable. Products in these reactions were calculated in the lowest possible spin state since higher spin states (e.g. triplet or quartet) would require the promotion of an electron out of the d-shell. The insertion product for the reaction with complex **I** is exothermic by 45.7 kcal/mol while the halogen addition product is exothermic by 28.7 kcal/mol (Scheme 5.12). While both fragment pathways are viable, the insertion product is favored by 17.0 kcal/mol. This energetic preference supports the observed experimental product preference (Figure 5.4). The reaction with complex **IV** resulted in oxidative addition and insertion products. The insertion product is depicted in Scheme 5.13. Instead of releasing the fluorenyl radical, the fluorenyl scaffold appears to abstract a hydrogen from the phenyl ring, resulting in the release of fluorene and the formation of Pd complexed with Cl and benzyne. DFT calculations suggest the reaction is exothermic by 20.8 kcal/mol, meaning the oxidative addition products (Scheme 5.9) are favored by at least 17.5 kcal/mol. This energetic preference is in accordance with the preference observed in experiments (Figure 5.4).



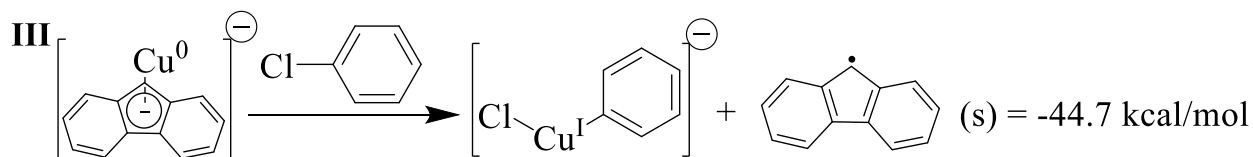
Scheme 5.12. Enthalpies for the reaction between chlorobenzene and complex **I**. Ion products calculated in the doublet, (d), spin state. The reactant ion was calculated in the singlet spin state. Calculations were completed at the M06/6-311+G** level. Detailed information on the structures of the calculated species are shown in Appendix C.



Scheme 5.13. Enthalpies for the reaction between chlorobenzene and complex **IV**. The insertion product is comprised of Pd complexed with Cl and benzyne. The reactant and product ions were calculated in the singlet, (s), spin state. Energetic information for the oxidative addition product (not shown) is depicted in Scheme 5.9. Calculations were completed with M06 functional and a mixed lan12dz/6-311+G** basis set. Detailed information on the structures of the calculated species are shown in Appendix C.

Of all the reactions with chlorobenzene, the Pd SAC model ion was the only metal complex to produce an experimentally observed oxidative addition product. This may be due to the relatively larger size of the Pd atom which allows for more effective cooling via vibrational modes. This is reflected in the calculations as the exothermicity for forming the Pd oxidative addition product is ~40-50 kcal/mol while the Co and Ni oxidative addition products are ~70-75 kcal/mol. The lower energy associated with the Pd reactions likely reduces the probability that a fragment ion would

be produced from every reaction collision. DFT calculations also suggested lower energies for the reaction between fluorobenzene and the Ni SAC model ion which featured an observed oxidative addition product (Scheme 5.6).



Scheme 5.14. Enthalpies for the reaction between chlorobenzene and complex **III**. Enthalpies The insertion product was calculated in the doublet, (d), spin state. Energetic information for the halogen addition product, (d), is depicted in Scheme 5.10. Calculations were completed at the M06/6-311+G** level. Detailed information on the structures of the calculated species are shown in Appendix C.

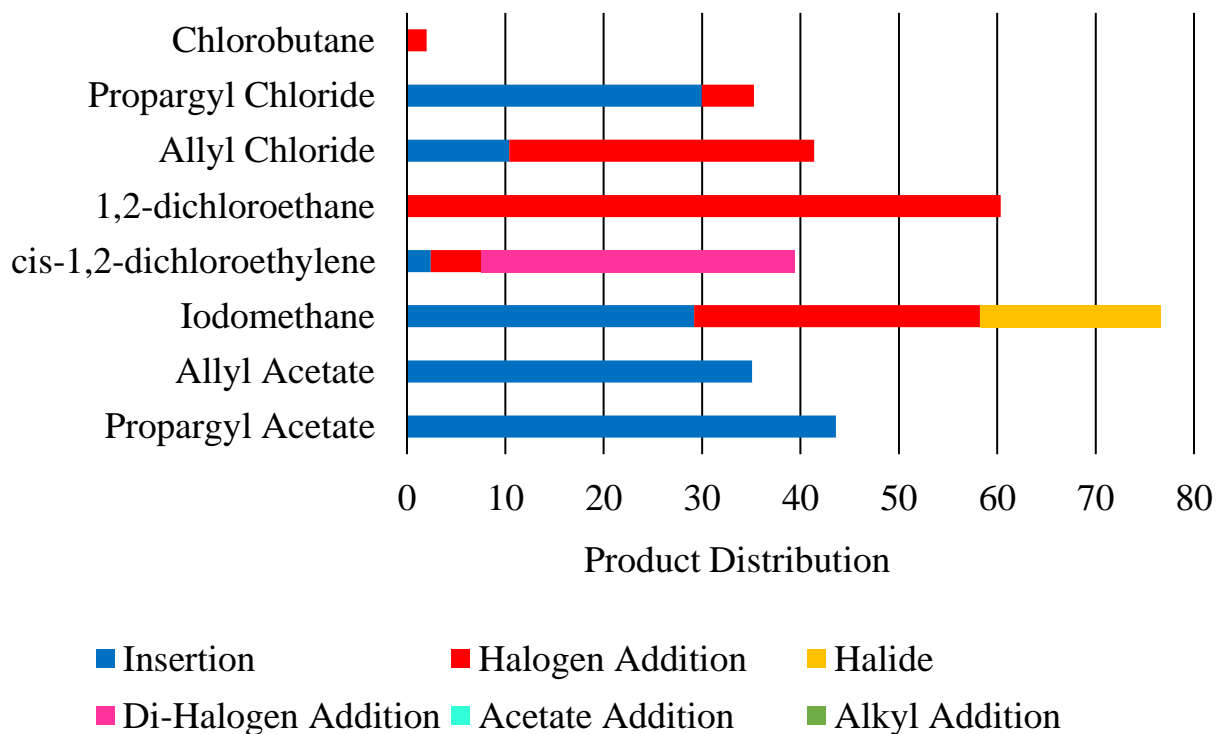
Formation of the insertion product in the reaction between chlorobenzene and complex **III** is depicted in Scheme 5.14. DFT calculations suggest the reaction is exothermic by 44.7 kcal/mol. Compared to the halogen addition product (Scheme 5.10, -27.1 kcal/mol) the insertion product is favored by 17.6 kcal/mol, which supports the preference for the insertion product observed in experiments. However, as mentioned earlier, complex **III** likely does not enact C-X insertion like the other metal complexes. Halogen addition occurs via the TS depicted in Scheme 5.10 while the insertion product likely forms via a TS which involves Cu insertion into the C-Cl bond with concerted loss of the fluorenyl radical. Since these products do not share a rate-limiting TS, the processes that form the products are fundamentally different. This means that differences in the energies of the TSs may also affect product preference.

5.4 Oxidative addition of Non-Aromatic Reagents by the SAC Model Complexes

The SAC model ions were also receptive to oxidative additions with non-aromatic reagents as shown in Figure 5.5. As can be seen in in panel (a), complex **II** has very little reactivity with

chlorobutane, which only allowed for the halogen addition product. More competitive reactions were observed with the other neutral reagents. Reactions with unsaturated carbon chains, propargyl and allyl chloride, displayed both insertion and oxidative addition products. Reagents with two halides were also tested. The sole product for the reaction with 1,2-dichloroethane was halogen addition while a di-halide addition peak appeared in the reaction with cis-1,2-dichloroethylene, along with the insertion and halogen addition products. Similar to the insertion product, the di-halogen addition product occurs with the loss of the support scaffold as the fluorenyl radical and presumably releases acetylene (Scheme 5.15). The reaction with the most competitive pathways was the iodomethane reaction, where a mix of the insertion, halogen addition, and halide products were observed. In addition to the halide reagents, allyl and propargyl acetate reagents were also included due their common use in C-C coupling reactions.¹³⁵ Both reagents resulted in the insertion ion as the sole product. As shown in Figure 5.5 (b), complex **III** displayed similar reactivity. The most notable difference is the appearance of the acetate addition and carbon-centered addition products in the reactions with allyl and propargyl acetate. Acetate addition products are formed in the same manner as halogen addition products. The carbon-centered addition product forms due to cleavage of the metal-oxygen bond and results in an acetoxy radical that will likely decompose via CO₂ loss (Scheme 5.16).

(a) Co Complex- Linear Halide Product Distribution



(b) Cu Complex - Linear Halide Product Distribution

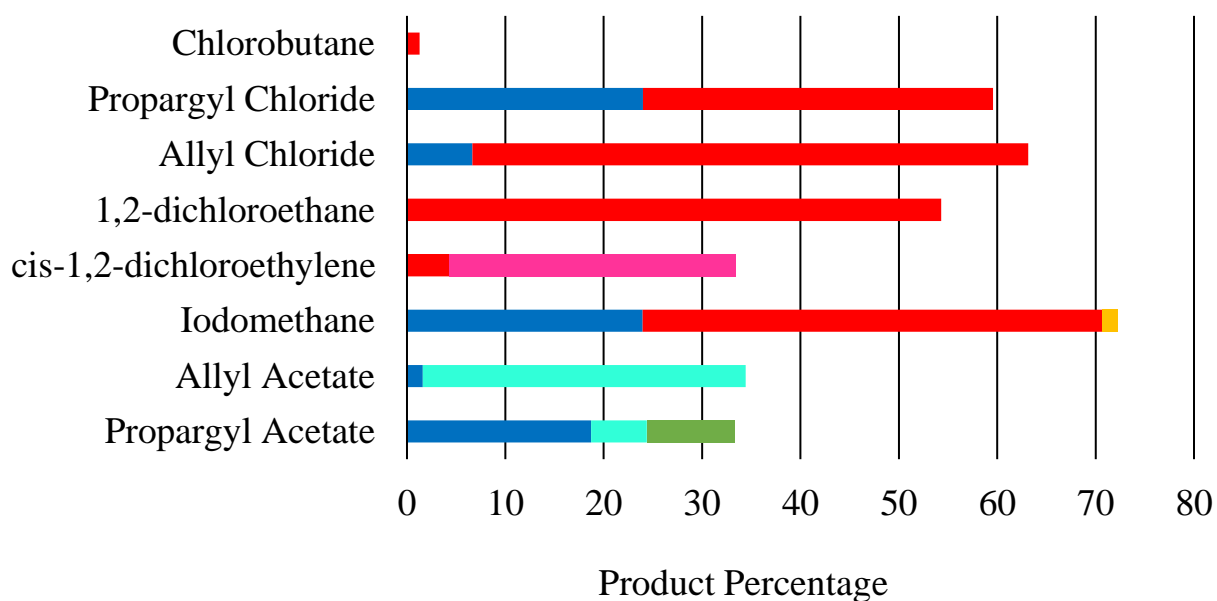
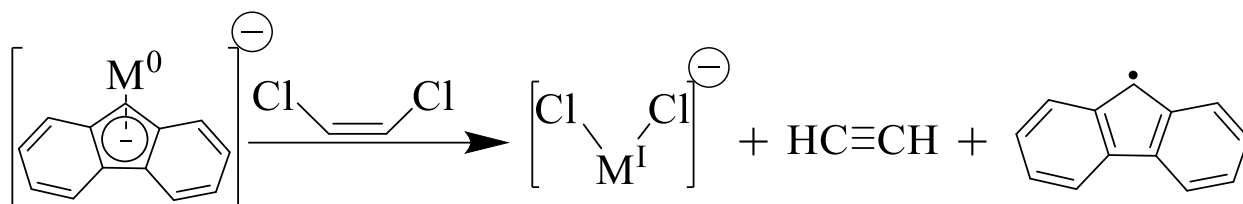
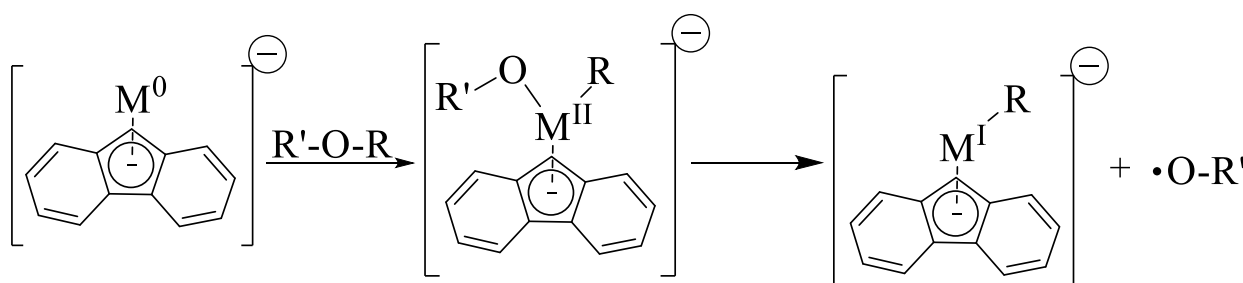


Figure 5.5. Product distributions for the oxidative addition reactions of various polar reagents by complexes **II**, panel (a), and **III**, panel (b). Products of reactions between the SAC model ions and adventitious species in the ion trap are not shown.



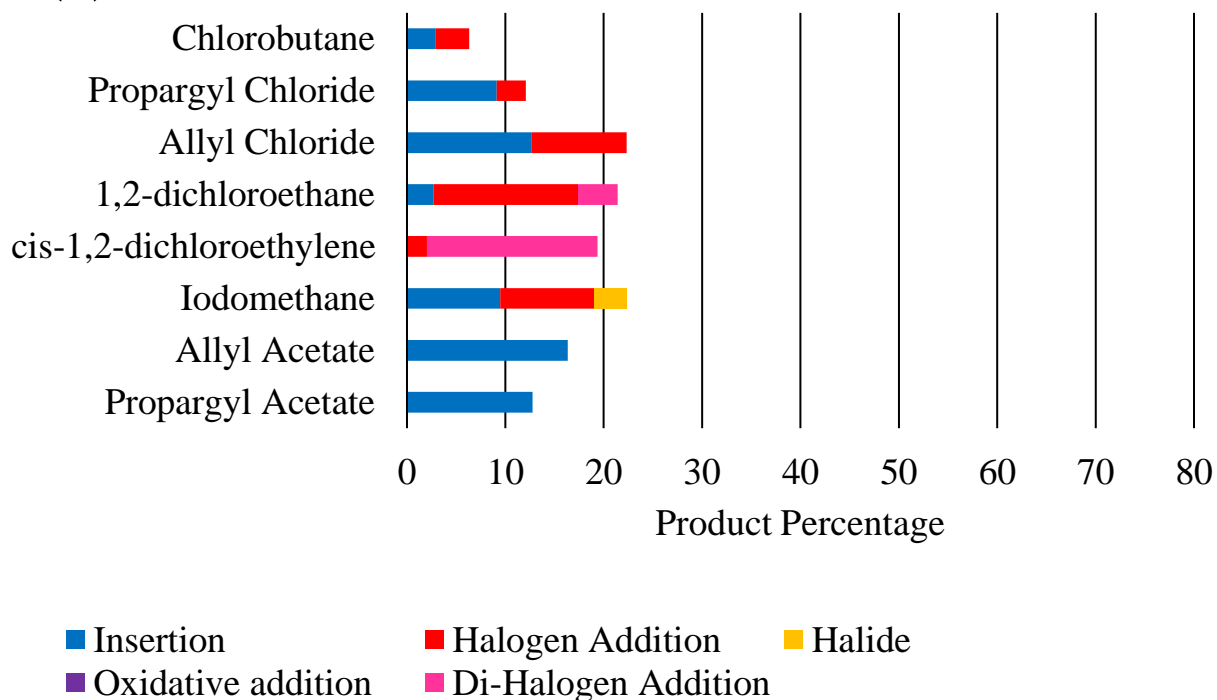
Scheme 5.15. Reaction of the SAC model ions with cis-1,2-dichloroethylene to produce the di-halogen addition product. The product ion is formed with the release of acetylene and the fluorenyl radical.



Scheme 5.16. Formation of the alkyl addition product.

Figure 5.6 depicts the product distributions for the reactions of complexes **I** and **IV** with the non-aromatic reagents. As shown in panel (a), complex **I** had little reactivity with chlorobutane and formed the insertion and halogen addition products. Once again more competitive reactions were observed with the rest of the neutral reagents listed in Figure 5.6. Reactions with the unsaturated halides, propargyl chloride and allyl chloride resulted in the insertion and halogen addition products. Insertion, halogen addition, and di-halogen addition products were observed in the reaction with 1,2-dichloroethane. The reaction with cis-1,2-dichloroethylene resulted in di-halogen addition and halogen addition products. The reaction with iodomethane resulted in a mix of insertion, halogen addition, and halide products. The only product observed in the reactions with allyl and propargyl acetates was the insertion product.

(a) Ni Complex - Linear Halide Product Distribution



(b) Pd Complex - Linear Halide Product Distribution

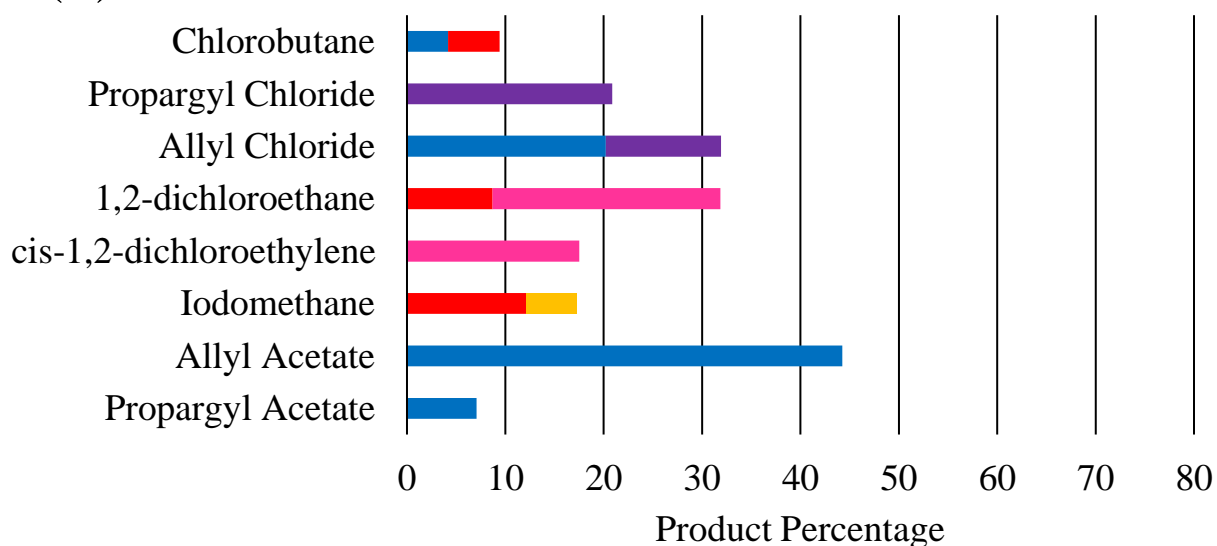
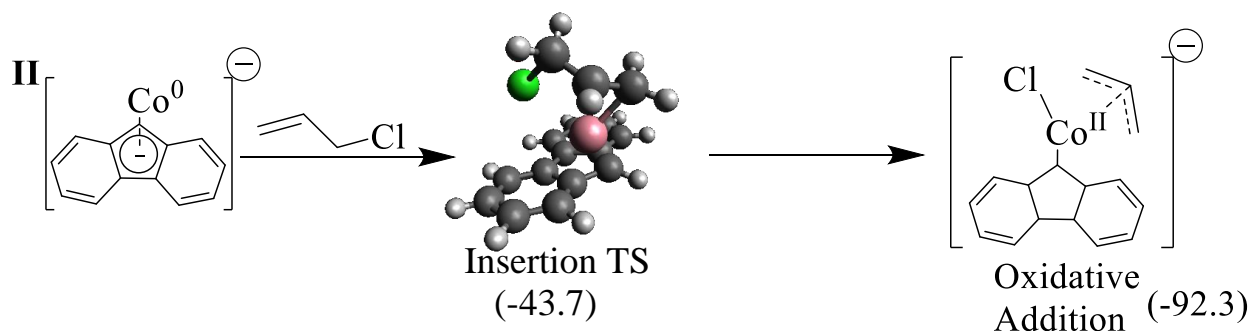


Figure 5.6. Product distributions for the oxidative addition reactions of various polar reagents by complexes I and IV. Products of reactions between the SAC model ions and adventitious species in the ion trap are not shown.

Similar results were observed with complex **IV**. One of the most notable differences was the appearance of the oxidative addition product in the reactions with propargyl chloride and allyl chloride. Also, the reaction with allyl acetate resulted in the insertion product but the reaction was relatively more competitive compared to the allyl acetate reaction with complex **I**. Of all the SAC model ions, the majority of the non-aromatic neutral reagents were most reactive with complexes **II** and **III**, similar to the reactions with aromatic reagents.

5.5 Computational Modelling for the Oxidative Addition of Non-Aromatic Reagents

Using allyl chloride as a sample reactant, computational modelling of reactions with the SAC model ions was carried out in order to gain more information on the thermodynamics of the oxidative additions. The reaction with complex **II** is shown in Scheme 5.17. DFT calculations suggest the metal center inserts into the C-Cl bond via a three-centered TS that is 43.7 kcal/mol below the reactants, resulting in a reaction that is exothermic by 92.3 kcal/mol.



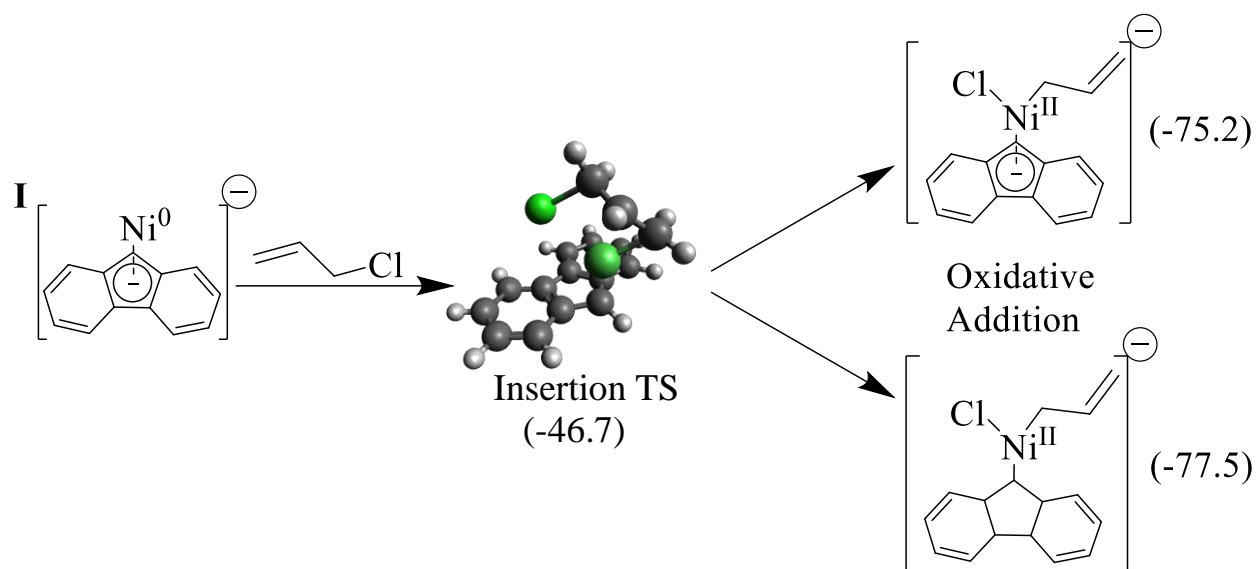
Scheme 5.17. Enthalpies for the TS state and oxidative addition product of the reaction between allyl chloride and complex **II**. Enthalpies in kcal/mol. Calculations were completed at the M06/6-311+G** level. Detailed information on the structures of the calculated species are shown in Appendix C.

In this case, as opposed to the results for the calculations of the chlorobenzene reaction, DFT calculations only suggested the η_1 structure where the metal is bound to the 9-carbon of the

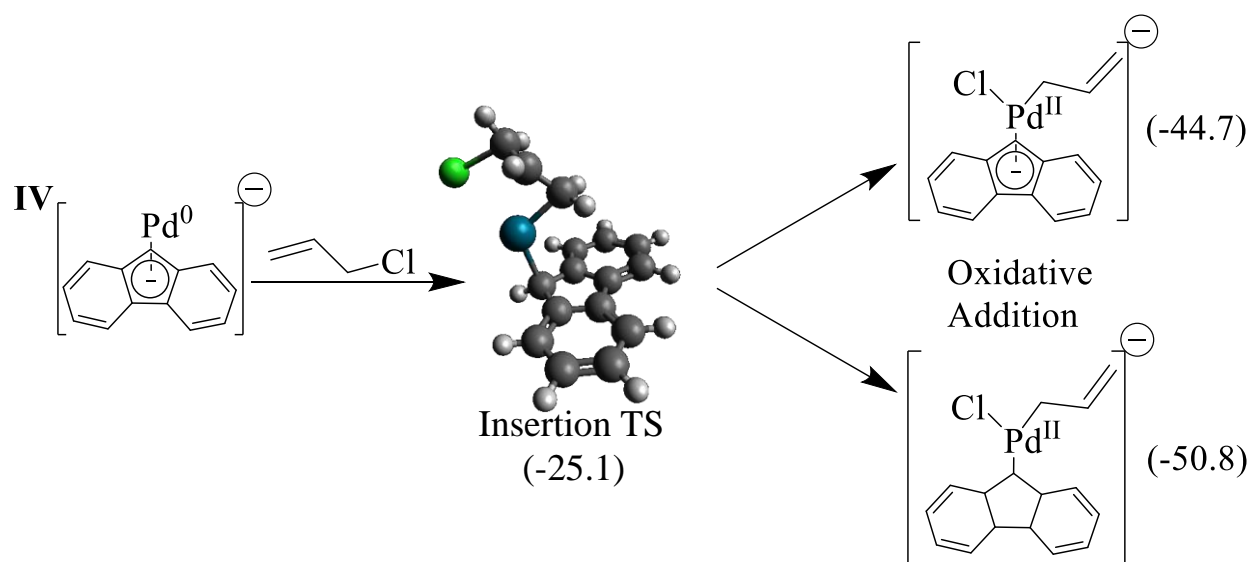
fluorenyl scaffold, despite efforts to optimize the η^5 structure where the metal is bound to the center ring of the fluorenyl scaffold.

The calculated transition states for the oxidative addition of allyl chloride by complexes **I** and **IV** are similar. Scheme 5.18 depicts the oxidative addition of allyl chloride to complex **I**. DFT calculations suggest the Ni center inserts into the C-Cl bond via a typical three-centered TS that is 46.7 kcal/mol below the reactants. As was the case with the aromatic reagents, DFT calculations indicate there are two possible oxidative addition products. Formation of the 9-fluorenyl complex is exothermic by 77.5 kcal/mol while forming the η^5 -fluorenyl product is exothermic by 75.2 kcal/mol. A similar TS that is 25.1 kcal/mol below the reactants was found for the reaction with complex **IV**, as shown in Scheme 5.19. Oxidative addition products with the η^5 -fluorenyl and 9-fluorenyl ligand structure are both possible and result in reactions that are exothermic by 44.7 and 50.8 kcal/mol, respectively. Once again, formation of the oxidative addition products of the reaction with complex **IV** are less exothermic than formation of the oxidative addition products for complexes **I** and **II**. Since complex **IV** was the only SAC model ion to display the intact oxidative addition product in the experiments with allyl chloride, exothermicities of ~ 50 kcal/mol or below may be required in order for the oxidative addition product to avoid fragmentation.

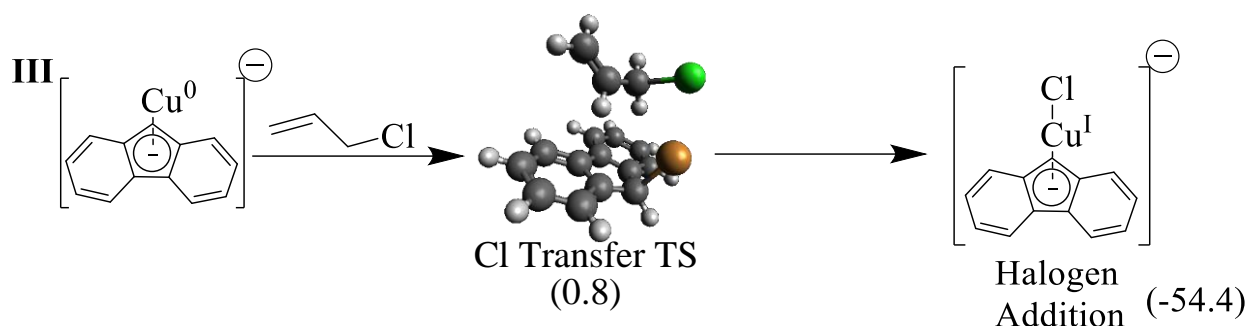
DFT calculations suggest a one-electron process for the reaction between complex **III** and allyl chloride. As shown in Scheme 5.20, complex **III** performs Cl abstraction via a one-electron transfer TS that is 0.8 kcal/mol above the reactants. This pathway directly leads to the halogen addition product and is exothermic by -54.4 kcal/mol. These results are similar to the pathway suggested for the chlorobenzene reaction and reinforces the rationale that the process is driven by the nature of the metal complex rather than the choice of polar reagent.



Scheme 5.18. Enthalpies for the TS and oxidative addition product of the reaction between allyl chloride and complex **I**. Calculations suggest formation of the oxidative addition product is favored in two different bonding schemes. Enthalpies are in kcal/mol. Calculations were completed at the M06/6-311+G** level. Detailed information on the structures of the calculated species are shown in Appendix C.

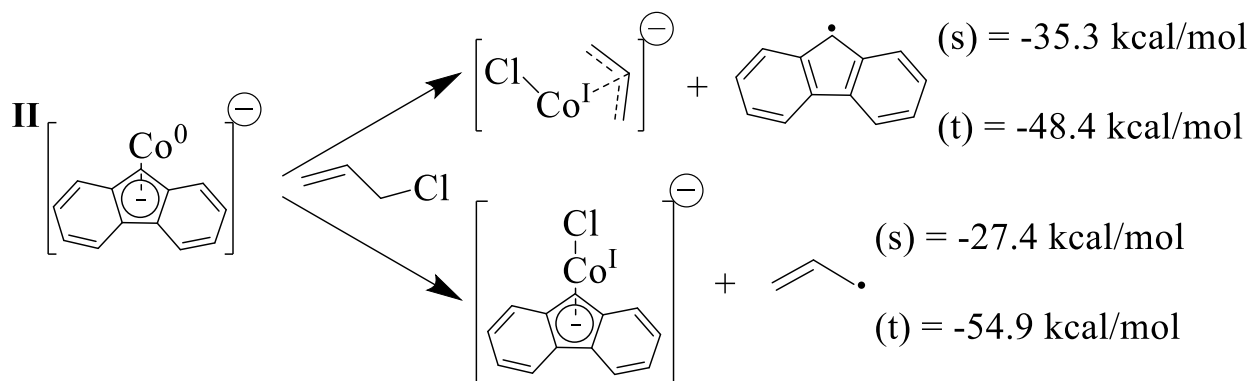


Scheme 5.19. Enthalpies for the TS and oxidative addition product of the reaction between allyl chloride and complex **IV**. Calculations suggest formation of the oxidative addition product is favored in two different bonding schemes. Enthalpies are in kcal/mol. Calculations were completed with M06 functional and a mixed lan12dz/6-311+G** basis set. Detailed information on the structures of the calculated species are shown in Appendix C.



Scheme 5.20. Enthalpies for the TS and halogen addition product of the reaction between allyl chloride and complex **III**. The TS is a one-electron process that leads to the halogen addition product. Enthalpies in kcal/mol. Calculations were completed at the M06/6-311+G** level. Detailed information on the structures of the calculated species are shown in Appendix C.

In addition to the transition states, the overall energetics for these reactions provide additional data for rationalizing the product distributions. Scheme 5.21 depicts the energetics for the reaction of allyl chloride with complex **II**. The insertion and halogen addition products were considered in both the singlet and triplet states. DFT calculations suggest that both products are more stable in the triplet state. Formation of the singlet and triplet states of the insertion product were exothermic by 35.3 kcal/mol and 48.4 kcal/mol, respectively. The Co center is bound to the allyl moiety in an η^3 fashion for both spin states. Formation of the halogen addition product is exothermic by 27.4 kcal/mol in the singlet state, while forming the triplet state is exothermic by 54.9 kcal/mol. When comparing the triplet states of each product, the halogen addition product is favored by 6.5 kcal/mol, which aligns with the product distribution for complex **II**, shown in Figure 5.5 (a).

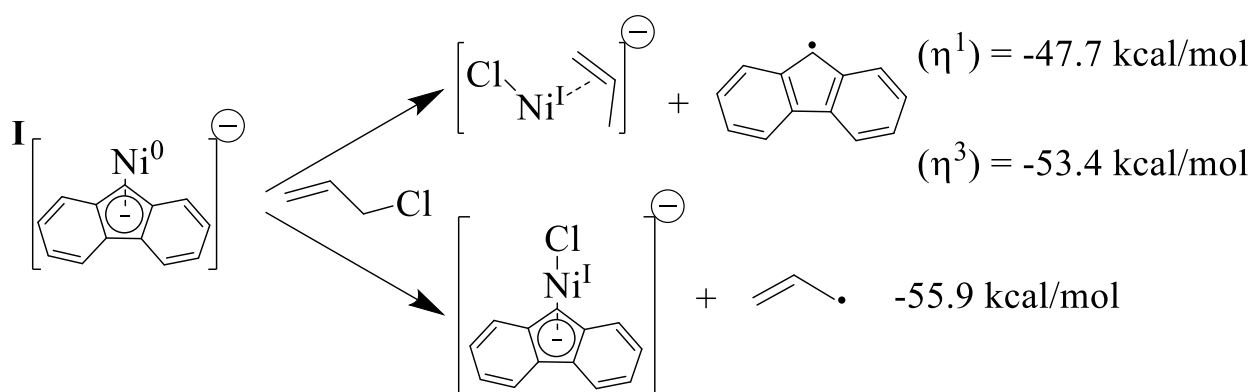


Scheme 5.21. Enthalpies for the reaction of allyl chloride with the Co SAC model ion. Complex **II** was calculated in the doublet, (d), spin state. Both singlet and triplet states were considered for the resulting product ion. (s) = singlet, (t) = triplet. Calculations were completed at the M06/6-311+G** level. Detailed information on the structures of the calculated species are shown in Appendix C.

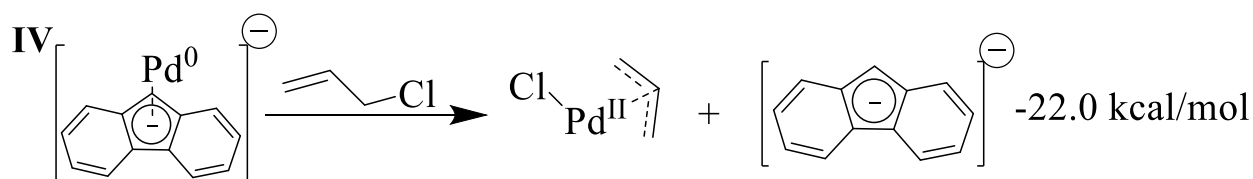
The overall energetics for the reactions of allyl chloride with complex **I** is depicted in Scheme 5.22. DFT calculations suggest that the insertion product can exist in two binding modes. When producing the η^1 -allyl insertion product, the reaction is exothermic by 47.7 kcal/mol while forming the η^3 -allyl insertion product results in a reaction that is exothermic by 53.4 kcal/mol. While the η^3 -binding mode is energetically favorable, both binding modes are possible. Formation of the halogen addition product was exothermic by 55.9 kcal/mol. Of the two observed products, the calculations suggest halogen addition is favored over the most stable insertion product by 2.5 kcal/mol. The small difference supports the almost equal formation of these products, as displayed in Figure 5.6 (a), and also suggests the insertion product mainly exists in the η^3 -binding mode.

The insertion product for the reaction with complex **IV** is depicted in Scheme 5.23. In this case, the fluorenyl anion was observed in the product spectrum. DFT calculations suggest formation of this ion is exothermic by 22.0 kcal/mol with the release of the neutral $\text{Pd}(\text{Cl})(\eta^3\text{-CH}_2\text{CH=CH}_2)$ complex. The η^3 -binding mode was the only option in this case since computational optimization

of the end-on η^1 binding mode led to the η^3 structure. Formation of the oxidative addition product (Scheme 5.19) is favored over the insertion product from an enthalpic perspective. However, formation of the insertion product leads to two products while the oxidative addition pathway only leads to the one product ion. Therefore, the insertion product is favored entropically and this may explain the preference for the insertion product observed in experiments (Figure 5.6), but it also depends on the efficiency of the oxidative product collisional cooling.

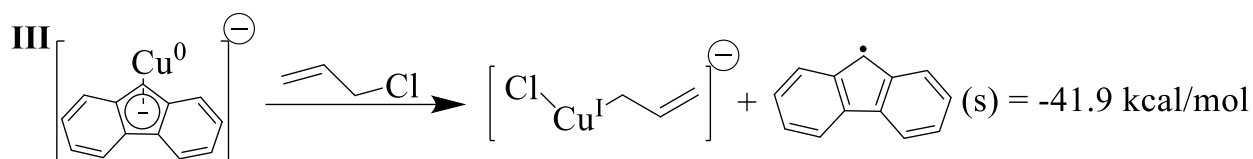


Scheme 5.22. Enthalpies for the reaction of allyl chloride with complex **I**. Ion reactants and products were calculated in the singlet state. DFT calculations suggest exothermic η^1 and η^3 binding modes for the insertion product. Calculations were completed at the M06/6-311+G** level. Detailed information on the structures of the calculated species are shown in Appendix C.



Scheme 5.23 Enthalpies for the reaction of allyl chloride with complex **IV**. Energetic information for the oxidative addition product (not shown) is depicted in Scheme 5.19. Ion reactants and products were calculated in the singlet (s), spin state. Calculations were completed with M06 functional and a mixed lanl2dz/6-311+G** basis set. Detailed information on the structures of the calculated species are shown in Appendix C.

DFT calculations also suggest favorable reactions leading to both products in the allyl chloride reaction with complex **III**. The insertion product was exothermic by 41.9 kcal/mol (Scheme 5.24), while the halogen addition product was exothermic by 54.4 kcal/mol (Scheme 5.20). In this case, the halogen addition product is favored by 12.5 kcal/mol. However, it is important to remember that the insertion and halogen addition products are formed via pathways with different TSs. As mentioned earlier, the differences in the energies of the TS will affect the product preference. Experimentally, halogen addition is favored over the insertion product (Figure 5.5) and therefore suggests that the TS leading to the insertion product may be higher in energy than the TS for halogen addition.



Scheme 5.24. Enthalpies for the reaction of allyl chloride with complex **III**. The reactant ion was calculated in the doublet, (d), spin state. Product ions were considered in the singlet spin state, (s). Calculations were completed at the M06/6-311+G** level. Detailed information on the structures of the calculated species are shown in Appendix C.

In this study, the oxidative addition reactivity of all four of our SAC model ions was tested. In most cases, experiments with various polar reagents led to fragmentation products that are indicative of oxidative addition. However, products that correlate to the full oxidative addition products were also observed and are supported by DFT calculations. Typical oxidative addition TSs for reactions with Co, Ni, and Pd SAC model ions were obtained via DFT calculations and provide further evidence of oxidative addition reactivity. However, it seems that the Cu SAC model ion preferentially activated polar bonds via a one-electron atom transfer process, due to the high 17-electron count of the metal complex. Our results suggest that graphene-supported SACs

that employ Co, Ni, or Pd may be able to engage in oxidative addition, a key step in many chemical transformations. Graphene-supported SACs that employ Cu likely cannot engage in oxidative additions on their own and may need a co-catalyst in order to complete desired transformations.

5.6 Experimental Section

All experiments were executed in a modified linear triple quadrupole ion trap mass spectrometer (modified Thermo Electron LTQ XL™) equipped with an electrospray ionization (ESI) source. Precursor complexes for all SAC model ions were introduced via ESI. Precursor complex solutions were made as follows:

Nickel precursor complex – Nickel(II) acetate tetrahydrate and fluorene-9-carboxylic acid were each dissolved in methanol at 10^{-4} M. Potassium oxalate monohydrate was dissolved in a water/methanol mixture at 10^{-4} M. These solutions were mixed in a 1:5:2.5 ratio by volume, respectively.

Cobalt precursor complex – Cobalt(II) benzoate and fluorene-9-carboxylic acid were each dissolved in methanol at 10^{-4} M. Potassium oxalate monohydrate was dissolved in a water/methanol mixture at 10^{-4} M. These solutions were mixed in a 1:4:0.6 ratio by volume, respectively.

Copper precursor complex – Copper(II) acetate and fluorene-9-carboxylic acid were each dissolved in methanol at 10^{-4} M. Potassium oxalate monohydrate was dissolved in a water/methanol mixture at 10^{-4} M. These solutions were mixed in a 1:4:1.5 ratio by volume, respectively.

Palladium precursor complex – Potassium tetrachloropalladate(II) and fluorene-9-carboxylic acid were each dissolved in methanol at 10^{-4} M. Potassium oxalate monohydrate was dissolved in a water/methanol mixture at 10^{-4} M. These solutions were mixed in a 1:1.5:0.5 ratio by volume, respectively.

Typical ESI conditions involved flow rates of $5\mu\text{L}/\text{min}$, needle potentials between 4-5 kV and heated capillary temperatures between 230-275 °C. A notched waveform was used to isolate the precursor complexes. The precursor complexes were subjected to sequential rounds of CID to form the respective SAC model ions. Once a steady signal of the ion of interest was achieved, neutral reagents were introduced into the ion trap via the external manifold, as previously described.^{36,68} Temperatures of the ion trap environment have been shown to be near room temperature.^{68,69} Reaction spectra were averaged over 200 scans in order to minimize noise. All neutral reagents were purchased commercially in the highest purity available and used without further purification. Density functional calculations were completed using the Gaussian16¹⁰¹ and Gaussian 09¹³⁶ suites of quantum mechanical programs. Calculations were completed using the M06 functional with an ECP basis set on Pd (lanl2dz) and a 6-311+G** basis set on all other atoms. Single point calculations at the M06/QZVP level with thermal enthalpy corrections from the calculations with the mixed ECP/6-311+G** basis set were performed for reported reaction energies. All transition states were verified using intrinsic reaction coordinate (IRC) calculations.

Chapter 6 - Conclusion

6.1 Highlights

SACs are considered to be the ultimate-limit in heterogenous catalysis since the atomic distribution can result in a catalyst with both homogeneous and heterogeneous characteristics.¹⁴ Understanding the underlying mechanisms of these catalysts is crucial to the advancement of SACs. However, as mentioned previously, surface analysis tools can become less effective for mechanistic studies at the atomic level. The goal of the work presented in this dissertation was to create an experimental model system that can be used to study the reactions and underlying mechanisms of graphene-supported SACs. We successfully generated a model ion in the gas-phase via sequential decarboxylative CID using a modified linear triple quadrupole ion trap mass spectrometer (modified Thermo Electron LTQ XLTM). The model ion consists of a zero-valent metal atom coordinated to the fluorenyl anion. Once again, the rationale is that if SACs operate through a single metal atom, the reactivity of these catalysts mainly depends on the local environment and therefore, metals supported on a simple polycyclic aromatic molecule, such as the fluorenyl anion, can serve as a model system for SACs supported on graphene.

The method for creating our model system is general and can be applied using a variety of metal centers. We generated the SAC model ion using Ni, Co, Cu and Pd. Three studies using our SAC model ions were detailed in Chapters 3, 4, and 5. The Ni SAC model was capable of the dehydrogenation of alkanes via C-H activation. Experiments and computational modelling suggest this process occurs via two C-H activations: C-H insertion followed by β -hydride elimination. Both the Ni and Co SAC model ions were capable of the amine and alcohol dehydrogenation via

similar mechanisms. Although not highlighted in those chapters, the potential energy surfaces suggest that the SAC models could also catalyze hydrogenations because the barriers in the reverse direction are modest and would be surmountable under mild conditions and hydrogen pressures. A study on the oxidative addition reactivity of the SAC model ions was also completed and suggests that the Ni, Co, and Pd SAC model ions can enact oxidative addition of polar reagents via a typical two-electron insertion process. Computational modelling suggest the Cu SAC model ion activates polar reagents via a one-electron transfer process. As mentioned previously, the structure of the fluorenyl anion, which serves as the carbon scaffold for our model ion, most closely resembles a Stone-Wales graphene defect.⁴⁶

6.2 Impact and Future Directions

As the field of single-atom catalysis continues, a wide variety of SACs are being created and studied.^{8,14-17} Our work with the model ions serves as a guide for condensed-phase chemists and suggests that if graphene containing Stone-Wales defects are used to trap atomic Ni, Co, or Pd, interesting and useful transformations can potentially be achieved. Simple alkanes can be made into valuable unsaturated feed stocks using a Ni active center. Amines and alcohols can be transformed into imine, aldehydes, and ketones using Ni and Co as the active centers. Introduction of co-catalysts may prove useful for achieving sequential transformations. Oxidative addition using the Ni, Co, and Pd active centers can act as a stepping stone in many important syntheses, including carbon coupling cycles. The suggested mechanisms for these processes can also help guide reagent choices and synthetic directions for the reactions that these SACs employ.

Of course, the most important question regarding any model is – Does the model accurately describe its target? Structural similarities, electronic similarities based on theoretical calculations, and our previously mentioned rationale give us good reason to believe our novel reactant system can serve as a reasonable model for graphene-supported SACs. In addition, we have demonstrated that the SAC models engage in mechanistic steps that are similar to those seen in condensed phase systems, e.g., oxidative addition, C-H activation. However, the only way to definitively test the efficacy of our model system is to compare our work to graphene-supported single-atom catalysts engaging in similar reaction systems. In order to accomplish this comparison several steps must be taken: (1) a graphene scaffold with sufficient Stone-Wales defects needs to be fabricated. (2) a method to stably anchor atomic distributions of metal atoms to the Stone-Wales defects on the graphene lattice must be developed. (3) alkane, amine, and alcohol dehydrogenation reactivity using Ni and Co graphene-supported SACs must be explored, as well as the oxidative addition reactivity of Ni, Co, Cu, and Pd graphene-supported SACs. As mention previously, Zhang et al. were able to trap Ni atoms on the defects of a graphene scaffold.³⁴ The major portion of these defects were Stone-Wales defects but a significant portion of the defects were not. Much more work and novel studies are needed to accomplish the goal of comparing our model system to an appropriate catalyst. However, if fabrication of an appropriate catalyst can be achieved, it is likely that many exciting discoveries await on the other side.

References

1. Copéret, C., Chabanas, M., Saint-Arroman, R. P. & Basset, J.-M. Homogeneous and Heterogeneous Catalysis: Bridging the Gap through Surface Organometallic Chemistry. *Angew. Chem., Int. Ed.* **42**, 156–181 (2003).
2. Roldan Cuenya, B. Metal Nanoparticle Catalysts Beginning to Shape-up. *Acc. Chem. Res.* **46**, 1682–1691 (2013).
3. Cao, S., Tao, F. (Feng), Tang, Y., Li, Y. & Yu, J. Size- and shape-dependent catalytic performances of oxidation and reduction reactions on nanocatalysts. *Chem. Soc. Rev.* **45**, 4747–4765 (2016).
4. Grabow, L. C. & Mavrikakis, M. Nanocatalysis Beyond the Gold-Rush Era. *Angewandte Chemie International Edition* **47**, 7390–7392 (2008).
5. Catalysis by design. *Nature Nanotechnology* **3**, 575–575 (2008).
6. Schauer mann, S., Nilius, N., Shaikhutdinov, S. & Freund, H.-J. Nanoparticles for Heterogeneous Catalysis: New Mechanistic Insights. *Acc. Chem. Res.* **46**, 1673–1681 (2013).
7. Pelletier, J. D. A. & Basset, J.-M. Catalysis by Design: Well-Defined Single-Site Heterogeneous Catalysts. *Acc. Chem. Res.* **49**, 664–677 (2016).
8. Yang, X.-F. *et al.* Single-Atom Catalysts: A New Frontier in Heterogeneous Catalysis. *Acc. Chem. Res.* **46**, 1740–1748 (2013).
9. Turner, M. *et al.* Selective oxidation with dioxygen by gold nanoparticle catalysts derived from 55-atom clusters. *Nature* **454**, 981–983 (2008).
10. Hughes, M. D. *et al.* Tunable gold catalysts for selective hydrocarbon oxidation under mild conditions. *Nature* **437**, 1132–1135 (2005).
11. Miller, J. T. *et al.* The effect of gold particle size on AuAu bond length and reactivity toward oxygen in supported catalysts. *Journal of Catalysis* **240**, 222–234 (2006).

12. Crespo-Quesada, M., Yarulin, A., Jin, M., Xia, Y. & Kiwi-Minsker, L. Structure Sensitivity of Alkynol Hydrogenation on Shape- and Size-Controlled Palladium Nanocrystals: Which Sites Are Most Active and Selective? *J. Am. Chem. Soc.* **133**, 12787–12794 (2011).
13. Molnár, Á., Sárkány, A. & Varga, M. Hydrogenation of carbon–carbon multiple bonds: chemo-, regio- and stereo-selectivity. *Journal of Molecular Catalysis A: Chemical* **173**, 185–221 (2001).
14. Liang, S., Hao, C. & Shi, Y. The Power of Single-Atom Catalysis. *ChemCatChem* **7**, 2559–2567 (2015).
15. Zhang Huabin, Liu Guigao, Shi Li & Ye Jinhua. Single-Atom Catalysts: Emerging Multifunctional Materials in Heterogeneous Catalysis. *Adv. Energy Mater.* **8**, 1701343 (2017).
16. Liu, J. Catalysis by Supported Single Metal Atoms. *ACS Catal.* **7**, 34–59 (2017).
17. Flytzani-Stephanopoulos, M. & Gates, B. C. Atomically Dispersed Supported Metal Catalysts. *Annual Review of Chemical and Biomolecular Engineering* **3**, 545–574 (2012).
18. Yan, H. *et al.* Single-Atom Pd₁/Graphene Catalyst Achieved by Atomic Layer Deposition: Remarkable Performance in Selective Hydrogenation of 1,3-Butadiene. *J. Am. Chem. Soc.* **137**, 10484–10487 (2015).
19. Derrien, M. L. Chapter 18 Selective Hydrogenation Applied to the Refining of Petrochemical Raw Materials Produced by Steam Cracking. in *Studies in Surface Science and Catalysis* (ed. Cerveny, L.) vol. 27 613–666 (Elsevier, 1986).
20. Cheng, N., Zhang, L., Doyle-Davis, K. & Sun, X. Single-Atom Catalysts: From Design to Application. *Electrochem. Energ. Rev.* **2**, 539–573 (2019).
21. Kyriakou, G. *et al.* Isolated Metal Atom Geometries as a Strategy for Selective Heterogeneous Hydrogenations. *Science* **335**, 1209–1212 (2012).
22. Zhang, X., Shi, H. & Xu, B.-Q. Catalysis by Gold: Isolated Surface Au³⁺ Ions are Active Sites for Selective Hydrogenation of 1,3-Butadiene over Au/ZrO₂ Catalysts. *Angew. Chem., Int. Ed.* **44**, 7132–7135 (2005).

23. Qiao, B. *et al.* Single-atom catalysis of CO oxidation using Pt₁/FeO_x. *Nat. Chem.* **3**, 634–641 (2011).
24. Wang, H. *et al.* Interaction between single gold atom and the graphene edge: A study via aberration-corrected transmission electron microscopy. *Nanoscale* **4**, 2920–2925 (2012).
25. Wang, H. *et al.* Atomic Bonding between Metal and Graphene. *J. Phys. Chem. C* **117**, 4632–4638 (2013).
26. Wu, P., Du, P., Zhang, H. & Cai, C. Graphyne-supported single Fe atom catalysts for CO oxidation. *Phys. Chem. Chem. Phys.* **17**, 1441–1449 (2014).
27. Krashennnikov, A. V., Lehtinen, P. O., Foster, A. S., Pyykkö, P. & Nieminen, R. M. Embedding Transition-Metal Atoms in Graphene: Structure, Bonding, and Magnetism. *Phys. Rev. Lett.* **102**, 126807 (2009).
28. Wang, H. *et al.* Doping Monolayer Graphene with Single Atom Substitutions. *Nano Lett.* **12**, 141–144 (2012).
29. Deng, D. *et al.* A single iron site confined in a graphene matrix for the catalytic oxidation of benzene at room temperature. *Sci. Adv.* **1**, e1500462 (2015).
30. Sun, S. *et al.* Single-atom Catalysis Using Pt/Graphene Achieved through Atomic Layer Deposition. *Sci. Rep.* **3**, 1775 (2013).
31. Rodríguez-Manzo, J. A., Cretu, O. & Banhart, F. Trapping of Metal Atoms in Vacancies of Carbon Nanotubes and Graphene. *ACS Nano* **4**, 3422–3428 (2010).
32. Markevich, A. V., Baldoni, M., Warner, J. H., Kirkland, A. I. & Besley, E. Dynamic Behavior of Single Fe Atoms Embedded in Graphene. *J. Phys. Chem. C* **120**, 21998–22003 (2016).
33. Robertson, A. W. *et al.* Dynamics of Single Fe Atoms in Graphene Vacancies. *Nano Lett.* **13**, 1468–1475 (2013).
34. Zhang, L. *et al.* Graphene Defects Trap Atomic Ni Species for Hydrogen and Oxygen Evolution Reactions. *Chem* **4**, 285–297 (2018).

35. Parkinson, G. S. Unravelling single atom catalysis: The surface science approach. *Chinese Journal of Catalysis* **38**, 1454–1459 (2017).
36. Gronert, S. Quadrupole ion trap studies of fundamental organic reactions. *Mass Spectrom. Rev.* **24**, 100–120 (2005).
37. O’Hair, R. A. J. The 3D quadrupole ion trap mass spectrometer as a complete chemical laboratory for fundamental gas-phase studies of metal mediated chemistry. *Chem. Commun.* **0**, 1469–1481 (2006).
38. Vikse, K. L., Henderson, M. A., Oliver, A. G. & McIndoe, J. S. Direct observation of key intermediates by negative-ion electrospray ionisation mass spectrometry in palladium-catalysed cross-coupling. *Chem. Commun.* **46**, 7412–7414 (2010).
39. Vikse, K., Khairallah, G. N., McIndoe, J. S. & O’Hair, R. A. J. Fixed-charge phosphine ligands to explore gas-phase coinage metal-mediated decarboxylation reactions. *Dalton Trans.* **42**, 6440–6449 (2013).
40. Vikse, K. L. & McIndoe, J. S. Mechanistic insights from mass spectrometry: examination of the elementary steps of catalytic reactions in the gas phase. *Pure Appl. Chem.* **87**, 361–377 (2015).
41. Armentrout, P. B. The Thermochemistry of Adsorbates on Transition Metal Cluster Ions: Relationship to Bulk-Phase Properties. *Eur. J. Mass Spectrom.* **9**, 531–538 (2003).
42. O’Hair, R. A. J. & Khairallah, G. N. Gas Phase Ion Chemistry of Transition Metal Clusters: Production, Reactivity, and Catalysis. *J. Cluster Sci.* **15**, 331–363 (2004).
43. Kim, Y. D. Chemical properties of mass-selected coinage metal cluster anions: towards obtaining molecular-level understanding of nanocatalysis. *Int. J. Mass Spectrom.* **238**, 17–31 (2004).
44. Böhme, D. K. & Schwarz, H. Gas-Phase Catalysis by Atomic and Cluster Metal Ions: The Ultimate Single-Site Catalysts. *Angew. Chem., Int. Ed.* **44**, 2336–2354 (2005).
45. Schwarz, H. Ménage-à-trois: single-atom catalysis, mass spectrometry, and computational chemistry. *Catal. Sci. Technol.* **7**, 4302–4314 (2017).

46. Ma, J., Alfè, D., Michaelides, A. & Wang, E. Stone-Wales defects in graphene and other planar sp²-bonded materials. *Phys. Rev. B* **80**, 033407 (2009).
47. Konermann, L., Ahadi, E., Rodriguez, A. D. & Vahidi, S. Unraveling the Mechanism of Electrospray Ionization. *Anal. Chem.* **85**, 2–9 (2013).
48. Gronert, S. Mass Spectrometric Studies of Organic Ion/Molecule Reactions. *Chem. Rev.* **101**, 329–360 (2001).
49. Armentrout, P. B. Kinetic energy dependence of ion–molecule reactions: guided ion beams and threshold measurements. *International Journal of Mass Spectrometry* **200**, 219–241 (2000).
50. Damrauer, R. Organometallic Chemistry in the Flowing Afterglow: A Review. *Organometallics* **23**, 1462–1479 (2004).
51. Briscese, S. M. J. & Riveros, J. M. Gas phase nucleophilic reactions of aromatic systems. *J. Am. Chem. Soc.* **97**, 230–231 (1975).
52. Moret, M.-E. & Chen, P. Ligand Binding Energies in Cationic Platinum(II) Complexes: A Quantitative Study in the Gas Phase. *Organometallics* **26**, 1523–1530 (2007).
53. Nguyen, S. & Fenn, J. B. Gas-phase ions of solute species from charged droplets of solutions. *PNAS* **104**, 1111–1117 (2007).
54. Dole, M. *et al.* Molecular Beams of Macroions. *J. Chem. Phys.* **49**, 2240–2249 (1968).
55. Iribarne, J. V. & Thomson, B. A. On the evaporation of small ions from charged droplets. *J. Chem. Phys.* **64**, 2287–2294 (1976).
56. The Nobel Prize in Chemistry 2002. *NobelPrize.org*
<https://www.nobelprize.org/prizes/chemistry/2002/fenn/lecture/>.
57. The Nobel Prize in Physics 1989. *NobelPrize.org*
<https://www.nobelprize.org/prizes/physics/1989/paul/lecture/>.
58. *LTQ Series Hardware Manual Revision D*, 172 (2015).

59. March, R. E. An Introduction to Quadrupole Ion Trap Mass Spectrometry. *Journal of Mass Spectrometry* **32**, 351–369 (1997).
60. Weil, C., Nappi, M., Cleven, C. D., Wollnik, H. & Cooks, R. G. Multiparticle Simulation of Ion Injection into the Quadrupole Ion Trap Under the Influence of Helium Buffer Gas Using Short Injection Times and DC Pulse Potentials. *Rapid Communications in Mass Spectrometry* **10**, 742–750 (1996).
61. Stafford, G. C., Kelley, P. E., Syka, J. E. P., Reynolds, W. E. & Todd, J. F. J. Recent improvements in and analytical applications of advanced ion trap technology. *International Journal of Mass Spectrometry and Ion Processes* **60**, 85–98 (1984).
62. Wong, P. S. H. Ion Trap Mass Spectrometry. *Current Separations* **16**, 85–93 (1997).
63. Louris, J. N., Amy, J. W., Ridley, T. Y. & Cooks, R. G. Injection of ions into a quadrupole ion trap mass spectrometer. *International Journal of Mass Spectrometry and Ion Processes* **88**, 97–111 (1989).
64. Mitchell Wells, J. & McLuckey, S. A. Collision-Induced Dissociation (CID) of Peptides and Proteins. in *Methods in Enzymology* vol. 402 148–185 (Academic Press, 2005).
65. Brodbelt-Lustig, J. S. & Cooks, R. G. Determination of relative gas-phase basicities by the proton-transfer equilibrium technique and the kinetic method in a quadrupole ion-trap. *Talanta* **36**, 255–260 (1989).
66. Nourse, B. D. & Kenttamaa, H. I. Effective ion temperatures in a quadrupole ion trap. *J. Phys. Chem.* **94**, 5809–5812 (1990).
67. Basic, C., Eyler, J. R. & Yost, R. A. Probing trapped ion energies via ion-molecule reaction kinetics: Quadrupole ion trap mass spectrometry. *J Am Soc Mass Spectrom* **3**, 716–726 (1992).
68. Gronert, S. Estimation of effective ion temperatures in a quadrupole ion trap. *J. Am. Soc. Mass Spectrom.* **9**, 845–848 (1998).
69. Donald, W. A., Khairallah, G. N. & O’Hair, R. A. J. The Effective Temperature of Ions Stored in a Linear Quadrupole Ion Trap Mass Spectrometer. *J. Am. Soc. Mass Spectrom.* **24**, 811–815 (2013).

70. Curtis, S., Renaud, J., Holmes, J. L. & Mayer, P. M. Old acid, new chemistry. Negative metal anions generated from alkali metal oxalates and others. *J. Am. Soc. Mass Spectrom.* **21**, 1944–1946 (2010).
71. Hale, R. D., Chan, C.-C., Weisbecker, C. S. & Attygalle, A. B. Gas-phase fragmentation of metal adducts of alkali-metal oxalate salts. *J. Mass Spectrom.* **49**, 195–200 (2014).
72. Brydon, S. C. *et al.* Experimental and DFT Studies on the Identity Exchange Reactions between Phenyl Chalcogen Iridium Ions and Alkenes. *J. Phys. Chem. A* **123**, 8200–8207 (2019).
73. Taubmann, S. & Alt, H. G. Heterogeneous catalysts for the dehydrogenation of saturated hydrocarbons. *Journal of Molecular Catalysis A: Chemical* **287**, 102–109 (2008).
74. Sattler, J. J. H. B., Ruiz-Martinez, J., Santillan-Jimenez, E. & Weckhuysen, B. M. Catalytic Dehydrogenation of Light Alkanes on Metals and Metal Oxides. *Chem. Rev.* **114**, 10613–10653 (2014).
75. Siri, G. J., Casella, M. L., Santori, G. F. & Ferretti, O. A. Tin/Platinum on Alumina as Catalyst for Dehydrogenation of Isobutane. Influence of the Preparation Procedure and of the Addition of Lithium on the Catalytic Properties. *Ind. Eng. Chem. Res.* **36**, 4821–4826 (1997).
76. Dobereiner, G. E. & Crabtree, R. H. Dehydrogenation as a Substrate-Activating Strategy in Homogeneous Transition-Metal Catalysis. *Chem. Rev.* **110**, 681–703 (2010).
77. Crabtree, R. H., Mihelcic, J. M. & Quirk, J. M. Iridium complexes in alkane dehydrogenation. *J. Am. Chem. Soc.* **101**, 7738–7740 (1979).
78. Göttker-Schnetmann, I., White, P. & Brookhart, M. Iridium Bis(phosphinite) p-XPCP Pincer Complexes: Highly Active Catalysts for the Transfer Dehydrogenation of Alkanes. *J. Am. Chem. Soc.* **126**, 1804–1811 (2004).
79. Gupta, M., Hagen, C., Flesher, R. J., Kaska, W. C. & Jensen, C. M. A highly active alkane dehydrogenation catalyst: stabilization of dihydrido rhodium and iridium complexes by a P–C–P pincer ligand. *Chem. Commun.* 2083–2084 (1996) doi:10.1039/CC9960002083.

80. Gupta, M., Hagen, C., Kaska, W. C., Cramer, R. E. & Jensen, C. M. Catalytic Dehydrogenation of Cycloalkanes to Arenes by a Dihydrido Iridium P–C–P Pincer Complex. *J. Am. Chem. Soc.* **119**, 840–841 (1997).
81. Baudry, D., Ephritikhine, M., Felkin, H. & Holmes-Smith, R. The selective catalytic conversion of cycloalkanes into cycloalkenes using a soluble rhenium polyhydride system. *J. Chem. Soc., Chem. Commun.* 788–789 (1983) doi:10.1039/C39830000788.
82. Braunstein, P. *et al.* Rhodium(I) and Iridium(I) Complexes with β -Keto Phosphine or Phosphino Enolate Ligands. Catalytic Transfer Dehydrogenation of Cyclooctane. *Organometallics* **15**, 5551–5567 (1996).
83. A. Miller, J. & K. Knox, L. Efficient and selective catalytic dehydrogenation of alkanes using rhodium(I) arsine complexes. *Journal of the Chemical Society, Chemical Communications* **0**, 1449–1450 (1994).
84. Huang, Z. *et al.* Highly Active and Recyclable Heterogeneous Iridium Pincer Catalysts for Transfer Dehydrogenation of Alkanes. *Advanced Synthesis & Catalysis* **351**, 188–206 (2009).
85. Xu, W. *et al.* Thermochemical alkane dehydrogenation catalyzed in solution without the use of a hydrogen acceptor. *Chem. Commun.* 2273–2274 (1997) doi:10.1039/A705105K.
86. Zhu, K., Achord, P. D., Zhang, X., Krogh-Jespersen, K. & Goldman, A. S. Highly Effective Pincer-Ligated Iridium Catalysts for Alkane Dehydrogenation. DFT Calculations of Relevant Thermodynamic, Kinetic, and Spectroscopic Properties. *J. Am. Chem. Soc.* **126**, 13044–13053 (2004).
87. Black, D. M., Payne, A. H. & Glish, G. L. Determination of Cooling Rates in a Quadrupole Ion Trap. *J. Am. Soc. Mass Spectrom.* **17**, 932–938 (2006).
88. Reed, A. E., Weinstock, R. B. & Weinhold, F. Natural population analysis. *J. Chem. Phys.* **83**, 735–746 (1985).

89. Ritter, D., Carroll, J. J. & Weisshaar, J. C. Kinetics of neutral transition metal atoms in the gas phase: reactions of scandium through copper with alkanes and alkenes. *J. Phys. Chem.* **96**, 10636–10645 (1992).
90. Curtis, S. *et al.* Reactions of Atomic Metal Anions in the Gas phase: Competition between Electron Transfer, Proton Abstraction and Bond Activation. *J. Phys. Chem. A* **115**, 14006–14012 (2011).
91. Zhao, Y.-X., Liu, Q.-Y., Zhang, M.-Q. & He, S.-G. Reactions of metal cluster anions with inorganic and organic molecules in the gas phase. *Dalton Trans.* **45**, 11471–11495 (2016).
92. Weisshaar, J. C. Bare transition metal atoms in the gas phase: reactions of M, M⁺, and M²⁺ with hydrocarbons. *Acc. Chem. Res.* **26**, 213–219 (1993).
93. van Koppen, P. A. M., Bowers, M. T., Fisher, E. R. & Armentrout, P. B. Relative Energetics of C-H and C-C Bond Activation of Alkanes: Reactions of Ni⁺ and Fe⁺ with Propane on the Lowest Energy (Adiabatic) Potential Energy Surfaces. *J. Am. Chem. Soc.* **116**, 3780–3791 (1994).
94. Eller, Karsten. & Schwarz, Helmut. Organometallic chemistry in the gas phase. *Chem. Rev.* **91**, 1121–1177 (1991).
95. Yi, S. S., Blomberg, M. R. A., Siegbahn, P. E. M. & Weisshaar, J. C. Statistical Modeling of Gas-Phase Organometallic Reactions Based on Density Functional Theory: Ni⁺ + C₃H₈. *J. Phys. Chem. A* **102**, 395–411 (1998).
96. Tjelta, B. L. & Armentrout, P. B. Ligand Effects in C–H and C–C Bond Activation by Gas-Phase Transition Metal–Ligand Complexes. *J. Am. Chem. Soc.* **118**, 9652–9660 (1996).
97. Albert, G. *et al.* Methane activation by rhodium cluster argon complexes. *Chem. Phys. Lett.* **268**, 235–241 (1997).
98. Chen, Y.-M., Sievers, M. R. & Armentrout, P. B. Activation of CH₄, C₂H₆, C₃H₈, and c-C₃H₆ by gas-phase Pd⁺ and the thermochemistry of Pd-ligand complexes. *Int. J. Mass Spectrom. Ion Processes* **167–168**, 195–212 (1997).

99. Innorta, G. & Torroni, S. Propane activation by $M_2C_5H_5$ (M=Ni and Co): An experimental and theoretical work. *J. Organomet. Chem.* **692**, 5563–5570 (2007).
100. Henderson, M. A., Kwok, S. & McIndoe, J. S. Gas-phase reactivity of ruthenium carbonyl cluster anions. *J. Am. Soc. Mass Spectrom.* **20**, 658–666 (2009).
101. Frisch, M. J. et al. *Gaussian 16 Rev. A.03.* (2016).
102. Gu, X.-Q., Chen, W., Morales-Morales, D. & Jensen, C. M. Dehydrogenation of secondary amines to imines catalyzed by an iridium PCP pincer complex: initial aliphatic or direct amino dehydrogenation? *Journal of Molecular Catalysis A: Chemical* **189**, 119–124 (2002).
103. Saidi, O., Blacker, A. J., Farah, M. M., Marsden, S. P. & Williams, J. M. J. Selective Amine Cross-Coupling Using Iridium-Catalyzed “Borrowing Hydrogen” Methodology. *Angew. Chem., Int. Ed.* **48**, 7375–7378 (2009).
104. Bernskoetter, W. H. & Brookhart, M. Kinetics and Mechanism of Iridium-Catalyzed Dehydrogenation of Primary Amines to Nitriles. *Organometallics* **27**, 2036–2045 (2008).
105. Matsu-ura, T., Sakaguchi, S., Obora, Y. & Ishii, Y. Guerbet Reaction of Primary Alcohols Leading to β -Alkylated Dimer Alcohols Catalyzed by Iridium Complexes. *J. Org. Chem.* **71**, 8306–8308 (2006).
106. Blank, B., Michlik, S. & Kempe, R. Selective Iridium-Catalyzed Alkylation of (Hetero)Aromatic Amines and Diamines with Alcohols under Mild Reaction Conditions. *Chemistry – A European Journal* **15**, 3790–3799 (2009).
107. Nicolau, G., Tarantino, G. & Hammond, C. Acceptorless Alcohol Dehydrogenation Catalysed by Pd/C. *ChemSusChem* **12**, 4953–4961 (2019).
108. Stubbs, J. M., Hazlehurst, R. J., Boyle, P. D. & Blacquiere, J. M. Catalytic Acceptorless Dehydrogenation of Amines with $Ru(PR_2NR'_2)$ and $Ru(dppp)$ Complexes. *Organometallics* **36**, 1692–1698 (2017).

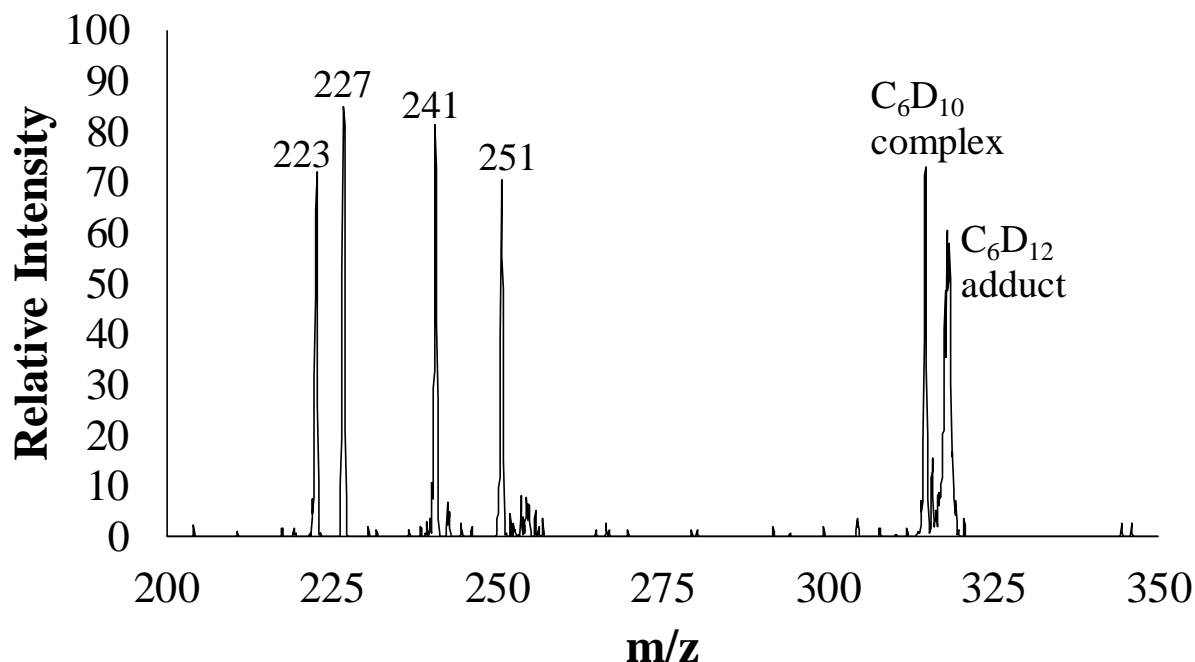
109. Sahoo, M. K. & Balaraman, E. Room temperature catalytic dehydrogenation of cyclic amines with the liberation of H₂ using water as a solvent. *Green Chem.* **21**, 2119–2128 (2019).
110. Zhang, J., Gandelman, M., Shimon, L. J. W., Rozenberg, H. & Milstein, D. Electron-Rich, Bulky Ruthenium PNP-Type Complexes. Acceptorless Catalytic Alcohol Dehydrogenation. *Organometallics* **23**, 4026–4033 (2004).
111. Jaiswal, G., Landge, V. G., Jagadeesan, D. & Balaraman, E. Iron-based nanocatalyst for the acceptorless dehydrogenation reactions. *Nature Communications* **8**, 1–13 (2017).
112. Siddiki, S. M. A. H., Toyao, T. & Shimizu, K. Acceptorless dehydrogenative coupling reactions with alcohols over heterogeneous catalysts. *Green Chem.* **20**, 2933–2952 (2018).
113. Ryabchuk, P. *et al.* Heterogeneous nickel-catalysed reversible, acceptorless dehydrogenation of N-heterocycles for hydrogen storage. *Chem. Commun.* **55**, 4969–4972 (2019).
114. Labinger, J. A. Tutorial on Oxidative Addition. *Organometallics* **34**, 4784–4795 (2015).
115. Vaska, L. & DiLuzio, J. W. CARBONYL AND HYDRIDO-CARBONYL COMPLEXES OF IRIIDIUM BY REACTION WITH ALCOHOLS. HYDRIDO COMPLEXES BY REACTION WITH ACID. *J. Am. Chem. Soc.* **83**, 2784–2785 (1961).
116. Vaska, L. & DiLuzio, J. W. Activation of Hydrogen by a Transition Metal Complex at Normal Conditions Leading to a Stable Molecular Dihydride. *J. Am. Chem. Soc.* **84**, 679–680 (1962).
117. Collman, J. P. & Roper, W. R. Preparation and Oxidative Addition Reactions of a Monomeric Ruthenium(0) Complex. *J. Am. Chem. Soc.* **87**, 4008–4009 (1965).
118. Maitlis, P. M., Haynes, A., Sunley, G. J. & Howard, M. J. Methanol carbonylation revisited: thirty years on. *J. Chem. Soc., Dalton Trans.* 2187–2196 (1996) doi:10.1039/DT9960002187.
119. Haynes, A. *et al.* Promotion of Iridium-Catalyzed Methanol Carbonylation: Mechanistic Studies of the Cativa Process. *J. Am. Chem. Soc.* **126**, 2847–2861 (2004).

120. Nicolaou, K. C., Bulger, P. G. & Sarlah, D. Palladium-Catalyzed Cross-Coupling Reactions in Total Synthesis. *Angew. Chem., Int. Ed.* **44**, 4442–4489 (2005).
121. Dounay, A. B. & Overman, L. E. The Asymmetric Intramolecular Heck Reaction in Natural Product Total Synthesis. *Chem. Rev.* **103**, 2945–2964 (2003).
122. de Vries, J. G. The Heck reaction in the production of fine chemicals. *Can. J. Chem.* **79**, 1086–1092 (2001).
123. Blaser, H.-U., Indolese, A., Naud, F., Nettekoven, U. & Schnyder, A. Industrial R&D on Catalytic C-C and C-N Coupling Reactions: A Personal Account on Goals, Approaches and Results. *Adv. Synth. Catal.* **346**, 1583–1598 (2004).
124. Yin & Liebscher, J. Carbon–Carbon Coupling Reactions Catalyzed by Heterogeneous Palladium Catalysts. *Chem. Rev.* **107**, 133–173 (2007).
125. Molnár, Á. Efficient, Selective, and Recyclable Palladium Catalysts in Carbon–Carbon Coupling Reactions. *Chem. Rev.* **111**, 2251–2320 (2011).
126. Rosen, B. M. *et al.* Nickel-Catalyzed Cross-Couplings Involving Carbon–Oxygen Bonds. *Chem. Rev.* **111**, 1346–1416 (2011).
127. Fürstner, A., Leitner, A., Méndez, M. & Krause, H. Iron-Catalyzed Cross-Coupling Reactions. *J. Am. Chem. Soc.* **124**, 13856–13863 (2002).
128. Feng, Z., Chen, F. & Zhang, X. Copper Catalyzed Cross-Coupling of Iodobenzoates with Bromozinc-difluorophosphonate. *Org. Lett.* **14**, 1938–1941 (2012).
129. The Nobel Prize in Chemistry 2010. *NobelPrize.org*
<https://www.nobelprize.org/prizes/chemistry/2010/summary/>.
130. Lee, E.-K. *et al.* Platinum single atoms dispersed on carbon nanotubes as reusable catalyst for Suzuki coupling reaction. *Journal of Catalysis* **352**, 388–393 (2017).

131. Zhang, X. *et al.* C–C Coupling on Single-Atom-Based Heterogeneous Catalyst. *J. Am. Chem. Soc.* **140**, 954–962 (2018).
132. Chen, Z. *et al.* A heterogeneous single-atom palladium catalyst surpassing homogeneous systems for Suzuki coupling. *Nature Nanotechnology* **1** (2018) doi:10.1038/s41565-018-0167-2.
133. Douvris, C. & Ozerov, O. V. Hydrodefluorination of Perfluoroalkyl Groups Using Silylium-Carborane Catalysts. *Science* **321**, 1188–1190 (2008).
134. Chock, P. B. & Halpern, J. Reactions of pentacyanocobaltate(II) with some organic halides. *J. Am. Chem. Soc.* **91**, 582–588 (1969).
135. Anka-Lufford, L. L., Prinsell, M. R. & Weix, D. J. Selective Cross-Coupling of Organic Halides with Allylic Acetates. *J. Org. Chem.* **77**, 9989–10000 (2012).
136. Frisch, M. J. *et al.* *Gaussian 09 Rev. C.01.* (2010).

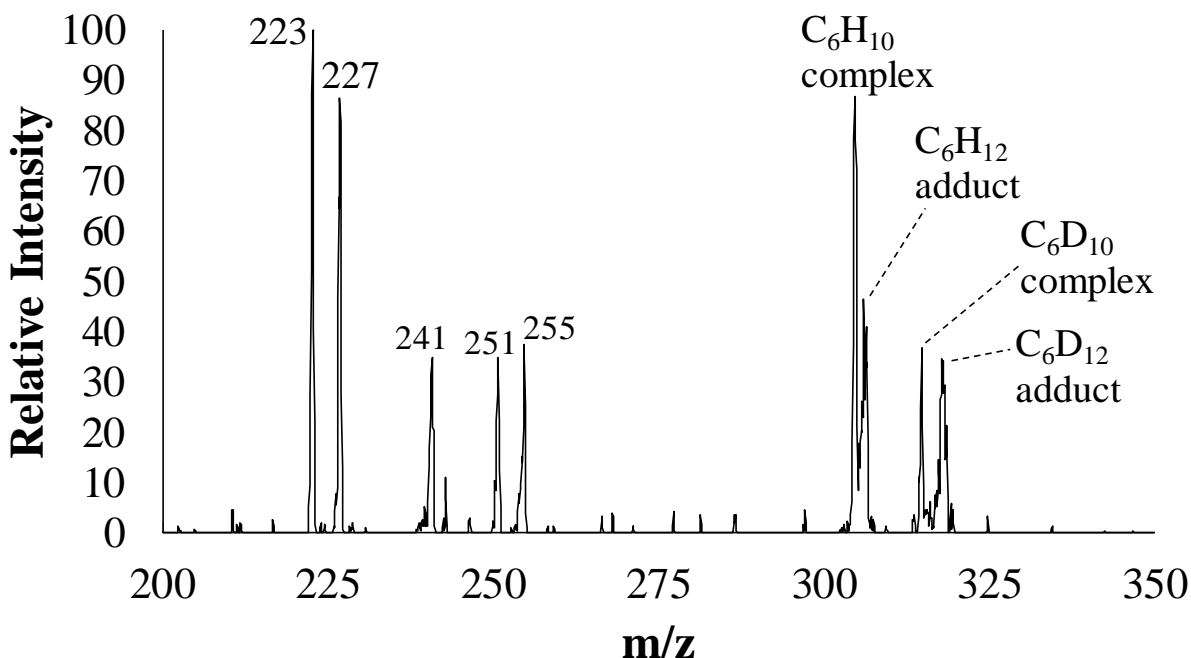
Appendix A – Spectra

A.1. Mass spectrum for reaction of complex I with cyclohexane-d₁₂.



The dehydrogenation and alkane adduct peaks (C₆D₁₀ complex and C₆D₁₂ adduct) appear at m/z 315 and 319, respectively. Peak broadening is observed for the alkane adduct peak due to the relative instability of the product ion during the instrument scans. Complex I appears at m/z 223. Adduct formation products of complex I with water and nitrogen appear at m/z 241 and 251, respectively. The peak at m/z 227 may be an adduct of fluorene-9-carboxylate and water formed through secondary reactions. There are also peaks (not shown) at m/z 90, an oxide from reaction with adventitious oxygen, and m/z 107, an unidentified adduct that is independent of the neutral reagent.

A.2. Mass spectrum for reaction of complex **I** with a 50% by volume solution of cyclohexane-d12 in cyclohexane.



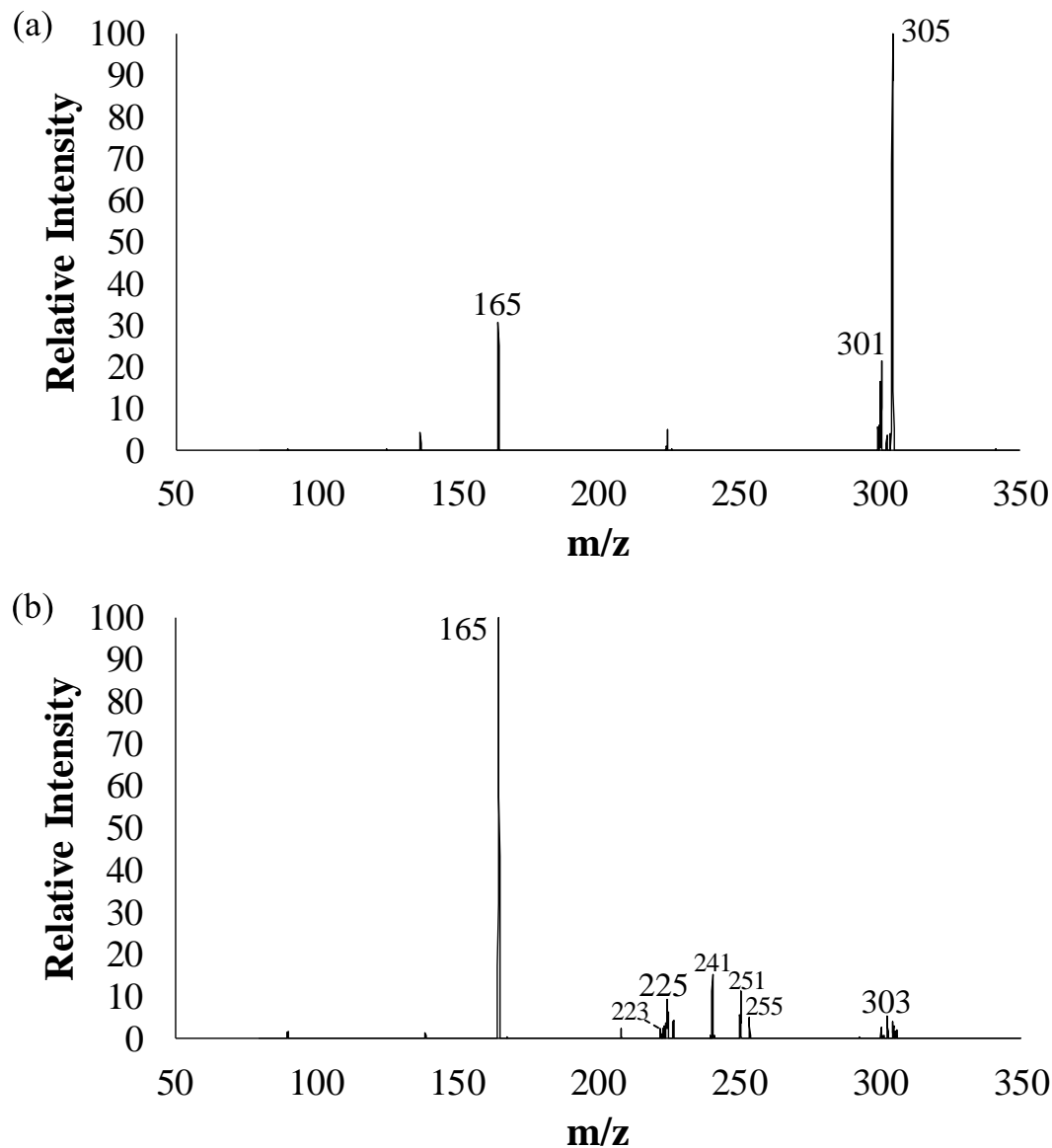
The dehydrogenation products of cyclohexane and cyclohexane-d12 (C₆H₁₀ and C₆D₁₀ complexes) appear at m/z 305 and 315, respectively. Relative kinetic analysis of these peaks provides a KIE value. The alkane adduct products (C₆H₁₂ and C₆D₁₂ adducts) appear at m/z 307 and 319, respectively. Peak broadening for the alkane adduct products is observed due to the relative instability of the product ions during the instrument scans. Complex **I** appears at m/z 223. Adduct formation products of complex **I** with water, nitrogen and methanol appear at m/z 241, 251 and 255, respectively. The peak at m/z 227 may be an adduct of fluorene-9-carboxylate and water formed through secondary reactions. There are also peaks (not shown) at m/z 90, an oxide from reaction with adventitious oxygen, and m/z 107, an unidentified adduct that is independent of the neutral reagent.

Relative Intensity of m/z 305 = 86.89

Relative Intensity of m/z 315 = 36.77

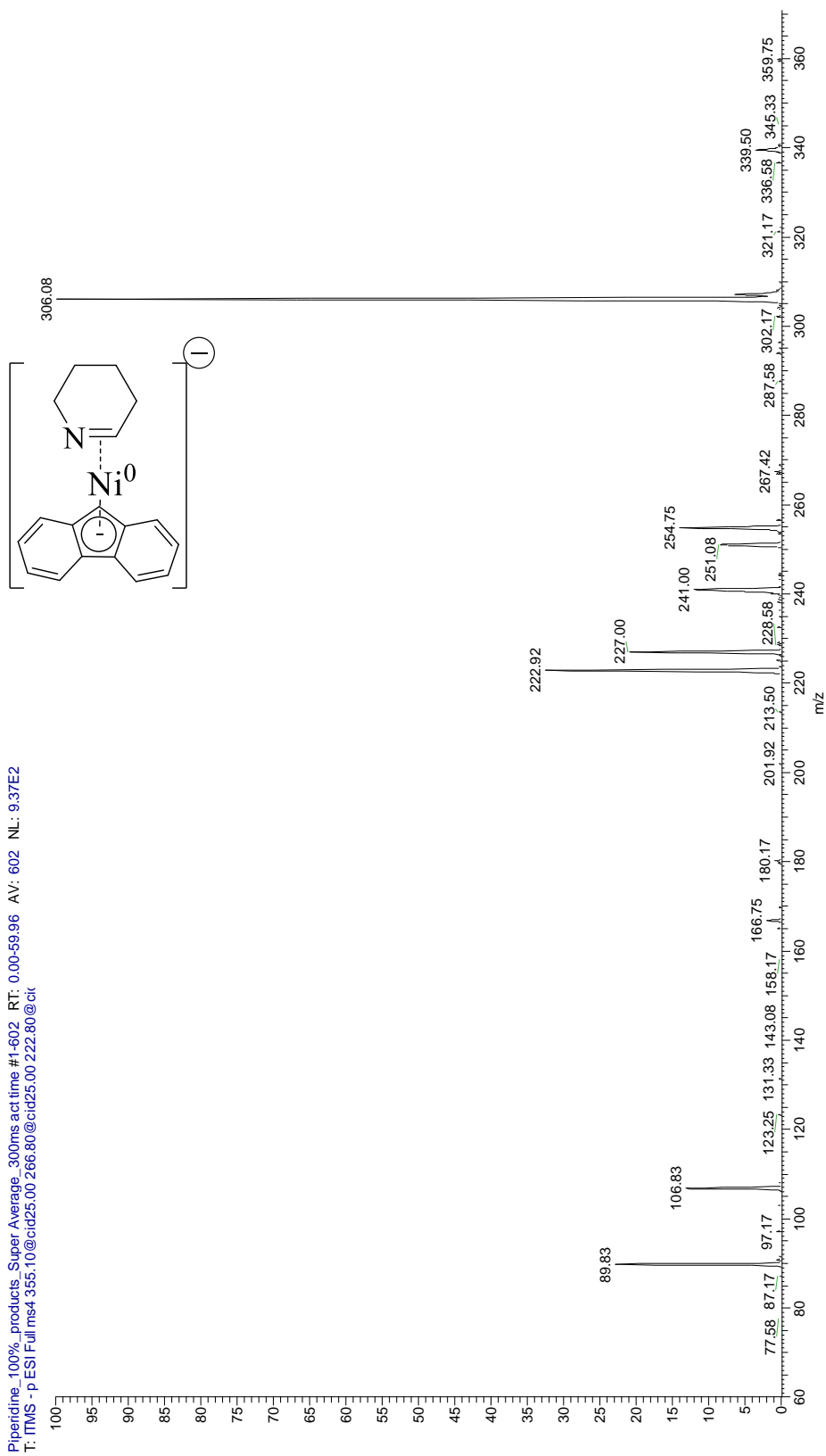
$$KIE = \frac{\text{Relative Intensity of C - H activation}}{\text{Relative Intensity of C - D activation}} = \frac{86.89}{36.77} = 2.4$$

A.3. Mass Spectra of the CID of the cyclohexene adduct.



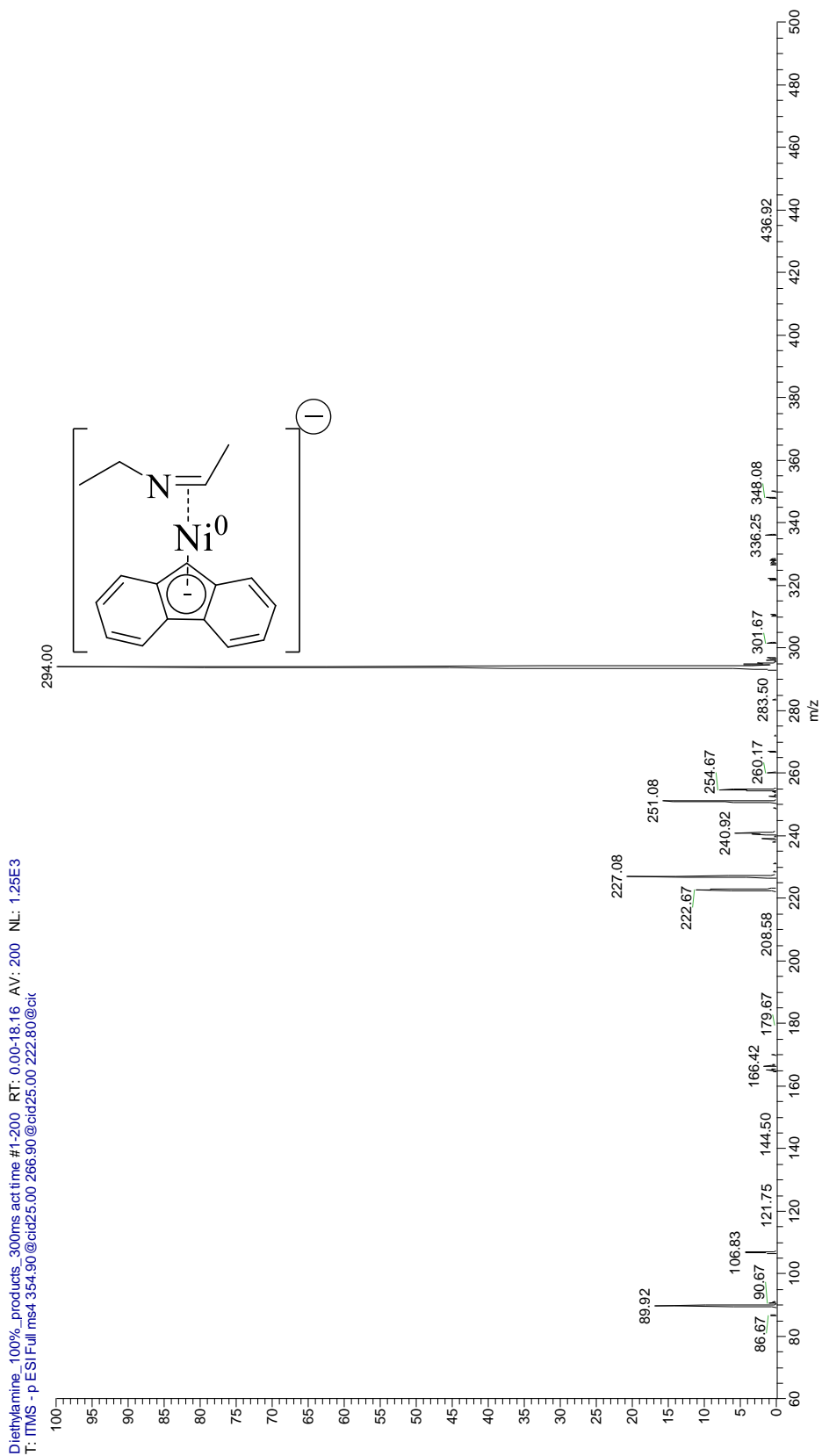
Panels (a) and (b) depict CID of the cyclohexene adduct (m/z 305) using 15 and 25 eV, respectively. The peaks at m/z 301, 303 and 225 correspond to the benzene adduct, cyclohexadiene adduct, and H_2 adduct, respectively. The peak at m/z 165 corresponds to the fluorenyl anion. This anion is relatively stable and is lost easily due to the energy introduced by CID. The peak at m/z 223 corresponds to complex I, which indicates the loss of cyclohexene and recovery of the reactant ion. Adduct formation with adventitious water, nitrogen and methanol appear at m/z 241, 251 and 255, respectively

A.4. Product spectrum for piperidine reaction with complex I.

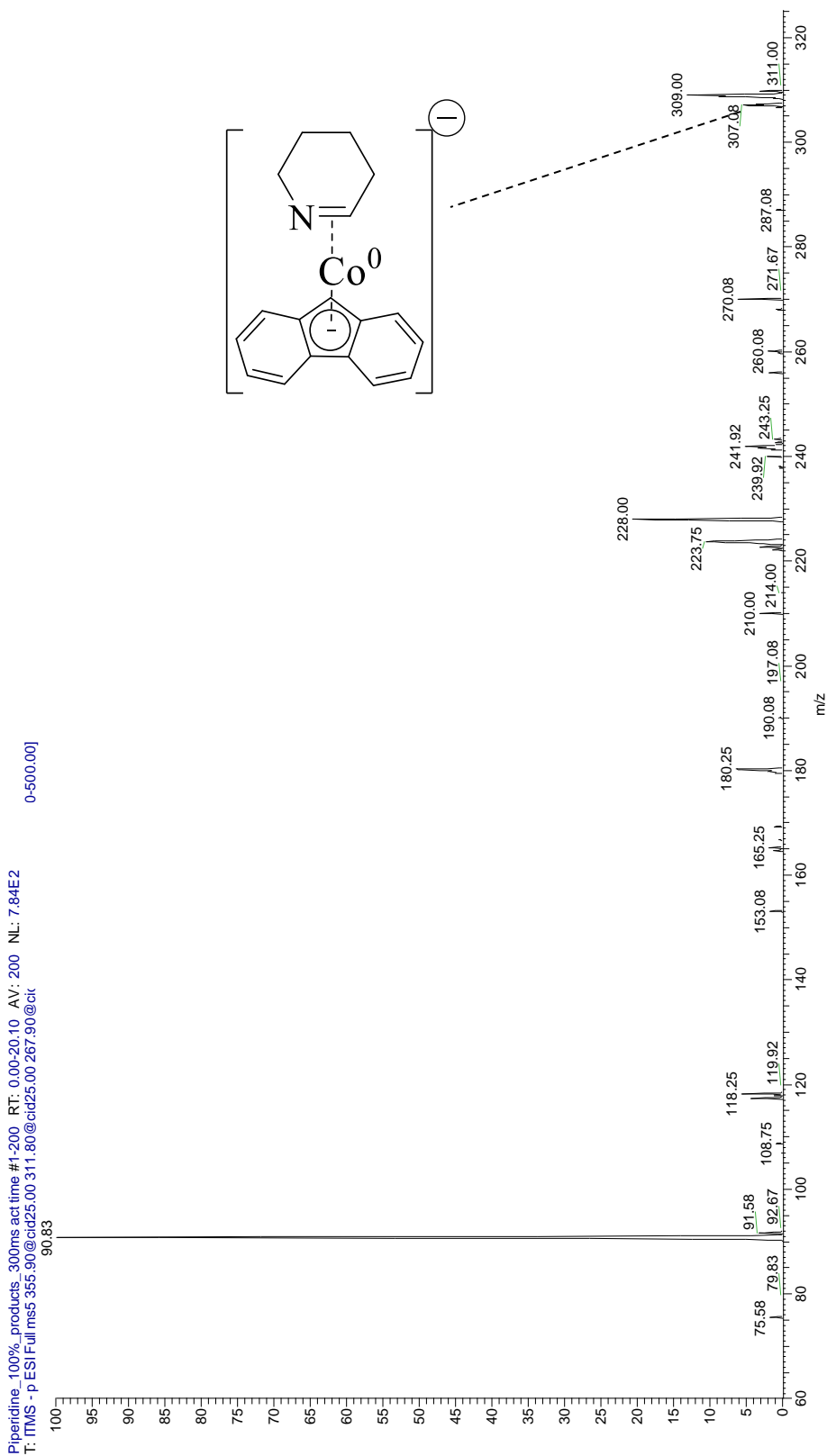


Piperidine_100%_products_Super_Average_300ms_act_time_#1-602_RT: 0.00-59.96 AV: 602 NL: 9.37E2
T: ITMS - p ESI Full ms4 355.10@cid25.00 266.80@cid25.00 222.80@cid

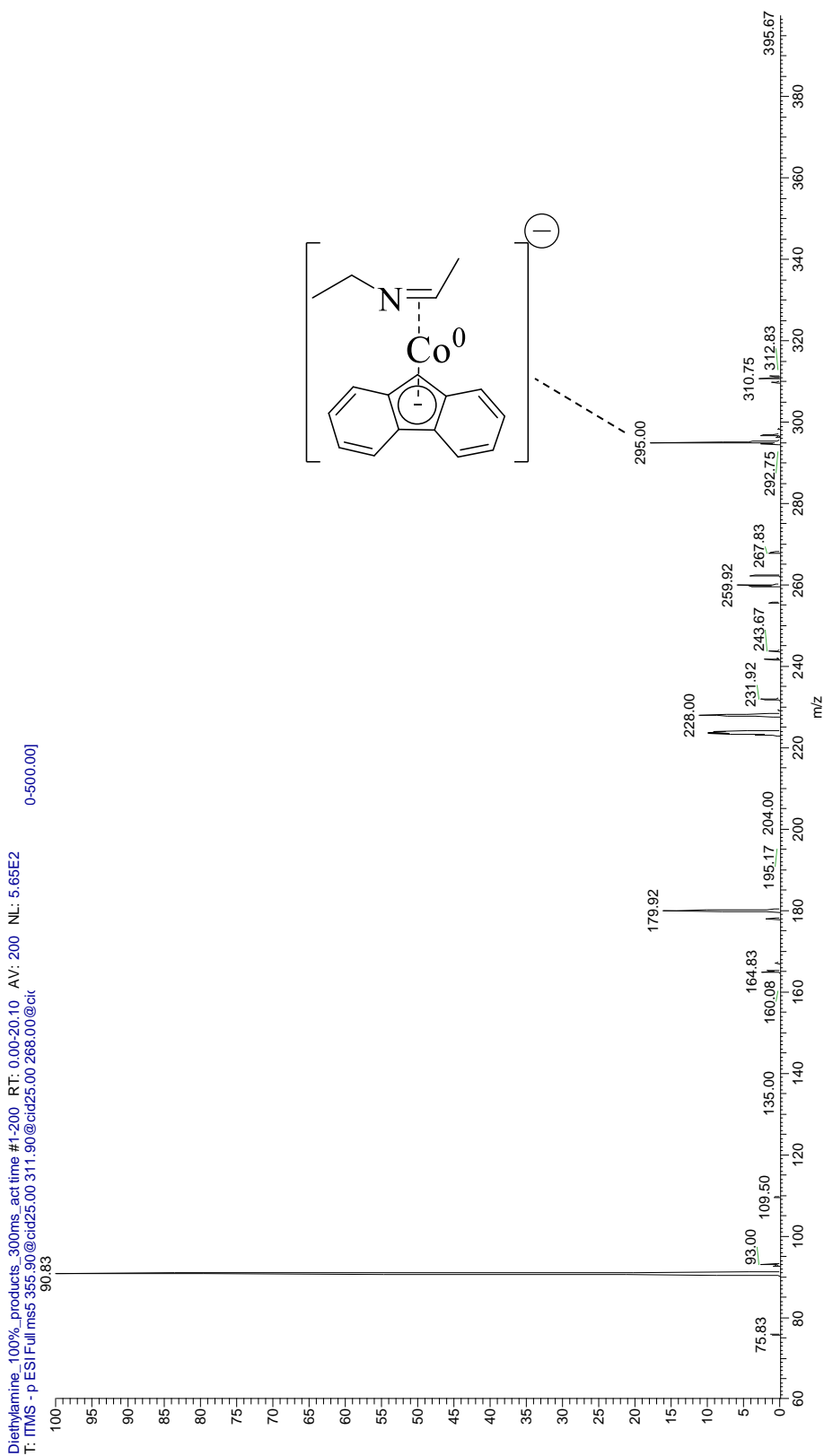
A.5. Product spectrum for diethylamine reaction with complex I.



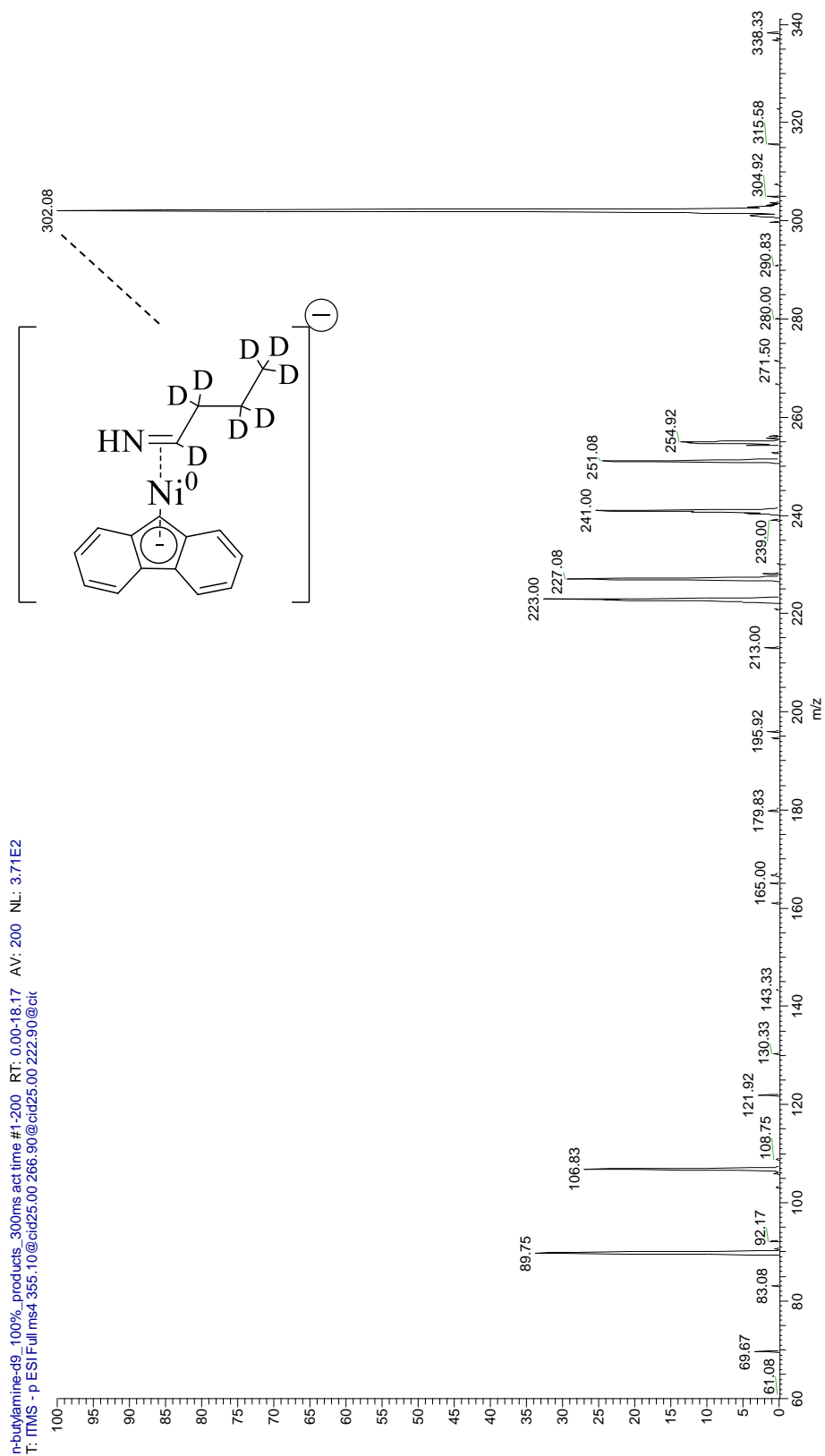
A.6. Product spectrum for piperidine reaction with complex II.



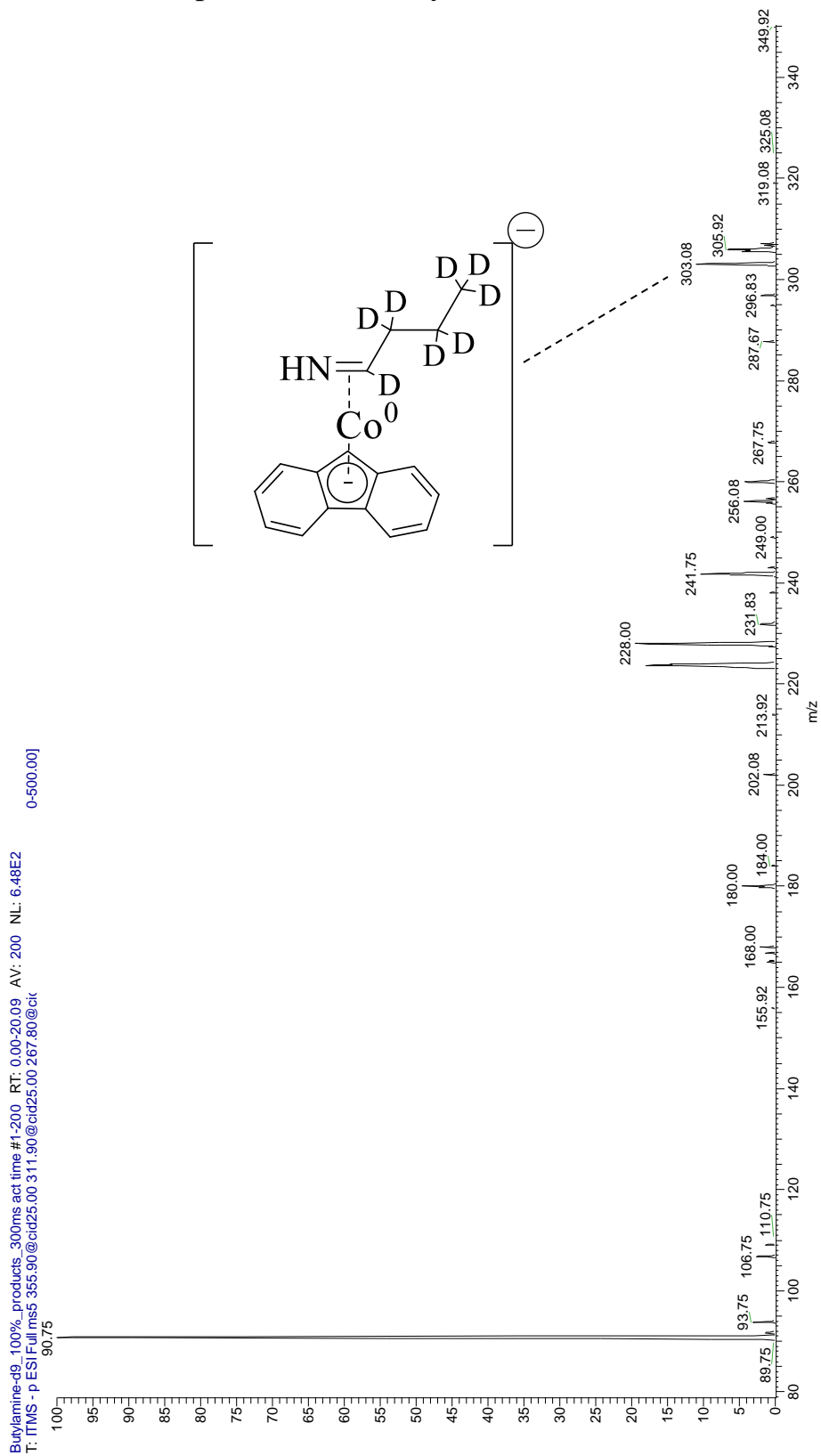
A.7. Product spectrum for diethylamine reaction with complex II.



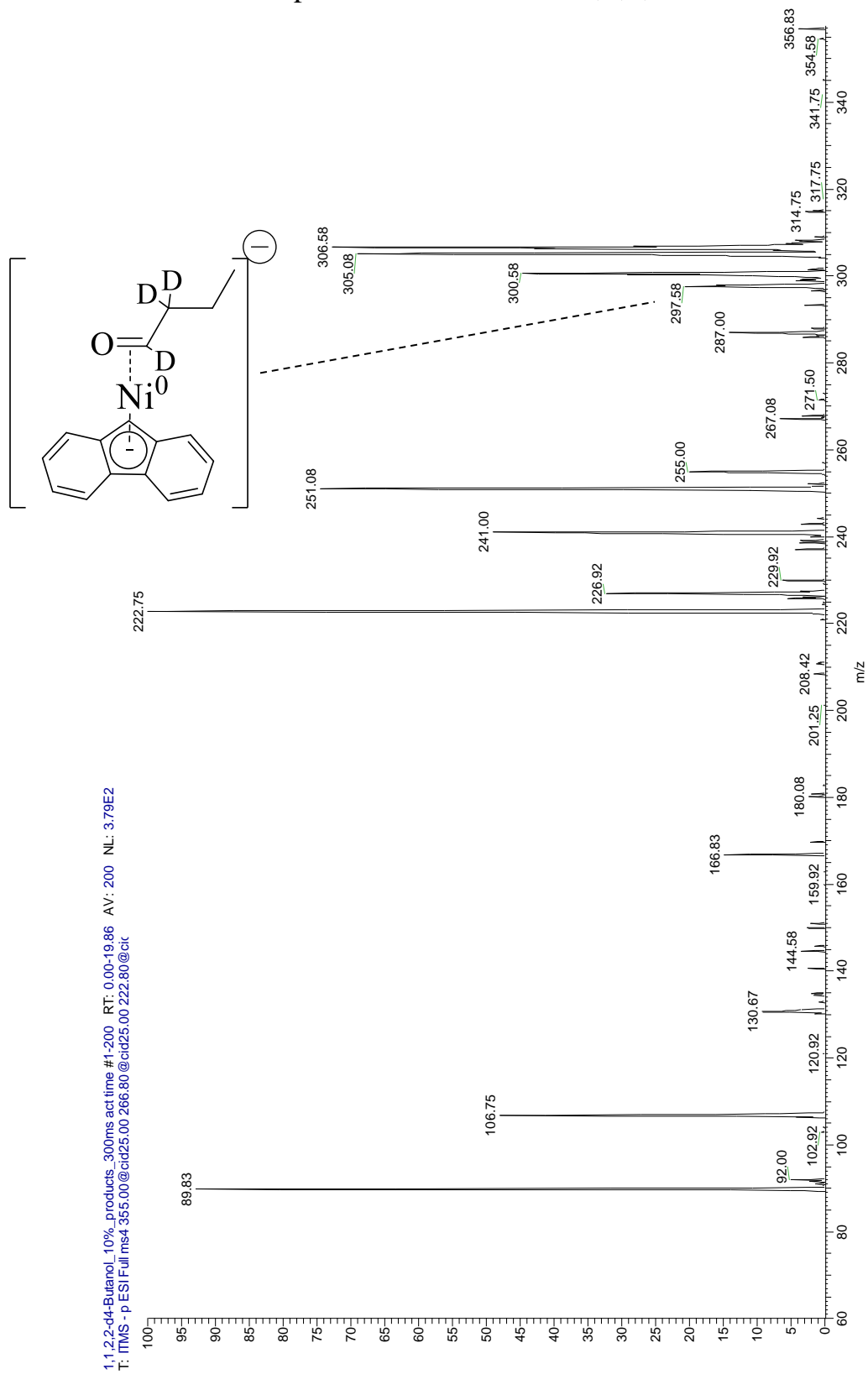
A.8. Product spectrum for n-butylamine-d₉ reaction with complex I.



A.9. Product spectrum for n-butylamine-d₉ reaction with complex II.

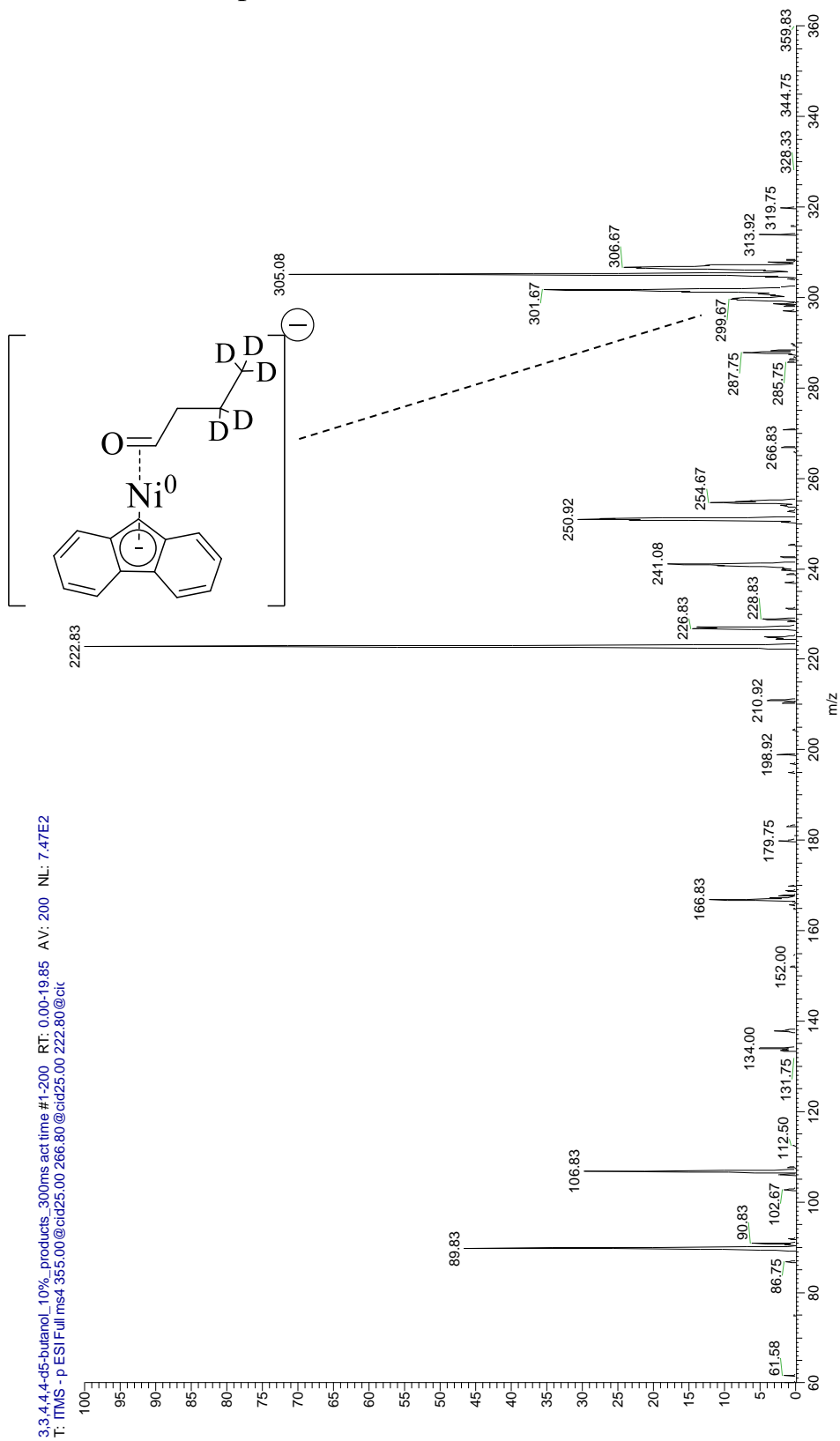


A.10. Product spectrum for n-butanol-1,1,2,2-d₄ reaction with complex I.



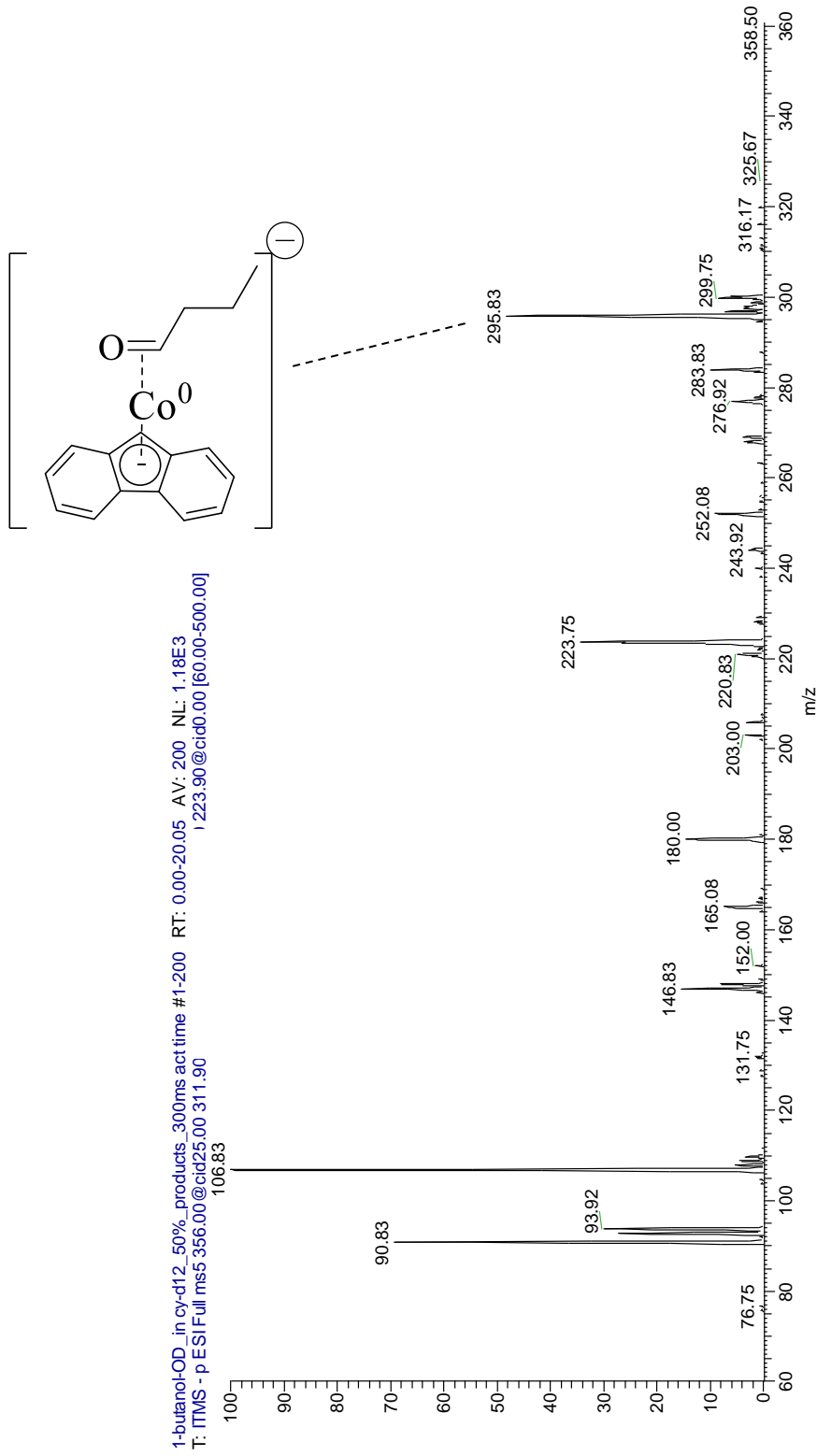
1,1,2,2-⁴D-Butanol_10%_products_300ms_act time #1-200 RT: 0.00-19.86 AV: 200 NL: 3.79E2
 T: ITMS - p ESI Full ms4 355.00@cid25.00 266.80@cid25.00 222.80@cid

A.11. Product spectrum for n-butanol-3,3,4,4-d₅ reaction with complex I.

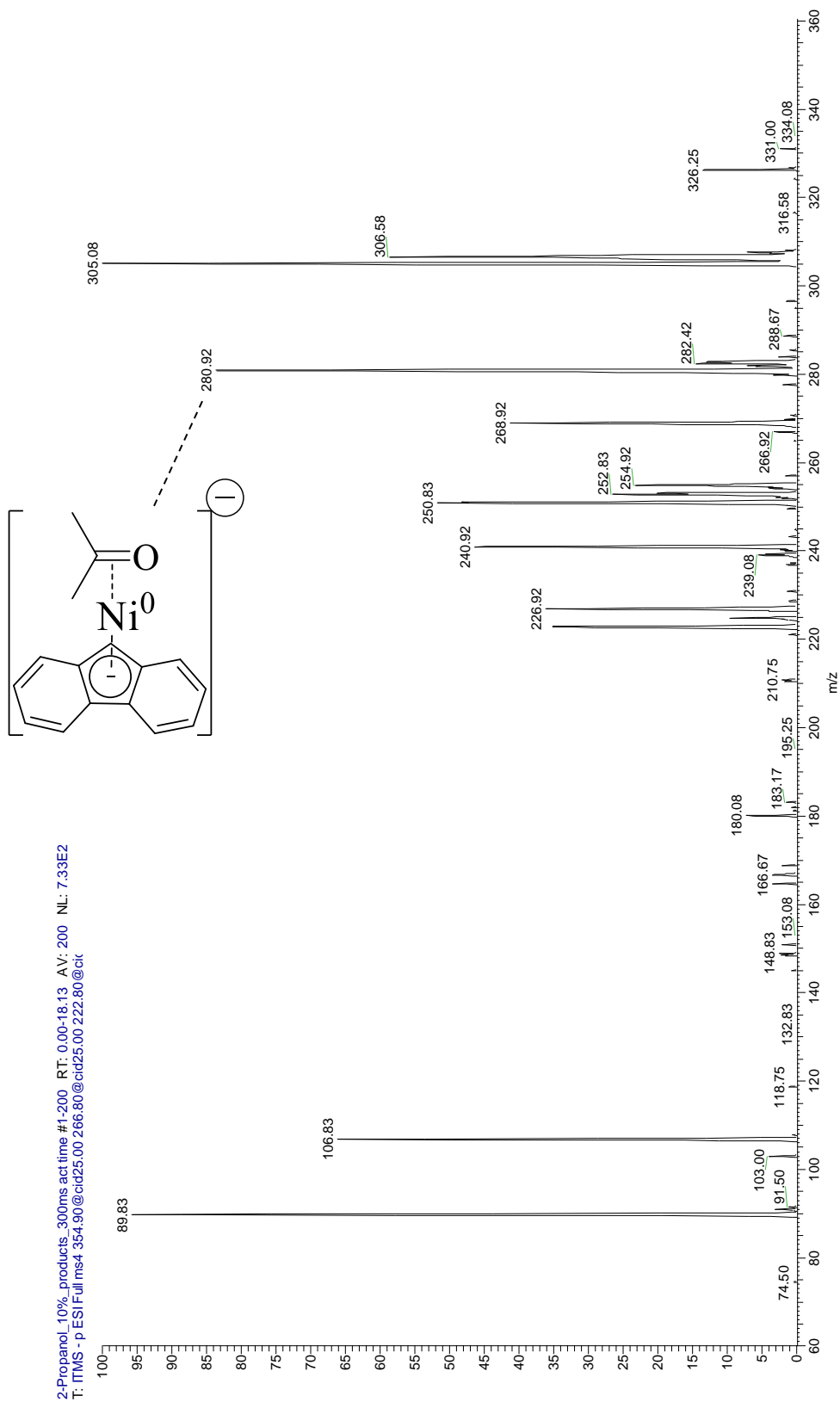


3,3,4,4-d₅-butanol_10%_products_300ms act time #1:200 RT: 0.00-19.85 AV: 200 NL: 7.47E2
 T: ITMS - p ESIFull ms4-355.00@cid25.00 266.80@cid25.00 222.80@cid

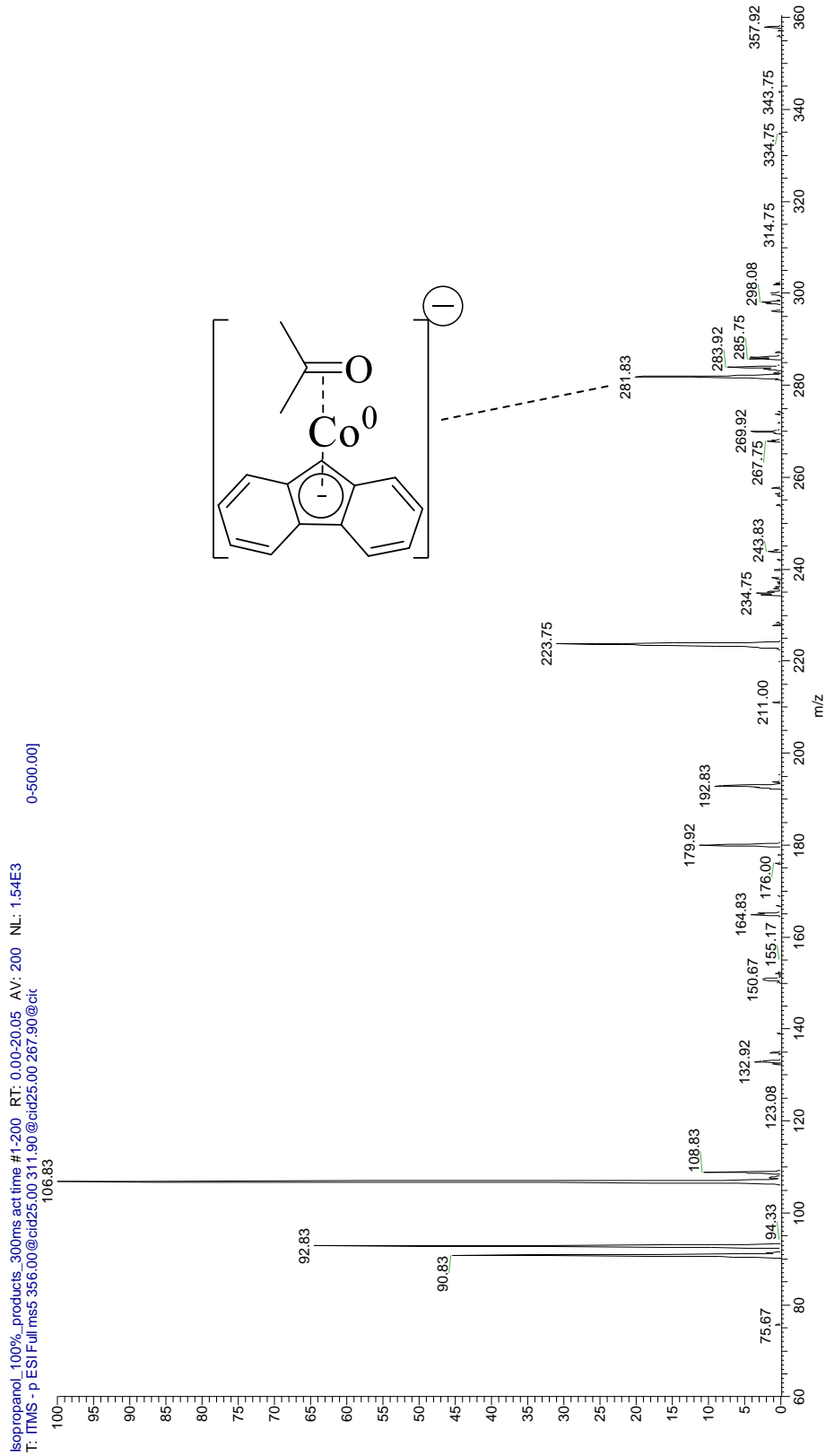
A.12. Product spectrum for n-butanol-OD reaction with complex II.



A.13. Product spectrum for isopropanol reaction with complex I.

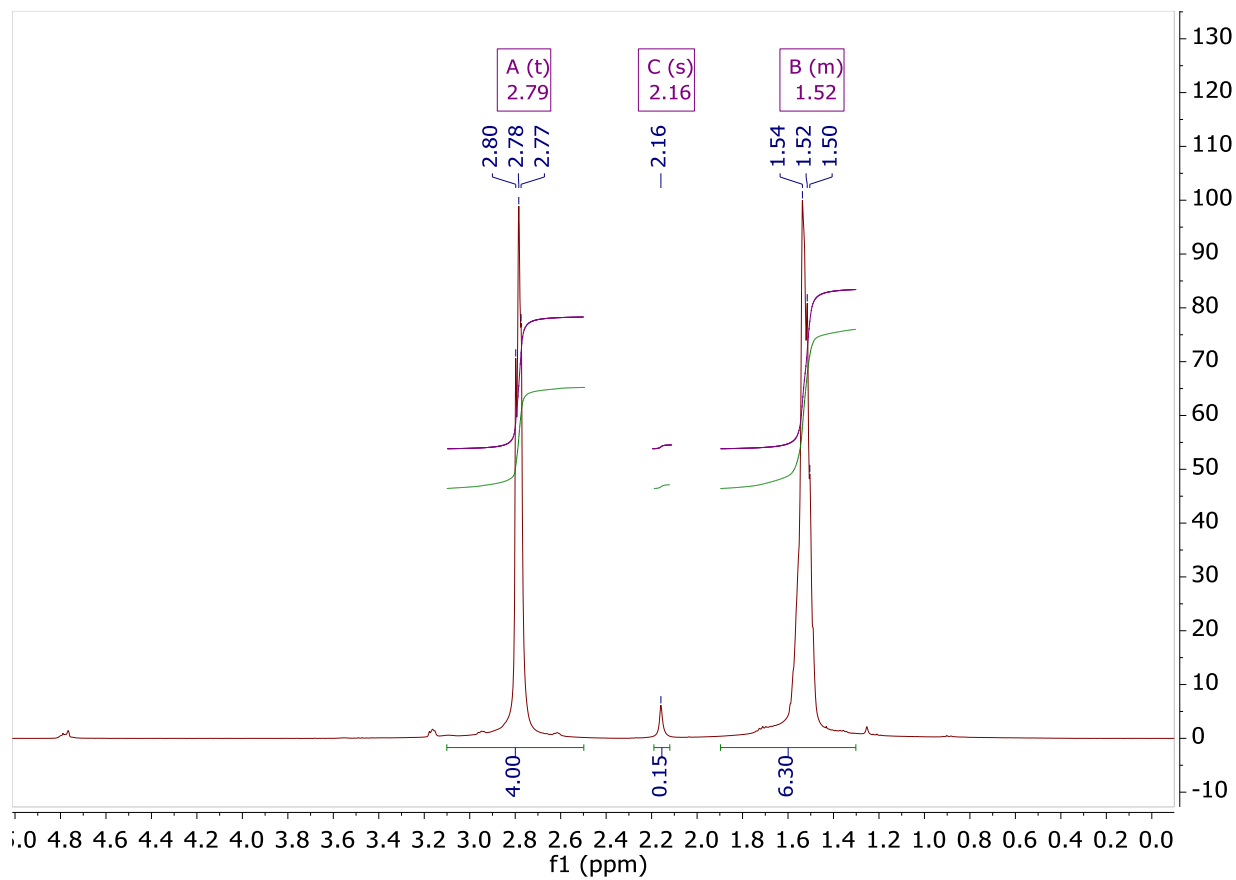


A.14. Product spectrum for isopropanol reaction with complex II.

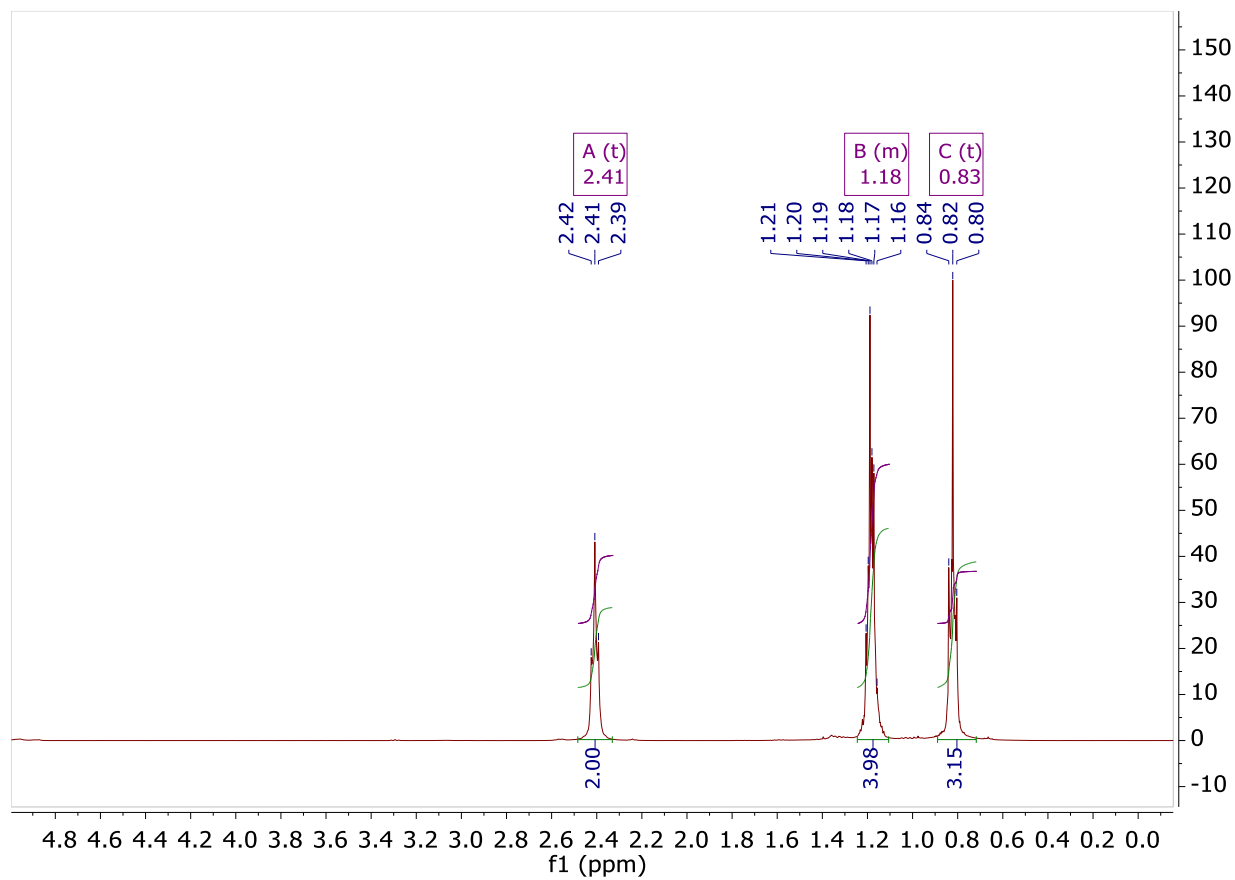


isopropanol_100%.productis_300ms.act.time.#1-200_RT: 0.00-20.05_AV: 200_NL: 1.54E3
 T: ITMS - p_ESI.Full.ms5.356.00@cid25.00.311.90@cid25.00.267.90@cit
 0-500.00]

A.15. ^1H -NMR spectrum for piperidine-ND.

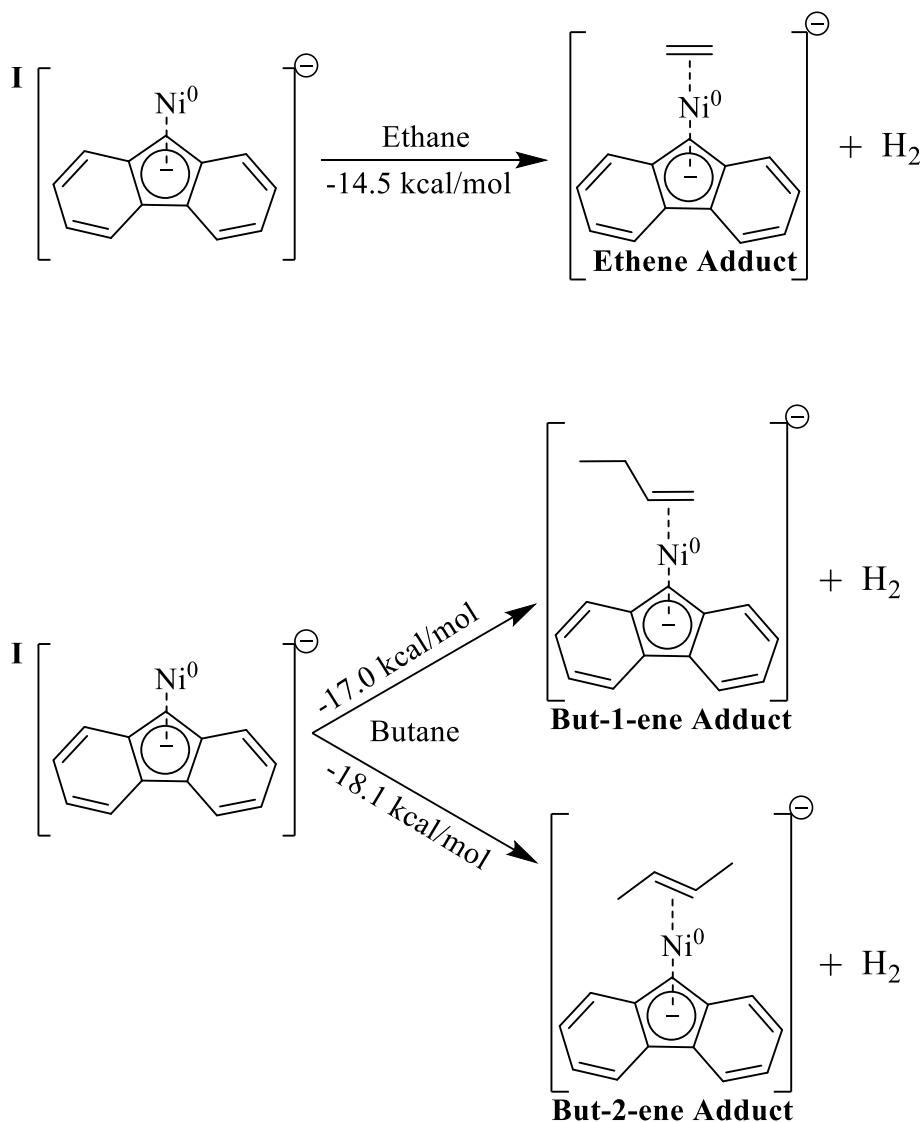


A.16. ^1H -NMR spectrum for butylamine- ND_2 .



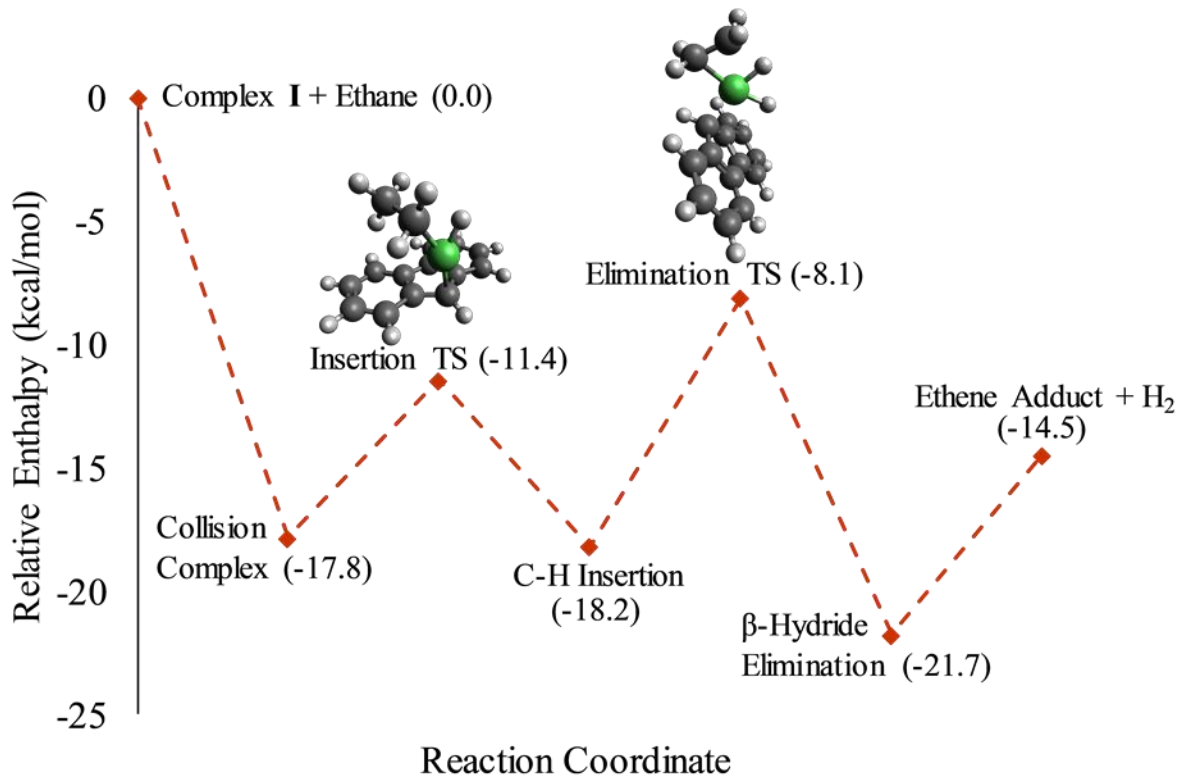
Appendix B – Thermodynamic data

B.1. Reaction enthalpies for the dehydrogenation of ethane and butane by complex I.



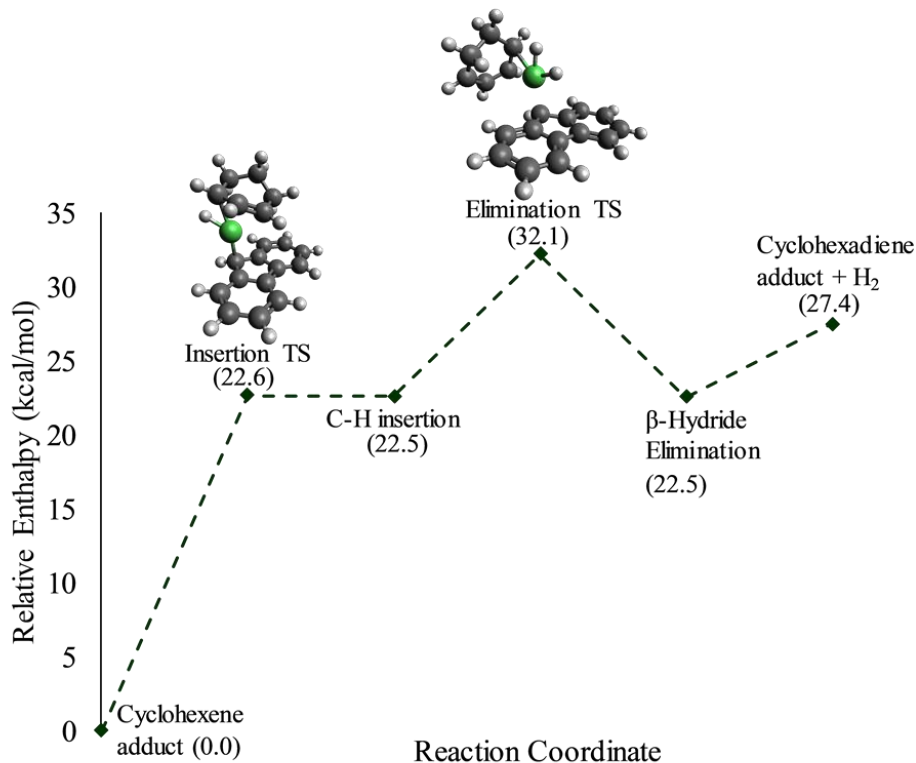
DFT calculations suggest exothermic enthalpies for the dehydrogenations of ethane and butane. Calculations were completed at the M06/6-311 + G** level. Detailed information on the structure and frequencies of the calculated species are shown in Appendix C.

B.2. Potential energy surface for the dehydrogenation of ethane by complex I.



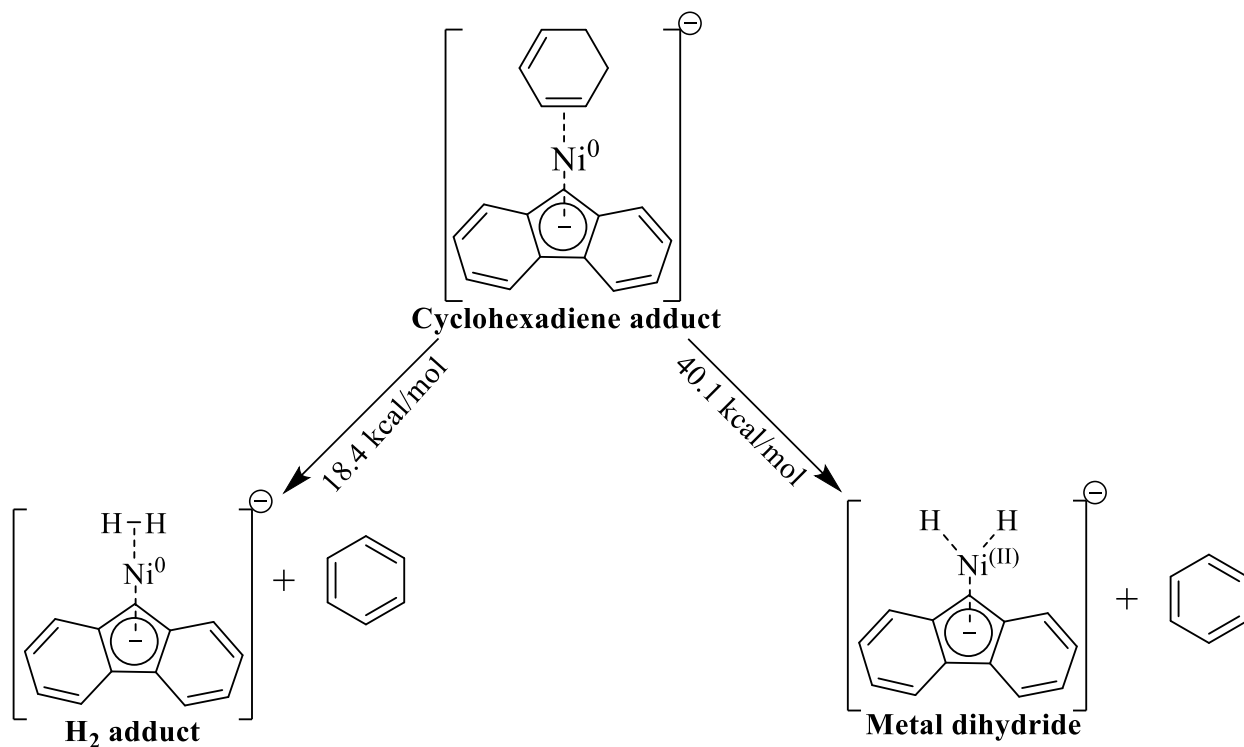
DFT calculations suggest the dehydrogenation of ethane by complex **I** occurs via the same mechanism as the dehydrogenation of cyclohexane. The overall reaction is exothermic by 14.5 kcal/mol. These computational results suggest that complex **I** can also dehydrogenate smaller alkanes. Calculations were completed at the M06/6-311 + G** level. Detailed information on the structure and frequencies of the calculated species are shown in Appendix C.

B.3. Potential energy surface for the dehydrogenation of cyclohexene.



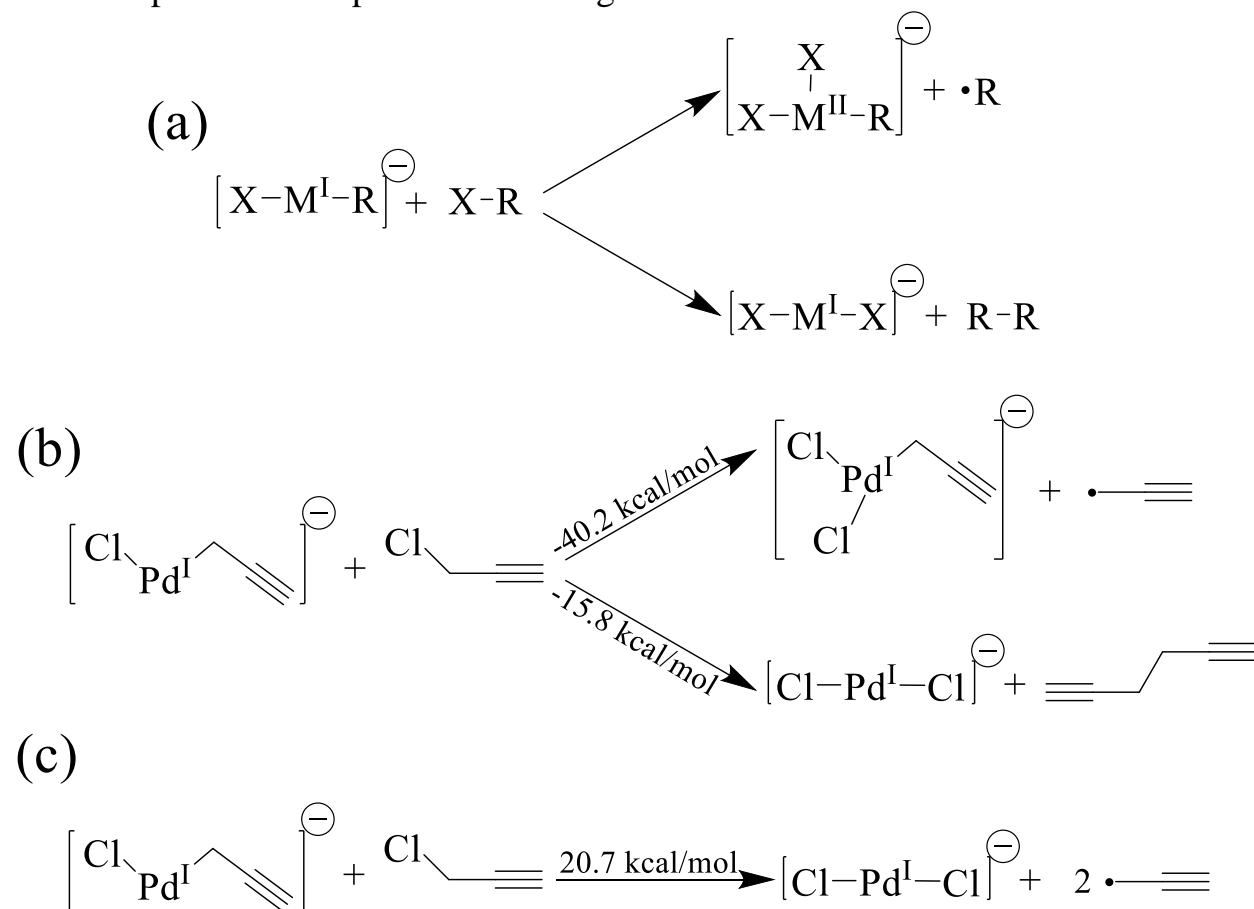
The dehydrogenation of cyclohexene occurs via the same mechanism as that of the dehydrogenation of cyclohexane. CID provides the cyclohexene adduct complex with the energy required to proceed with the reaction. Calculations were completed at the M06/6-311 + G** level. Detailed information on the structure and frequencies of the calculated species are shown in Appendix C.

B.4. Reaction enthalpies for the formation of the H₂ adduct and the metal dihydride species.



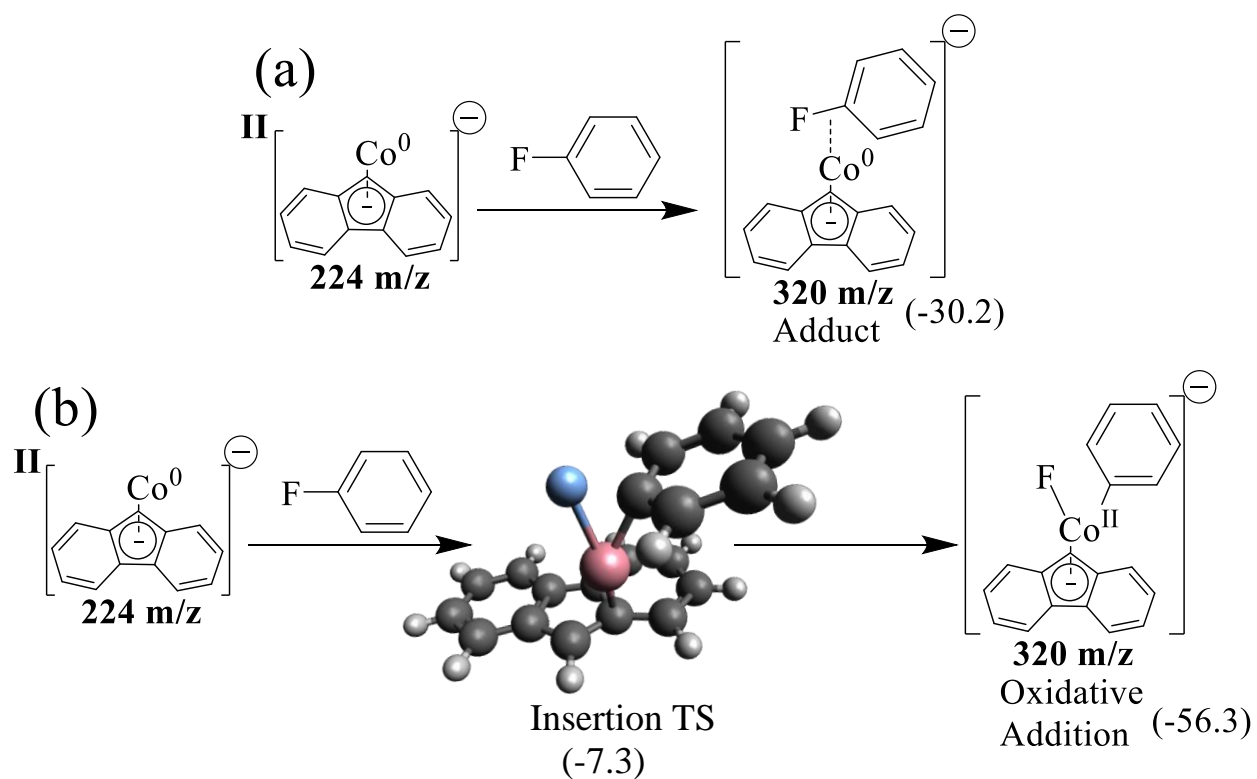
The H₂ adduct and the metal dihydride ions are isobaric and therefore indistinguishable using mass spectrometry. Comparisons of the energies of formation acquired via DFT calculations indicate formation of the H₂ adduct is favorable by 21.7 kcal/mol. Detailed information on the structure and frequencies of the calculated species are shown in Appendix C.

B.5. Reaction pathways commonly observed for the secondary reactions between insertion products and polar neutral reagents.



Insertion products often react with the neutral reagents resulting two secondary products. Panel (a) depicts the general reactions. A second halogen group can add to the insertion product, presumably releasing an organic radical. Alternatively, the metal center can swap the organic ligand with the halogen group of the reagent, presumably releasing a carbon-coupled product. The secondary reactions of the insertion product from the reaction between propargyl chloride and complex **IV** are shown as an example in panel (b). DFT calculations suggest the second halogen addition is exothermic by 40.2 kcal/mol while the carbon coupling is exothermic by 15.8 kcal/mol. The possibility of forming the dihalide anion via the release of two propargyl radicals was also explored computationally, as shown in panel (c). DFT calculations suggest this process is endothermic by 20.7 kcal/mol. Therefore, formation of the dihalide anion via the carbon coupling pathway is favored by 36.5 kcal/mol. Detailed information on the structure and frequencies of the calculated species are shown in Appendix C.

B.6. Comparison of adduct formation and oxidative addition of fluorobenzene by complex II.



Appendix C – Computational Data

C.1. Gas-phase dehydrogenation of alkanes

Complex I (s)

M06/6-311+G** Enthalpy = -2008.56485

C	0.00000	0.97574	0.80445
C	-0.72273	-1.10703	-0.03491
C	-1.15689	0.13142	0.50938
C	-2.52458	0.34980	0.69500
C	-3.43278	-0.62352	0.31251
C	-3.00185	-1.82506	-0.26579
C	-1.64738	-2.06779	-0.43805
C	1.15688	0.13142	0.50933
C	0.72269	-1.10703	-0.03494
C	3.43275	-0.62360	0.31252
C	2.52457	0.34975	0.69498
C	1.64732	-2.06785	-0.43802
C	3.00180	-1.82514	-0.26577
Ni	0.00005	2.27549	-0.57527
H	0.00004	1.60663	1.70175
H	-2.86512	1.29354	1.11581
H	-4.49797	-0.44935	0.44984
H	-3.73269	-2.56954	-0.57259
H	-1.31040	-3.00802	-0.87232
H	4.49794	-0.44946	0.44987
H	2.86513	1.29349	1.11578
H	1.31031	-3.00808	-0.87225
H	3.73261	-2.56965	-0.57254

Cyclohexane (s)

M06/6-311+G** Enthalpy = -235.566343

C	-0.98166	-1.06811	0.23219
C	0.43424	-1.38409	-0.23219
C	1.41590	-0.31604	0.23220
C	0.98166	1.06811	-0.23219
C	-0.43424	1.38409	0.23219
C	-1.41590	0.31604	-0.23220
H	-1.68288	-1.83108	-0.12632
H	-1.01631	-1.10572	1.33229
H	0.44959	-1.43296	-1.33228
H	0.74435	-2.37287	0.12634
H	1.46601	-0.32716	1.33230
H	2.42722	-0.54187	-0.12643
H	1.01631	1.10572	-1.33229

H	1.68288	1.83108	0.12632
H	-0.74435	2.37287	-0.12634
H	-0.44959	1.43296	1.33228
H	-2.42722	0.54187	0.12643
H	-1.46601	0.32716	-1.33230

Hydrogen molecule (s)

M06/6-311+G** Enthalpy = -1.157449

H	0.00000	-0.00000	0.37368
H	0.00000	-0.00000	-0.37368

Collision complex of I with cyclohexane (s)

M06/6-311+G** Enthalpy = -2244.155879

C	1.94437	-2.98951	-1.17572
C	1.99662	-1.63416	-1.45846
C	1.73914	-0.70671	-0.44891
C	1.37907	-1.14384	0.86574
C	1.36350	-2.52259	1.13657
C	1.64005	-3.42449	0.12638
C	1.36171	1.16207	0.86627
C	1.72823	0.73099	-0.44859
C	1.97135	1.66262	-1.45786
C	1.89889	3.01692	-1.17459
C	1.58857	3.44671	0.12783
C	1.32576	2.54037	1.13770
C	1.10316	0.00691	1.70082
H	1.23655	0.00764	2.78339
Ni	-0.80649	-0.00653	1.38127
H	1.10190	-2.87079	2.13398
H	1.61068	-4.49172	0.33734
H	2.14362	-3.71950	-1.95647
H	2.24296	-1.29384	-2.46390
H	2.22174	1.32622	-2.46362
H	2.08675	3.75016	-1.95512
H	1.54333	4.51330	0.33928
H	1.05928	2.88426	2.13532
C	-1.89165	-0.01039	-2.11367
C	-1.87336	-1.27072	-1.25865
C	-3.02632	-1.28640	-0.26472
C	-3.09721	-0.02297	0.58772
C	-3.04507	1.24364	-0.26131
C	-1.89200	1.24780	-1.25531
H	-1.90926	-2.16683	-1.89345
H	-2.79275	-0.01620	-2.75223
H	-3.97708	-1.36934	-0.82220
H	-2.95830	-2.16962	0.38210

H	-0.92533	-1.31572	-0.70103
H	-1.02630	-0.00308	-2.79000
H	-0.94464	1.30537	-0.69764
H	-1.94129	2.14499	-1.88770
H	-2.99026	2.12607	0.38785
H	-3.99691	1.31391	-0.81869
H	-2.43259	-0.01939	1.51469
H	-4.05940	-0.03083	1.12502

Insertion TS for the dehydrogenation of cyclohexane (s)

M06/6-311+G** Enthlapy = -2244.152541

Imaginary frequency = -585.98

H	1.10265	3.81894	-0.19633
C	0.34110	3.06842	0.00634
C	-1.60158	1.14873	0.57809
C	-0.10068	2.25561	-1.02635
C	-0.15597	2.92944	1.31127
C	-1.12176	1.97176	1.59314
C	-1.09256	1.27377	-0.76911
H	0.28484	2.38773	-2.03518
H	0.22270	3.57095	2.10305
C	-2.56390	0.08222	0.56822
C	-4.29694	-2.00588	-0.02889
C	-2.59257	-0.46378	-0.75495
C	-3.38158	-0.44118	1.56811
C	-4.24680	-1.48216	1.27384
C	-3.48572	-1.50950	-1.03232
H	-3.34411	-0.02580	2.57451
H	-4.89195	-1.89287	2.04668
H	-3.52862	-1.93526	-2.03328
H	-4.98503	-2.81997	-0.24870
C	-1.64630	0.22772	-1.58197
H	-1.65003	0.20025	-2.66653
Ni	0.29649	-0.20454	-0.86556
H	-1.49870	1.85684	2.60878
H	1.72375	0.06001	0.65630
C	2.05271	-0.62134	-0.16718
H	1.20646	-1.29105	-1.26761
C	2.48295	-1.93574	0.47849
H	1.63489	-2.37914	1.01455
H	2.75973	-2.65709	-0.30988
C	3.22432	0.02866	-0.89241
H	3.51926	-0.60663	-1.74489
H	2.91430	0.99130	-1.31748
C	4.42680	0.21722	0.02937
H	4.15809	0.93582	0.81950

H	5.27218	0.65629	-0.52002
C	3.67525	-1.74516	1.40972
H	3.37669	-1.09769	2.24899
H	3.98393	-2.70519	1.84747
H	5.18918	-1.78770	-0.11519
H	5.69389	-0.94839	1.35095
C	4.84229	-1.09950	0.67326

C-H insertion of cyclohexane with I (s)

M06/6-311+G** Enthalpy = -2244.156108

C	1.28469	-0.06471	1.48877
C	1.61448	-0.80332	-0.70394
C	1.41249	-1.22526	0.64575
C	1.33154	-2.59821	0.92224
C	1.41351	-3.51033	-0.11292
C	1.57482	-3.08957	-1.44343
C	1.67532	-1.73923	-1.73589
C	1.53279	1.07542	0.64484
C	1.68977	0.63375	-0.70453
C	1.77117	3.34741	-0.11551
C	1.59509	2.44953	0.92033
C	1.84806	1.55742	-1.73714
C	1.88821	2.91118	-1.44565
Ni	-0.72220	0.03917	1.96402
C	-2.85117	1.39816	-1.30502
C	-2.68025	0.13218	-2.13317
C	-2.98439	-1.10367	-1.29761
C	-2.08567	-1.15499	-0.05972
C	-2.19733	0.11502	0.77406
C	-1.95131	1.36078	-0.06738
H	-1.80469	0.09430	2.96031
H	1.51531	-0.07607	2.56165
H	1.17285	-2.93554	1.94502
H	1.33988	-4.57415	0.10300
H	1.62171	-3.82682	-2.24079
H	1.80454	-1.41024	-2.76623
H	1.80822	4.41327	0.09964
H	1.47222	2.80229	1.94284
H	1.94248	1.21594	-2.76721
H	2.01128	3.63905	-2.24353
H	-2.62787	2.28830	-1.90978
H	-3.90471	1.48200	-0.99039
H	-3.31616	0.16343	-3.02934
H	-1.63707	0.07569	-2.48552
H	-4.04087	-1.07359	-0.98312
H	-2.85689	-2.01599	-1.89708

H	-1.04817	-1.29075	-0.40231
H	-2.32436	-2.03510	0.55141
H	-3.19737	0.17003	1.22746
H	-2.09405	2.26519	0.53819
H	-0.90570	1.38271	-0.41130

Elimination TS for the dehydrogenation of cyclohexane (s)

M06/6-311+G** Enthlapy = -2244.144737

Imaginary frequency = -579.14

C	0.47707	-0.12210	0.83891
C	2.66763	-0.23146	-0.03002
C	1.61851	-0.98555	0.55835
C	1.79941	-2.35454	0.76730
C	2.98282	-2.95816	0.37261
C	4.00038	-2.21677	-0.23990
C	3.84289	-0.85319	-0.44204
C	0.94842	1.21893	0.50819
C	2.24774	1.15134	-0.06050
C	0.98901	3.60694	0.21526
C	0.33610	2.46557	0.65366
C	2.88471	2.30209	-0.51535
C	2.25508	3.53068	-0.37660
Ni	-0.88311	-0.62014	-0.57988
C	-3.98008	0.81449	-0.56620
C	-3.88083	-0.51919	-1.28763
C	-2.74705	-1.36567	-0.73486
C	-2.34876	-1.20747	0.63286
C	-2.90596	-0.10268	1.51287
C	-4.14323	0.57127	0.92662
H	-1.68584	-0.93084	-1.77950
H	-0.01132	-0.21074	-1.74361
H	-0.05669	-0.26475	1.78150
H	1.00153	-2.94093	1.22070
H	3.12197	-4.02565	0.53095
H	4.91571	-2.71268	-0.55376
H	4.63797	-0.27386	-0.90927
H	3.87391	2.24178	-0.96698
H	2.74454	4.43724	-0.72413
H	0.50834	4.57706	0.32374
H	-0.65834	2.53493	1.09270
H	-2.76629	-2.39507	-1.10307
H	-2.01775	-2.10600	1.15613
H	-4.82877	-1.06509	-1.14449
H	-3.76074	-0.36842	-2.36817
H	-3.06277	1.39566	-0.75156
H	-4.82142	1.39984	-0.96070

H	-3.15124	-0.50488	2.50659
H	-2.14599	0.67489	1.69538
H	-4.35026	1.51033	1.45742
H	-5.02278	-0.07609	1.07572

β -hydride elimination of cyclohexane with **I** (s)

M06/6-311+G** Enthalpy = -2244.167832

C	-0.54260	-0.16399	-0.99551
C	-2.09363	1.25422	0.05278
C	-0.83552	1.20009	-0.62254
C	-0.11372	2.38993	-0.79844
C	-0.61189	3.57752	-0.29276
C	-1.83212	3.61814	0.39885
C	-2.56965	2.45686	0.57045
C	-1.71462	-0.92227	-0.62856
C	-2.64541	-0.07641	0.04727
C	-3.23200	-2.76706	-0.31724
C	-2.03802	-2.27421	-0.81210
C	-3.83411	-0.59600	0.55613
C	-4.12960	-1.93815	0.37366
Ni	0.84867	-0.74959	0.45863
C	2.63883	-1.47629	0.76528
C	2.35508	-1.33957	-0.62211
C	3.00935	-0.26775	-1.47803
C	4.14482	0.45352	-0.75609
C	3.78952	0.74991	0.69383
C	3.62167	-0.55801	1.45375
H	0.48016	-0.60439	2.01555
H	-0.20399	-0.32457	1.61920
H	0.03173	-0.40442	-1.88935
H	0.84136	2.37413	-1.32186
H	-0.04581	4.49698	-0.42811
H	-2.19814	4.56231	0.79452
H	-3.52306	2.48730	1.09669
H	-3.47860	-3.81766	-0.45764
H	-1.33799	-2.93036	-1.32712
H	-4.53385	0.05107	1.08388
H	-5.05721	-2.35143	0.76202
H	2.56529	-2.47649	1.20111
H	2.04280	-2.23669	-1.16467
H	2.26498	0.47641	-1.80272
H	3.40000	-0.71210	-2.40613
H	4.41063	1.37445	-1.29294
H	5.04368	-0.18469	-0.76299
H	2.84787	1.31976	0.73466
H	4.56635	1.37012	1.16222

H	3.30735	-0.36160	2.48835
H	4.61528	-1.04238	1.52193

Cyclohexene adduct with I (s)

M06/6-311+G** Enthlapy = -2243.004322

C	-0.81077	-2.86751	0.25952
C	0.12516	-2.54298	-0.89051
C	1.44060	-2.08213	-0.67597
C	2.00266	-1.88139	0.71015
C	0.90903	-1.81958	1.76910
C	-0.06960	-2.97129	1.58912
C	-0.32949	1.21590	-1.65023
C	-1.12173	1.37324	0.55419
C	-1.48730	1.09044	-0.80467
C	-2.82888	0.77577	-1.09230
C	-3.74746	0.69138	-0.06592
C	-3.37084	0.91549	1.27159
C	-2.06396	1.25675	1.57627
C	0.75520	1.59952	-0.78202
C	0.27509	1.69229	0.56961
C	2.94938	2.22534	0.00173
C	2.10799	1.90180	-1.04219
C	1.15287	2.00214	1.60828
C	2.48392	2.26339	1.33012
Ni	0.27104	-0.64274	-1.24139
H	-1.33877	-3.81255	0.05961
H	-1.59491	-2.09839	0.34336
H	-0.09878	-3.03488	-1.84098
H	2.18312	-2.24956	-1.46186
H	2.68475	-2.71721	0.95797
H	2.61210	-0.96639	0.74496
H	1.35567	-1.84305	2.77281
H	0.36952	-0.86510	1.68199
H	0.49562	-3.91806	1.61586
H	-0.78711	-3.00712	2.42005
H	-0.35830	1.38551	-2.72336
H	-3.12724	0.57192	-2.11904
H	-4.78050	0.43328	-0.29061
H	-4.11088	0.82433	2.06272
H	-1.77160	1.43599	2.61047
H	3.99685	2.44011	-0.20025
H	2.48520	1.84711	-2.06157
H	0.79187	2.03539	2.63580
H	3.17312	2.50379	2.13579

Insertion TS for dehydrogenation of cyclohexene (s)

M06/6-311+G** Enthalpy = -2242.96826

Imaginary frequency = -762.78

C	-0.20949	2.41248	-1.40917
C	-0.16334	3.58081	-0.66747
C	0.65248	3.68598	0.46849
C	1.44995	2.61679	0.85151
C	2.28474	-1.94696	-0.90296
C	3.23281	-2.34784	0.02109
C	3.63005	-1.50418	1.06967
C	3.08775	-0.23150	1.17946
H	0.52366	-0.22352	-2.63056
H	1.96882	-2.61689	-1.70056
H	3.67536	-3.33885	-0.06059
H	4.36946	-1.84743	1.78909
H	3.40542	0.43064	1.98422
H	2.09127	2.70010	1.72818
H	0.66088	4.60807	1.04443
H	-0.77794	4.42912	-0.96249
H	-0.86884	2.33159	-2.27235
Ni	-0.76568	-1.00258	-0.53428
C	-1.64962	-1.73341	1.01907
C	-1.27055	-0.44904	1.42666
C	-2.24208	0.70000	1.24872
C	-3.63265	0.16937	0.91310
C	-3.61458	-0.78473	-0.27908
C	-2.53233	-1.86397	-0.13774
H	-2.89304	-2.87981	-0.31204
H	-1.13779	-2.61399	1.40783
H	-0.51571	-0.34839	2.20585
H	-2.29222	1.29525	2.17321
H	-4.02199	-0.36640	1.79154
H	-4.32384	0.99928	0.71192
H	-4.60264	-1.25584	-0.38866
H	-3.44274	-0.20434	-1.19575
H	-1.91100	1.40095	0.46615
C	0.57108	1.31382	-1.02588
C	1.43575	1.44244	0.10338
C	1.70069	-0.67431	-0.79131
C	2.14721	0.19965	0.24894
C	0.67385	-0.02021	-1.57231
H	-1.77832	-1.81849	-1.40486

C-H insertion of cyclohexene with I (s)

M06/6-311+G** Enthalpy = -2242.96835

C	-0.86921	-0.12360	-1.56750
---	----------	----------	----------

C	-2.15507	0.48550	0.30457
C	-1.97640	-0.49791	-0.71176
C	-2.80952	-1.62324	-0.72018
C	-3.77264	-1.76988	0.26297
C	-3.92670	-0.81279	1.27614
C	-3.11667	0.31227	1.29799
C	-0.45686	1.18585	-1.10352
C	-1.20118	1.54047	0.05990
C	0.75951	3.25408	-0.89988
C	0.52518	2.06791	-1.57355
C	-0.93660	2.72925	0.73782
C	0.03864	3.58831	0.25589
Ni	0.70979	-1.23760	-0.85033
C	2.81458	0.61927	1.24538
C	1.95136	-0.29913	2.10340
C	1.24649	-1.36192	1.26444
C	2.10281	-2.01893	0.21476
C	3.39195	-1.39717	-0.05509
C	3.74952	-0.18168	0.39110
H	1.14293	-1.77072	-2.16289
H	-0.85094	-0.38795	-2.62189
H	-2.68052	-2.38355	-1.48796
H	-4.41692	-2.64666	0.25722
H	-4.68386	-0.95511	2.04317
H	-3.23923	1.06038	2.08007
H	1.52660	3.93412	-1.26408
H	1.11341	1.80110	-2.44937
H	-1.49949	2.98732	1.63386
H	0.25099	4.51994	0.77410
H	3.36901	1.31509	1.88980
H	2.15897	1.24713	0.61689
H	2.59791	-0.81368	2.83017
H	1.21690	0.28575	2.67218
H	0.34314	-0.81582	0.79428
H	0.74463	-2.10062	1.90000
H	2.09980	-3.11034	0.20822
H	4.07780	-1.95088	-0.69648
H	4.69979	0.25736	0.09487

Elimination TS for dehydrogenation of cyclohexene (s)

M06/6-311+G** Enthalpy = -2242.953089

Imaginary frequency = -714.54

C	-0.50326	-0.27666	-0.89241
C	-2.62711	0.06923	0.07382
C	-1.78379	-0.88639	-0.55085
C	-2.25318	-2.18793	-0.73619

C	-3.51719	-2.53307	-0.28392
C	-4.33140	-1.59614	0.36304
C	-3.88622	-0.29435	0.54281
C	-0.67165	1.13415	-0.55364
C	-1.92868	1.33476	0.07535
C	-0.20242	3.47603	-0.27472
C	0.18127	2.22623	-0.73502
C	-2.29311	2.59197	0.54931
C	-1.42954	3.66311	0.37285
Ni	0.88119	-0.90508	0.45246
C	3.75595	0.71515	0.65446
C	3.83030	-0.70684	1.20407
C	2.73443	-1.59495	0.64765
C	2.40217	-1.41418	-0.73918
C	2.98626	-0.28941	-1.45502
C	3.63933	0.71013	-0.84190
H	0.01316	-0.66086	1.65658
H	1.52956	-1.23143	1.72411
H	2.10791	-2.28243	-1.32866
H	2.86036	-0.25894	-2.53775
H	2.79556	-2.62827	0.99748
H	3.80405	-0.69087	2.30101
H	4.79884	-1.14676	0.91067
H	2.87574	1.21728	1.09014
H	4.63360	1.28891	0.98172
H	4.02358	1.55541	-1.40830
H	-1.61581	-2.92899	-1.21595
H	-3.88060	-3.54906	-0.42421
H	-5.31492	-1.89085	0.72091
H	-4.52269	0.43854	1.03662
H	-0.05144	-0.52951	-1.85408
H	1.14956	2.08148	-1.21189
H	-3.25203	2.73710	1.04486
H	-1.70458	4.65089	0.73474
H	0.46376	4.32566	-0.40999

β -hydride elimination of cyclohexene with **I** (s)

M06/6-311+G** Enthalpy = -2242.968418

C	-0.58047	0.28908	-0.96514
C	-1.92388	-1.35789	0.03894
C	-0.67953	-1.11332	-0.61444
C	0.21931	-2.17687	-0.78151
C	-0.10888	-3.43085	-0.29776
C	-1.32379	-3.66056	0.36571
C	-2.22771	-2.62403	0.53584
C	-1.85833	0.86212	-0.60517

C	-2.66393	-0.12055	0.04247
C	-3.63341	2.45991	-0.29395
C	-2.37255	2.15364	-0.77572
C	-3.92319	0.21071	0.53878
C	-4.40912	1.49835	0.37017
Ni	0.80113	0.87949	0.47206
C	4.57495	-0.14408	0.36911
C	3.50086	0.25664	1.37908
C	2.64911	1.41145	0.86443
C	2.37215	1.44346	-0.53289
C	2.94623	0.41145	-1.39486
C	3.97191	-0.35165	-0.99308
H	0.39511	0.82475	2.02656
H	-0.29256	0.55722	1.63134
H	-0.05845	0.61264	-1.86536
H	1.17881	-2.00341	-1.26576
H	0.59224	-4.25335	-0.42380
H	-1.55295	-4.65332	0.74521
H	-3.17401	-2.80094	1.04565
H	-4.02904	3.46519	-0.42460
H	-1.77018	2.91343	-1.27087
H	-4.52845	-0.54043	1.04481
H	-5.39287	1.76499	0.74855
H	5.09671	-1.05034	0.70549
H	5.34156	0.65016	0.31589
H	2.87241	-0.62868	1.56399
H	3.95791	0.51655	2.34361
H	2.73011	2.35397	1.40814
H	2.11793	2.39271	-1.01138
H	2.51990	0.26877	-2.38880
H	4.38593	-1.11763	-1.64625

Cyclohexadiene adduct with **I** (s)

M06/6-311+G** Enthalpy = -2241.803149

C	0.76247	-0.49067	-1.26438
C	1.78287	1.23193	-0.02969
C	0.69124	0.90076	-0.92339
C	-0.32969	1.86508	-1.14252
C	-0.20694	3.12216	-0.54004
C	0.86953	3.43707	0.28460
C	1.86061	2.48717	0.54611
C	1.96923	-0.98693	-0.66600
C	2.59281	0.04928	0.09652
C	3.76182	-2.46708	-0.03152
C	2.58604	-2.24432	-0.72567
C	3.77052	-0.19853	0.79723

C	4.35647	-1.45339	0.73546
C	-4.21650	-1.72372	-0.08014
C	-4.39836	-0.23210	-0.14606
C	-3.53579	0.57459	0.49036
C	-2.37616	0.04523	1.20325
C	-1.93687	-1.27869	0.91438
C	-2.73699	-2.10778	-0.08236
Ni	-0.80091	0.05636	0.08043
H	0.26562	-0.96539	-2.10554
H	-1.12468	1.68516	-1.86421
H	-0.97283	3.87202	-0.72803
H	0.92660	4.42021	0.74482
H	2.68263	2.73016	1.21829
H	4.23428	-3.44639	-0.07693
H	2.13237	-3.04447	-1.30764
H	4.23295	0.59315	1.38524
H	5.27808	-1.65413	1.27594
H	-4.68523	-2.10571	0.84502
H	-4.73872	-2.21843	-0.91043
H	-5.25068	0.17575	-0.68630
H	-3.68123	1.65530	0.47478
H	-2.10688	0.52038	2.14895
H	-1.39255	-1.83162	1.68119
H	-2.62762	-3.17881	0.13709
H	-2.34450	-1.96567	-1.10092

Insertion TS for the dehydrogenation of cyclohexadiene (s)

M06/6-311+G** Enthalpy = -2241.762524

Imaginary Frequency = -699.60

C	1.74374	2.22097	-1.16171
C	2.23621	2.99687	-0.13589
C	2.49656	2.45261	1.13883
C	2.26607	1.11391	1.38443
C	0.64375	-2.72845	-1.32218
C	0.74878	-3.71223	-0.35688
C	1.21568	-3.42071	0.93394
C	1.59766	-2.12813	1.26033
H	0.75747	-0.12617	-2.83303
H	0.25540	-2.96465	-2.31054
H	0.45504	-4.73188	-0.59729
H	1.27932	-4.21225	1.67614
H	1.95601	-1.89767	2.26265
H	2.46051	0.69379	2.37012
H	2.86969	3.09626	1.93117
H	2.41080	4.05717	-0.30485
H	1.52883	2.65794	-2.13438

C	-1.77987	-0.14035	1.41047
C	-1.66101	1.20738	0.96103
C	-2.90920	1.77994	0.34038
H	-1.03528	-0.53130	2.10383
H	-1.04818	1.88434	1.56579
H	-3.67489	2.02381	1.10972
H	-4.02669	1.04442	-1.45999
H	-2.68408	2.70628	-0.20090
C	1.50865	0.84071	-0.94728
C	1.78163	0.29184	0.35780
C	1.00739	-1.40984	-1.00914
C	1.51077	-1.12345	0.30066
C	0.94043	-0.19026	-1.76714
C	-2.80668	-0.97413	0.97925
C	-3.61433	-0.54715	-0.08931
H	-4.22245	-1.27320	-0.62626
H	-2.84562	-2.00494	1.32179
H	-1.81124	0.55173	-1.24817
Ni	-0.48410	0.55350	-0.45302
C	-3.43789	0.72518	-0.60114

C-H insertion of cyclohexadiene with **I** (s)

M06/6-311+G** Enthalpy = -2241.770718

C	-1.21121	-0.45503	1.74984
C	-1.08010	-1.28597	-0.41932
C	-0.72261	-1.53663	0.95313
C	0.05042	-2.68049	1.25755
C	0.42615	-3.53367	0.24792
C	0.07655	-3.28137	-1.09820
C	-0.66041	-2.16768	-1.43127
C	-2.02037	0.37251	0.90165
C	-1.91198	-0.10787	-0.44600
C	-3.41885	2.16355	0.10857
C	-2.78662	1.52405	1.15502
C	-2.54020	0.57550	-1.49226
C	-3.29579	1.69850	-1.21307
Ni	0.24306	0.33235	0.49255
C	3.94918	1.17447	0.43945
C	3.20052	2.27950	0.28440
C	2.12378	2.30908	-0.76258
C	1.47185	0.94543	-0.90874
C	2.42277	-0.15035	-0.88123
C	3.63070	-0.04558	-0.26443
H	1.00683	1.15704	1.44466
H	-1.14169	-0.37798	2.82728
H	0.34640	-2.87236	2.28615

H	1.02150	-4.41274	0.48320
H	0.40553	-3.96820	-1.87362
H	-0.92024	-1.96702	-2.46929
H	-4.01240	3.05374	0.30433
H	-2.86485	1.90991	2.16883
H	-2.43214	0.22342	-2.51666
H	-3.79349	2.23260	-2.01831
H	4.77603	1.17207	1.14923
H	3.41961	3.18155	0.85237
H	1.37399	3.07547	-0.53448
H	2.59117	2.61065	-1.72769
H	0.79391	0.90582	-1.77450
H	2.11770	-1.10790	-1.30461
H	4.28384	-0.90961	-0.17067

Elimination TS for dehydrogenation of cyclohexadiene (s)

M06/6-311+G** Enthalpy = -2241.769174

Imaginary frequency = -609.43

C	0.47514	-0.23534	0.88457
C	2.61491	-0.00417	-0.07930
C	1.72876	-0.90853	0.56050
C	2.13793	-2.22596	0.77191
C	3.38563	-2.63687	0.32953
C	4.24196	-1.75022	-0.33343
C	3.85666	-0.43325	-0.53889
C	0.70967	1.16128	0.52577
C	1.97547	1.29223	-0.10387
C	0.35638	3.51975	0.21389
C	-0.08896	2.29624	0.68865
C	2.40203	2.52343	-0.59337
C	1.59217	3.63803	-0.43240
Ni	-0.91903	-0.81971	-0.46551
C	-4.36388	0.38834	-0.54402
C	-3.94651	-0.73357	-1.17838
C	-2.85165	-1.54080	-0.64202
C	-2.46887	-1.25771	0.73698
C	-2.94723	-0.06849	1.34743
C	-3.82416	0.77163	0.71906
H	-0.04464	-0.70593	-1.68019
H	-1.75747	-1.24439	-1.62461
H	-2.08013	-2.05556	1.36837
H	-2.59884	0.16829	2.35231
H	-2.87672	-2.59429	-0.92915
H	-4.39461	-1.03032	-2.12420
H	-5.14795	0.99624	-0.99153
H	-4.14713	1.69388	1.19314

H	1.46656	-2.92864	1.26325
H	3.70214	-3.66548	0.48965
H	5.21124	-2.09614	-0.68419
H	4.52614	0.26012	-1.04580
H	0.01211	-0.45449	1.85018
H	-1.06537	2.20982	1.16146
H	3.36783	2.61446	-1.08830
H	1.91598	4.60630	-0.80628
H	-0.26889	4.40185	0.33455

β -hydride elimination of cyclohexadiene with **I** (s)

M06/6-311+G** Enthalpy = -2241.800892

C	-0.70858	-0.02161	1.52286
C	-2.11385	0.16081	-0.35045
C	-1.70126	-0.69561	0.71683
C	-2.27255	-1.97513	0.81340
C	-3.18406	-2.39402	-0.13863
C	-3.55216	-1.56341	-1.20832
C	-3.01730	-0.28818	-1.31081
C	-0.62253	1.31425	0.98748
C	-1.43968	1.42214	-0.17702
C	0.05028	3.60551	0.67595
C	0.11041	2.43177	1.40627
C	-1.47092	2.60488	-0.91328
C	-0.72910	3.69681	-0.48757
Ni	0.84789	-1.19213	0.71667
H	1.39537	-2.46221	1.53719
H	0.81307	-2.12220	2.04208
C	4.06901	-0.48961	-0.52845
C	3.40264	0.76037	-0.64218
C	2.06255	0.80818	-0.90946
C	1.28425	-0.38351	-1.03813
C	1.95399	-1.64671	-0.88640
C	3.36623	-1.65336	-0.66407
H	-0.61251	-0.20370	2.59234
H	-1.98451	-2.63660	1.62883
H	-3.61921	-3.38855	-0.06287
H	-4.26140	-1.92032	-1.95089
H	-3.31263	0.36426	-2.13170
H	0.62616	4.47008	0.99999
H	0.74464	2.36284	2.28840
H	-2.08251	2.67610	-1.81190
H	-0.75077	4.62568	-1.05205
H	5.14069	-0.51602	-0.34380
H	3.96704	1.68374	-0.53446
H	1.56646	1.76892	-1.02973

H	0.32498	-0.31934	-1.55517
H	1.49680	-2.55390	-1.28316
H	3.88299	-2.61064	-0.60812

Benzene adduct of **I** (s)

M06/6-311+G** Enthalpy = -2240.634598

C	0.06778	0.89853	-1.72114
C	-0.61756	1.65591	0.39418
C	-1.06824	1.25926	-0.90791
C	-2.44717	1.29129	-1.18555
C	-3.33713	1.65051	-0.19323
C	-2.89202	1.99077	1.09699
C	-1.53727	1.99603	1.38453
C	1.22959	1.12097	-0.89450
C	0.81460	1.57082	0.40225
C	3.52113	1.24080	-0.15444
C	2.60592	0.98826	-1.15657
C	1.75727	1.80145	1.40241
C	3.10500	1.63414	1.13034
Ni	-0.02779	-0.98283	-1.06738
C	0.48640	-2.13732	1.95594
C	1.22181	-2.44024	0.83744
C	0.58817	-2.71493	-0.40963
C	-0.84100	-2.65662	-0.47940
C	-1.56929	-2.32707	0.70093
C	-0.92474	-2.07945	1.88684
H	0.07546	0.91773	-2.80860
H	-2.80572	1.00239	-2.17203
H	-4.40420	1.65983	-0.40717
H	-3.61513	2.25462	1.86484
H	-1.19078	2.26485	2.38171
H	4.58405	1.12255	-0.35616
H	2.93830	0.65733	-2.13900
H	1.43442	2.11298	2.39510
H	3.84572	1.81237	1.90600
H	0.99138	-1.90733	2.89058
H	2.30800	-2.46818	0.89370
H	1.16530	-3.20052	-1.19694
H	-1.37581	-3.09700	-1.32134
H	-2.65449	-2.26743	0.65080
H	-1.49801	-1.80354	2.76809

H₂ adduct of **I** (s)

M06/6-311+G** Enthalpy = -2009.766017

C	0.00133	0.89815	1.05959
---	---------	---------	---------

C	-0.70313	-1.06791	-0.01664
C	-1.14473	0.11624	0.65772
C	-2.52390	0.30886	0.85255
C	-3.42212	-0.61816	0.36166
C	-2.98456	-1.75656	-0.33766
C	-1.63015	-1.97788	-0.52405
C	1.15771	0.13366	0.65454
C	0.73255	-1.05699	-0.01835
C	3.44518	-0.56524	0.35234
C	2.53389	0.34792	0.84526
C	1.67209	-1.95285	-0.52796
C	3.02340	-1.71064	-0.34523
Ni	-0.03385	1.96945	-0.59134
H	-0.49129	2.81909	-1.79307
H	0.37470	2.84500	-1.79190
H	-0.00235	1.59152	1.89943
H	-2.87455	1.19928	1.37106
H	-4.48911	-0.46033	0.50679
H	-3.71279	-2.46430	-0.72637
H	-1.28923	-2.86595	-1.05495
H	4.50998	-0.39096	0.49464
H	2.87218	1.24395	1.36237
H	1.34344	-2.84625	-1.05767
H	3.76141	-2.40732	-0.73547

Cyclohexene (s)

M06/6-311+G** Enthalpy = -234.360263

C	-1.48548	0.04230	-0.11119
C	-0.66261	1.29329	-0.05983
C	0.66260	1.29331	0.05978
C	1.48546	0.04231	0.11134
C	0.68620	-1.17714	-0.32814
C	-0.68615	-1.17721	0.32802
H	-1.86434	-0.10477	-1.13504
H	-2.37937	0.16116	0.51468
H	-1.19208	2.24253	-0.11939
H	1.19206	2.24257	0.11908
H	1.86397	-0.10486	1.13532
H	2.37955	0.16119	-0.51423
H	0.55962	-1.15192	-1.42050
H	1.23356	-2.09743	-0.09581
H	-1.23351	-2.09746	0.09554
H	-0.55954	-1.15221	1.42037

1,3-Cyclohexadiene (s)

M06/6-311+G** Enthalpy = -233.156888

C	0.10742	1.41311	0.06511
C	1.24886	0.71925	0.11540
C	1.24756	-0.72145	-0.11549
C	0.10490	-1.41328	-0.06497
C	-1.18114	-0.71401	0.26152
C	-1.17980	0.71612	-0.26156
H	0.10762	2.49185	0.19616
H	2.19401	1.22047	0.30498
H	2.19182	-1.22437	-0.30500
H	0.10326	-2.49208	-0.19563
H	-2.04114	-1.26442	-0.13399
H	-1.30255	-0.70458	1.35869
H	-2.03895	1.26808	0.13359
H	-1.30090	0.70666	-1.35877

Benzene (s)

M06/6-311+G** Enthalpy = -232.007738

C	-0.63772	1.23357	-0.00000
C	-1.38720	0.06455	-0.00001
C	-0.74953	-1.16903	0.00001
C	0.63772	-1.23357	-0.00000
C	1.38721	-0.06454	-0.00000
C	0.74953	1.16903	0.00001
H	-1.13651	2.19816	-0.00003
H	-2.47195	0.11488	0.00001
H	-1.33545	-2.08332	0.00004
H	1.13652	-2.19815	0.00001
H	2.47195	-0.11490	-0.00006
H	1.33546	2.08331	0.00006

Dihydride species of I (s)

M06/6-311+G** Enthalpy = -2009.731424

C	3.55177	-0.25355	0.28227
H	4.58711	0.05678	0.40484
C	3.27144	-1.50631	-0.26965
H	4.08809	-2.15815	-0.57045
C	1.95616	-1.92161	-0.43005
H	1.73789	-2.90202	-0.85013
C	0.92539	-1.07511	-0.03714
C	1.20512	0.20458	0.49109
C	2.52680	0.60200	0.66092
H	2.74627	1.58999	1.06022
C	-0.51532	-1.24998	-0.03636
C	-0.04630	0.91730	0.78583

C	-1.09505	-0.07748	0.50261
H	-0.09917	1.45475	1.73460
C	-1.31058	-2.32422	-0.42214
H	-0.86082	-3.21984	-0.84756
C	-2.68487	-2.24776	-0.24467
H	-3.31893	-3.08058	-0.53915
C	-3.25826	-1.10314	0.31780
H	-4.33643	-1.05937	0.45586
C	-2.47550	-0.01961	0.68861
H	-2.92127	0.88449	1.09533
Ni	-0.46240	2.28793	-0.51945
H	-1.35749	3.08323	0.50705
H	0.37707	1.61781	-1.64056

Ethane (s)

M06/6-311+G** Enthalpy = -79.697777

C	-0.75853	-0.00000	0.00000
C	0.75853	0.00000	-0.00000
H	-1.16023	0.71079	0.72886
H	-1.16023	-0.98662	0.25111
H	-1.16022	0.27583	-0.97998
H	1.16023	-0.71084	-0.72881
H	1.16022	-0.27576	0.98000
H	1.16023	0.98660	-0.25118

Collision complex of I with ethane (s)

M06/6-311+G** Enthalpy = -2088.29103

C	0.42308	-0.38738	-1.44987
C	0.40026	1.35932	0.12923
C	-0.33096	0.73704	-0.94605
C	-1.55568	1.31989	-1.35196
C	-2.06021	2.40348	-0.66014
C	-1.37567	2.95533	0.43861
C	-0.14742	2.43613	0.82223
C	1.65556	-0.40063	-0.70085
C	1.63858	0.64855	0.27310
C	3.86002	-1.01477	0.05614
C	2.79446	-1.21092	-0.80387
C	2.71489	0.81531	1.14467
C	3.82158	-0.01220	1.03907
Ni	-0.91874	-1.21619	-0.25291
C	-2.33177	-2.08887	1.00761
C	-3.67413	-1.40872	1.22149
H	0.33044	-0.79402	-2.45500
H	-2.10013	0.89701	-2.19406
H	-3.01296	2.83427	-0.96354

H	-1.80478	3.79832	0.97474
H	0.39422	2.87893	1.65778
H	4.73940	-1.65128	-0.02243
H	2.82738	-2.00391	-1.54923
H	2.69087	1.60212	1.89784
H	4.66659	0.11765	1.71129
H	-1.49371	-1.44012	1.40143
H	-2.19459	-2.37730	-0.08449
H	-2.24844	-3.03233	1.55798
H	-3.84740	-1.19255	2.28251
H	-3.71279	-0.45916	0.67895
H	-4.50483	-2.03368	0.87126

Insertion TS for dehydrogenation of ethane (s)

M06/6-311+G** Enthalpy = -2088.280881

Imaginary frequency = -583.35

C	-1.90628	1.02096	-1.40121
C	-2.57880	2.02025	-0.72510
C	-1.97545	2.70924	0.34135
C	-0.67850	2.40524	0.72186
C	2.78667	-0.77818	-0.85173
C	3.80471	-0.40546	0.00305
C	3.61534	0.59648	0.97099
C	2.39554	1.24426	1.06670
Ni	-0.62656	-1.60633	-0.26324
C	-0.59641	0.67887	-1.01876
C	0.02659	1.41066	0.04531
C	1.53545	-0.14495	-0.76350
C	1.35966	0.90007	0.19869
C	0.31723	-0.32589	-1.50828
H	-0.62607	-2.85210	0.47335
C	-2.07673	-1.29089	2.07910
H	-1.90938	-0.23745	1.82577
H	-3.02766	-1.35061	2.63354
H	-1.27617	-1.58480	2.76777
C	-2.08546	-2.17409	0.83799
H	-2.37346	-3.19934	1.10671
H	-2.83746	-1.83087	0.10036
H	4.77053	-0.90248	-0.06502
H	2.93926	-1.57252	-1.57986
H	4.43009	0.86179	1.64013
H	2.24816	2.02686	1.80995
H	0.27167	-0.75832	-2.50533
H	-0.20952	2.94398	1.54420
H	-2.53065	3.48305	0.86571
H	-3.59660	2.27342	-1.01456

H	-2.39046	0.47735	-2.21066
---	----------	---------	----------

C-H insertion of ethane with I (s)

M06/6-311+G** Enthalpy = -2088.291636

C	0.08955	1.43761	-1.24607
C	0.86459	0.54141	0.76290
C	1.26417	1.09630	-0.49781
C	2.63248	1.16532	-0.80750
C	3.56172	0.70679	0.10624
C	3.16515	0.15915	1.33718
C	1.82244	0.07069	1.66246
C	-1.03681	1.21719	-0.39789
C	-0.57739	0.57476	0.80878
C	-3.29968	1.02958	0.41352
C	-2.42643	1.42431	-0.57073
C	-1.50116	0.17490	1.79134
C	-2.84362	0.40115	1.59561
Ni	-0.26978	-0.62900	-1.09052
H	-0.03711	-1.08684	-2.46890
C	-0.70213	-2.45710	-0.65752
C	0.22236	-3.01546	0.41686
H	0.07645	1.94091	-2.20454
H	2.95115	1.56545	-1.76751
H	4.62146	0.76068	-0.13409
H	3.91817	-0.20211	2.03288
H	1.51322	-0.36814	2.60957
H	-4.36739	1.18555	0.27625
H	-2.79125	1.88866	-1.48419
H	-1.15101	-0.31774	2.69689
H	-3.56412	0.08668	2.34616
H	-0.72162	-3.12954	-1.52363
H	-1.73821	-2.39262	-0.27758
H	1.27120	-3.00715	0.09130
H	-0.02055	-4.05523	0.70164
H	0.18195	-2.41594	1.33611

Elimination TS for dehydrogenation of ethane (s)

M06/6-311+G** Enthalpy = -2088.27558

Imaginary frequency = -672.33

C	0.25580	0.30997	0.90489
C	-1.87127	-0.02976	-0.05467
C	-1.02142	0.92390	0.56423
C	-1.48588	2.22744	0.74846
C	-2.74915	2.57644	0.29805
C	-3.56911	1.64156	-0.34530

C	-3.12970	0.33759	-0.52240
C	0.07994	-1.10047	0.57637
C	-1.17924	-1.29808	-0.05272
C	0.52169	-3.45457	0.33050
C	0.91653	-2.20313	0.77521
C	-1.55408	-2.55686	-0.51398
C	-0.70335	-3.63574	-0.32302
Ni	1.64952	0.83085	-0.47708
C	3.58962	1.21990	-0.66100
C	3.23910	0.92230	0.68883
H	3.16863	1.73078	1.41602
H	3.50011	-0.04885	1.10920
H	4.17859	0.49260	-1.22232
H	3.85692	2.24606	-0.91976
H	2.36602	1.17847	-1.71359
H	0.70087	0.87293	-1.65292
H	0.72431	0.57527	1.85451
H	-0.84392	2.96779	1.22269
H	-3.10778	3.59452	0.43625
H	-4.55208	1.93975	-0.70197
H	-3.77014	-0.39408	-1.01304
H	-2.51364	-2.69737	-1.00970
H	-0.98735	-4.62443	-0.67529
H	1.87946	-2.06988	1.26458
H	1.17651	-4.31018	0.48297

β -hydride elimination of ethane with **I** (s)

M06/6-311+G** Enthalpy = -2088.297324

C	-0.04969	0.28556	-1.34255
C	0.91808	-1.32992	0.06219
C	1.19065	-0.27359	-0.85489
C	2.52323	0.06530	-1.11928
C	3.54424	-0.59882	-0.46207
C	3.26936	-1.61303	0.46755
C	1.95692	-1.97642	0.72804
C	-1.08985	-0.54999	-0.78157
C	-0.51178	-1.50343	0.10999
C	-3.26313	-1.45595	-0.26366
C	-2.48030	-0.55734	-0.96684
C	-1.31801	-2.38461	0.82589
C	-2.69238	-2.36331	0.64083
Ni	-0.45932	1.95577	-0.14725
C	-0.22887	2.87431	1.57521
C	0.44522	1.63499	1.53759
H	-1.31772	2.57157	-1.37242
H	-1.36904	3.12728	-0.73628

H	-0.12091	0.67239	-2.35898
H	2.74808	0.86991	-1.81770
H	4.57881	-0.32647	-0.66221
H	4.08747	-2.11236	0.98086
H	1.74079	-2.76854	1.44401
H	-4.34194	-1.45423	-0.40711
H	-2.93883	0.15509	-1.65099
H	-0.87060	-3.09721	1.51788
H	-3.32933	-3.05113	1.19155
H	0.33138	3.80785	1.49460
H	-1.16857	2.97116	2.12185
H	1.52847	1.59210	1.40743
H	0.02069	0.75874	2.03181

Ethene adduct of **I** (s)

M06/6-311+G** Enthalpy = -2087.128228

C	0.20233	-0.36300	-1.42941
C	1.41126	0.85561	0.16947
C	1.47388	-0.22093	-0.77311
C	2.68611	-0.91330	-0.92826
C	3.77733	-0.56783	-0.15546
C	3.69997	0.46634	0.79422
C	2.52016	1.17278	0.95396
C	-0.63419	0.69080	-0.90413
C	0.09473	1.41947	0.09775
C	-2.53771	2.11686	-0.49402
C	-1.95697	1.08111	-1.19929
C	-0.52260	2.44960	0.80520
C	-1.83197	2.79638	0.51425
Ni	-0.90267	-1.36182	-0.06587
C	-1.46035	-2.77886	1.12250
C	-2.38155	-1.71374	1.11045
H	0.06609	-0.83495	-2.39931
H	2.75532	-1.72856	-1.64620
H	4.71347	-1.10961	-0.27632
H	4.57039	0.71126	1.39794
H	2.46027	1.98036	1.68256
H	-3.56440	2.40392	-0.71140
H	-2.51873	0.54626	-1.96250
H	0.02356	2.98189	1.58294
H	-2.31857	3.59794	1.06460
H	-1.68094	-3.70517	0.58829
H	-0.75709	-2.89478	1.94935
H	-3.31954	-1.79231	0.55596
H	-2.39794	-0.97308	1.91378

Butane (s)

M06/6-311+G** Enthalpy = -158.220605

C	1.93837	-0.11771	0.00009
C	0.55918	0.51452	-0.00010
C	-0.55918	-0.51452	-0.00010
C	-1.93837	0.11771	0.00009
H	2.07919	-0.75204	0.88296
H	2.73521	0.63186	0.00001
H	2.07928	-0.75233	-0.88256
H	0.44606	1.16853	-0.87680
H	0.44590	1.16872	0.87645
H	-0.44590	-1.16870	0.87647
H	-0.44605	-1.16856	-0.87678
H	-2.73521	-0.63186	-0.00053
H	-2.07909	0.75275	-0.88229
H	-2.07938	0.75163	0.88322

But-1-ene adduct of I (s)

M06/6-311+G** Enthalpy = -2165.655091

C	-0.37051	-0.30634	-1.41384
C	-1.08253	1.45040	-0.03530
C	-0.14293	1.07133	-1.04180
C	0.80091	2.01567	-1.47487
C	0.82129	3.27592	-0.90720
C	-0.08878	3.63504	0.10099
C	-1.03756	2.72328	0.53309
C	-1.53672	-0.72801	-0.67373
C	-1.95162	0.32579	0.19502
C	-3.35261	-2.07263	0.16100
C	-2.26786	-1.92457	-0.68307
C	-3.03515	0.14902	1.05463
C	-3.73563	-1.04597	1.03905
Ni	1.20589	-1.19924	-0.57861
C	1.87452	0.56962	2.23140
C	2.93280	-0.23398	1.49153
C	2.38502	-1.51290	0.91326
C	2.88482	-2.11645	-0.25434
H	-0.12654	-0.69796	-2.40873
H	1.52765	1.74081	-2.23744
H	1.56051	4.00177	-1.24005
H	-0.04501	4.62881	0.53957
H	-1.74743	2.99974	1.31172
H	-3.91436	-3.00462	0.15434
H	-1.96353	-2.73721	-1.34033
H	-3.33639	0.95097	1.72744
H	-4.58435	-1.19132	1.70284

H	1.05555	0.84846	1.55875
H	2.28440	1.48985	2.66403
H	1.43958	-0.02237	3.04705
H	3.76604	-0.46164	2.18135
H	3.36308	0.37346	0.68218
H	1.86733	-2.14514	1.64567
H	2.79010	-3.19341	-0.40525
H	3.71377	-1.65286	-0.79703

But-2-ene adduct of **I** (s)

M06/6-311+G** Enthalpy = -2165.656834

C	-0.32577	0.32039	-1.69221
C	-1.58607	0.87090	0.21204
C	-1.56359	0.09405	-0.99499
C	-2.68363	-0.69737	-1.31147
C	-3.75628	-0.74402	-0.44490
C	-3.75522	-0.01283	0.75794
C	-2.67478	0.79000	1.08084
C	0.41232	1.26590	-0.89119
C	-0.35334	1.59830	0.28172
C	2.16317	2.73149	-0.10936
C	1.67103	1.87784	-1.07454
C	0.17821	2.45150	1.24858
C	1.42932	3.01445	1.05838
Ni	0.68677	-0.92980	-0.50853
C	3.40756	-1.79998	-0.07793
C	2.12874	-1.49454	0.65110
C	1.04684	-2.39349	0.71391
C	0.04709	-2.38233	1.83942
H	-0.16300	0.12879	-2.74891
H	-2.68732	-1.28571	-2.22720
H	-4.61604	-1.36535	-0.68809
H	-4.60740	-0.07868	1.42982
H	-2.67500	1.36072	2.00869
H	3.14340	3.18453	-0.24372
H	2.25983	1.64210	-1.95928
H	-0.38981	2.67364	2.15117
H	1.84890	3.67864	1.80990
H	4.18878	-2.18858	0.59658
H	3.81501	-0.90411	-0.56384
H	3.24094	-2.55064	-0.85946
H	2.21956	-0.74240	1.44538
H	1.14706	-3.34775	0.18374
H	-0.97146	-2.58018	1.48157
H	0.27780	-3.13355	2.61367
H	0.02567	-1.39871	2.32480

C.2. Gas-phase dehydrogenation of amines and alcohols

Complex I (s)

M06/6-311+G** Enthalpy = -2008.56485

C	0.00000	0.97574	0.80445
C	-0.72273	-1.10703	-0.03491
C	-1.15689	0.13142	0.50938
C	-2.52458	0.34980	0.69500
C	-3.43278	-0.62352	0.31251
C	-3.00185	-1.82506	-0.26579
C	-1.64738	-2.06779	-0.43805
C	1.15688	0.13142	0.50933
C	0.72269	-1.10703	-0.03494
C	3.43275	-0.62360	0.31252
C	2.52457	0.34975	0.69498
C	1.64732	-2.06785	-0.43802
C	3.00180	-1.82514	-0.26577
Ni	0.00005	2.27549	-0.57527
H	0.00004	1.60663	1.70175
H	-2.86512	1.29354	1.11581
H	-4.49797	-0.44935	0.44984
H	-3.73269	-2.56954	-0.57259
H	-1.31040	-3.00802	-0.87232
H	4.49794	-0.44946	0.44987
H	2.86513	1.29349	1.11578
H	1.31031	-3.00808	-0.87225
H	3.73261	-2.56965	-0.57254

Complex II (d)

M06/6-311+G** Enthalpy = -1883.009415

C	-0.00000	0.93981	0.92100
C	-0.72219	-1.08675	-0.02366
C	-1.15265	0.11945	0.59537
C	-2.52357	0.34631	0.76268
C	-3.43264	-0.59728	0.31553
C	-3.00436	-1.77341	-0.31388
C	-1.64994	-2.01600	-0.48708
C	1.15266	0.11947	0.59537
C	0.72222	-1.08674	-0.02366

C	3.43266	-0.59722	0.31553
C	2.52357	0.34635	0.76268
C	1.64998	-2.01598	-0.48708
C	3.00440	-1.77336	-0.31389
Co	-0.00004	2.29667	-0.65077
H	-0.00001	1.59415	1.79379
H	-2.86591	1.26916	1.22678
H	-4.49816	-0.41920	0.44392
H	-3.73740	-2.49413	-0.66755
H	-1.31479	-2.93192	-0.97138
H	4.49818	-0.41913	0.44391
H	2.86590	1.26920	1.22678
H	1.31485	-2.93190	-0.97138
H	3.73746	-2.49407	-0.66756

Butylamine (s)

M06/6-311+G** Enthalpy = -213.532389

C	-2.50870	-0.30693	-0.01540
C	-1.24051	0.52431	0.04278
C	0.01598	-0.32437	-0.03923
C	1.28984	0.49330	0.01242
N	2.45729	-0.37017	-0.08902
H	-2.55904	-0.88102	-0.94756
H	-3.40876	0.31225	0.04246
H	-2.54568	-1.02509	0.81188
H	-1.23598	1.25572	-0.77804
H	-1.22323	1.11428	0.97025
H	0.01419	-0.91830	-0.96370
H	0.01905	-1.05205	0.78834
H	1.30469	1.18852	-0.83793
H	1.27538	1.11968	0.92398
H	2.50074	-1.00637	0.70136
H	3.31793	0.16571	-0.09131

Collision complex of I with butylamine (s)

M06/6-311+G** Enthalpy = -2222.148875

C	-1.15565	1.48034	1.16223
C	-0.89624	0.79374	-1.07734
C	-1.81497	0.86255	0.03790
C	-3.14976	0.42889	-0.17314
C	-3.50719	-0.12726	-1.38336
C	-2.57962	-0.26553	-2.43637
C	-1.28337	0.20411	-2.27934
C	0.17117	1.81624	0.70817
C	0.33692	1.39092	-0.65323
C	2.44201	2.63556	0.68149

C	1.24150	2.45791	1.34824
C	1.55816	1.57275	-1.30333
C	2.60894	2.19014	-0.64063
Ni	-0.93276	-0.46074	1.43315
C	3.78772	-1.51948	-1.01348
C	2.42447	-2.18643	-1.02039
C	1.68487	-1.98305	0.28955
C	0.35569	-2.70955	0.32296
N	-0.43150	-2.33318	1.51137
H	-1.30100	-2.86271	1.55771
H	-1.65361	1.96764	1.99733
H	-3.87427	0.51221	0.63425
H	-4.52687	-0.48155	-1.52662
H	-2.88887	-0.72044	-3.37433
H	-0.57152	0.12622	-3.10186
H	3.27230	3.12292	1.18914
H	1.13071	2.79171	2.37868
H	1.68589	1.23276	-2.33154
H	3.56167	2.33763	-1.14492
H	4.30825	-1.63603	-1.97051
H	4.42866	-1.94392	-0.23031
H	3.68272	-0.44680	-0.81107
H	2.52715	-3.26212	-1.23565
H	1.81224	-1.76795	-1.83270
H	2.31271	-2.32038	1.13129
H	1.50195	-0.90965	0.45105
H	0.52750	-3.80134	0.28399
H	-0.23675	-2.43147	-0.55777
H	0.09101	-2.52502	2.36625

N-H Insertion TS for the dehydrogenation of butylamine by complex **I** (s)

M06/6-311+G** Enthalpy = -2222.121498

Imaginary frequency = -993.78

H	-5.52139	-1.63513	-0.09056
C	-4.63616	-1.00432	-0.14289
C	-2.39753	0.63946	-0.30054
C	-3.61700	-1.17857	0.77614
C	-4.54411	-0.03147	-1.15073
C	-3.42789	0.78584	-1.22885
C	-2.47299	-0.37200	0.70852
H	-3.69237	-1.94740	1.54303
H	-5.35399	0.08149	-1.86749
C	-1.16066	1.34871	-0.11502
C	1.25965	2.40988	0.76593
C	-0.49697	0.76875	1.02328
C	-0.57397	2.40471	-0.81192

C	0.62988	2.93587	-0.37814
C	0.71847	1.34734	1.46041
H	-1.06820	2.81803	-1.69033
H	1.08859	3.76271	-0.91464
H	1.22668	0.93635	2.33097
H	2.20089	2.84267	1.10050
C	-1.27197	-0.34714	1.50403
H	-1.19732	-0.77344	2.49998
Ni	0.06922	-1.16039	0.22706
H	-3.35986	1.54664	-2.00530
H	1.18106	-2.08821	0.57848
C	2.56727	-1.10610	-1.10517
H	2.30543	-0.04045	-1.05607
N	1.35318	-1.86912	-0.88189
H	2.92880	-1.28312	-2.13568
C	3.71266	-1.39306	-0.13811
H	3.97055	-2.46097	-0.20674
H	3.34316	-1.22938	0.88593
C	4.94926	-0.53819	-0.38327
H	5.79763	-0.94637	0.18396
H	5.23520	-0.60909	-1.44452
C	4.75103	0.92117	-0.00282
H	4.47000	1.00847	1.05386
H	3.94731	1.38963	-0.58010
H	5.66269	1.50903	-0.15889
H	1.49092	-2.85201	-1.09587

N-H insertion of butylamine by complex **I** (s)

M06/6-311+G** Enthalpy = -2222.146214

C	1.32604	0.07296	-1.59334
C	1.85202	0.90031	0.53863
C	2.30472	0.06781	-0.52645
C	3.51893	-0.61554	-0.38540
C	4.24617	-0.48440	0.78458
C	3.78437	0.31715	1.83782
C	2.58799	1.00640	1.71585
C	0.33003	1.04732	-1.19948
C	0.61353	1.51320	0.11847
C	-1.64289	2.42636	-1.21591
C	-0.80803	1.53176	-1.86040
C	-0.25098	2.39777	0.75924
C	-1.37713	2.85521	0.09321
Ni	0.18155	-1.40584	-0.82483
N	-0.66862	-2.46988	0.36617
C	-2.06681	-2.36852	0.70340
C	-2.56469	-0.93924	0.60056

C	-3.98626	-0.74801	1.09753
C	-4.47488	0.67905	0.91620
H	-0.16676	-1.83073	-2.18000
H	1.58724	-0.11968	-2.62975
H	3.87504	-1.25697	-1.18916
H	5.18757	-1.01855	0.89488
H	4.36811	0.39587	2.75156
H	2.22861	1.63215	2.53138
H	-2.53064	2.79536	-1.72591
H	-1.03973	1.17833	-2.86306
H	-0.03861	2.73109	1.77406
H	-2.05852	3.54680	0.58280
H	-0.36609	-3.43778	0.44388
H	-2.24688	-2.72022	1.74108
H	-2.71844	-3.00359	0.06417
H	-2.48507	-0.61055	-0.44735
H	-1.87964	-0.28535	1.16257
H	-4.65869	-1.44183	0.56929
H	-4.04271	-1.02831	2.16071
H	-5.48229	0.83039	1.32199
H	-4.49249	0.95225	-0.14559
H	-3.79583	1.38644	1.40758

α -C elimination TS for the dehydrogenation of butylamine by complex I

M06/6-311+G** Enthalpy = -2222.128333

Imaginary frequency = -488.48

C	-0.67753	-0.07604	1.02583
C	-2.51023	0.63481	-0.27736
C	-1.41333	1.07593	0.50821
C	-1.18368	2.44761	0.65316
C	-2.02208	3.34787	0.01592
C	-3.08809	2.90861	-0.77965
C	-3.33142	1.55164	-0.92906
C	-1.47454	-1.22821	0.61957
C	-2.55197	-0.80892	-0.20236
C	-2.21415	-3.50262	0.36271
C	-1.32703	-2.58564	0.90503
C	-3.42472	-1.73993	-0.75893
C	-3.25560	-3.08745	-0.47509
Ni	1.02034	0.15733	-0.04220
C	2.83336	0.93470	0.23610
H	2.07902	0.18877	-1.07270
H	0.49963	-0.59303	-1.21177
H	-0.30602	-0.03804	2.05260
H	-0.33188	2.78443	1.23970
H	-1.84365	4.41587	0.12386

H	-3.72430	3.63503	-1.27969
H	-4.16387	1.20793	-1.54152
H	-4.24061	-1.41408	-1.40251
H	-3.93354	-3.82388	-0.89982
H	-2.09522	-4.56184	0.58156
H	-0.50272	-2.91944	1.53302
H	3.02813	1.82743	-0.37367
N	2.02334	1.15566	1.31028
C	4.03539	0.01637	0.31826
H	4.77672	0.49099	0.98382
H	3.73373	-0.92131	0.80896
C	4.69305	-0.29185	-1.01499
H	3.97616	-0.82652	-1.65105
H	4.91464	0.65196	-1.53473
C	5.96436	-1.10732	-0.86127
H	6.42551	-1.33935	-1.82733
H	5.75816	-2.05864	-0.35600
H	6.70803	-0.57303	-0.25685
H	2.19846	0.43450	2.01736

β -hydride elimination of butylamine complex **I** (s)

M06/6-311+G** Enthalpy = -2222.143431

C	-0.56967	0.38945	1.57675
C	0.47250	1.71502	-0.06302
C	0.65904	1.04376	1.17935
C	1.90368	1.13028	1.81323
C	2.93732	1.82583	1.20773
C	2.75871	2.45081	-0.03480
C	1.52592	2.39656	-0.66736
C	-1.54976	0.79872	0.58871
C	-0.90674	1.54747	-0.44373
C	-3.62504	1.01849	-0.62030
C	-2.93425	0.57714	0.49490
C	-1.61588	1.96992	-1.56401
C	-2.97296	1.69960	-1.65868
Ni	-0.85358	-1.57165	0.87187
H	-1.57279	-1.82180	2.33164
H	-1.80791	-2.45628	1.85588
N	-0.97908	-2.90948	-0.49910
C	-0.13079	-1.91917	-0.90104
C	1.32594	-2.29070	-1.02624
C	2.28359	-1.11685	-1.07710
C	3.72101	-1.54055	-1.31543
H	-0.82214	0.33692	2.63562
H	2.06051	0.63436	2.76979
H	3.90635	1.88472	1.69925

H	3.58701	2.98333	-0.49566
H	1.37795	2.89431	-1.62510
H	-4.69444	0.83181	-0.69578
H	-3.45408	0.04251	1.28804
H	-1.10848	2.51777	-2.35721
H	-3.53673	2.02555	-2.52912
H	-1.92214	-2.71832	-0.84931
H	-0.47117	-1.15421	-1.61866
H	1.45290	-2.89792	-1.94340
H	1.58807	-2.95853	-0.19186
H	2.21303	-0.55734	-0.13841
H	1.96707	-0.41456	-1.86228
H	4.06165	-2.22721	-0.52951
H	4.40202	-0.68149	-1.32247
H	3.83138	-2.06572	-2.27389

Butan-1-imine adduct of complex **I** (s)

M06/6-311+G** Enthalpy = -2220.981595

C	-0.85555	-0.37386	-1.39212
C	-0.70812	1.62418	-0.16877
C	-0.10440	0.85087	-1.20471
C	1.04601	1.34621	-1.83595
C	1.58710	2.55193	-1.42855
C	1.00722	3.29387	-0.38732
C	-0.13726	2.82909	0.24002
C	-1.99781	-0.26626	-0.50877
C	-1.89087	0.92510	0.26615
C	-4.06466	-0.76668	0.62035
C	-3.11020	-1.09707	-0.32443
C	-2.85091	1.23075	1.23010
C	-3.93614	0.38776	1.40765
Ni	0.38930	-1.70106	-0.59807
C	3.54643	1.14371	1.58471
C	2.39318	0.15829	1.55940
C	2.75720	-1.15069	0.87779
C	1.60568	-2.11871	0.81864
N	1.58379	-3.09206	-0.12752
H	-0.93023	-0.85728	-2.37344
H	1.52061	0.76495	-2.62466
H	2.48483	2.92830	-1.91495
H	1.46052	4.23121	-0.07463
H	-0.59281	3.40564	1.04402
H	-4.92544	-1.41650	0.76473
H	-3.20617	-2.00878	-0.91157
H	-2.75539	2.13388	1.83146
H	-4.69243	0.62046	2.15321

H	4.42106	0.72428	2.10054
H	3.27360	2.07930	2.08520
H	3.85267	1.39894	0.56272
H	1.53391	0.60616	1.04242
H	2.05387	-0.05098	2.58547
H	3.60335	-1.61698	1.41805
H	3.11588	-0.96084	-0.14435
H	1.10676	-2.26944	1.79075
H	0.96708	-3.84918	0.17843

C-H insertion TS for the dehydrogenation of butylamine by complex **I** (s)

M06/6-311+G** Enthalpy = -2222.124968

Imaginary frequency = -575.50

H	-3.24103	-3.03885	0.94745
C	-2.24472	-2.60529	0.88958
C	0.30090	-1.47131	0.79319
C	-1.66606	-2.40413	-0.34922
C	-1.58666	-2.23636	2.07669
C	-0.32246	-1.67022	2.02477
C	-0.36977	-1.83323	-0.43600
H	-2.19245	-2.68812	-1.25780
H	-2.07667	-2.39102	3.03457
C	1.57593	-0.91516	0.43589
C	3.83986	0.10268	-0.81368
C	1.65604	-0.90102	-0.99443
C	2.61557	-0.40006	1.20843
C	3.74505	0.10916	0.58824
C	2.81708	-0.39489	-1.59943
H	2.53741	-0.39444	2.29511
H	4.56039	0.51354	1.18286
H	2.89810	-0.37439	-2.68461
H	4.73370	0.50335	-1.28778
C	0.43954	-1.42225	-1.54754
H	0.31261	-1.73228	-2.57879
Ni	-0.91244	0.07089	-0.95489
H	0.18284	-1.37438	2.94354
H	-2.08098	0.87448	0.59884
C	-1.95782	1.55205	-0.28600
H	-1.23267	1.34476	-1.62051
C	-1.24229	2.80402	0.18799
H	-1.08280	3.47529	-0.67038
N	-3.25739	1.89691	-0.88027
H	-3.60923	1.09271	-1.39072
H	-1.89507	3.35900	0.88862
C	0.08399	2.50489	0.86531
H	0.72657	1.95032	0.16551

H	-0.08367	1.81759	1.70825
C	0.79621	3.75466	1.34852
H	0.18919	4.30284	2.08150
H	0.99547	4.43928	0.51446
H	1.75710	3.51755	1.81830
H	-3.93116	2.09819	-0.14338

N-H elimination TS for the dehydrogenation of butylamine by complex **I** (s)

M06/6-311+G** Enthalpy = -2222.109855

Imaginary frequency = -1106.53

C	-0.33576	-0.32781	-0.84632
C	-2.48719	0.33867	-0.16161
C	-1.73683	-0.70982	-0.75779
C	-2.39308	-1.88159	-1.14179
C	-3.75169	-2.01452	-0.90662
C	-4.48008	-0.99278	-0.28449
C	-3.84775	0.18394	0.08846
C	-0.29974	1.05918	-0.40220
C	-1.58763	1.44464	0.06818
C	0.50884	3.26000	0.15599
C	0.73887	1.99889	-0.36893
C	-1.79701	2.70876	0.61069
C	-0.74914	3.61658	0.65750
Ni	0.57241	-1.05718	0.78665
C	2.39705	-1.60397	0.53063
C	3.45847	-0.57907	0.22923
H	0.76841	-1.77924	2.17653
H	-0.39781	-1.27895	2.06217
H	0.26026	-0.65203	-1.70053
H	-1.82990	-2.69149	-1.60180
H	-4.26144	-2.92995	-1.20004
H	-5.54331	-1.12365	-0.09861
H	-4.41456	0.98353	0.56322
H	-2.78074	2.98888	0.98462
H	-0.90350	4.60848	1.07489
H	1.31938	3.98540	0.18319
H	1.72522	1.73478	-0.74724
H	2.52148	-2.54268	-0.02430
H	4.43885	-0.86524	0.66057
N	2.02586	-1.79978	1.88242
H	3.18951	0.38144	0.70138
C	3.64199	-0.36447	-1.26452
H	2.67589	-0.07960	-1.70223
H	3.91138	-1.32236	-1.73342
C	4.69391	0.68214	-1.58404
H	4.82585	0.82152	-2.66256

H	5.66814	0.40524	-1.16154
H	4.41950	1.65438	-1.15591
H	2.35952	-1.01158	2.44436

β -C elimination TS for the dehydrogenation of butylamine by complex I (s)

M06/6-311+G** Enthalpy = -2222.115428

Imaginary frequency = -575.99

C	-0.44730	-0.00466	0.96923
C	-2.40534	0.60708	-0.19479
C	-1.31580	1.09810	0.57212
C	-1.22210	2.46947	0.82051
C	-2.17191	3.32859	0.29112
C	-3.22340	2.84349	-0.49570
C	-3.34026	1.48259	-0.73917
C	-1.14978	-1.19963	0.51632
C	-2.30202	-0.83418	-0.22823
C	-1.67888	-3.51402	0.12637
C	-0.86114	-2.55292	0.69981
C	-3.10348	-1.80742	-0.81725
C	-2.79157	-3.14782	-0.63970
Ni	1.15139	0.26128	-0.25351
C	3.12592	0.67758	-0.05161
H	2.20621	0.49929	-1.27063
H	0.41289	0.02568	-1.56438
H	-0.04588	0.00061	1.98648
H	-0.39285	2.85542	1.41183
H	-2.09629	4.39742	0.48034
H	-3.95031	3.53660	-0.91211
H	-4.16407	1.10328	-1.34209
H	-3.97553	-1.52156	-1.40363
H	-3.41314	-3.91712	-1.09137
H	-1.44979	-4.56870	0.26464
H	0.01514	-2.84705	1.27621
H	3.34658	1.73097	-0.25187
C	2.47860	0.44082	1.19698
C	4.22285	-0.24469	-0.54815
H	5.04419	-0.23706	0.18476
H	3.85375	-1.27811	-0.57981
C	4.73843	0.14111	-1.92186
H	3.92839	0.10970	-2.65965
H	5.14006	1.16203	-1.91680
N	2.76972	-0.76265	1.95002
H	2.00326	-0.93464	2.59730
H	2.76665	-1.56393	1.32198
H	2.29244	1.29801	1.84551
H	5.53434	-0.52896	-2.26461

Diethylamine (s)

M06/6-311+G** Enthalpy = -213.526877

C	-2.43857	-0.36746	-0.02731
C	-1.21259	0.51598	0.02173
N	0.00000	-0.27140	-0.08306
C	1.21258	0.51595	0.02194
C	2.43859	-0.36745	-0.02740
H	-2.45467	-0.95154	-0.95219
H	-2.44809	-1.07142	0.81345
H	-3.35762	0.22276	0.02759
H	-1.22895	1.13587	0.94068
H	-1.22557	1.22330	-0.81952
H	-0.00008	-1.00031	0.62731
H	1.22897	1.13558	0.94108
H	1.22552	1.22353	-0.81909
H	3.35763	0.22277	0.02769
H	2.45468	-0.95123	-0.95248
H	2.44812	-1.07170	0.81312

Collision complex of **II** with diethylamine (d)

M06/6-311+G** Enthalpy = -2096.567244

C	-0.00146	-1.55842	-1.57871
C	-0.71738	-1.30135	0.63910
C	-1.15601	-1.46233	-0.73345
C	-2.54509	-1.45041	-1.00656
C	-3.45228	-1.30314	0.02818
C	-3.01939	-1.12409	1.35823
C	-1.66747	-1.10225	1.65896
C	1.15341	-1.46364	-0.73367
C	0.71513	-1.30200	0.63895
C	3.44999	-1.30710	0.02764
C	2.54252	-1.45300	-1.00699
C	1.66569	-1.10410	1.65876
C	3.01746	-1.12774	1.35784
Co	0.00131	0.31588	-0.71726
C	1.21494	2.65049	0.54832
N	0.00154	2.26056	-0.19176
C	-1.21225	2.65113	0.54736
H	0.00206	2.75989	-1.08730
H	-0.00174	-1.76626	-2.64232
H	-2.88980	-1.55562	-2.03425
H	-4.51855	-1.29451	-0.19035
H	-3.75423	-0.98600	2.14849
H	-1.33387	-0.94448	2.68461
H	4.51624	-1.29960	-0.19102

H	2.88693	-1.55846	-2.03475
H	1.33243	-0.94598	2.68446
H	3.75259	-0.99065	2.14800
H	1.13926	3.71209	0.85433
H	-1.13630	3.71267	0.85347
H	-1.23351	2.04349	1.46092
H	1.23511	2.04292	1.46194
C	-2.46997	2.42297	-0.25677
H	-3.34911	2.73017	0.32105
H	-2.56741	1.36298	-0.52027
H	-2.45450	3.00756	-1.18599
C	2.47330	2.42173	-0.25466
H	3.35197	2.72898	0.32384
H	2.45877	3.00601	-1.18409
H	2.57069	1.36165	-0.51780

N-H insertion TS for the dehydrogenation of diethylamine by complex **II** (d)

M06/6-311+G** Enthalpy = -2096.555342

Imaginary frequency = -1010.10

H	-2.47867	-3.72539	-0.15589
C	-1.59499	-3.10955	0.00277
C	0.67927	-1.56261	0.46004
C	-1.12010	-2.33553	-1.03408
C	-0.97443	-3.11666	1.26805
C	0.15506	-2.34342	1.48868
C	0.02481	-1.51473	-0.83093
H	-1.61566	-2.34011	-2.00296
H	-1.38479	-3.72806	2.06736
C	1.84149	-0.72261	0.37852
C	3.91545	0.98906	-0.34508
C	1.88752	-0.16860	-0.94249
C	2.82185	-0.39008	1.31384
C	3.85413	0.46173	0.95478
C	2.94797	0.68064	-1.28567
H	2.77618	-0.80050	2.32162
H	4.62167	0.72346	1.67917
H	2.99610	1.10913	-2.28541
H	4.73341	1.65477	-0.61283
C	0.73740	-0.60944	-1.68755
H	0.65129	-0.54928	-2.76717
H	0.64009	-2.35147	2.46429
C	-1.23524	2.97058	0.73835
H	-1.59326	3.81331	0.10348
C	-3.22281	1.68419	0.37426
H	-3.68146	2.44774	-0.29495
N	-1.78130	1.70831	0.28911

H	-1.50148	1.69760	-1.06785
Co	-0.74005	0.40440	-0.62470
H	-3.51810	1.97486	1.39888
H	-1.62594	3.17736	1.75132
C	-3.79301	0.32032	0.05160
H	-4.88518	0.31586	0.15397
H	-3.36757	-0.44112	0.71509
H	-3.54130	0.02981	-0.97550
C	0.27830	2.97001	0.76765
H	0.66216	3.92896	1.13671
H	0.69007	2.79889	-0.23377
H	0.65686	2.16756	1.41096

N-H insertion of diethylamine by complex **II** (d)

M06/6-311+G** Enthalpy = -2096.586764

C	0.29712	1.55671	-1.59250
C	1.17128	1.00552	0.49398
C	1.46807	1.09571	-0.91098
C	2.74486	0.70028	-1.36931
C	3.67913	0.25385	-0.46693
C	3.38171	0.16027	0.91251
C	2.14326	0.52167	1.38858
C	-0.67432	1.89642	-0.59186
C	-0.15970	1.50928	0.69122
C	-2.72216	2.58453	0.46675
C	-1.97444	2.43092	-0.67892
C	-0.95464	1.65414	1.83924
C	-2.21724	2.19415	1.72418
Co	-0.23482	-0.29726	-0.86358
H	-0.77795	-0.71947	-2.18932
N	-0.59142	-1.94081	-0.11310
C	-0.29844	-2.20205	1.27347
C	-1.33824	-3.00047	-0.74022
H	0.22334	1.78409	-2.64808
H	2.97337	0.74450	-2.43162
H	4.66194	-0.05241	-0.81766
H	4.13739	-0.21621	1.59716
H	1.91183	0.43198	2.44870
H	-3.72715	2.99492	0.40263
H	-2.38149	2.70368	-1.64989
H	-0.57426	1.34063	2.80960
H	-2.83852	2.31212	2.60838
H	-0.19847	-1.25068	1.81760
H	-1.07600	-3.05531	-1.80544
H	-1.06542	-3.98560	-0.30869
H	-1.13486	-2.73538	1.77288

C	0.98486	-3.00563	1.47056
H	0.92419	-3.97191	0.95416
H	1.19018	-3.20055	2.53366
H	1.82998	-2.45215	1.04439
C	-2.84863	-2.81901	-0.62104
H	-3.40434	-3.64901	-1.08213
H	-3.13624	-1.88196	-1.11139
H	-3.15219	-2.74744	0.43113

α -C elimination TS for the dehydrogenation of diethylamine by complex **II** (d)

M06/6-311+G** Enthalpy = -2096.562689

Imaginary frequency = -461.82

C	-0.27542	-0.51145	0.71890
C	-1.75100	1.25250	0.21635
C	-0.45699	0.93227	0.71694
C	0.41458	1.97084	1.06906
C	0.00638	3.28600	0.90739
C	-1.25863	3.59495	0.39242
C	-2.13653	2.57805	0.04494
C	-1.57095	-1.04892	0.34091
C	-2.45267	0.00980	-0.00450
C	-3.32487	-2.61653	-0.16139
C	-2.03177	-2.36492	0.26832
C	-3.74238	-0.25646	-0.45384
C	-4.17976	-1.57052	-0.53055
C	3.04304	-0.01757	-1.05492
C	3.00719	-1.81833	0.45805
H	0.29755	-0.98821	1.51450
H	1.40492	1.72956	1.44955
H	0.68233	4.09386	1.18083
H	-1.55128	4.63462	0.26689
H	-3.12364	2.81499	-0.34984
H	-4.40641	0.56116	-0.73111
H	-5.18743	-1.79181	-0.87386
H	-3.68180	-3.64275	-0.22134
H	-1.36735	-3.18702	0.53021
H	2.26738	-2.45666	-0.07911
N	2.76692	-0.40303	0.22403
H	1.81042	-0.23342	-2.16468
H	-0.01742	-0.53547	-1.89912
Co	1.07848	-0.39086	-0.85470
H	3.68034	-0.68779	-1.65710
H	3.99163	-2.11613	0.04954
C	2.96002	-2.13760	1.93712
H	3.71624	-1.55138	2.47061

H	3.14123	-3.20231	2.12741
H	1.98561	-1.87356	2.35943
C	3.34791	1.44338	-1.27839
H	4.36021	1.67645	-0.92110
H	2.64083	2.06939	-0.72481
H	3.28044	1.70815	-2.33903

β -hydride elimination of diethylamine by complex **II** (d)

M06/6-311+G** Enthalpy = -2096.568495

C	-0.72948	-0.60924	1.08933
C	-2.58546	0.25542	-0.05763
C	-2.03371	-0.90882	0.56170
C	-2.78960	-2.08891	0.57259
C	-4.03339	-2.11525	-0.03316
C	-4.55820	-0.97697	-0.66349
C	-3.83298	0.20429	-0.67534
C	-0.51717	0.78520	0.83827
C	-1.63555	1.32662	0.09514
C	0.61195	2.91597	0.56913
C	0.62838	1.60041	1.05321
C	-1.61213	2.63387	-0.35157
C	-0.48509	3.42955	-0.11443
Co	0.89666	-0.18026	-0.28467
H	-0.11535	-0.64477	-1.67132
H	0.01094	0.13035	-1.82389
C	2.55251	-2.48168	0.58707
C	2.19682	-1.62325	-0.60377
N	2.73037	-0.38436	-0.86704
C	3.73703	0.15722	0.01748
H	-0.25501	-1.19342	1.87391
H	-2.39155	-2.98363	1.04781
H	-4.61423	-3.03543	-0.02615
H	-5.53481	-1.02409	-1.13866
H	-4.24036	1.09252	-1.15627
H	1.47607	3.55308	0.74734
H	1.42485	1.27976	1.72598
H	-2.45522	3.03775	-0.91061
H	-0.45872	4.45246	-0.48124
H	3.54862	-2.95040	0.50461
H	1.81684	-3.28770	0.68767
H	1.93251	-2.20761	-1.49485
H	3.67535	1.25415	-0.03217
H	2.53765	-1.91827	1.52876
H	3.59966	-0.10243	1.08786
C	5.13120	-0.28519	-0.40801
H	5.31128	0.00100	-1.44998

H	5.22768	-1.37542	-0.34389
H	5.91065	0.16408	0.22145

N-ethylethanamine adduct of complex **II** (d)

M06/6-311+G** Enthalpy = -2095.388263

C	0.97127	0.78009	-1.63358
C	0.50569	1.48356	0.56798
C	0.08594	1.56604	-0.80641
C	-1.04310	2.35030	-1.13082
C	-1.73798	2.98823	-0.11922
C	-1.34019	2.87897	1.22270
C	-0.22174	2.12819	1.56330
C	1.95422	0.23084	-0.73528
C	1.67239	0.64616	0.60714
C	3.85448	-0.99948	0.09269
C	3.06936	-0.59075	-0.96963
C	2.46977	0.20902	1.66331
C	3.55810	-0.61054	1.40920
Co	-0.50189	-0.54378	-1.15335
C	-2.67954	-0.85245	0.55392
N	-2.04695	-1.50059	-0.58331
C	-0.94457	-2.28472	-0.35273
H	1.11843	0.92074	-2.70153
H	-1.36702	2.43156	-2.16658
H	-2.61644	3.58113	-0.36576
H	-1.91317	3.38366	1.99634
H	0.08165	2.04046	2.60578
H	4.71483	-1.63977	-0.09163
H	3.30097	-0.91286	-1.98309
H	2.23768	0.51200	2.68344
H	4.18582	-0.95425	2.22750
H	-3.15549	0.06983	0.19235
H	-0.78724	-3.07034	-1.10325
H	-1.97146	-0.52842	1.33813
C	-0.34308	-2.59977	0.99384
H	0.68231	-2.96151	0.85697
H	-0.89952	-3.38551	1.53262
H	-0.28260	-1.72386	1.64867
C	-3.73658	-1.75642	1.17084
H	-3.28142	-2.66979	1.57162
H	-4.46582	-2.05682	0.41017
H	-4.26842	-1.25387	1.98845

α -C insertion TS for the dehydrogenation of diethylamine by complex **II** (d)

M06/6-311+G** Enthalpy = -2096.549096

Imaginary frequency = -737.25

H	-3.10105	-3.21780	0.81135
C	-2.12496	-2.73781	0.77773
C	0.36526	-1.47581	0.74460
C	-1.55215	-2.45928	-0.45178
C	-1.49026	-2.38984	1.98211
C	-0.25680	-1.75091	1.96082
C	-0.27363	-1.83579	-0.50722
H	-2.05591	-2.74512	-1.37280
H	-1.97596	-2.60689	2.92990
C	1.61375	-0.84695	0.41626
C	3.84545	0.30574	-0.77845
C	1.71732	-0.80383	-1.01325
C	2.61605	-0.29487	1.21442
C	3.72765	0.28171	0.62194
C	2.86091	-0.22971	-1.58874
H	2.52209	-0.31513	2.29980
H	4.51254	0.71454	1.23742
H	2.95860	-0.18706	-2.67213
H	4.72548	0.75866	-1.23086
C	0.53231	-1.36334	-1.59580
H	0.43892	-1.65159	-2.63666
H	0.22473	-1.46200	2.89471
H	-2.14705	0.84367	0.63352
C	-2.05027	1.56094	-0.21588
C	-3.44319	1.94507	-0.66906
H	-3.40576	2.64783	-1.51326
H	-3.98646	1.05708	-1.00977
H	-1.46453	1.32808	-1.50038
Co	-0.97083	0.01759	-0.91359
N	-1.34412	2.73027	0.29879
H	-1.22582	3.39303	-0.46838
H	-4.00609	2.42323	0.14344
C	-0.02672	2.41300	0.82989
H	0.59912	1.86579	0.09750
H	-0.16181	1.72463	1.67657
C	0.69372	3.66237	1.28418
H	0.12112	4.18708	2.05726
H	0.83926	4.35626	0.44620
H	1.68341	3.41476	1.68141

N-H elimination TS for the dehydrogenation of diethylamine by complex **II** (d)

M06/6-311+G** Enthalpy = -2096.529526

Imaginary frequency = -1078.24

C	0.46250	-0.16041	-1.07594
C	2.14492	0.90868	0.17727

C	0.98830	1.11933	-0.62846
C	0.52943	2.42757	-0.82824
C	1.19081	3.48489	-0.22184
C	2.30917	3.26819	0.58998
C	2.78609	1.97957	0.78906
C	1.42966	-1.14020	-0.61748
C	2.42598	-0.50714	0.17282
C	2.52508	-3.24806	-0.23911
C	1.50420	-2.51928	-0.82693
C	3.43465	-1.25387	0.77464
C	3.48503	-2.62449	0.56804
C	-3.87129	-0.76463	0.66194
N	-3.08082	0.41056	0.30151
C	-2.96639	-0.52270	-2.05978
H	0.01017	-0.26347	-2.06303
H	-0.34362	2.60739	-1.45213
H	0.83155	4.50026	-0.37544
H	2.80480	4.11219	1.06328
H	3.66076	1.81075	1.41551
H	4.18465	-0.76589	1.39541
H	4.27075	-3.21784	1.02918
H	2.57973	-4.32313	-0.39841
H	0.74889	-3.01686	-1.43352
H	-4.78059	-0.74772	0.04229
H	-2.39247	-0.31805	-2.97109
H	-2.71838	-1.54810	-1.75644
C	-2.60765	0.49459	-1.00871
H	-2.07848	0.35707	1.34897
H	-0.46360	-0.51635	1.53985
Co	-1.14622	0.00143	0.22770
H	-3.36301	-1.71998	0.43676
H	-2.56711	1.52592	-1.38010
H	-4.03411	-0.51399	-2.34237
C	-4.24338	-0.72920	2.12815
H	-4.88022	-1.57929	2.39619
H	-4.77635	0.19782	2.36398
H	-3.34229	-0.77025	2.75010

Butanol (s)

M06/6-311+G** Enthalpy = -233.421458			
C	-2.49089	-0.29317	0.00003
C	-1.21550	0.52871	-0.00003
C	0.03087	-0.33919	-0.00009
C	1.30218	0.47094	0.00007
O	2.39684	-0.42184	0.00011
H	-2.53968	-0.94092	-0.88260

H	-3.38498	0.33692	0.00007
H	-2.53959	-0.94091	0.88267
H	-1.19988	1.19136	-0.87728
H	-1.19979	1.19135	0.87722
H	0.03299	-0.99795	-0.87950
H	0.03290	-0.99813	0.87919
H	1.32424	1.12547	0.88783
H	1.32439	1.12561	-0.88757
H	3.21475	0.07811	-0.00078

Collision complex of **I** with butanol (s)

M06/6-311+G** Enthalpy = -2242.02351

C	1.29826	-0.10596	-1.59457
C	2.01278	0.75687	0.47199
C	2.33826	-0.14262	-0.59184
C	3.54128	-0.85626	-0.53262
C	4.37326	-0.71681	0.56512
C	4.02909	0.13335	1.62800
C	2.85390	0.86752	1.57937
C	0.35319	0.88847	-1.14415
C	0.77550	1.40407	0.13660
C	-1.51689	2.42339	-1.07527
C	-0.79353	1.45985	-1.74963
C	0.01056	2.35931	0.80136
C	-1.13680	2.86658	0.20652
Ni	-0.17466	-1.16690	-0.86599
C	-4.36947	0.73079	0.78291
C	-3.69503	-0.60126	0.51085
C	-2.48284	-0.81093	1.40279
C	-1.85375	-2.17296	1.25408
O	-1.52422	-2.39975	-0.12203
H	-0.88931	-3.13281	-0.19397
H	1.46692	-0.37521	-2.63605
H	3.80648	-1.53394	-1.34254
H	5.30342	-1.28005	0.61140
H	4.69219	0.22128	2.48562
H	2.59491	1.53853	2.39772
H	-2.40894	2.84252	-1.53874
H	-1.10434	1.12295	-2.73631
H	0.32236	2.72179	1.78088
H	-1.73316	3.61842	0.71848
H	-5.22382	0.90052	0.11854
H	-3.65749	1.55140	0.63434
H	-4.73321	0.78848	1.81733
H	-3.36865	-0.64914	-0.53571
H	-4.40745	-1.42929	0.65510

H	-1.72622	-0.04332	1.18235
H	-2.77043	-0.68900	2.45953
H	-0.94508	-2.24332	1.86633
H	-2.56062	-2.95914	1.57044

O-H insertion TS for the dehydrogenation of butanol by complex **I** (s)

M06/6-311+G** Enthalpy = -2242.005957

Imaginary frequency = -1205.86

H	-0.79142	3.89754	0.89038
C	-0.08090	3.14492	0.55470
C	1.74528	1.24454	-0.34346
C	0.18232	2.05434	1.36041
C	0.53758	3.29417	-0.69898
C	1.44379	2.34604	-1.14400
C	1.09496	1.06659	0.92585
H	-0.31275	1.94328	2.32287
H	0.29835	4.15425	-1.31919
C	2.65586	0.14358	-0.51953
C	4.24490	-2.12615	-0.30244
C	2.52911	-0.71005	0.61820
C	3.55178	-0.16961	-1.54004
C	4.34562	-1.30063	-1.43211
C	3.34880	-1.84116	0.71286
H	3.63478	0.47616	-2.41301
H	5.05133	-1.54925	-2.22096
H	3.26669	-2.49876	1.57613
H	4.87765	-3.00832	-0.22881
C	1.51318	-0.18844	1.50094
H	1.45123	-0.43665	2.55659
H	1.92579	2.46271	-2.11370
C	-2.92602	-0.45395	0.18168
H	-3.09411	-0.41307	1.27524
H	-2.75963	0.59240	-0.13508
O	-1.82367	-1.26193	-0.13098
C	-4.16919	-0.99418	-0.49922
H	-4.34041	-2.02627	-0.15912
H	-3.97804	-1.05574	-1.58037
C	-5.40131	-0.14611	-0.23696
H	-5.57197	-0.07670	0.84754
H	-5.21148	0.88281	-0.57508
C	-6.64435	-0.68971	-0.91848
H	-7.52809	-0.07071	-0.72809
H	-6.86786	-1.70600	-0.57209
H	-6.50203	-0.74269	-2.00453
H	-1.18839	-1.67879	0.96508
Ni	-0.19995	-0.61057	0.54812

O-H insertion of butanol by complex I (s)

M06/6-311+G** Enthalpy = -2242.039687

C	-1.83636	0.40072	1.43533
C	-2.12063	-0.02832	-0.84923
C	-2.46303	-0.46845	0.46273
C	-3.25326	-1.61499	0.61340
C	-3.67787	-2.30216	-0.50925
C	-3.32159	-1.87671	-1.79671
C	-2.54125	-0.74518	-1.96749
C	-1.23243	1.47479	0.67638
C	-1.34575	1.18557	-0.71665
C	0.00951	3.46001	0.12224
C	-0.54940	2.63351	1.07827
C	-0.75615	2.02162	-1.66322
C	-0.08440	3.15789	-1.24474
Ni	-0.07639	-0.50433	1.18768
H	0.06266	-0.64441	2.62950
O	1.44724	-1.24767	0.54384
C	2.62122	-0.53833	0.63261
C	3.67328	-1.11495	-0.30534
C	4.99852	-0.37634	-0.25175
C	6.04255	-0.96588	-1.18386
H	-2.17808	0.50122	2.45980
H	-3.51545	-1.96475	1.60941
H	-4.28963	-3.19400	-0.39351
H	-3.65763	-2.44160	-2.66238
H	-2.26337	-0.41532	-2.96675
H	0.54445	4.35437	0.43368
H	-0.44681	2.85921	2.13728
H	-0.82644	1.78422	-2.72313
H	0.37826	3.81685	-1.97473
H	3.04052	-0.55240	1.66482
H	2.50104	0.54188	0.38336
H	3.27191	-1.09665	-1.32969
H	3.81954	-2.17614	-0.05256
H	4.83378	0.68227	-0.50095
H	5.37735	-0.38383	0.78136
H	6.99567	-0.42587	-1.14092
H	5.69355	-0.94406	-2.22348
H	6.24191	-2.01511	-0.93332

α -C elimination TS for the dehydrogenation of butanol by complex I (s)

M06/6-311+G** Enthalpy = -2242.031766

Imaginary Frequency = -546.11

C	-0.64631	0.07261	-0.98922
---	----------	---------	----------

C	-2.53062	-0.61406	0.24812
C	-1.41406	-1.06881	-0.50234
C	-1.20010	-2.44355	-0.64342
C	-2.07047	-3.33363	-0.03576
C	-3.15541	-2.88104	0.72611
C	-3.38507	-1.52114	0.87015
C	-1.43805	1.23514	-0.60938
C	-2.54861	0.83000	0.17583
C	-2.15048	3.51978	-0.36835
C	-1.25987	2.59176	-0.88440
C	-3.42512	1.77304	0.70639
C	-3.22601	3.11831	0.43302
Ni	1.04630	-0.16098	0.08800
C	3.98665	-0.04545	-0.34584
C	2.80598	-0.98570	-0.19469
H	2.00531	-0.13550	1.20089
H	0.53722	0.59857	1.23357
H	-0.19960	0.03047	-1.98518
H	-0.34002	-2.79511	-1.20889
H	-1.90448	-4.40368	-0.14232
H	-3.81784	-3.59958	1.20278
H	-4.23288	-1.16730	1.45512
H	-4.26693	1.45784	1.32122
H	-3.90659	3.86386	0.83698
H	-2.00866	4.57762	-0.57990
H	-0.41127	2.91441	-1.48488
H	3.02808	-1.84867	0.46655
H	4.70649	-0.53693	-1.02293
H	3.64577	0.86082	-0.86504
O	2.03693	-1.19261	-1.21392
C	4.67958	0.30846	0.95563
H	3.98232	0.87037	1.59053
H	4.91148	-0.61544	1.50666
C	5.95006	1.11160	0.74052
H	6.43453	1.38013	1.68574
H	5.73550	2.04231	0.20165
H	6.67722	0.55017	0.14081

β -hydride elimination of butanol by complex **I** (s)

M06/6-311+G** Enthalpy = -2242.044551

C	-0.82032	-0.13242	-1.43264
C	-1.50260	1.31115	0.30187
C	-1.91837	0.25461	-0.55804
C	-3.23076	-0.22413	-0.45082
C	-4.07943	0.30481	0.50623
C	-3.64898	1.31324	1.37864

C	-2.36126	1.81674	1.27420
C	0.22454	0.83830	-1.16078
C	-0.16377	1.68711	-0.08659
C	2.28738	2.06931	-1.33004
C	1.45869	1.05448	-1.78141
C	0.68677	2.69137	0.36823
C	1.91272	2.88343	-0.25361
Ni	-0.44205	-1.92033	-0.49510
H	-1.31910	-3.17987	-1.06257
H	-1.43012	-2.59231	-1.63166
C	4.34382	-0.01643	0.96672
C	2.90158	-0.28776	1.35218
C	2.28850	-1.43216	0.56352
C	0.83176	-1.68822	0.91569
O	0.36969	-2.90809	0.88075
H	-1.02071	-0.40146	-2.47179
H	-3.57503	-1.01841	-1.11087
H	-5.09595	-0.07397	0.58961
H	-4.32899	1.70333	2.13170
H	-2.02946	2.61335	1.93859
H	3.24882	2.23373	-1.81269
H	1.76672	0.41797	-2.60988
H	0.38722	3.33208	1.19636
H	2.58388	3.66613	0.09114
H	4.97696	-0.89536	1.14722
H	4.76875	0.82531	1.52636
H	4.41525	0.22817	-0.10020
H	2.30444	0.62028	1.19417
H	2.83472	-0.51335	2.42739
H	2.84356	-2.36498	0.75290
H	2.40030	-1.22154	-0.51181
H	0.42693	-1.00589	1.69261

Butanal adduct of complex I (s)

M06/6-311+G** Enthalpy = -2240.880468

C	-0.80528	-0.41346	-1.40870
C	-0.64094	1.62666	-0.25297
C	-0.05482	0.82462	-1.27270
C	1.09007	1.29474	-1.92822
C	1.64406	2.50765	-1.55768
C	1.08091	3.27838	-0.52979
C	-0.06017	2.83771	0.12075
C	-1.93757	-0.27276	-0.50834
C	-1.81692	0.94034	0.22462
C	-3.98149	-0.73550	0.67459
C	-3.04394	-1.09745	-0.27635

C	-2.75737	1.27943	1.19613
C	-3.83925	0.44350	1.42025
Ni	0.40729	-1.77665	-0.67173
C	3.17218	1.22083	1.90866
C	2.11799	0.13612	1.78831
C	2.60909	-1.07838	1.01829
C	1.51978	-2.10608	0.81681
O	1.63728	-3.05542	-0.05838
H	-0.93298	-0.88351	-2.39331
H	1.55372	0.68953	-2.70533
H	2.53873	2.86528	-2.06315
H	1.54420	4.21965	-0.24477
H	-0.50190	3.43532	0.91692
H	-4.83826	-1.38080	0.85698
H	-3.14805	-2.02953	-0.82871
H	-2.64967	2.20111	1.76618
H	-4.58136	0.70006	2.17213
H	4.07866	0.84536	2.40263
H	2.80826	2.08329	2.47836
H	3.45789	1.58650	0.91483
H	1.22970	0.54161	1.28488
H	1.78363	-0.17938	2.78818
H	2.99808	-0.77559	0.03515
H	3.45564	-1.54224	1.55870
H	0.92351	-2.30511	1.73385

C-H insertion TS for the dehydrogenation of butanol by complex **I** (s)

M06/6-311+G** Enthalpy = -2242.01632

Imaginary Frequency = -589.70

H	1.57629	3.56958	-0.66474
C	0.74648	2.92219	-0.38897
C	-1.37662	1.27781	0.37081
C	0.27370	1.99945	-1.30548
C	0.19271	3.02588	0.89814
C	-0.86300	2.20718	1.27291
C	-0.80304	1.14692	-0.94892
H	0.71004	1.93412	-2.29972
H	0.59756	3.74896	1.60147
C	-2.43213	0.30874	0.47302
C	-4.32273	-1.69634	0.10593
C	-2.46176	-0.42976	-0.75315
C	-3.32857	0.01052	1.49844
C	-4.27168	-0.98811	1.31802
C	-3.43449	-1.42678	-0.91841
H	-3.29239	0.56666	2.43426
H	-4.97778	-1.22256	2.11074

H	-3.47723	-1.99382	-1.84650
H	-5.07311	-2.47361	-0.02476
C	-1.42245	0.04078	-1.62319
H	-1.38327	-0.15524	-2.68944
Ni	0.38771	-0.50382	-0.70328
H	-1.28646	2.28623	2.27327
H	1.70928	-0.06998	0.84906
C	1.96378	-1.00095	0.27615
H	1.29556	-1.64706	-0.92059
C	3.37162	-0.85918	-0.25022
H	3.64786	-1.77067	-0.80301
H	3.37255	-0.03549	-0.98048
C	4.40712	-0.58942	0.83217
H	4.12834	0.32899	1.36883
H	4.36983	-1.39844	1.57207
O	1.92576	-2.11202	1.17255
H	0.99844	-2.34746	1.26405
C	5.80989	-0.45665	0.26625
H	6.55516	-0.25434	1.04373
H	5.86268	0.35905	-0.46583
H	6.11161	-1.37558	-0.25174

O-H elimination TS for the dehydrogenation of butanol by complex **I** (s)

M06/6-311+G** Enthalpy = -2242.004001

Imaginary Frequency = -1607.41

C	-0.24525	0.12731	-0.91212
C	-1.89659	-1.28741	-0.01988
C	-0.56726	-1.23906	-0.52629
C	0.18831	-2.41648	-0.56978
C	-0.35746	-3.59544	-0.09251
C	-1.65380	-3.63043	0.43778
C	-2.42293	-2.47801	0.47468
C	-1.48632	0.87034	-0.75419
C	-2.47040	0.03200	-0.16101
C	-3.07560	2.67417	-0.76399
C	-1.81217	2.19612	-1.06210
C	-3.73104	0.53569	0.15294
C	-4.03241	1.85356	-0.15041
Ni	0.44793	0.67819	0.84681
H	1.50712	1.36957	2.12187
H	0.61002	0.98825	2.48107
H	0.44714	0.34682	-1.72328
H	1.20269	-2.39684	-0.96267
H	0.23138	-4.50945	-0.12120
H	-2.05632	-4.56643	0.81641
H	-3.43442	-2.50649	0.87627

H	-4.47699	-0.10317	0.62257
H	-5.01413	2.25573	0.08624
H	-1.06409	2.84476	-1.51397
H	-3.32913	3.70568	-0.99745
O	2.52068	1.74066	1.45267
C	2.17849	1.24397	0.25497
H	2.00736	2.00523	-0.53870
C	3.03160	0.09467	-0.24292
H	2.62195	-0.30087	-1.18550
H	2.99670	-0.72300	0.49390
C	4.48155	0.51604	-0.45535
H	4.86038	0.92765	0.48844
H	4.51169	1.34182	-1.18220
C	5.35848	-0.62811	-0.93112
H	5.35562	-1.44903	-0.20362
H	6.40006	-0.32058	-1.08120
H	4.99240	-1.03791	-1.88112

β -C elimination TS for the dehydrogenation of butanol by complex I (s)

M06/6-311+G** Enthalpy = -2242.007527

Imaginary Frequency = -594.07

C	-0.42621	0.04208	-0.97028
C	-2.34064	-0.68839	0.20099
C	-1.21192	-1.11541	-0.54703
C	-1.01334	-2.48225	-0.75727
C	-1.89867	-3.39585	-0.20732
C	-2.98839	-2.97104	0.56144
C	-3.21008	-1.61684	0.76560
C	-1.22420	1.19108	-0.55132
C	-2.35050	0.75730	0.19355
C	-1.93050	3.46661	-0.22477
C	-1.03604	2.55637	-0.76609
C	-3.23012	1.68034	0.75115
C	-3.01967	3.03558	0.54071
Ni	1.16473	-0.16188	0.26961
C	3.12713	-0.61850	0.13917
C	2.47487	-0.58293	-1.12682
H	2.28865	-1.52459	-1.65055
H	3.35478	-1.62475	0.50671
H	2.15793	-0.28832	1.35750
H	0.43341	0.24100	1.53401
H	-0.03885	0.03978	-1.99419
H	-0.15695	-2.82116	-1.33745
H	-1.74127	-4.46042	-0.36732
H	-3.66316	-3.70563	0.99398
H	-4.06463	-1.28443	1.35306

H	-4.08302	1.34352	1.33847
H	-3.70237	3.76631	0.96733
H	-0.17546	2.90354	-1.33714
H	-1.77993	4.53177	-0.38696
O	2.77945	0.48297	-2.00273
H	1.97725	1.00265	-2.10420
C	4.19226	0.39867	0.48734
H	5.05637	0.22997	-0.17326
H	3.82290	1.40022	0.24223
C	4.62803	0.33767	1.93937
H	5.42536	1.05750	2.15514
H	5.00223	-0.66104	2.19836
H	3.78656	0.55590	2.60662

Collision complex of **II** with butanol (d)

M06/6-311+G** Enthalpy = -2116.4539

C	-1.40283	0.42969	-1.60934
C	-0.72310	1.39682	0.42122
C	-0.54132	1.41419	-1.00912
C	0.37087	2.35131	-1.55510
C	1.09431	3.17168	-0.71423
C	0.94357	3.11308	0.68448
C	0.03397	2.22840	1.24238
C	-2.16914	-0.14171	-0.52618
C	-1.73798	0.42387	0.71314
C	-3.72588	-1.52138	0.68808
C	-3.18234	-1.10853	-0.51579
C	-2.27986	-0.02421	1.91841
C	-3.27156	-0.99179	1.90604
Co	0.38132	-0.55935	-1.48301
C	2.90030	0.07920	2.53018
C	2.11941	-0.63041	1.44061
C	2.86046	-1.83967	0.89421
C	2.12257	-2.60473	-0.17701
O	2.02265	-1.79847	-1.35761
H	1.64900	-2.33356	-2.09019
H	-1.73798	0.44042	-2.64307
H	0.50675	2.40579	-2.63320
H	1.80542	3.87588	-1.14164
H	1.53746	3.76429	1.32093
H	-0.09836	2.18777	2.32415
H	-4.50719	-2.27855	0.69430
H	-3.51874	-1.54797	-1.45293
H	-1.93005	0.39248	2.86243
H	-3.70401	-1.34130	2.84062

H	2.35726	0.95591	2.89744
H	3.87043	0.42755	2.15380
H	3.09608	-0.58400	3.38351
H	1.90027	0.07316	0.62510
H	1.13618	-0.94568	1.82015
H	3.83684	-1.52807	0.49454
H	3.07151	-2.54053	1.71811
H	2.66952	-3.52528	-0.43077
H	1.11424	-2.88293	0.16686

O-H insertion TS for the dehydrogenation of butanol by complex **II** (d)

M06/6-311+G** Enthalpy = -2116.440413

Imaginary Frequency = -1204.15

H	0.93053	3.71728	-0.91809
C	0.18599	3.00117	-0.57553
C	-1.73615	1.20086	0.33880
C	-0.14817	1.93604	-1.39147
C	-0.40518	3.17858	0.68626
C	-1.35808	2.27573	1.13800
C	-1.11674	0.99393	-0.95058
H	0.31391	1.82134	-2.36952
H	-0.10855	4.01833	1.30885
C	-2.70458	0.15252	0.51910
C	-4.42106	-2.02539	0.30496
C	-2.64460	-0.69528	-0.62982
C	-3.60444	-0.12025	1.54853
C	-4.46057	-1.20502	1.44193
C	-3.52558	-1.77890	-0.72159
H	-3.64011	0.52098	2.42804
H	-5.16816	-1.42093	2.23873
H	-3.49428	-2.43065	-1.59269
H	-5.10180	-2.87115	0.23364
C	-1.61450	-0.22688	-1.52220
H	-1.55712	-0.50156	-2.57047
H	-1.81831	2.41283	2.11585
C	2.96600	-0.37465	-0.02327
H	3.07242	-0.10033	-1.09130
H	2.81033	0.57694	0.51708
O	1.87237	-1.23215	0.16201
C	4.24506	-1.03283	0.45727
H	4.39166	-1.96903	-0.10138
H	4.11951	-1.32158	1.51097
C	5.46260	-0.13840	0.30353
H	5.56601	0.15634	-0.75110
H	5.29906	0.79624	0.85935
C	6.74264	-0.80207	0.77906

H	7.61632	-0.15082	0.66579
H	6.93773	-1.72282	0.21613
H	6.66866	-1.07998	1.83732
H	1.36845	-1.59374	-0.97569
Co	0.20885	-0.55687	-0.55835

O-H insertion of butanol by complex **II** (d)

M06/6-311+G** Enthalpy = -2116.488508

C	-2.52219	0.04762	-0.88550
C	-1.20057	0.74298	0.90277
C	-2.04593	1.19571	-0.16580
C	-2.22017	2.58123	-0.36472
C	-1.57769	3.46872	0.46592
C	-0.72777	3.01947	1.50068
C	-0.53373	1.67358	1.71593
C	-2.09884	-1.11534	-0.15691
C	-1.22971	-0.69299	0.90526
C	-1.72037	-3.40282	0.48244
C	-2.33051	-2.49300	-0.34884
C	-0.59520	-1.64691	1.71754
C	-0.84587	-2.98428	1.50938
Co	-0.51149	0.00272	-1.26146
O	1.31118	-0.07225	-1.47626
H	-0.73713	0.01016	-2.73211
C	2.08486	-0.21268	-0.34783
C	3.55808	0.00133	-0.66877
C	4.46412	-0.12589	0.54249
C	5.93179	0.07562	0.20789
H	-3.24521	0.06123	-1.69098
H	-2.84600	2.93488	-1.18077
H	-1.70641	4.53782	0.31403
H	-0.21854	3.74790	2.12642
H	0.12934	1.32735	2.50656
H	-1.89293	-4.46640	0.33532
H	-2.97408	-2.82426	-1.16051
H	0.09066	-1.32503	2.49905
H	-0.36057	-3.73052	2.13320
H	1.98028	-1.22094	0.11656
H	1.81186	0.50593	0.46132
H	3.67103	0.99682	-1.12380
H	3.85415	-0.72399	-1.44159
H	4.15462	0.60396	1.30522
H	4.32091	-1.11554	1.00177
H	6.57906	-0.01299	1.08832
H	6.09893	1.06719	-0.23054
H	6.26911	-0.66310	-0.52961

α -C elimination TS for the dehydrogenation of butanol by complex II (d)

M06/6-311+G** Enthalpy = -2116.472284

Imaginary Frequency = -416.44

C	-0.73829	-0.18578	1.08363
C	-2.36680	0.83148	-0.27807
C	-1.25346	1.07644	0.57423
C	-0.79995	2.39078	0.74502
C	-1.44074	3.42322	0.07752
C	-2.52608	3.17460	-0.77119
C	-2.98758	1.87849	-0.95163
C	-1.67676	-1.18879	0.61082
C	-2.63929	-0.58657	-0.24260
C	-2.74952	-3.31120	0.25123
C	-1.75611	-2.56052	0.85908
C	-3.62053	-1.35462	-0.86295
C	-3.67649	-2.71803	-0.61485
C	3.98947	-0.29529	0.31501
C	2.82101	0.66871	0.39221
H	-0.32053	-0.24814	2.08905
H	0.05509	2.58176	1.39012
H	-1.09048	4.44492	0.20890
H	-3.00565	4.00099	-1.29018
H	-3.83360	1.68270	-1.60905
H	-4.34424	-0.88626	-1.52861
H	-4.44120	-3.32879	-1.08843
H	-2.80826	-4.38080	0.44256
H	-1.02882	-3.03596	1.51448
H	3.05914	1.66287	-0.03884
H	4.69479	-0.01967	1.11734
H	3.62496	-1.30305	0.56222
O	2.08148	0.64718	1.46731
C	4.71387	-0.30464	-1.01724
H	4.01757	-0.63084	-1.80098
H	5.00529	0.72320	-1.28038
C	5.94061	-1.19921	-1.00577
H	6.45112	-1.21342	-1.97504
H	5.66688	-2.23228	-0.75985
H	6.66540	-0.86771	-0.25189
H	2.03059	0.12554	-1.09048
H	0.39972	-0.68604	-1.20826
Co	1.00556	-0.00003	-0.00473

β -hydride elimination of butanol by complex **II** (d)

M06/6-311+G** Enthalpy = -2116.482982

C	-1.21899	-0.27342	1.57008
C	-1.99897	0.82314	-0.35104
C	-2.29004	-0.18885	0.60815
C	-3.48798	-0.90451	0.49137
C	-4.35049	-0.63035	-0.55482
C	-4.04587	0.34994	-1.51071
C	-2.86808	1.07222	-1.40931
C	-0.30903	0.79499	1.23157
C	-0.74820	1.43051	0.02239
C	1.64304	2.21704	1.20795
C	0.89490	1.22170	1.82187
C	0.02161	2.41807	-0.57475
C	1.22022	2.80871	0.01345
Co	0.43660	-1.38459	0.74662
H	1.56887	-1.92361	1.73624
H	0.89543	-1.75951	2.25087
O	0.14672	-1.62107	-1.09196
C	1.43057	-1.79128	-0.87437
C	2.39840	-0.72439	-1.33648
C	3.72558	-0.74195	-0.59970
C	4.67908	0.33011	-1.09661
H	-1.38142	-0.62089	2.58727
H	-3.73146	-1.68057	1.21484
H	-5.27993	-1.18948	-0.64427
H	-4.73463	0.53773	-2.33060
H	-2.62570	1.83563	-2.14713
H	2.57818	2.53951	1.66177
H	1.23275	0.77919	2.75709
H	-0.30839	2.87985	-1.50413
H	1.83135	3.57733	-0.45349
H	1.83347	-2.82254	-0.95463
H	1.91665	0.25780	-1.21345
H	2.58603	-0.84146	-2.42061
H	4.18972	-1.73627	-0.69484
H	3.52962	-0.59946	0.47236
H	4.90177	0.19966	-2.16343
H	5.63206	0.32567	-0.55439
H	4.22918	1.32371	-0.97674

Butanal adduct of complex **II** (d)

M06/6-311+G** Enthalpy = -2115.310158

C	0.36750	0.66617	-1.72816
C	0.21795	1.67668	0.38606
C	-0.45957	1.47677	-0.85768

C	-1.72260	2.06869	-1.04454
C	-2.30694	2.77075	-0.01023
C	-1.66267	2.91042	1.23228
C	-0.40392	2.36829	1.42560
C	1.59524	0.43065	-0.99545
C	1.49458	1.02334	0.29874
C	3.79004	-0.37134	-0.41879
C	2.76863	-0.25157	-1.34316
C	2.52566	0.86857	1.22631
C	3.66918	0.17509	0.86871
Co	-0.73031	-0.93948	-1.20674
C	-2.15032	-1.70671	-0.07394
C	-2.03232	-1.61846	1.43183
C	-0.63765	-1.48215	2.03501
C	0.28991	-2.66252	1.79794
O	-1.48425	-2.59143	-0.77504
H	0.32056	0.71563	-2.81682
H	-2.24598	1.93623	-1.98945
H	-3.29174	3.21105	-0.15107
H	-2.15481	3.45014	2.03726
H	0.09986	2.48088	2.38484
H	4.69573	-0.91141	-0.68578
H	2.85948	-0.70604	-2.32792
H	2.43136	1.29334	2.22477
H	4.47772	0.05063	1.58465
H	-3.15547	-1.41681	-0.44094
H	-2.63503	-0.75311	1.74634
H	-2.52309	-2.51159	1.86619
H	-0.75197	-1.32232	3.11848
H	-0.17269	-0.56897	1.64250
H	-0.15633	-3.59702	2.16524
H	1.24795	-2.51379	2.31010
H	0.49059	-2.79541	0.73078

α -C insertion TS for the dehydrogenation of butanol by complex **II** (d)

M06/6-311+G** Enthalpy = -2116.446042

Imaginary Frequency = -667.57

H	1.80256	3.24883	-0.80397
C	0.92217	2.68556	-0.50052
C	-1.33858	1.26782	0.32505
C	0.36815	1.76690	-1.38471
C	0.38754	2.88733	0.77772
C	-0.73829	2.17686	1.18795
C	-0.78873	1.03573	-0.99389
H	0.77508	1.65460	-2.38699
H	0.85784	3.59791	1.45242

C	-2.46752	0.38983	0.47117
C	-4.51844	-1.46565	0.19809
C	-2.56361	-0.39677	-0.72012
C	-3.37956	0.21351	1.51011
C	-4.40295	-0.71112	1.37644
C	-3.61571	-1.31585	-0.83908
H	-3.29297	0.80672	2.41942
H	-5.12198	-0.85067	2.17986
H	-3.71080	-1.91759	-1.74115
H	-5.33101	-2.18322	0.10284
C	-1.49250	-0.05119	-1.61203
H	-1.48293	-0.29478	-2.66917
H	-1.14329	2.32808	2.18768
H	1.64910	-0.23361	0.88661
C	1.99550	-1.10843	0.26392
C	3.38981	-0.80900	-0.23147
H	3.75142	-1.66283	-0.82484
H	3.32590	0.04784	-0.91866
C	4.38367	-0.50187	0.88002
H	4.01438	0.36012	1.45466
H	4.41317	-1.34641	1.57939
O	2.05524	-2.25880	1.10930
H	1.15554	-2.59235	1.16969
C	5.77410	-0.21163	0.34341
H	6.48829	0.01889	1.14188
H	5.75861	0.64188	-0.34594
H	6.16594	-1.07116	-0.21466
H	1.33797	-1.75030	-0.89763
Co	0.39463	-0.58681	-0.70216

O-H elimination TS for the dehydrogenation of butanol by complex **II** (d)

M06/6-311+G** Enthalpy = -2116.441915

Imaginary Frequency = -1572.76

C	0.34230	-0.06351	1.30040
C	1.93322	-1.14127	-0.03435
C	0.77102	-1.33731	0.77792
C	0.23681	-2.62803	0.91383
C	0.83628	-3.68507	0.25788
C	1.96617	-3.48605	-0.55413
C	2.50933	-2.22329	-0.70421
C	1.32127	0.90282	0.87735
C	2.27641	0.25375	0.02089
C	2.52842	2.96825	0.59253
C	1.48073	2.27889	1.15826
C	3.31978	0.98794	-0.55304
C	3.44847	2.33224	-0.26707

H	-1.40175	0.94405	-1.91865
H	-0.75424	0.21262	-2.19851
H	-0.36387	0.06745	2.11438
H	-0.65008	-2.78503	1.52467
H	0.42265	-4.68578	0.35894
H	2.41192	-4.33323	-1.06925
H	3.38211	-2.07244	-1.33681
H	4.03051	0.49662	-1.21544
H	4.25700	2.90882	-0.70845
H	0.76300	2.78380	1.80162
H	2.64463	4.02948	0.80068
O	-2.09015	1.77721	-1.21814
C	-2.08944	1.04242	-0.07932
H	-2.04459	1.66604	0.83790
C	-3.13255	-0.04672	0.03592
H	-2.91314	-0.66850	0.91992
H	-3.06220	-0.70687	-0.84166
C	-4.54963	0.50883	0.13599
H	-4.72666	1.15545	-0.73345
H	-4.61768	1.16172	1.01921
C	-5.60405	-0.58077	0.21243
H	-5.56476	-1.22311	-0.67586
H	-6.62045	-0.17585	0.28536
H	-5.43974	-1.22702	1.08420
Co	-0.31847	0.43464	-0.55005

Piperidine (s)

M06/6-311+G** Enthalpy = -251.61086

C	1.43920	0.10003	0.23553
C	0.79574	-1.19954	-0.22984
C	-0.65864	-1.25477	0.20536
N	-1.36700	-0.09504	-0.31078
C	-0.82603	1.15158	0.20532
C	0.62198	1.29809	-0.22981
H	2.47286	0.17186	-0.12169
H	1.48719	0.10331	1.33564
H	1.33848	-2.06583	0.16608
H	0.83607	-1.25931	-1.32598
H	-1.14090	-2.16215	-0.17429
H	-0.69475	-1.30317	1.31417
H	-2.35940	-0.16401	-0.11771
H	-1.42905	1.98360	-0.17441
H	-0.86851	1.19463	1.31413
H	0.65380	1.36285	-1.32594
H	1.03974	2.23108	0.16617

2,3,4,5-tetrahydropyridine adduct of complex I (s)

M06/6-311+G** Enthalpy = -2259.056693

C	-0.83812	0.93583	-1.64869
C	-1.57370	0.85788	0.58188
C	-1.86031	0.43912	-0.75979
C	-3.01804	-0.32335	-1.00005
C	-3.82466	-0.69392	0.05675
C	-3.51074	-0.32392	1.37734
C	-2.39201	0.44902	1.63584
C	0.07488	1.68034	-0.82005
C	-0.37044	1.63494	0.54674
C	1.94699	3.02755	-0.11294
C	1.23168	2.42757	-1.12764
C	0.38398	2.23312	1.55468
C	1.54228	2.92133	1.23205
Ni	0.31486	-0.63195	-1.24743
C	2.37400	-1.67618	1.66110
C	0.86880	-1.87773	1.70383
C	0.44525	-2.74129	0.52407
N	0.95242	-2.33510	-0.78214
C	1.99621	-1.47224	-0.82846
C	2.76999	-0.96066	0.37515
H	-0.96501	1.07601	-2.71902
H	-3.25433	-0.64061	-2.01389
H	-4.71134	-1.29622	-0.13003
H	-4.15303	-0.64469	2.19371
H	-2.15077	0.73906	2.65790
H	2.85107	3.58413	-0.35199
H	1.57325	2.49183	-2.15900
H	0.06305	2.15856	2.59335
H	2.13615	3.38984	2.01265
H	2.72903	-1.11576	2.53553
H	2.86020	-2.66507	1.69752
H	0.55893	-2.35813	2.64246
H	0.36056	-0.90417	1.65343
H	-0.65133	-2.78277	0.45811
H	0.78412	-3.77901	0.70969
H	2.56026	-1.47906	-1.77058
H	3.84892	-1.07934	0.19537
H	2.60087	0.12111	0.48694

3,4-dihydropyridine adduct of complex I (s)

M06/6-311+G** Enthalpy = -2257.865654

C	0.83479	-0.45318	-1.69935
C	0.90641	-1.49296	0.40612
C	0.28181	-1.51267	-0.88676

C	-0.69057	-2.49872	-1.15300
C	-1.06557	-3.37653	-0.15644
C	-0.49106	-3.31166	1.12647
C	0.49453	-2.37764	1.40142
C	1.85308	0.17087	-0.89295
C	1.88719	-0.44638	0.39737
C	3.63631	1.63067	-0.19293
C	2.75974	1.20591	-1.17176
C	2.76471	0.01556	1.37933
C	3.63707	1.04927	1.08691
Ni	-0.83523	0.47717	-1.07732
C	-2.45250	0.21115	1.28463
C	-2.53853	0.46919	-0.19525
C	-2.24177	1.77385	-0.66475
N	-1.93513	2.83690	0.22608
C	-1.58087	2.53653	1.41251
C	-1.40835	1.13361	1.90921
H	0.83497	-0.45337	-2.78715
H	-1.16242	-2.53869	-2.13286
H	-1.83004	-4.12343	-0.35968
H	-0.81692	-4.00462	1.89812
H	0.94790	-2.33643	2.39114
H	4.33211	2.43849	-0.40997
H	2.75382	1.68193	-2.15037
H	2.76936	-0.44266	2.36759
H	4.32733	1.41276	1.84398
H	-3.43674	0.39500	1.75476
H	-2.19567	-0.83811	1.48519
H	-3.24789	-0.14516	-0.75679
H	-2.66543	2.12183	-1.60849
H	-1.35678	3.36244	2.09711
H	-1.43453	1.10092	3.00558
H	-0.40510	0.78878	1.59955

2,3-dihydropyridine adduct of complex I (s)

M06/6-311+G** Enthalpy = -2257.874823

C	0.65498	-0.48703	-1.21585
C	1.69685	1.28284	-0.07021
C	0.57946	0.91378	-0.91457
C	-0.46664	1.85298	-1.11551
C	-0.34207	3.12690	-0.54911
C	0.75904	3.47947	0.22381
C	1.77538	2.55177	0.47120
C	1.89252	-0.95102	-0.64770
C	2.52838	0.11382	0.05965
C	3.72309	-2.39075	-0.03499

C	2.51991	-2.20218	-0.69269
C	3.73339	-0.09806	0.72411
C	4.33189	-1.34789	0.67804
Ni	-0.85827	0.03929	0.15364
C	-1.81337	-1.36830	1.03412
C	-2.65159	-2.25313	0.14799
C	-3.45820	-1.41219	-0.83464
N	-4.22960	-0.33409	-0.23158
C	-3.65546	0.25442	0.75378
C	-2.38330	-0.09531	1.36425
H	0.14317	-0.98934	-2.03218
H	-1.28722	1.64167	-1.79919
H	-1.12760	3.85848	-0.72485
H	0.81754	4.47483	0.65626
H	2.61746	2.82435	1.10597
H	4.20533	-3.36559	-0.06765
H	2.05496	-3.02416	-1.23368
H	4.20686	0.71613	1.27084
H	5.27483	-1.52161	1.19011
H	-1.20530	-1.87886	1.78422
H	-2.02654	-2.96453	-0.40910
H	-3.34670	-2.85493	0.76285
H	-4.13975	-2.04388	-1.42028
H	-2.75102	-0.95614	-1.55272
H	-4.19590	1.10637	1.18818
H	-2.14698	0.39497	2.31013

Pyridine adduct of complex **I** (s)

M06/6-311+G** Enthalpy = -2256.695172

C	-0.69150	-0.22817	-1.45852
C	-1.58378	1.29386	0.09625
C	-0.58886	1.11222	-0.92483
C	0.27361	2.18585	-1.23083
C	0.18494	3.35952	-0.50950
C	-0.75730	3.51120	0.52341
C	-1.63865	2.48408	0.81986
C	-1.81644	-0.83084	-0.79131
C	-2.35295	0.08450	0.16921
C	-3.51262	-2.42084	-0.15970
C	-2.43050	-2.08326	-0.94924
C	-3.43333	-0.28596	0.97037
C	-4.01274	-1.53278	0.80833
Ni	0.79490	-0.44245	-0.11389
C	1.94497	-1.40008	1.12357
C	2.90548	-2.13670	0.36793
C	3.95036	-1.49066	-0.23357

N	4.14557	-0.14336	-0.18075
C	3.26701	0.55290	0.50194
C	2.15195	0.01604	1.20480
H	-0.33795	-0.52616	-2.44230
H	1.02662	2.06784	-2.00745
H	0.86521	4.17829	-0.73388
H	-0.79519	4.44119	1.08507
H	-2.37509	2.60772	1.61283
H	-3.98412	-3.39377	-0.28306
H	-2.04258	-2.78739	-1.68300
H	-3.82624	0.40783	1.71239
H	-4.85925	-1.82657	1.42390
H	1.30879	-1.92573	1.83540
H	2.81866	-3.21760	0.28447
H	4.68783	-2.05268	-0.80548
H	3.42514	1.63405	0.53777
H	1.65410	0.63970	1.94849

Pyridine (s)

M06/6-311+G** Enthalpy = -248.060176

C	0.00001	1.37613	-0.00001
C	1.19220	0.66873	0.00001
C	1.13552	-0.71869	-0.00000
N	-0.00001	-1.41003	-0.00000
C	-1.13553	-0.71867	-0.00001
C	-1.19219	0.66875	0.00002
H	0.00002	2.46210	-0.00005
H	2.15026	1.17811	0.00001
H	2.05471	-1.30281	0.00003
H	-2.05472	-1.30279	0.00001
H	-2.15025	1.17813	0.00003

Fluorenyl anion (s)

M06/6-311+G** Enthalpy = -500.386466

C	-0.00000	1.76290	0.00000
C	0.71565	-0.44908	-0.00000
C	1.13845	0.93036	0.00000
C	2.52338	1.20321	0.00000
C	3.43320	0.16517	0.00000
C	3.01171	-1.17981	0.00000
C	1.65728	-1.47647	-0.00000
C	-1.13844	0.93038	-0.00000
C	-0.71564	-0.44910	0.00000
C	-3.43319	0.16517	0.00000
C	-2.52338	1.20321	-0.00000
C	-1.65728	-1.47648	0.00000

C	-3.01171	-1.17981	0.00000
H	0.00000	2.84808	-0.00000
H	2.87303	2.23532	0.00000
H	4.49982	0.38676	0.00000
H	3.74973	-1.97913	0.00000
H	1.32819	-2.51597	-0.00000
H	-4.49981	0.38676	0.00000
H	-2.87306	2.23533	-0.00000
H	-1.32820	-2.51599	0.00000
H	-3.74973	-1.97913	-0.00000

2,3,4,5-tetrahydropyridine complex with nickel (s)

M06/6-311+G** Enthalpy = -1758.58921

C	1.09640	1.45313	-0.01625
C	2.21477	0.43759	-0.20829
C	1.63351	-0.90149	-0.62865
C	0.71578	-1.41048	0.46946
N	-0.28485	-0.45847	0.94538
C	-0.10963	0.85446	0.67758
Ni	-1.55660	0.00821	-0.29288
H	1.45397	2.31693	0.55847
H	0.78507	1.85286	-0.99215
H	2.94704	0.80638	-0.93440
H	2.75417	0.30289	0.74072
H	1.06383	-0.78375	-1.56307
H	2.42493	-1.63537	-0.82188
H	0.18824	-2.32093	0.15979
H	1.32275	-1.69903	1.34351
H	-0.66608	1.54030	1.32870

Fluorene (s)

M06/6-311+G** Enthalpy = -500.941638

C	-0.00000	1.81796	0.00012
C	-0.73049	-0.44807	0.00010
C	-1.17548	0.88102	0.00006
C	-2.52910	1.16749	-0.00005
C	-3.44040	0.11600	-0.00011
C	-2.99867	-1.20431	-0.00006
C	-1.64134	-1.49708	0.00003
C	1.17548	0.88102	0.00001
C	0.73049	-0.44807	0.00007
C	3.44040	0.11600	-0.00011
C	2.52910	1.16750	-0.00008
C	1.64134	-1.49708	0.00007
C	2.99867	-1.20430	-0.00003
H	-0.00003	2.47477	-0.87962

H	0.00003	2.47438	0.88016
H	-2.87853	2.19687	-0.00007
H	-4.50573	0.32545	-0.00021
H	-3.72437	-2.01198	-0.00011
H	-1.30135	-2.52922	0.00008
H	4.50573	0.32546	-0.00021
H	2.87853	2.19687	-0.00015
H	1.30135	-2.52922	0.00013
H	3.72437	-2.01198	-0.00003

Ni complex with imine ring (s)

M06/6-311+G** Enthalpy = -1756.833025

C	-0.54936	1.13839	0.77632
N	-1.56414	1.31844	0.00998
C	-1.84240	0.17980	-0.86368
C	-1.68909	-1.14352	-0.18127
C	-0.64715	-1.27964	0.65126
C	0.19201	-0.11282	0.94544
Ni	1.58611	-0.00336	-0.32411
H	-0.25046	1.98591	1.40503
H	-2.83959	0.30115	-1.30725
H	-1.10381	0.23353	-1.69841
H	-2.37581	-1.95856	-0.40046
H	-0.44152	-2.22326	1.15438
H	0.76493	-0.16703	1.88368

Hydrogen abstraction product from CID of butan-1-imine adduct of complex I (d)

M06/6-311+G** Enthalpy = -1719.945394

C	-2.29525	0.42714	-0.56610
C	-1.48922	0.66046	0.70428
C	0.01448	0.42961	0.57675
C	0.72401	1.34877	-0.31016
N	1.91323	1.83337	-0.21638
Ni	0.46228	-1.29799	-0.06356
H	-2.16169	-0.60676	-0.90536
H	-3.36585	0.61778	-0.40477
H	-1.96561	1.07880	-1.38373
H	-1.86990	-0.01227	1.48469
H	-1.69485	1.68754	1.06667
H	0.49139	0.42364	1.57467
H	0.15798	1.68350	-1.19440
H	2.34797	1.44210	0.62792

Dehydrogenation product of hydrogen abstraction product from CID of butan-1-imine adduct of complex I (d)

M06/6-311+G** Enthalpy = -1718.755244

C	1.09171	1.23074	0.40754
C	-0.20119	0.61765	0.45131
C	-1.21442	0.70556	-0.50411
C	-2.48001	0.06501	-0.40715
N	-2.97233	-0.76123	0.46942
Ni	1.48836	-0.52037	-0.13844
H	1.28323	1.96631	-0.38123
H	1.59051	1.44977	1.35565
H	-0.47739	0.14530	1.39987
H	-1.01460	1.27113	-1.41502
H	-3.16967	0.31846	-1.22867
H	-2.25634	-0.96577	1.17411

Butan-1-imine adduct of complex **II** (d)

M06/6-311+G** Enthalpy = -2095.416763

C	-0.83382	0.26086	-1.66244
C	-1.75182	0.74671	0.44446
C	-1.88083	-0.07351	-0.71845
C	-2.91818	-1.01831	-0.76970
C	-3.76362	-1.16657	0.31307
C	-3.60132	-0.39098	1.47321
C	-2.59852	0.56163	1.53704
C	-0.11622	1.36888	-1.06862
C	-0.65391	1.64677	0.22493
C	1.47565	3.14667	-0.74365
C	0.94700	2.15227	-1.54363
C	-0.08868	2.63870	1.02686
C	0.97174	3.38693	0.54572
Co	0.37127	-1.22006	-0.98782
C	0.88785	-1.98556	0.72027
C	1.65094	-1.06902	1.64727
C	2.81251	-0.28643	1.04487
C	4.04903	-1.13424	0.79389
N	1.49768	-2.61957	-0.33726
H	-0.92633	0.11515	-2.73973
H	-3.03044	-1.64860	-1.64994
H	-4.55941	-1.90749	0.27485
H	-4.26715	-0.54082	2.31937
H	-2.47527	1.16790	2.43341
H	2.30694	3.74514	-1.11013
H	1.36736	1.95310	-2.52781
H	-0.48472	2.82753	2.02379
H	1.41798	4.16229	1.16324
H	0.03017	-2.46477	1.22261
H	0.92134	-0.36343	2.07341
H	2.03368	-1.65625	2.50609

H	3.06414	0.54416	1.72031
H	2.47884	0.18037	0.10681
H	4.40088	-1.59391	1.72815
H	4.87392	-0.53556	0.38832
H	3.81513	-1.93877	0.09076
H	0.99821	-3.47614	-0.58222

1st dehydrogenation of the butan-1-imine adduct with complex **II** (s)

M06/6-311+G** Enthalpy = -2094.242395

C	-0.72981	0.08274	-1.63394
C	-1.63850	0.88117	0.37951
C	-1.81581	-0.05456	-0.68271
C	-2.93209	-0.90259	-0.65975
C	-3.81739	-0.84057	0.40009
C	-3.61480	0.05230	1.46421
C	-2.52756	0.90973	1.45358
C	0.06180	1.19894	-1.15774
C	-0.47023	1.66493	0.08194
C	1.75234	2.91017	-1.02443
C	1.17630	1.85362	-1.70403
C	0.14113	2.71614	0.76529
C	1.24829	3.33904	0.21458
Co	0.45345	-1.44253	-1.02378
C	1.43609	-2.27021	0.30898
C	1.89905	-2.07298	1.70913
C	1.92158	-0.60569	2.11933
C	2.95168	0.19270	1.34214
N	1.47435	-3.03564	-0.64735
H	-0.84820	-0.14193	-2.69733
H	-3.08179	-1.62064	-1.46380
H	-4.67890	-1.50462	0.41909
H	-4.31661	0.07057	2.29428
H	-2.37446	1.61088	2.27286
H	2.62010	3.41089	-1.44852
H	1.59371	1.51021	-2.64886
H	-0.25785	3.05291	1.72129
H	1.72893	4.16260	0.73684
H	1.21413	-2.63667	2.35702
H	2.89675	-2.52487	1.83036
H	2.12072	-0.53526	3.19793
H	0.92333	-0.17872	1.94809
H	3.96496	-0.19353	1.51760
H	2.93122	1.25337	1.61368
H	2.74809	0.13331	0.26590

2nd dehydrogenation of the butan-1-imine adduct with complex **II** (d)

M06/6-311+G** Enthalpy = -2093.063894

C	0.50102	-0.76249	-1.84788
C	1.20497	-0.95742	0.37263
C	1.60952	-0.58044	-0.96227
C	2.91741	-0.06430	-1.15217
C	3.76709	0.04636	-0.07892
C	3.35890	-0.31044	1.22708
C	2.08961	-0.78911	1.45474
C	-0.55828	-1.34998	-1.08428
C	-0.14496	-1.45845	0.29086
C	-2.71913	-2.20728	-0.45446
C	-1.86733	-1.75414	-1.43297
C	-1.05039	-1.89463	1.26957
C	-2.32227	-2.27078	0.89907
Co	0.01098	0.69660	-0.39016
C	-1.47303	2.96487	-1.59549
C	-1.47709	1.93593	-0.49709
C	-0.69454	2.18459	0.70109
C	-1.11894	1.76151	1.98427
N	-1.45507	1.41539	3.04228
H	0.50871	-0.62419	-2.92203
H	3.24102	0.23098	-2.14824
H	4.77076	0.43783	-0.22997
H	4.04696	-0.17752	2.05747
H	1.76215	-1.04002	2.46167
H	-3.72945	-2.50869	-0.72297
H	-2.19676	-1.68501	-2.46755
H	-0.75176	-1.91340	2.31513
H	-3.03311	-2.59823	1.65219
H	-0.47467	3.40773	-1.71020
H	-2.17717	3.79389	-1.40980
H	-1.73870	2.51726	-2.56088
H	-2.43195	1.41826	-0.35769
H	-0.04235	3.06223	0.71863

Nitrile complex with **II** (d)

M06/6-311+G** Enthalpy = -1975.853287

C	0.00004	1.36285	1.27476
C	0.72634	0.45731	-0.73055
C	1.16379	1.09580	0.48289
C	2.54433	1.22936	0.73664
C	3.44906	0.79277	-0.20792
C	3.01761	0.17273	-1.39804
C	1.67810	-0.01709	-1.65458
C	-1.16376	1.09561	0.48300
C	-0.72628	0.45709	-0.73042

C	-3.44902	0.79286	-0.20793
C	-2.54432	1.22927	0.73669
C	-1.67807	-0.01701	-1.65465
C	-3.01752	0.17291	-1.39815
Co	-0.00004	-0.65375	0.88590
C	-0.00009	-2.51618	0.49316
N	-0.00005	-3.67663	0.35781
H	0.00008	1.81448	2.26110
H	2.88361	1.68283	1.66566
H	4.51481	0.90314	-0.02314
H	3.75803	-0.18724	-2.10771
H	1.35124	-0.53729	-2.55182
H	-4.51477	0.90328	-0.02324
H	-2.88358	1.68277	1.66571
H	-1.35121	-0.53713	-2.55195
H	-3.75797	-0.18686	-2.10790

Methane (s)

M06/6-311+G** Enthalpy = -40.440289

C	0.00000	-0.00000	-0.00000
H	-0.39491	0.32237	0.96433
H	0.93448	-0.54160	0.15245
H	0.18390	0.87288	-0.62774
H	-0.72348	-0.65363	-0.48903

Methyl radical (d)

M06/6-311+G** Enthalpy = -39.777625

C	0.00000	0.00000	0.00000
H	-0.24999	-1.05138	-0.00000
H	-0.78555	0.74217	-0.00000
H	1.03552	0.30920	-0.00000

Ethyl radical (d)

M06/6-311+G** Enthalpy = -79.042613

C	0.68839	0.00008	-0.00108
C	-0.78886	-0.00000	-0.02275
H	1.10521	-0.88353	-0.49603
H	1.08950	-0.00525	1.02625
H	1.10503	0.88856	-0.48720
H	-1.34867	0.92571	0.04999
H	-1.34829	-0.92597	0.04992

Propane (s)

M06/6-311+G** Enthalpy = -118.95915

C	1.25959	-0.25900	0.00000
---	---------	----------	---------

C	-0.00000	0.58948	-0.00000
C	-1.25959	-0.25900	-0.00000
H	2.16782	0.35110	-0.00036
H	1.29404	-0.90838	-0.88256
H	1.29440	-0.90786	0.88292
H	-0.00000	1.25074	-0.87614
H	-0.00002	1.25069	0.87618
H	-1.29413	-0.90825	0.88264
H	-1.29429	-0.90800	-0.88283
H	-2.16782	0.35108	0.00018

Carbon monoxide complex with **I** (s)

M06/6-311+G** Enthalpy = -2121.942283

C	-0.00029	-0.15462	-1.72865
C	0.71737	-1.05494	0.30650
C	1.14919	-0.51831	-0.96151
C	2.53796	-0.43355	-1.22250
C	3.43634	-0.87496	-0.28092
C	3.00717	-1.39420	0.96098
C	1.66296	-1.47104	1.25538
C	-1.14992	-0.51772	-0.96145
C	-0.71833	-1.05459	0.30651
C	-3.43723	-0.87284	-0.28066
C	-2.53864	-0.43207	-1.22235
C	-1.66410	-1.46998	1.25551
C	-3.00829	-1.39227	0.96123
Ni	0.00044	1.14142	-0.07241
C	0.00142	2.70543	0.60079
O	0.00228	3.78222	1.04220
H	-0.00023	0.20295	-2.75052
H	2.88387	-0.01871	-2.16693
H	4.50275	-0.80937	-0.48641
H	3.74480	-1.71856	1.69040
H	1.33001	-1.86042	2.21599
H	-4.50361	-0.80654	-0.48607
H	-2.88437	-0.01706	-2.16677
H	-1.33132	-1.85951	2.21612
H	-3.74606	-1.71608	1.69075

Carbon monoxide complex with **II** (d)

M06/6-311+G** Enthalpy = -1996.372711

C	0.00002	-0.07540	1.76426
C	-0.72030	-1.04930	-0.22787
C	-1.14761	-0.45793	1.01895

C	-2.53553	-0.33289	1.26505
C	-3.43777	-0.81385	0.34486
C	-3.01536	-1.39639	-0.86931
C	-1.67242	-1.49329	-1.16377
C	1.14762	-0.45796	1.01894
C	0.72031	-1.04933	-0.22787
C	3.43777	-0.81397	0.34486
C	2.53555	-0.33299	1.26505
C	1.67240	-1.49339	-1.16376
C	3.01534	-1.39651	-0.86931
Co	-0.00014	1.02715	-0.25258
C	0.00012	2.71992	-0.55969
O	0.00036	3.87915	-0.70416
H	0.00003	0.40380	2.73501
H	-2.87894	0.13200	2.18669
H	-4.50337	-0.72323	0.54451
H	-3.75649	-1.74092	-1.58562
H	-1.34148	-1.92268	-2.10771
H	4.50338	-0.72340	0.54452
H	2.87898	0.13188	2.18669
H	1.34145	-1.92279	-2.10768
H	3.75646	-1.74109	-1.58560

Acetone adduct of complex I (s)

M06/6-311+G** Enthalpy = -2201.626384

C	-0.00052	0.21999	-1.60114
C	0.71844	1.58315	0.17403
C	1.15310	0.78910	-0.92721
C	2.52719	0.66965	-1.17390
C	3.43221	1.28597	-0.32875
C	2.99994	2.03332	0.77734
C	1.64481	2.18235	1.02583
C	-1.15554	0.78633	-0.92734
C	-0.72294	1.58143	0.17392
C	-3.43594	1.27746	-0.32917
C	-2.52926	0.66340	-1.17419
C	-1.65091	2.17827	1.02564
C	-3.00564	2.02589	0.77695
Ni	0.00323	-1.58225	-0.80694
O	0.00558	-3.22287	0.13039
C	0.00269	-2.22465	0.96628
C	1.27161	-1.87405	1.70965
C	-1.26935	-1.87867	1.70658
H	-0.00036	0.02978	-2.67872
H	2.87519	0.06715	-2.01104
H	4.49875	1.18112	-0.51655

H	3.73086	2.49687	1.43507
H	1.30579	2.76994	1.87800
H	-4.50220	1.16993	-0.51707
H	-2.87563	0.05998	-2.01136
H	-1.31349	2.76666	1.87789
H	-3.73778	2.48760	1.43462
H	2.14723	-2.13774	1.11002
H	1.31196	-0.80112	1.93565
H	1.32271	-2.42087	2.66680
H	-1.31467	-0.80569	1.93140
H	-1.32023	-2.42466	2.66422
H	-2.14252	-2.14667	1.10529

Acetone adduct of complex **II** (d)

M06/6-311+G** Enthalpy = -2076.065968

C	-0.00015	-1.40105	-1.56321
C	0.71932	-1.08738	0.63821
C	1.14965	-1.30686	-0.72389
C	2.54145	-1.34663	-0.99310
C	3.43915	-1.18418	0.03216
C	3.01083	-0.95562	1.36204
C	1.66934	-0.89626	1.65852
C	-1.14993	-1.30674	-0.72387
C	-0.71955	-1.08730	0.63823
C	-3.43940	-1.18373	0.03222
C	-2.54173	-1.34633	-0.99305
C	-1.66952	-0.89598	1.65854
C	-3.01103	-0.95517	1.36208
Co	0.00000	0.54770	-0.62985
C	0.00027	2.37785	-0.06222
O	0.00031	2.25119	-1.38749
H	-0.00017	-1.59368	-2.62871
H	2.88772	-1.50211	-2.01259
H	4.50552	-1.21224	-0.18126
H	3.74987	-0.80777	2.14499
H	1.33535	-0.70462	2.67705
H	-4.50577	-1.21164	-0.18119
H	-2.88803	-1.50177	-2.01254
H	-1.33549	-0.70434	2.67705
H	-3.75003	-0.80718	2.14503
C	1.26889	2.88314	0.58553
H	2.14622	2.43278	0.10814
H	1.29445	2.63370	1.65449
H	1.35473	3.98180	0.49631
C	-1.26821	2.88375	0.58532
H	-1.35379	3.98238	0.49541

H	-1.29375	2.63498	1.65443
H	-2.14568	2.43333	0.10826

Ethane adduct with complex I (s)

M06/6-311+G** Enthalpy = -2088.291295

C	-0.45306	-0.40336	-1.46510
C	-0.31365	1.34268	0.10873
C	0.36505	0.68621	-0.98036
C	1.60667	1.21272	-1.41121
C	2.17259	2.27554	-0.73446
C	1.53627	2.86009	0.37648
C	0.29552	2.39555	0.78755
C	-1.67238	-0.35180	-0.69485
C	-1.58355	0.69562	0.27683
C	-3.89145	-0.84963	0.10481
C	-2.85345	-1.10199	-0.77464
C	-2.63316	0.91969	1.16768
C	-3.78331	0.15106	1.08428
Ni	0.86896	-1.29337	-0.29706
C	2.29260	-2.14833	0.96984
C	3.39453	-1.25048	1.50666
H	-0.40159	-0.81461	-2.47157
H	2.11502	0.76333	-2.26202
H	3.13699	2.66246	-1.05915
H	2.01334	3.68483	0.90034
H	-0.20896	2.86350	1.63260
H	-4.80384	-1.43997	0.04413
H	-2.94141	-1.89330	-1.51732
H	-2.55411	1.70530	1.91837
H	-4.60785	0.32560	1.77165
H	2.38779	-3.18464	1.31240
H	1.27977	-1.80819	1.34228
H	2.34031	-2.21143	-0.16377
H	4.38441	-1.57808	1.16639
H	3.24633	-0.22025	1.16699
H	3.40741	-1.24170	2.60304

Dimethyl complex with II (d)

M06/6-311+G** Enthalpy = -1962.737458

C	-0.15337	0.33126	1.64573
C	-0.80706	-1.09840	-0.07620
C	-1.28160	-0.22092	0.95888
C	-2.66791	-0.00318	1.08813
C	-3.53976	-0.65248	0.24253
C	-3.07016	-1.51647	-0.76753

C	-1.71733	-1.72961	-0.93508
C	1.01616	-0.27618	1.10577
C	0.62637	-1.10916	-0.00567
C	3.31895	-0.83025	0.66693
C	2.39355	-0.15299	1.41630
C	1.60704	-1.78293	-0.76048
C	2.93060	-1.64539	-0.42789
Co	0.10252	1.09427	-0.32694
H	-0.19450	1.00631	2.49206
H	-3.03850	0.68256	1.84719
H	-4.60994	-0.48613	0.34301
H	-3.78279	-2.00655	-1.42617
H	-1.35497	-2.38178	-1.72748
H	4.37650	-0.72994	0.90038
H	2.70443	0.48494	2.24064
H	1.31075	-2.39953	-1.60709
H	3.69458	-2.15326	-1.01084
C	1.22144	1.66255	-1.83511
H	1.62691	2.67733	-1.72739
H	0.58390	1.65073	-2.73427
H	2.04963	0.95312	-1.98673
C	-0.55740	2.91266	-0.09049
H	-1.39263	2.93213	0.62812
H	-0.90673	3.33339	-1.04498
H	0.24809	3.56015	0.28590

Carbon monoxide

M06/6-311+G** Enthalpy = -113.277543			
C	0.00000	-0.00000	-0.64360
O	0.00000	0.00000	0.48270

C.3. Oxidative addition of polar reagents

DFT calculations were performed using the M06 functional with an effective core potential (ECP) basis set on Pd (lanl2dz) and a 6-311+G** basis set on the other atoms. Energies are reported from single-point calculations at the M06/QZVP level with thermal enthalpy corrections from the calculations with the mixed ECP/6-311+G** basis set for all reactions.

Complex **IV** (s)

M06 function with mixed lanl2dz/6-311+G** basis set Enthalpy = -628.626077031			
C	-0.00000	-0.49553	0.95691
C	0.72003	1.49168	-0.07737
C	1.15154	0.30233	0.58257
C	2.52142	0.11413	0.80972

C	3.42979	1.04929	0.34987
C	3.00351	2.19211	-0.34784
C	1.65109	2.41141	-0.55743
C	-1.15154	0.30234	0.58256
C	-0.72002	1.49169	-0.07737
C	-3.42978	1.04932	0.34987
C	-2.52142	0.11415	0.80972
C	-1.65106	2.41143	-0.55743
C	-3.00349	2.19214	-0.34784
Pd	-0.00001	-2.15928	-0.36597
H	-0.00001	-1.08294	1.88026
H	2.86126	-0.78415	1.32234
H	4.49361	0.89486	0.52008
H	3.73670	2.90660	-0.71458
H	1.31702	3.30809	-1.07847
H	-4.49359	0.89490	0.52008
H	-2.86126	-0.78412	1.32234
H	-1.31700	3.30810	-1.07847
H	-3.73667	2.90663	-0.71458

Fluorobenzene (s)

M06/6-311+G** Enthalpy = -331.422792819

C	0.00000	1.21043	0.26003
C	0.00000	0.00000	0.92554
C	-0.00000	-1.21043	0.26003
C	0.00000	-1.20158	-1.12793
C	0.00000	-0.00000	-1.82403
C	0.00000	1.20158	-1.12793
F	0.00000	0.00000	2.26554
H	0.00000	2.13330	0.83015
H	-0.00000	-2.13330	0.83015
H	0.00000	-2.14353	-1.66765
H	0.00000	-0.00000	-2.90916
H	0.00000	2.14353	-1.66765

Fluorobenzene adduct with complex **IV** (s)

M06 function with mixed lanl2dz/6-311+G** basis set Enthalpy = -958.440018

C	1.02475	-0.15012	-1.36561
C	2.28759	1.14541	0.13074
C	1.31398	1.19174	-0.91215
C	0.82356	2.43964	-1.32404
C	1.26218	3.59076	-0.69782
C	2.19184	3.53658	0.35407
C	2.70128	2.31595	0.76542
C	1.92878	-1.00799	-0.63386
C	2.67296	-0.22999	0.30443

C	3.11328	-2.96733	0.11687
C	2.18305	-2.38475	-0.72293
C	3.59024	-0.84015	1.15892
C	3.81124	-2.20483	1.06809
Pd	-0.92969	-0.56677	-0.41154
C	-2.40390	-0.56919	2.06544
C	-2.72549	0.76662	2.19920
C	-3.22305	1.48400	1.10187
C	-3.40629	0.86331	-0.11543
C	-3.09000	-0.50395	-0.24991
C	-2.60195	-1.25231	0.84265
F	-3.63954	-1.16175	-1.30877
H	0.73584	-0.36271	-2.39562
H	0.07871	2.49099	-2.11663
H	0.87414	4.55637	-1.01609
H	2.51192	4.45495	0.84020
H	3.43142	2.27220	1.57276
H	3.30337	-4.03667	0.04820
H	1.62826	-2.98981	-1.43813
H	4.14231	-0.24411	1.88468
H	4.52909	-2.68784	1.72656
H	-2.02325	-1.12651	2.91668
H	-2.56700	1.26945	3.14815
H	-3.44841	2.54159	1.20246
H	-3.81205	1.38629	-0.97554
H	-2.58706	-2.33723	0.79602

Insertion TS for oxidative addition of fluorobenzene by complex **IV** (s)

M06 function with mixed lanl2dz/6-311+G** basis set Enthalpy = -960.031194858

Imaginary frequency = -329.17

H	1.86462	2.48635	-1.89194
C	0.93998	2.16648	-1.41772
C	-1.41623	1.36818	-0.14235
C	0.30103	1.02473	-1.88191
C	0.43402	2.89525	-0.33640
C	-0.74151	2.49984	0.29380
C	-0.89329	0.58571	-1.24543
H	0.68212	0.49424	-2.75193
H	0.96951	3.77293	0.01538
C	-2.63433	0.73606	0.27948
C	-4.88365	-0.85282	0.64053
C	-2.82588	-0.42415	-0.53875
C	-3.55789	1.06577	1.26940
C	-4.68110	0.27632	1.45193
C	-3.97626	-1.20462	-0.34023
H	-3.39946	1.94519	1.89218

H	-5.40875	0.52846	2.21899
H	-4.14610	-2.08844	-0.95234
H	-5.77241	-1.46231	0.79155
C	-1.73751	-0.54844	-1.45385
H	-1.71588	-1.20271	-2.31785
H	-1.13064	3.07729	1.13112
C	3.30571	-0.94979	-0.38158
H	3.24623	-1.69638	-1.16828
C	4.39959	-0.11007	-0.25472
H	5.21741	-0.19268	-0.96769
C	4.46443	0.83234	0.77108
H	5.32758	1.48484	0.86340
C	3.41643	0.91665	1.68364
H	3.45669	1.64518	2.49059
C	2.30913	0.08772	1.58052
H	1.48655	0.14568	2.28761
C	2.23684	-0.79695	0.50466
F	1.61088	-2.38636	0.96357
Pd	0.39277	-0.97543	-0.28708

C-F insertion of fluorobenzene by complex **IV** (s)

M06 function with mixed lanl2dz/6-311+G** basis set Enthalpy = -960.074967684

C	-1.70489	-0.53852	-1.33753
C	-1.68955	1.41420	-0.04799
C	-1.07523	0.71678	-1.16125
C	0.13086	1.22817	-1.71453
C	0.60230	2.47370	-1.24837
C	-0.03439	3.15232	-0.23130
C	-1.18226	2.61381	0.38388
C	-2.78794	-0.59580	-0.38494
C	-2.78749	0.58673	0.40601
C	-4.70381	-1.36288	0.84522
C	-3.76474	-1.56571	-0.15457
C	-3.73139	0.77398	1.40635
C	-4.69336	-0.20321	1.62611
Pd	0.50692	-0.66453	-0.43817
F	0.77084	-2.61929	0.10584
C	2.38881	-0.32867	0.20971
C	3.36170	-1.31439	0.05619
C	4.65473	-1.10316	0.52282
C	4.98850	0.08368	1.16691
C	4.01472	1.05829	1.34334
C	2.72340	0.85425	0.86190
H	-1.60139	-1.18931	-2.19759
H	0.54232	0.80997	-2.63016
H	1.50013	2.89415	-1.69375

H	0.36461	4.10128	0.11650
H	-1.64750	3.13897	1.21606
H	-5.45914	-2.12291	1.03118
H	-3.77541	-2.47960	-0.74319
H	-3.71935	1.67870	2.01142
H	-5.43771	-0.07034	2.40643
H	3.08050	-2.26214	-0.39515
H	5.40693	-1.88003	0.39591
H	5.99851	0.24317	1.53746
H	4.25888	1.98620	1.85802
H	1.97304	1.63249	1.00243

Complex I (s)

M06/6-311+G** Enthalpy = -2008.96933413

C	-0.00000	0.97574	0.80445
C	-0.72273	-1.10703	-0.03491
C	-1.15689	0.13142	0.50938
C	-2.52458	0.34980	0.69500
C	-3.43278	-0.62352	0.31251
C	-3.00185	-1.82506	-0.26579
C	-1.64738	-2.06779	-0.43805
C	1.15688	0.13142	0.50933
C	0.72269	-1.10703	-0.03494
C	3.43275	-0.62360	0.31252
C	2.52457	0.34975	0.69498
C	1.64732	-2.06785	-0.43802
C	3.00180	-1.82514	-0.26577
Ni	0.00005	2.27549	-0.57527
H	0.00004	1.60663	1.70175
H	-2.86512	1.29354	1.11581
H	-4.49797	-0.44935	0.44984
H	-3.73269	-2.56954	-0.57259
H	-1.31040	-3.00802	-0.87232
H	4.49794	-0.44945	0.44987
H	2.86513	1.29349	1.11578
H	1.31031	-3.00808	-0.87225
H	3.73261	-2.56965	-0.57254

Fluorobenzene adduct with complex I (s)

M06/6-311+G** Enthalpy = -2340.45181297

C	0.71883	0.39116	-1.76292
C	1.98066	0.29763	0.21607
C	1.68499	-0.37778	-1.01277
C	2.33309	-1.59551	-1.28912
C	3.19737	-2.13746	-0.35870
C	3.44579	-1.49333	0.86641

C	2.84090	-0.27999	1.14810
C	0.46981	1.57877	-0.98062
C	1.22374	1.51665	0.23558
C	-0.42403	3.69936	-0.26670
C	-0.33650	2.70538	-1.22076
C	1.10406	2.52379	1.19206
C	0.28242	3.61068	0.94605
Ni	-0.74830	-0.61403	-0.85224
C	-2.48801	-0.86926	-0.09018
C	-1.70723	-2.05667	0.04018
C	-0.99494	-2.23859	1.26211
C	-1.06647	-1.31811	2.27907
C	-1.85520	-0.15481	2.13014
C	-2.56824	0.06266	0.97818
F	-3.52310	-0.84663	-0.99896
H	0.59399	0.33100	-2.84156
H	2.12600	-2.11726	-2.22177
H	3.68679	-3.08617	-0.56988
H	4.11853	-1.94956	1.58841
H	3.03714	0.22220	2.09457
H	-1.05979	4.56345	-0.44945
H	-0.91173	2.77142	-2.14237
H	1.65687	2.45616	2.12826
H	0.18440	4.40084	1.68636
H	-1.87008	-2.89721	-0.63256
H	-0.38937	-3.13409	1.38260
H	-0.49141	-1.46862	3.18815
H	-1.87701	0.58893	2.92172
H	-3.19023	0.94399	0.84790

Insertion TS of fluorobenzene by complex **I** (s)

M06/6-311+G** Enthalpy = -2340.40729146

Imaginary frequency = -220.52

H	-2.23066	2.26727	1.67045
C	-1.25750	1.98966	1.27247
C	1.21623	1.28670	0.17088
C	-0.62206	0.85641	1.76447
C	-0.69392	2.75009	0.24183
C	0.53768	2.40198	-0.30384
C	0.63846	0.47871	1.22685
H	-1.05947	0.29466	2.58719
H	-1.23127	3.61413	-0.14053
C	2.46667	0.67754	-0.18683
C	4.75319	-0.88222	-0.44643
C	2.61845	-0.50472	0.60673
C	3.44833	1.04060	-1.10801

C	4.58894	0.26566	-1.23893
C	3.78669	-1.26746	0.46426
H	3.32126	1.93527	-1.71609
H	5.36106	0.54544	-1.95123
H	3.92515	-2.16576	1.06341
H	5.65684	-1.47871	-0.55486
C	1.46670	-0.67616	1.44209
H	1.43778	-1.31845	2.31653
Ni	-0.34790	-0.95719	0.28519
H	0.96375	2.99730	-1.11041
C	-3.07917	-1.38776	0.27614
H	-2.95360	-2.24577	0.93088
C	-4.20195	-0.58671	0.32831
H	-4.98838	-0.82340	1.04279
C	-4.34703	0.51467	-0.51990
H	-5.23653	1.13528	-0.47118
C	-3.34941	0.77622	-1.46433
H	-3.45923	1.61904	-2.14418
C	-2.21441	-0.00337	-1.55015
H	-1.42678	0.20996	-2.26729
C	-2.01741	-1.01750	-0.58561
F	-1.19661	-2.22878	-1.06454

C-F insertion of fluorobenzene by complex **I** (s)

M06/6-311+G** Enthalpy = -2340.4716168

C	2.06636	0.66359	1.14101
C	1.00558	0.90204	-0.89794
C	1.44887	1.60777	0.27875
C	1.12130	2.97485	0.42780
C	0.43734	3.61362	-0.57457
C	0.03065	2.92695	-1.74442
C	0.30273	1.59387	-1.90890
C	2.22655	-0.56521	0.42497
C	1.53537	-0.44463	-0.82555
C	2.76564	-2.83996	-0.12523
C	2.81887	-1.79056	0.76875
C	1.49173	-1.52736	-1.71294
C	2.11162	-2.70978	-1.36308
Ni	0.04400	0.06157	0.85253
C	-1.71022	-0.40177	0.26563
F	-0.35625	-0.13305	2.62925
C	-2.00952	-0.90739	-1.00480
C	-3.31220	-1.21261	-1.39053
C	-4.36647	-1.01250	-0.50914
C	-4.09444	-0.51670	0.76155
C	-2.78876	-0.22579	1.14127

H	2.41568	0.85716	2.14701
H	1.41664	3.50536	1.32931
H	0.18708	4.66612	-0.46736
H	-0.52001	3.46516	-2.51103
H	-0.02892	1.06786	-2.80096
H	3.22957	-3.78879	0.13239
H	3.30778	-1.90504	1.73269
H	0.97731	-1.43518	-2.66710
H	2.08767	-3.55492	-2.04585
H	-1.20756	-1.08598	-1.72064
H	-3.50312	-1.61114	-2.38618
H	-5.38683	-1.24530	-0.80620
H	-4.90971	-0.36192	1.46732
H	-2.57721	0.12967	2.14673

Complex II (d)

M06/6-311+G** Enthalpy = -1883.39625103

C	-0.00000	0.93981	0.92100
C	-0.72219	-1.08675	-0.02366
C	-1.15265	0.11945	0.59537
C	-2.52357	0.34631	0.76268
C	-3.43264	-0.59728	0.31553
C	-3.00436	-1.77342	-0.31388
C	-1.64994	-2.01600	-0.48708
C	1.15266	0.11947	0.59537
C	0.72222	-1.08674	-0.02366
C	3.43266	-0.59722	0.31553
C	2.52357	0.34635	0.76268
C	1.64998	-2.01598	-0.48708
C	3.00440	-1.77336	-0.31389
Co	-0.00004	2.29667	-0.65077
H	-0.00001	1.59415	1.79379
H	-2.86591	1.26916	1.22678
H	-4.49816	-0.41921	0.44392
H	-3.73740	-2.49414	-0.66755
H	-1.31479	-2.93192	-0.97138
H	4.49818	-0.41913	0.44391
H	2.86590	1.26920	1.22678
H	1.31485	-2.93190	-0.97138
H	3.73746	-2.49407	-0.66756

Chlorobenzene (s)

M06/6-311+G** Enthalpy = -691.776106302

C	0.00000	1.20902	-0.17651
C	0.00000	1.20099	-1.56427
C	0.00000	0.00000	-2.26040

C	-0.00000	-1.20099	-1.56427
C	-0.00000	-1.20902	-0.17651
C	-0.00000	0.00000	0.50126
Cl	-0.00000	0.00000	2.24915
H	0.00000	2.14031	0.37987
H	0.00000	2.14382	-2.10264
H	0.00000	0.00000	-3.34570
H	-0.00000	-2.14382	-2.10264
H	-0.00000	-2.14031	0.37987

Insertion TS for oxidative addition of chlorobenzene by complex **II** (d)

M06/6-311+G** Enthalpy = -2575.21211857

Imaginary frequency = -219.22

H	1.63168	3.76719	-0.49858
C	0.79548	3.10088	-0.29894
C	-1.34223	1.39830	0.26871
C	0.41691	2.18947	-1.26515
C	0.14204	3.17295	0.94276
C	-0.91283	2.31928	1.22397
C	-0.67382	1.31194	-1.01187
H	0.93469	2.14962	-2.22118
H	0.47766	3.88914	1.68761
C	-2.42129	0.44592	0.25089
C	-4.30586	-1.50919	-0.33105
C	-2.36942	-0.24431	-1.00031
C	-3.39616	0.12936	1.19362
C	-4.33862	-0.84382	0.90329
C	-3.33650	-1.21984	-1.27517
H	-3.41767	0.64500	2.15222
H	-5.10457	-1.09638	1.63201
H	-3.31523	-1.75501	-2.22268
H	-5.05319	-2.27022	-0.54569
C	-1.24317	0.22642	-1.75984
H	-1.10593	0.05713	-2.82259
Co	0.44649	-0.32861	-0.51203
H	-1.41543	2.37108	2.18862
C	2.35293	-1.53961	-0.67615
H	1.75031	-2.30904	-1.15403
C	3.64336	-1.24817	-1.13550
H	3.99741	-1.70633	-2.05751
C	4.48187	-0.42193	-0.41195
H	5.48681	-0.21209	-0.76688
C	4.04295	0.11560	0.81900
H	4.70804	0.76675	1.38304
C	2.78604	-0.14116	1.30309

H	2.43408	0.28666	2.23800
C	1.89270	-0.90409	0.51207
Cl	0.50881	-1.98464	1.48962

η_5 C-Cl insertion of chlorobenzene by complex **II** (d)

M06/6-311+G** Enthalpy = -2575.292339

C	2.38604	-0.23940	0.67253
C	1.17913	0.80707	-1.01300
C	2.05009	1.02525	0.11288
C	2.32209	2.35397	0.51740
C	1.79135	3.39738	-0.19757
C	0.95619	3.17661	-1.31875
C	0.64359	1.90191	-1.71913
C	1.85357	-1.25409	-0.17861
C	1.06267	-0.62400	-1.19949
C	1.17688	-3.39811	-1.02976
C	1.87442	-2.66503	-0.10277
C	0.34468	-1.40407	-2.12465
C	0.41451	-2.77296	-2.04323
Co	0.24599	-0.06111	0.75867
C	-1.61232	0.14809	0.30476
Cl	-0.12212	-0.71478	2.84461
C	-2.43778	-0.97111	0.14065
C	-3.76914	-0.85060	-0.24121
C	-4.32569	0.40575	-0.45926
C	-3.53055	1.53274	-0.29170
C	-2.19519	1.39998	0.08131
H	2.97076	-0.40603	1.56802
H	2.95027	2.53540	1.38571
H	2.00309	4.41877	0.10894
H	0.54328	4.02903	-1.85111
H	-0.02541	1.73032	-2.55923
H	1.19002	-4.48375	-0.97369
H	2.43052	-3.15361	0.69295
H	-0.27464	-0.92119	-2.87708
H	-0.14196	-3.38657	-2.74620
H	-2.02501	-1.96444	0.32053
H	-4.38140	-1.74304	-0.36399
H	-5.36859	0.50446	-0.75244
H	-3.95264	2.52384	-0.45379
H	-1.59121	2.30157	0.19645

η_1 C-Cl insertion of chlorobenzene by complex **II** (d)

M06/6-311+G** Enthalpy = -2575.28859277

C	0.01067	0.64364	-1.57942
C	1.83772	-0.55503	-0.70353

C	0.71446	-0.63868	-1.55939
C	0.41433	-1.84915	-2.18033
C	1.20827	-2.95757	-1.92955
C	2.29658	-2.88026	-1.05452
C	2.61254	-1.67989	-0.43718
C	0.87697	1.54801	-0.81742
C	1.94249	0.81356	-0.24226
C	1.68944	3.52598	0.27905
C	0.76570	2.91346	-0.55537
C	2.85513	1.43509	0.60438
C	2.72641	2.79161	0.86320
Co	-1.73407	0.57637	-0.55428
C	-1.06305	-0.38117	0.91260
Cl	-3.90968	0.63572	-0.39988
C	-0.38743	0.25903	1.95321
C	0.12933	-0.46665	3.02201
C	-0.02595	-1.84634	3.07500
C	-0.71393	-2.49199	2.05323
C	-1.23146	-1.76559	0.98786
H	-0.39194	0.99698	-2.53815
H	-0.45423	-1.92516	-2.83202
H	0.97400	-3.90607	-2.40730
H	2.89166	-3.76772	-0.85565
H	3.45655	-1.61917	0.24718
H	1.60279	4.58939	0.48882
H	-0.05093	3.48763	-0.98973
H	3.66024	0.86274	1.06121
H	3.43272	3.28884	1.52302
H	-0.23543	1.33777	1.92301
H	0.66582	0.05183	3.81479
H	0.38668	-2.41497	3.90493
H	-0.84224	-3.57242	2.08272
H	-1.76076	-2.28729	0.19136

Insertion TS for oxidative addition of chlorobenzene by complex **I** (s)

M06/6-311+G** Enthalpy = -2700.79494209

Imaginary frequency = -179.62

H	2.03717	3.36551	-0.70107
C	1.11954	2.82908	-0.46912
C	-1.21767	1.45342	0.18875
C	0.65935	1.86725	-1.34709
C	0.44795	3.10240	0.73476
C	-0.71353	2.41756	1.05990
C	-0.51922	1.14401	-1.03515
H	1.19695	1.65509	-2.26914
H	0.84450	3.85409	1.41271

C	-2.39585	0.62694	0.22975
C	-4.48242	-1.15056	-0.22539
C	-2.38652	-0.20038	-0.93708
C	-3.43205	0.53057	1.15544
C	-4.47512	-0.35405	0.92886
C	-3.45436	-1.08065	-1.14996
H	-3.42535	1.15258	2.04937
H	-5.28998	-0.43200	1.64430
H	-3.46733	-1.71561	-2.03407
H	-5.30904	-1.83820	-0.39272
C	-1.19067	0.05368	-1.69580
H	-1.06805	-0.20889	-2.74219
Ni	0.38739	-0.61664	-0.48258
H	-1.23234	2.63299	1.99302
C	2.48649	-1.57704	-0.59176
H	2.05949	-2.43297	-1.10589
C	3.72070	-1.04107	-0.97135
H	4.21706	-1.42452	-1.86073
C	4.32466	-0.04894	-0.21759
H	5.28750	0.35483	-0.51757
C	3.70189	0.41893	0.95244
H	4.17285	1.20981	1.53215
C	2.48266	-0.07398	1.35488
H	1.96795	0.31429	2.22906
C	1.84359	-1.03249	0.54316
Cl	0.47324	-2.14878	1.36643

η_5 C-Cl insertion of chlorobenzene by complex I (s)

M06/6-311+G** Enthalpy = -2700.85970191

C	2.23462	0.66763	0.73889
C	0.90237	0.87877	-1.14020
C	1.54062	1.60746	-0.07751
C	1.28050	2.98672	0.06370
C	0.46579	3.61249	-0.84910
C	-0.14186	2.89667	-1.90561
C	0.05998	1.54585	-2.04994
C	2.22268	-0.59933	0.07953
C	1.34267	-0.50052	-1.05085
C	2.51148	-2.93718	-0.38994
C	2.77915	-1.84874	0.41015
C	1.07762	-1.62925	-1.84216
C	1.66898	-2.82944	-1.51526
Ni	0.18593	0.08199	0.74683
C	-1.58746	-0.39504	0.27562
Cl	-0.17242	0.11021	2.90849

C	-1.92231	-1.67342	-0.17604
C	-3.21983	-1.98655	-0.57393
C	-4.21772	-1.02084	-0.53143
C	-3.90392	0.25681	-0.07971
C	-2.60792	0.55948	0.32286
H	2.74710	0.89220	1.66568
H	1.71846	3.53737	0.89210
H	0.26552	4.67625	-0.74861
H	-0.79590	3.42231	-2.59597
H	-0.44291	0.98717	-2.83592
H	2.94410	-3.90352	-0.14346
H	3.40608	-1.94582	1.29265
H	0.39697	-1.55556	-2.68719
H	1.47245	-3.71114	-2.11956
H	-1.15445	-2.44659	-0.21992
H	-3.45276	-2.99302	-0.91888
H	-5.23182	-1.26189	-0.84231
H	-4.67782	1.02171	-0.03594
H	-2.38247	1.56168	0.68720

η_1 C-Cl insertion of chlorobenzene by complex **I** (s)

M06/6-311+G** Enthalpy = -2700.86319131

C	-0.05000	0.44893	-1.54585
C	1.89779	-0.55347	-0.67505
C	0.74519	-0.78263	-1.46002
C	0.49569	-2.05812	-1.95730
C	1.37063	-3.09107	-1.65226
C	2.49053	-2.86820	-0.84694
C	2.75749	-1.59881	-0.35500
C	0.79590	1.46892	-0.91425
C	1.93183	0.85714	-0.33703
C	1.52276	3.58114	-0.03441
C	0.60412	2.84006	-0.76433
C	2.83857	1.60418	0.40771
C	2.63098	2.96771	0.55688
Ni	-1.78541	0.30614	-0.63051
C	-1.03629	-0.31632	0.94231
Cl	-3.93325	0.41746	-0.45487
C	-0.50018	0.54794	1.89569
C	0.05948	0.04906	3.06783
C	0.08929	-1.31927	3.30662
C	-0.45816	-2.18547	2.36701
C	-1.01958	-1.68794	1.19688
H	-0.48974	0.69580	-2.52526
H	-0.39576	-2.24431	-2.55355
H	1.17623	-4.09129	-2.03217

H	3.15223	-3.69550	-0.60382
H	3.62835	-1.42520	0.27406
H	1.37410	4.65111	0.08974
H	-0.27431	3.31663	-1.19535
H	3.69927	1.12568	0.87092
H	3.33071	3.56402	1.13677
H	-0.49349	1.62189	1.71729
H	0.48532	0.73825	3.79467
H	0.53746	-1.70871	4.21756
H	-0.43960	-3.25957	2.54110
H	-1.43029	-2.38023	0.46417

Insertion TS for oxidative addition of chlorobenzene by complex **IV** (s)

M06 function with mixed lanl2dz/6-311+G** basis set Enthalpy = -1320.43033185

Imaginary frequency = -87.02

H	1.13649	4.03481	-0.96991
C	0.33997	3.35588	-0.67148
C	-1.69666	1.64173	0.12322
C	0.20217	2.14323	-1.31905
C	-0.51065	3.71591	0.38586
C	-1.52531	2.85869	0.78173
C	-0.80730	1.25472	-0.92331
H	0.89639	1.85702	-2.10748
H	-0.37263	4.66927	0.89028
C	-2.67491	0.59528	0.27190
C	-4.33330	-1.62006	0.02651
C	-2.36509	-0.42346	-0.67955
C	-3.77989	0.46676	1.11096
C	-4.60809	-0.63829	0.99216
C	-3.22854	-1.52184	-0.79852
H	-4.00140	1.23942	1.84621
H	-5.47545	-0.74406	1.63901
H	-3.01043	-2.30362	-1.52419
H	-4.99704	-2.47744	-0.06533
C	-1.15863	-0.06820	-1.39505
H	-0.99299	-0.37520	-2.42778
H	-2.19501	3.14123	1.59317
C	3.22633	-0.51007	-0.59200
H	3.44120	-1.28848	-1.31668
C	3.81629	0.74140	-0.67438
H	4.50344	0.94946	-1.49122
C	3.53369	1.72774	0.26476
H	3.98705	2.71088	0.18145
C	2.65315	1.44867	1.30631
H	2.40705	2.21978	2.03145

C	2.06265	0.20239	1.42463
H	1.38148	-0.02623	2.23772
C	2.30087	-0.76014	0.43143
Cl	2.09184	-2.59255	0.93411
Pd	0.41413	-1.24338	-0.36507

η_5 C-Cl insertion of chlorobenzene by complex **IV** (s)

M06 function with mixed lanl2dz/6-311+G** basis set Enthalpy = -1320.4648284

C	2.11551	0.91908	1.04428
C	0.97734	1.08693	-0.96808
C	1.26881	1.75939	0.27844
C	0.64368	3.00336	0.54457
C	-0.16385	3.56838	-0.40875
C	-0.41496	2.92449	-1.64517
C	0.14431	1.70463	-1.92578
C	2.56582	-0.14802	0.19014
C	1.85551	-0.07032	-1.04856
C	3.67440	-2.11927	-0.61856
C	3.46907	-1.19405	0.39250
C	2.06669	-1.01292	-2.04824
C	2.98275	-2.03319	-1.83190
Pd	-0.08501	-0.04023	0.79309
C	-1.82464	-0.58240	-0.04281
Cl	-0.69634	-1.02462	2.86877
C	-1.82153	-1.41941	-1.15779
C	-3.00709	-1.71579	-1.82374
C	-4.21161	-1.18018	-1.38403
C	-4.22006	-0.35388	-0.26654
C	-3.03679	-0.06182	0.40436
H	2.49293	1.13457	2.03579
H	0.82253	3.50235	1.49355
H	-0.63697	4.52641	-0.20843
H	-1.07454	3.39798	-2.36671
H	-0.06451	1.20088	-2.86701
H	4.38062	-2.93161	-0.46556
H	3.99515	-1.28475	1.33947
H	1.51742	-0.95156	-2.98577
H	3.16202	-2.77369	-2.60674
H	-0.88522	-1.84764	-1.51413
H	-2.98765	-2.37068	-2.69311
H	-5.13800	-1.41037	-1.90458
H	-5.15911	0.06311	0.09280
H	-3.05654	0.56406	1.29309

η_1 C-Cl insertion of chlorobenzene by complex **IV** (s)

M06 function with mixed lanl2dz/6-311+G** basis set Enthalpy = -1320.47855209

C	0.18643	0.44515	-1.55510
C	2.11997	-0.56236	-0.65226
C	0.97237	-0.79112	-1.44432
C	0.72883	-2.06604	-1.94654
C	1.60347	-3.09802	-1.63861
C	2.71964	-2.87476	-0.82770
C	2.98153	-1.60607	-0.33173
C	1.02262	1.46063	-0.90353
C	2.15283	0.84863	-0.31575
C	1.74822	3.57393	-0.02452
C	0.83479	2.83305	-0.76069
C	3.05606	1.59536	0.43354
C	2.85044	2.95959	0.57755
Pd	-1.72782	0.28292	-0.61762
C	-0.81859	-0.35126	1.01514
Cl	-4.03461	0.19171	0.01275
C	-0.26630	0.54844	1.91850
C	0.35789	0.07495	3.06855
C	0.42953	-1.28869	3.32158
C	-0.13995	-2.18119	2.42109
C	-0.76685	-1.71716	1.27045
H	-0.21113	0.69147	-2.54864
H	-0.15928	-2.25250	-2.54740
H	1.41274	-4.09763	-2.02176
H	3.38217	-3.70114	-0.58395
H	3.85023	-1.43125	0.29997
H	1.60074	4.64445	0.09559
H	-0.03971	3.31022	-1.19870
H	3.91265	1.11604	0.90347
H	3.54652	3.55587	1.16174
H	-0.29768	1.61739	1.72228
H	0.79946	0.78406	3.76550
H	0.92680	-1.65506	4.21607
H	-0.09109	-3.25150	2.60880
H	-1.20176	-2.42221	0.56698

Complex III (d)

M06/6-311+G** Enthalpy = -2141.19650422

C	0.86971	0.88973	0.00000
C	-1.16008	-0.04096	0.72117
C	0.05190	0.57173	1.15151
C	0.27902	0.74026	2.52303
C	-0.66962	0.30744	3.43214
C	-1.85500	-0.30910	3.00463
C	-2.09688	-0.48588	1.65093
C	0.05190	0.57173	-1.15151

C	-1.16008	-0.04096	-0.72117
C	-0.66962	0.30744	-3.43214
C	0.27902	0.74026	-2.52303
C	-2.09688	-0.48588	-1.65093
C	-1.85500	-0.30910	-3.00463
Cu	2.35895	-0.56987	-0.00000
H	1.54809	1.74300	0.00000
H	1.20732	1.19348	2.86579
H	-0.49118	0.43766	4.49749
H	-2.58145	-0.64966	3.73826
H	-3.01863	-0.96006	1.31676
H	-0.49118	0.43766	-4.49749
H	1.20732	1.19348	-2.86579
H	-3.01863	-0.96006	-1.31676
H	-2.58145	-0.64966	-3.73826

Cl Transfer TS for halogen abstraction of chlorobenzene by complex **III** (d)

M06/6-311+G** Enthalpy = -2832.97456964

Imaginary frequency = -261.52

H	-0.92483	-3.76326	2.29041
C	-0.56874	-2.76236	2.05554
C	0.30469	-0.19405	1.46938
C	0.67629	-2.60098	1.47447
C	-1.38972	-1.65901	2.33030
C	-0.95473	-0.37710	2.03583
C	1.12984	-1.31306	1.15909
H	1.29035	-3.46655	1.23266
H	-2.37587	-1.81264	2.76174
C	1.01236	0.99583	1.06778
C	2.80926	2.90762	0.15871
C	2.25471	0.59032	0.50002
C	0.67890	2.34596	1.15166
C	1.57562	3.30134	0.69890
C	3.15069	1.57115	0.05488
H	-0.27805	2.64654	1.57570
H	1.32775	4.35782	0.76428
H	4.10036	1.27677	-0.38805
H	3.50442	3.66789	-0.19120
C	2.32774	-0.85794	0.47564
H	3.27484	-1.38982	0.54535
H	-1.59882	0.47868	2.23354
Cl	-0.59928	-0.70884	-2.18192
Cu	1.63079	-1.25551	-1.40797
C	-3.09795	-0.53906	-0.82555
C	-4.04067	0.09762	-0.02969
H	-4.87521	-0.47035	0.37677

C	-3.91475	1.45321	0.25911
H	-4.64751	1.94570	0.89233
C	-2.83709	2.17094	-0.24938
H	-2.72445	3.22721	-0.01228
C	-1.89326	1.54604	-1.05478
H	-1.03350	2.09034	-1.43898
H	-3.16579	-1.60461	-1.03214
C	-2.05302	0.20295	-1.34628

Chlorine addition product of complex **III** (s)
M06/6-311+G** Enthalpy = -2601.53662625

C	0.16034	-0.00077	1.11590
C	-1.67644	0.72461	-0.17347
C	-0.59881	1.15568	0.64313
C	-0.41733	2.52364	0.86287
C	-1.27600	3.43271	0.26841
C	-2.31993	3.00383	-0.56108
C	-2.51978	1.65090	-0.78396
C	-0.60224	-1.15487	0.64299
C	-1.67859	-0.72051	-0.17355
C	-1.28611	-3.42984	0.26793
C	-0.42474	-2.52338	0.86250
C	-2.52470	-1.64423	-0.78412
C	-2.32881	-2.99778	-0.56144
Cu	1.86993	-0.00240	0.12200
Cl	3.78290	-0.00390	-0.84588
H	0.52199	-0.00138	2.14885
H	0.40895	2.86735	1.48222
H	-1.13157	4.49746	0.43688
H	-2.97306	3.73613	-1.02874
H	-3.33618	1.31505	-1.42122
H	-1.14480	-4.49504	0.43622
H	0.40055	-2.86961	1.48175
H	-3.34013	-1.30590	-1.42131
H	-2.98411	-3.72810	-1.02918

Phenyl radical (d)
M06/6-311+G** Enthalpy = -231.478175565

C	-0.00000	1.20778	-0.62840
C	-0.00000	1.21909	0.76725
C	0.00000	0.00000	1.39100
C	-0.00000	-1.21909	0.76725
C	-0.00000	-1.20778	-0.62840
C	-0.00000	-0.00000	-1.31607

H	-0.00000	2.14646	-1.17567
H	-0.00000	2.15483	1.31865
H	-0.00000	-2.15483	1.31865
H	-0.00000	-2.14646	-1.17567
H	-0.00000	-0.00000	-2.40172

C-Cl insertion of chlorobenzene by cobalt (s)

M06/6-311+G** Enthalpy = -2074.57720962

Co	1.05842	-0.34852	0.00009
C	-0.56251	0.46628	-0.00064
C	-0.95999	-0.86179	-0.00026
C	-2.28316	-1.26225	0.00002
C	-3.26158	-0.25780	0.00007
C	-2.88524	1.07979	0.00021
C	-1.53623	1.45731	-0.00018
Cl	3.07726	0.34145	0.00001
H	-0.14207	-1.64647	0.00060
H	-2.57118	-2.31266	0.00022
H	-4.31540	-0.52662	-0.00010
H	-3.65807	1.84777	0.00045
H	-1.27196	2.51397	0.00092

C-Cl insertion of chlorobenzene by cobalt (t)

M06/6-311+G** Enthalpy = -2074.61296068

Co	-1.24100	-0.00002	-0.00007
C	0.73342	-0.00003	-0.00004
C	1.49412	1.18624	0.00001
C	2.88549	1.19506	0.00012
C	3.59572	0.00003	0.00018
C	2.88554	-1.19502	0.00012
C	1.49417	-1.18626	0.00001
Cl	-3.44181	0.00002	-0.00006
H	0.97976	2.14762	-0.00003
H	3.42177	2.14357	0.00016
H	4.68370	0.00005	0.00027
H	3.42186	-2.14351	0.00016
H	0.97984	-2.14766	-0.00004

Fluorenyl radical (d)

M06/6-311+G** Enthalpy = -500.607194889

C	-0.00000	1.73948	-0.00019
C	0.72970	-0.45317	-0.00006
C	1.15515	0.90498	0.00003
C	2.51757	1.21056	0.00001
C	3.43783	0.17166	0.00000
C	3.01396	-1.15701	0.00003

C	1.65512	-1.47680	0.00002
C	-1.15515	0.90499	0.00001
C	-0.72970	-0.45317	-0.00008
C	-3.43783	0.17166	0.00002
C	-2.51757	1.21056	0.00003
C	-1.65512	-1.47680	-0.00001
C	-3.01396	-1.15701	0.00003
H	-0.00000	2.82388	0.00098
H	2.85051	2.24489	-0.00012
H	4.50065	0.39270	-0.00007
H	3.75231	-1.95304	0.00004
H	1.33737	-2.51624	0.00015
H	-4.50065	0.39270	-0.00006
H	-2.85051	2.24488	-0.00006
H	-1.33737	-2.51624	0.00009
H	-3.75230	-1.95305	0.00001

C-Cl insertion of chlorobenzene by nickel (d)

M06/6-311+G** Enthalpy = -2200.21044365

Ni	-1.21629	-0.08174	-0.00000
C	0.72395	-0.03425	0.00002
C	1.43805	1.17908	0.00001
C	2.82791	1.24079	-0.00000
C	3.58249	0.07312	-0.00001
C	2.91910	-1.14786	-0.00000
C	1.52783	-1.19087	0.00001
Cl	-3.38150	0.08082	-0.00001
H	0.88578	2.11898	0.00003
H	3.32841	2.20869	-0.00001
H	4.66967	0.11429	-0.00003
H	3.49093	-2.07543	-0.00000
H	1.05109	-2.17178	0.00002

Chlorine addition product of complex I (d)

M06/6-311+G** Enthalpy = -2469.31154699

C	0.29503	-0.40581	1.40929
C	0.46132	1.36037	-0.13059
C	-0.34940	0.77931	0.91152
C	-1.62088	1.33914	1.18314
C	-2.04050	2.44577	0.45592
C	-1.24116	3.00662	-0.54472
C	0.00269	2.46131	-0.84213
C	1.57264	-0.46858	0.75239
C	1.67353	0.58817	-0.20192
C	3.77705	-1.19553	0.11555
C	2.65004	-1.35098	0.90205

C	2.81225	0.72055	-0.99428
C	3.86276	-0.16771	-0.83569
Ni	-1.29018	-0.85106	0.08138
Cl	-2.56961	-2.23227	-0.96004
H	0.07998	-0.88129	2.36111
H	-2.23627	0.94007	1.98602
H	-3.01450	2.88080	0.66653
H	-1.60408	3.86502	-1.10369
H	0.61279	2.89256	-1.63411
H	4.61108	-1.88437	0.23142
H	2.59274	-2.16094	1.62637
H	2.87758	1.52166	-1.72877
H	4.75685	-0.07097	-1.44617

Palladium complex with chlorine and benzyne (s)

M06 function with mixed lanl2dz/6-311+G** basis set Enthalpy = -819.192506035

C	-2.20265	1.43643	-0.00004
C	-1.06854	0.65670	-0.00005
C	-1.07342	-0.66201	-0.00023
C	-2.21547	-1.43046	0.00002
C	-3.41242	-0.68715	0.00008
C	-3.40624	0.70393	0.00003
Pd	0.83747	-0.00658	0.00001
Cl	3.23039	0.00979	0.00001
H	-2.21155	2.52439	0.00011
H	-2.23487	-2.51835	0.00005
H	-4.36618	-1.21226	0.00013
H	-4.35524	1.23757	0.00003

Fluorene (s)

M06/6-311+G** Enthalpy = -501.243597684

C	0.00000	1.81796	0.00012
C	-0.73049	-0.44807	0.00010
C	-1.17548	0.88102	0.00006
C	-2.52910	1.16749	-0.00005
C	-3.44040	0.11601	-0.00011
C	-2.99867	-1.20431	-0.00006
C	-1.64134	-1.49708	0.00003
C	1.17548	0.88102	0.00001
C	0.73049	-0.44807	0.00007
C	3.44040	0.11600	-0.00011
C	2.52910	1.16750	-0.00008
C	1.64134	-1.49708	0.00007
C	2.99867	-1.20430	-0.00003
H	-0.00003	2.47477	-0.87962

H	0.00003	2.47438	0.88016
H	-2.87853	2.19687	-0.00007
H	-4.50573	0.32546	-0.00021
H	-3.72437	-2.01197	-0.00011
H	-1.30135	-2.52922	0.00008
H	4.50573	0.32546	-0.00021
H	2.87853	2.19687	-0.00015
H	1.30135	-2.52922	0.00013
H	3.72437	-2.01198	-0.00003

C-Cl insertion of chlorobenzene by copper (s)

M06/6-311+G** Enthalpy = -2332.43608783

Cu	-1.19376	-0.00024	-0.00001
C	0.72507	-0.00024	0.00001
C	1.48423	-1.18523	0.00001
C	2.87614	-1.19511	-0.00000
C	3.58482	0.00033	-0.00000
C	2.87566	1.19551	-0.00000
C	1.48377	1.18507	0.00001
Cl	-3.35251	0.00024	0.00001
H	0.96821	-2.14562	0.00001
H	3.41303	-2.14330	-0.00000
H	4.67286	0.00056	-0.00001
H	3.41220	2.14390	-0.00000
H	0.96736	2.14525	0.00001

Allyl Chloride (s)

M06/6-311+G** Enthalpy = -577.471325939

C	-2.20670	-0.20324	-0.30554
C	-1.12214	-0.12139	0.45198
C	0.03113	0.74917	0.12752
Cl	1.53100	-0.24243	-0.11109
H	-3.04408	-0.83742	-0.03570
H	-2.29721	0.36546	-1.22789
H	-1.03843	-0.70720	1.36586
H	-0.12919	1.31066	-0.79498
H	0.26818	1.44249	0.93747

Insertion TS for oxidative addition of allyl chloride by complex **II** (d)

M06/6-311+G** Enthalpy = -2460.93532908

Imaginary frequency = -275.33

C	-1.09370	1.63194	-1.50209
C	-1.44789	2.77409	-0.77662
C	-0.66453	3.24352	0.27206
C	0.50501	2.57245	0.63710

C	2.79312	-1.54208	-0.88987
C	3.85041	-1.53271	0.00482
C	3.97614	-0.52169	0.96668
C	3.03941	0.49860	1.02772
H	0.50361	-0.71079	-2.61690
H	2.69978	-2.34180	-1.62215
H	4.59315	-2.32702	-0.03375
H	4.80901	-0.54112	1.66505
H	3.13438	1.28689	1.77260
H	1.09390	2.92435	1.48257
H	-0.97789	4.12485	0.82543
H	-2.35503	3.31071	-1.04683
H	-1.65969	1.35422	-2.38898
C	0.10397	0.95458	-1.16243
C	0.88840	1.43914	-0.05247
C	1.83166	-0.52737	-0.83653
C	1.97914	0.51268	0.12683
C	0.64075	-0.29850	-1.61987
C	-2.84120	-1.55428	0.00413
H	-3.67513	-1.09513	-0.52682
C	-1.89087	-2.40322	-0.66625
H	-2.12263	-2.74666	-1.67688
H	-1.34631	-3.14028	-0.07038
C	-2.81826	-1.41173	1.42035
H	-2.51643	-2.27404	2.01303
H	-3.61340	-0.83040	1.87980
Cl	-1.17049	-0.25847	2.06953
Co	-1.17698	-0.57824	-0.61330

η_1 C-Cl insertion of allyl chloride by complex **II** (d)

M06/6-311+G** Enthalpy = -2461.01529286

C	-0.14272	-0.38008	-1.19177
C	-2.11528	0.35452	-0.14268
C	-1.48737	-0.74323	-0.79236
C	-2.18534	-1.94782	-0.91496
C	-3.45921	-2.05838	-0.38259
C	-4.06453	-0.98087	0.27779
C	-3.39251	0.22577	0.39819
C	-0.01523	1.02618	-0.85020
C	-1.18372	1.45760	-0.15393
C	0.96471	3.18911	-0.45624
C	1.05750	1.91769	-1.00338
C	-1.24993	2.73275	0.39738
C	-0.17463	3.59793	0.24554
Co	1.34283	-0.71999	0.24406
Cl	2.94955	-1.14282	-1.29546

C	0.15936	-1.04348	1.87094
C	1.33307	-0.33905	2.19145
C	2.57638	-0.90371	1.86814
H	0.32691	-0.80559	-2.07488
H	-1.71845	-2.79672	-1.41017
H	-3.99976	-2.99813	-0.47348
H	-5.06283	-1.09363	0.69280
H	-3.86177	1.06602	0.90783
H	1.79672	3.88018	-0.57046
H	1.95098	1.59936	-1.53479
H	-2.13749	3.05194	0.94168
H	-0.21625	4.59715	0.67176
H	0.14617	-2.13361	1.93839
H	-0.81207	-0.56382	1.95741
H	1.26605	0.73313	2.39345
H	3.48631	-0.31340	1.90641
H	2.71346	-1.98486	1.91945

Insertion TS for oxidative addition of allyl chloride by complex I (s)

M06/6-311+G** Enthalpy = -2586.514317

Imaginary frequency = -222.28

C	-1.37392	-2.12084	-1.40223
C	-2.25123	-2.88413	-0.65277
C	-2.93348	-2.33587	0.44290
C	-2.74148	-1.00879	0.79074
C	-0.04244	2.73777	-1.01677
C	-0.44502	3.72222	-0.13226
C	-1.34685	3.44148	0.90495
C	-1.86416	2.16332	1.04768
H	0.01853	0.22925	-2.67029
H	0.67960	2.95899	-1.80113
H	-0.04882	4.73062	-0.23480
H	-1.63649	4.22864	1.59655
H	-2.56391	1.94228	1.85216
H	-3.26548	-0.58513	1.64595
H	-3.60737	-2.95967	1.02478
H	-2.40882	-3.92941	-0.91005
H	-0.83409	-2.55888	-2.23983
Ni	1.33324	-0.41617	-0.60161
C	-1.16465	-0.77573	-1.06596
C	-1.87033	-0.22092	0.04183
C	-0.54700	1.43718	-0.88241
C	-1.48816	1.16527	0.15289
C	-0.27514	0.22256	-1.62196
C	3.13219	-0.83187	0.09232
H	3.46469	-1.83958	-0.16020

C	3.09681	0.18741	-0.92071
H	3.56288	-0.03659	-1.88129
H	3.19434	1.23677	-0.62042
C	2.85886	-0.55992	1.47090
H	2.85645	0.49064	1.75784
H	3.31950	-1.20123	2.22076
Cl	0.91024	-1.00522	1.98647

η_5 C-Cl insertion of allyl chloride by complex **I** (s)

M06/6-311+G** Enthalpy = -2586.56109951

C	-0.73555	-0.17634	-1.79310
C	0.23801	-1.38823	-0.08140
C	0.44796	-0.86243	-1.40632
C	1.72308	-0.98838	-2.00281
C	2.71718	-1.65013	-1.32783
C	2.49963	-2.18663	-0.03685
C	1.28150	-2.06284	0.58209
C	-1.75535	-0.45627	-0.82695
C	-1.15216	-1.16168	0.26545
C	-3.83033	-0.42284	0.38164
C	-3.10277	-0.07154	-0.73651
C	-1.90739	-1.48937	1.39811
C	-3.24011	-1.13196	1.44338
Ni	0.01343	0.75823	-0.03966
Cl	-0.11317	2.86216	-0.70374
C	0.74850	1.18003	1.72207
C	2.16953	1.41119	1.49682
C	3.18236	0.60988	1.86155
H	-0.86959	0.39589	-2.70228
H	1.90363	-0.55898	-2.98490
H	3.70095	-1.74714	-1.77978
H	3.31817	-2.68587	0.47472
H	1.12656	-2.45393	1.58578
H	-4.87569	-0.13315	0.45416
H	-3.55551	0.50817	-1.53672
H	-1.44341	-2.01109	2.23262
H	-3.83862	-1.38459	2.31467
H	0.55283	0.34950	2.41501
H	0.20174	2.08042	2.01744
H	2.40594	2.31585	0.93191
H	4.21253	0.83034	1.59467
H	3.00373	-0.30710	2.42074

η_1 C-Cl insertion of allyl chloride by complex **I** (s)

M06/6-311+G** Enthalpy = -2586.56495127

C	0.08004	-0.33960	-1.12582
---	---------	----------	----------

C	1.92179	0.76411	-0.15287
C	0.74775	0.94716	-0.92206
C	0.38012	2.23216	-1.31381
C	1.17049	3.31061	-0.94584
C	2.32040	3.12795	-0.17200
C	2.69685	1.85482	0.23140
C	1.00843	-1.32375	-0.56068
C	2.08472	-0.65956	0.07405
C	1.94988	-3.42684	0.11724
C	0.95447	-2.71631	-0.53610
C	3.06927	-1.38086	0.74453
C	3.00039	-2.76569	0.76182
Ni	-1.70415	-0.45675	-0.31564
Cl	-3.84994	-0.84205	-0.23597
C	-1.19484	0.01501	1.46245
C	-1.80927	1.32286	1.67840
C	-1.15214	2.48726	1.75734
H	-0.31610	-0.54463	-2.13423
H	-0.53518	2.38427	-1.88207
H	0.88309	4.31514	-1.24674
H	2.91758	3.98874	0.11774
H	3.59187	1.71209	0.83427
H	1.90878	-4.51324	0.13961
H	0.12443	-3.23481	-1.01167
H	3.88884	-0.86566	1.24225
H	3.76367	-3.34194	1.27839
H	-0.10893	0.00995	1.60302
H	-1.67774	-0.79585	2.02177
H	-2.89874	1.33009	1.74086
H	-1.67866	3.42950	1.88312
H	-0.06779	2.53429	1.67480

Insertion TS for oxidative addition of allyl chloride by complex **IV** (s)

M06 function with mixed lanl2dz/6-311+G** basis set Enthalpy = -1206.13727102

Imaginary frequency = -271.21

C	0.54736	2.45768	-1.17996
C	1.04985	3.57669	-0.54004
C	2.07358	3.46849	0.41309
C	2.61516	2.22833	0.71196
C	1.89637	-2.39782	-0.91384
C	2.90139	-3.02394	-0.19774
C	3.70370	-2.30711	0.70135
C	3.51329	-0.94395	0.86764
H	0.33835	-0.29090	-2.35536
H	1.26368	-2.96854	-1.59121
H	3.06809	-4.09114	-0.32689

H	4.48009	-2.82220	1.26132
H	4.14718	-0.38223	1.55225
H	3.41803	2.14332	1.44290
H	2.44246	4.36042	0.91304
H	0.63876	4.55687	-0.77148
H	-0.27091	2.54751	-1.89169
C	1.06713	1.19461	-0.87458
C	2.13537	1.09378	0.06014
C	1.67526	-1.02671	-0.74377
C	2.52056	-0.29482	0.13708
C	0.69564	-0.13282	-1.33527
C	-2.29781	-0.40150	1.79339
H	-2.33513	-1.40634	2.20900
C	-1.05091	0.27038	1.71932
H	-0.19477	-0.13834	2.25500
H	-1.03068	1.35731	1.60080
C	-3.51115	0.20384	1.42193
H	-3.49981	1.26963	1.21312
H	-4.44223	-0.17526	1.82502
Cl	-4.30042	-0.32034	-0.63541
Pd	-1.13315	-0.48489	-0.19083

η_5 C-Cl insertion of allyl chloride by complex **IV** (s)

M06 function with mixed lanl2dz/6-311+G** basis set Enthalpy = -1206.16946453

C	1.02089	-0.04283	1.71674
C	0.32055	-1.51008	0.06099
C	0.01408	-0.98052	1.37083
C	-1.17616	-1.40351	2.01616
C	-1.98104	-2.32980	1.40512
C	-1.66573	-2.85654	0.13050
C	-0.52267	-2.46550	-0.52780
C	2.08146	-0.16394	0.74886
C	1.65619	-1.04898	-0.28811
C	4.15486	0.14431	-0.42422
C	3.33834	0.43726	0.65771
C	2.48322	-1.32567	-1.36794
C	3.73781	-0.73189	-1.43085
Pd	-0.39873	0.80309	0.01211
Cl	-0.64345	3.15902	0.41113
C	-1.61421	0.98636	-1.67920
C	-2.88877	0.49793	-1.19994
C	-3.42077	-0.70744	-1.46983
H	1.07556	0.51621	2.64226
H	-1.43203	-0.99480	2.99034
H	-2.89574	-2.65231	1.89610
H	-2.33477	-3.58128	-0.32532

H	-0.28048	-2.87466	-1.50697
H	5.13615	0.60752	-0.49472
H	3.66629	1.13461	1.42445
H	2.15138	-1.99805	-2.15663
H	4.39713	-0.94364	-2.26836
H	-1.14780	0.35987	-2.44933
H	-1.57449	2.05145	-1.90981
H	-3.43005	1.17234	-0.53306
H	-4.35935	-1.03374	-1.03096
H	-2.91976	-1.40381	-2.13827

η_1 C-Cl insertion of allyl chloride by complex **IV** (s)

M06 function with mixed lanl2dz/6-311+G** basis set Enthalpy = -1206.18004172

C	-0.45891	-0.29388	-1.22336
C	-2.18121	0.80967	-0.05278
C	-1.09642	0.99248	-0.94444
C	-0.78439	2.27719	-1.38776
C	-1.52463	3.35567	-0.93019
C	-2.57661	3.17428	-0.02495
C	-2.90689	1.90166	0.41632
C	-1.32278	-1.27700	-0.56843
C	-2.32386	-0.61448	0.18211
C	-2.19607	-3.38235	0.18831
C	-1.27383	-2.67036	-0.56166
C	-3.23489	-1.33830	0.94796
C	-3.17001	-2.72293	0.94696
Pd	1.54966	-0.37958	-0.47065
Cl	3.90109	-0.64124	0.02081
C	0.98229	-0.01344	1.46679
C	1.03376	1.43401	1.64432
C	2.07228	2.09068	2.17271
H	-0.15645	-0.49556	-2.25914
H	0.05560	2.42784	-2.06268
H	-1.27836	4.35926	-1.26830
H	-3.13495	4.03580	0.33178
H	-3.72950	1.75912	1.11467
H	-2.15680	-4.46890	0.19853
H	-0.49859	-3.18729	-1.12321
H	-3.99493	-0.82448	1.53370
H	-3.87525	-3.30108	1.53829
H	1.74595	-0.55615	2.03069
H	-0.01182	-0.45542	1.57118
H	0.16214	2.00043	1.31363
H	2.06975	3.17173	2.27596
H	2.97352	1.55886	2.46984

Cl Transfer TS for halogen abstraction from allyl chloride by complex **III** (d)

M06/6-311+G** Enthalpy = -2718.66566036

Imaginary frequency = -808.60

H	2.46309	3.99579	0.29643
C	1.59894	3.33597	0.32735
C	-0.60693	1.65597	0.44707
C	1.29188	2.56125	-0.77656
C	0.82178	3.27581	1.49479
C	-0.27711	2.43395	1.55575
C	0.18411	1.70456	-0.73426
H	1.91879	2.59254	-1.66567
H	1.09068	3.88532	2.35357
C	-1.67724	0.71552	0.21906
C	-3.48931	-1.14713	-0.75214
C	-1.52366	0.19656	-1.09561
C	-2.72437	0.29003	1.03362
C	-3.63054	-0.63830	0.54856
C	-2.44925	-0.74124	-1.56899
H	-2.82151	0.67448	2.04752
H	-4.44879	-0.98194	1.17602
H	-2.32966	-1.16486	-2.56431
H	-4.20430	-1.88076	-1.11783
C	-0.31299	0.73399	-1.69761
H	-0.26610	0.93632	-2.76747
H	-0.87841	2.37900	2.46177
C	-0.16914	-2.40637	2.78150
C	0.15809	-1.71674	1.67729
H	-0.50913	-1.73240	0.81496
C	1.40044	-0.99287	1.51980
Cl	2.64017	-2.06343	0.32265
Cu	1.06188	-0.78777	-1.59609
H	0.47160	-2.40139	3.66114
H	-1.09360	-2.97198	2.84301
H	1.35564	-0.05953	0.96214
H	2.00614	-0.91269	2.42242

C-Cl insertion of allyl chloride by cobalt (s)

M06/6-311+G** Enthalpy = -1960.31577242

Co	-0.05950	-0.00019	-0.04107
Cl	-2.14684	0.00003	0.00071
C	1.53031	1.21384	0.23418
C	1.89641	0.00024	-0.37415
C	1.53091	-1.21349	0.23417
H	1.57899	2.13692	-0.33425
H	1.53160	1.32307	1.31837
H	2.13454	0.00028	-1.43687

H	1.57999	-2.13665	-0.33409
H	1.53188	-1.32260	1.31838

C-Cl insertion of allyl chloride by cobalt (t)
M06/6-311+G** Enthalpy = -1960.33472821

Co	-0.06238	-0.00019	-0.08677
Cl	-2.26249	0.00005	0.04161
C	1.63287	1.26606	0.25120
C	1.90055	0.00021	-0.32836
C	1.63329	-1.26573	0.25124
H	1.83203	2.15837	-0.33642
H	1.68036	1.40162	1.33247
H	2.12015	0.00023	-1.40122
H	1.83286	-2.15797	-0.33634
H	1.68096	-1.40125	1.33252

Chlorine addition product of complex II (s)
M06/6-311+G** Enthalpy = -2343.69283139

C	-0.13698	0.06394	1.63434
C	0.44360	-1.07973	-0.28183
C	0.95100	-0.62135	0.99155
C	2.32878	-0.77484	1.28971
C	3.14757	-1.40333	0.38461
C	2.64623	-1.86952	-0.85784
C	1.32682	-1.70870	-1.19539
C	-1.36004	-0.30429	0.94950
C	-1.00598	-0.97764	-0.25659
C	-3.67162	-0.42946	0.30407
C	-2.69931	-0.03222	1.21707
C	-1.98722	-1.35813	-1.16418
C	-3.32156	-1.08593	-0.87527
Co	0.51123	0.99809	-0.01666
Cl	0.50775	3.01860	-0.77065
H	-0.09984	0.52325	2.61665
H	2.71914	-0.40868	2.23661
H	4.20524	-1.52162	0.60643
H	3.32832	-2.34631	-1.55758
H	0.95341	-2.06678	-2.15298
H	-4.71889	-0.22017	0.50935
H	-2.97795	0.50213	2.12253
H	-1.71446	-1.85555	-2.09259
H	-4.09772	-1.38354	-1.57600

Chlorine addition product of complex II (t)
M06/6-311+G** Enthalpy = -2343.7364343

C	-0.00002	-0.28888	1.75611
---	----------	----------	---------

C	0.71925	-1.10876	-0.31073
C	1.14906	-0.62596	0.97797
C	2.53748	-0.53680	1.23718
C	3.43637	-0.91520	0.26900
C	3.00930	-1.37772	-0.99430
C	1.66479	-1.46302	-1.28408
C	-1.14912	-0.62591	0.97797
C	-0.71933	-1.10873	-0.31073
C	-3.43644	-0.91504	0.26899
C	-2.53754	-0.53667	1.23717
C	-1.66488	-1.46295	-1.28408
C	-3.00939	-1.37758	-0.99430
Co	0.00005	1.09579	0.08636
Cl	0.00011	3.14012	-0.69031
H	-0.00002	0.03142	2.79024
H	2.88346	-0.16740	2.19999
H	4.50248	-0.84310	0.47262
H	3.74725	-1.65028	-1.74380
H	1.33190	-1.80977	-2.26064
H	-4.50255	-0.84290	0.47260
H	-2.88350	-0.16726	2.19998
H	-1.33200	-1.80972	-2.26065
H	-3.74735	-1.65010	-1.74381

Allyl radical (d)

M06/6-311+G** Enthalpy = -117.214980533

C	1.21928	-0.19622	-0.00000
C	-0.00010	0.44674	-0.00000
C	-1.21926	-0.19641	-0.00000
H	2.15482	0.35110	-0.00000
H	1.27326	-1.28184	-0.00000
H	-0.00017	1.53664	0.00001
H	-1.27300	-1.28198	0.00001
H	-2.15447	0.35147	-0.00000

η_1 C-Cl insertion of allyl chloride by nickel (d)

M06/6-311+G** Enthalpy = -2085.90885746

Ni	-0.43126	0.25727	-0.06030
Cl	-2.49722	-0.42726	0.03527
C	1.43445	0.91636	-0.04379
C	2.35536	-0.09956	0.45922
C	3.21277	-0.86648	-0.23523
H	1.69024	1.23449	-1.06553
H	1.39623	1.80196	0.60594
H	2.31501	-0.26765	1.54061
H	3.80921	-1.63818	0.24372

H 3.30197 -0.77277 -1.31711

η_5 C-Cl insertion of allyl chloride by nickel (d)

M06/6-311+G** Enthalpy = -2085.9161639

C	-1.61403	-1.24773	0.24254
C	-1.88400	0.00038	-0.35401
C	-1.61170	1.24812	0.24263
Ni	0.05758	0.00004	-0.06431
Cl	2.23688	-0.00043	0.02495
H	-1.63564	-1.35560	1.32751
H	-1.78831	-2.15904	-0.32347
H	-2.13812	0.00061	-1.41888
H	-1.63436	1.35598	1.32762
H	-1.78448	2.15975	-0.32336

C-Cl insertion of allyl chloride by palladium (s)

M06 function with mixed lanl2dz/6-311+G** basis set Enthalpy = -705.461510892

Pd	-0.02549	-0.24940	-0.04143
Cl	-2.29039	0.14250	0.02736
C	1.15152	1.45204	0.23168
C	1.95360	0.45894	-0.39271
C	2.10852	-0.74392	0.28620
H	0.81357	2.31458	-0.33388
H	1.17649	1.57577	1.31286
H	2.21880	0.54405	-1.44308
H	2.52074	-1.61109	-0.21936
H	2.09749	-0.77589	1.37324

Fluorenyl anion (s)

M06/6-311+G** Enthalpy = -500.669784424

C	-1.76290	0.00000	0.00000
C	0.44908	-0.71565	-0.00000
C	-0.93036	-1.13845	-0.00000
C	-1.20321	-2.52338	-0.00000
C	-0.16517	-3.43320	-0.00000
C	1.17981	-3.01171	-0.00000
C	1.47647	-1.65728	-0.00000
C	-0.93038	1.13844	0.00000
C	0.44910	0.71564	0.00000
C	-0.16517	3.43319	0.00000
C	-1.20321	2.52338	0.00000
C	1.47648	1.65728	0.00000
C	1.17981	3.01171	0.00000
H	-2.84808	0.00000	0.00000
H	-2.23532	-2.87303	-0.00000
H	-0.38676	-4.49982	-0.00000

H	1.97913	-3.74973	-0.00000
H	2.51597	-1.32819	-0.00000
H	-0.38676	4.49981	0.00000
H	-2.23533	2.87306	0.00000
H	2.51599	1.32820	0.00000
H	1.97913	3.74973	0.00000

C-Cl insertion of allyl chloride by copper (d)

M06/6-311+G** Enthalpy = -2218.12427584

Cu	0.35295	-0.30727	0.00019
Cl	2.40424	0.40765	-0.00044
C	-1.47054	-0.98911	0.00079
C	-2.59456	-0.00754	-0.00166
C	-2.49827	1.32130	0.00069
H	-1.60345	-1.66176	-0.86569
H	-1.60376	-1.65728	0.87072
H	-3.61900	-0.41314	-0.00545
H	-3.37986	1.96125	-0.00071
H	-1.52148	1.80361	0.00413